

# **INTEGRATED DATA FLOW AND RISK AGGREGATION FOR CONSEQUENCE-BASED RISK MANAGEMENT OF SEISMIC REGIONAL LOSSES**

Joshua Steelman, Junho Song, and Jerome F. Hajjar

A Report of the Mid-America Earthquake Center

*Mid-America Earthquake Center  
1241 Newmark Civil Engineering Laboratory  
205 North Mathews Avenue  
University of Illinois at Urbana-Champaign  
Urbana, Illinois 61801*

January 2007



## **ACKNOWLEDGEMENTS**

This research was supported by the Mid-America Earthquake Center, headquartered at the University of Illinois at Urbana-Champaign, under NSF Grant No. EEC-97010785, and by the University of Illinois at Urbana-Champaign. The authors would like to thank the researchers throughout the MAE Center who have provided guidance and information for this research. In particular, Mr. Ray Foltz is recognized for his contributions conducting extensive research into available lifeline fragilities from various literature resources.



## **TABLE OF CONTENTS**

ACKNOWLEDGEMENTS	2
1. INTRODUCTION	6
2. Inventory database	7
2.1 MAEViz Implementation	7
2.1.1 Prompt user to map inventory to fragilities immediately after loading inventory.	8
2.1.1.1 Building Stock Inventory	8
2.1.1.2 Transportation Lifeline Inventory	10
2.1.1.3 Utility Lifeline Inventory	12
2.1.2 Modify inventory databases to store period for individual items after mapping to fragilities.	23
2.1.2.1 Building Stock Inventory	23
2.1.2.2 Utility Lifeline Inventory	25
2.1.3 Partition total value of inventory items into component values.	27
2.1.3.1 Building Stock Inventory	27
2.1.3.2 Utility Lifeline Inventory	28
2.1.4 Prompt user for level of building stock structure type uncertainty to consider.	35
2.2.1 Building Stock	36
2.2.2 Transportation Systems	42
2.2.3 Utility Systems	43
2.2.4 HAZUS Inventory Data	43
3. HAZARD DEFINITION	44
3.1 MAEViz Implementation	44
3.1.1 Within the Embayment, calculate hazard appropriate to specific inventory items (user option).	45
3.1.1.1 Building Stock Hazard	45
3.1.1.2 Transportation Lifeline Hazard	47
3.1.1.3 Utility Lifeline Hazard	48
3.1.2 Implement MAEC liquefaction hazard estimation algorithm (Memphis).	53
3.1.3 Implement typical USGS CEUS attenuation combinations.	56
3.1.4 Implement typical USGS WUS attenuation combinations.	60
3.1.5 Implement Toro and Silva soil amplification factors.	62
3.2 Background	68
3.2.1 Hazard Definition Overview	68
3.2.2 Seismic Source Definition	68
3.2.3 Ground Motion Attenuation	69
3.2.3.1 Attenuation to Locations Inside the Mississippi Embayment	69
3.2.3.2 USGS Attenuation to Locations Inside the CEUS but Outside the Mississippi Embayment	71
3.2.3.3 Toro and Silva site factors (84°W to 96°W, 36°N to 40°N)	71
3.2.3.4 MAEC Attenuation to Locations Inside the CEUS but Outside the Mississippi Embayment	71
3.2.3.5 USGS Attenuation to WUS Locations	72
3.2.3.6 Attenuation to Locations outside the US	72



3.2.4 Implementation of Scenario-Based Ground Shaking Hazard Models	72
3.2.5 Implementation of Probabilistic Ground Shaking Hazard Models	73
3.2.6 Ground Failure Hazard (Liquefaction)	74
4. Engineering engines (fragility curves)	75
4.1 MAEViz Implementation	75
4.1.1 Implement Parametric Fragilities.	76
4.1.2 Propagate hazard uncertainty effects through evaluation of vulnerability.	79
4.1.3 Implement generalized (HAZUS) nonstructural building fragilities.	81
4.1.4 Combine ground shaking and ground failure probabilities of damage.	84
4.1.5 Implement transportation lifeline fragilities.	88
4.1.6 Implement utility lifeline fragilities.	90
4.2 Background	119
4.2.1. Building structures	119
4.2.1.1 Building Structural Damage	119
4.2.1.2 Building Nonstructural and Contents Damage	123
4.2.1.3. Parametric fragility curves	124
4.2.2 Transportation systems	124
4.2.3 Utility Lifeline Fragilities	125
4.2.3.1 Buried Pipelines	125
4.2.3.2 Water Tanks	127
4.2.3.3 Tunnels	128
4.2.3.4 Electric System	128
4.2.4 Combined Damage from Ground Shaking and Ground Failure	129
5. Social and economic LOSSES	130
5.1 MAEViz Implementation	130
5.1.1 Implement Building Structural Damage Factors and Compute Loss of Structural Value.	131
5.1.2 Implement Damage Factors and Compute Losses of Building Nonstructural and Contents.	133
5.1.3 Implement Bridge Repair Factors and Calculate Expected Economic Loss for Bridges.	136
5.1.4 Implement utility lifeline damage factors.	139
5.1.5 Adjust Loss Calculations to Consider Inventory Uncertainty.	147
5.1.6 Scale losses to account for inflation.	152
5.1.7 Aggregate Losses of Inventory within Study Region.	153
5.1.8 Calculate Fiscal Losses (Property Tax Revenue).	158
5.2 Background	159
5.2.1. Economic Loss for Building structures	159
5.2.1.1 Building Structural Damage	159
5.2.1.2 Building Nonstructural and Contents losses	159
5.2.2. Social Impacts	159
6. NETWORK MODELING	160
7. SYSTEM INTERDEPENDENCIES	160



8. Decision Support	160
9. Conclusions	161
REFERENCES	162
APPENDIX A – SUPPLEMENTARY INVENTORY INFORMATION	167
A.2.1.3.2 Utility Component Mapping Data	167
APPENDIX B – SUPPLEMENTARY HAZARD INFORMATION	174
B.3.2.3.1 Attenuation to Locations Inside the Mississippi Embayment	174
B.3.2.6 Estimating Probability of Liquefaction-Induced Ground Failure	175
APPENDIX C – SUPPLEMENTARY Fragility INFORMATION	180
C4.2.1 Supplementary Fragility Data	180
Appendix D – direct economic loss example for buildings	<b>Error! Bookmark not defined.</b>



## 1. INTRODUCTION

This report documents the integrated flow of data within the Consequence-based Risk Management (CRM) framework established within the Mid-America Earthquake (MAE) Center for seismic regional loss assessment. This data flow is being implemented in MAEViz, the risk management software of the MAE Center. The report also provides an efficient framework for incorporating the uncertainties systematically into each key contribution to the loss assessment process. Supplementary documents to this report provide detailed examples of the quantitative data flow and associated aggregation of uncertainty.

This report first identifies the algorithmic methodologies and inputs/outputs (I/O) used in the MAE Center research efforts on seismic hazard, inventory, structural damage, and social and economic losses, *from source to society*. This helps identify possible incompatibilities between I/O's and missing information, and enables gaps in the data threads to be identified. This report then provides recommendations for filling of several of these identified gaps in the CRM data threads.

Based on these results and the CRM framework encompassed within the MAE Center, this report also suggests a method to systematically incorporate aleatory and epistemic uncertainties identified by MAE Center research efforts into MAEViz.

In the sections that follow, the general flow of the document is intended to first outline suggested modifications to MAEViz, accompanied by examples, then proceed into a more detailed description of the information available for use in MAEViz. The examples focus on applications for the Memphis Testbed.



## 2. INVENTORY DATABASE

### 2.1 MAEViz Implementation

Inventory is the collective group of entities that are subject to a projected hazard in a particular risk assessment. Inventory is incorporated into MAEViz as point-wise data for buildings, bridges, and utility facilities, and line-type data for utility pipelines.

The following upgrades are recommended for MAEViz handling of inventory:

- Prompt user to map inventory to fragilities immediately after loading inventory.
  - Building stock
  - Bridges
  - Components of electric generation facilities and substations
  - Water tanks
- Modify inventory databases to store period for individual items after mapping to fragilities.
  - Building stock
  - Components of electric generation facilities
- Partition total value of inventory items into component values.
  - Building stock
  - Components of electric generation facilities and substations
- Prompt user for level of building stock inventory uncertainty to consider.



2.1.1 Prompt user to map inventory to fragilities immediately after loading inventory.

2.1.1.1 Building Stock Inventory

**Algorithm**

Inputs: structure type, occupancy, number of stories, year built from building stock inventory database. Parametric fragilities by Jeong and Elnashai also require soil type (Uplands or Lowlands), time-history source/site (7.5 Blytheville/Memphis, 6.5 Marked Tree/Memphis, 5.5 Memphis/Memphis), hazard uncertainty inclusion (50<sup>th</sup> and 84<sup>th</sup> percentile), and hazard parameter (PGA, 0.2 sec Sa, or 1.0 sec Sa) inputs.

Process: use Table C.4.2.1-1 with Inputs to assign fragilities to individual inventory items. Prompt user to accept default mapping or modify by creating new mapping checks or changing existing mapping checks.

Outputs: modified building stock inventory database with each entity keyed to building fragility database

**Example**

Three buildings were selected at random from the available building stock inventory for Memphis and Shelby County, TN. The example will use the following three buildings:

**Table 2.1.1.1-1 Example Building Inventory Data**

	Structural type	Occupancy Class	Stories	Year Constructed	Appraised Value (\$)	Latitude	Longitude
Inventory 1 (I1)	C1	Industrial	3	1926	136,400	35.13554 N	90.03732 W
Inventory 2 (I2)	URM	Retail Trade	2	1972	415,393	35.22057 N	89.90675 W
Inventory 3 (I3)	URM	Industrial	2	1971	811,346	35.03183 N	89.89023 W

The data presented in Table 2.1.1.1-1 is obtained directly from the inventory database. Fragilities can be mapped to the inventory items using either the default mapping scheme provided in Table C.4.2.1-1 or in accordance with a user-specified mapping scheme. For this example, inventory item I1 will be evaluated using fragilities developed by the MAE Center for evaluating damage to gravity load designed concrete frames (Concrete Frame, Bracci Gravity Designed, Fragility ID Code: SF\_C1\_10), and inventory items I2 and I3 will be evaluated using MAE Center URM fragilities (Unreinforced Masonry, Wen and Li, Fragility ID Code: SF\_URM\_41). Note that the URM mappings are not consistent with the default mapping shown in Appendix C, as shown in Table 2.1.1.1-2, since the example preceded the development of the mapping scheme.



**Table 2.1.1.1-2 Example Building Mapping**

	Default Mapped Fragility	Default Fragility ID Code	Override Fragility	Override Fragility ID Code
Inventory 1 (I1)	Concrete Frame – Bracci Gravity Designed	SF_C1_10	Concrete Frame – Bracci Gravity Designed	SF_C1_10
Inventory 2 (I2)	Adapted HAZUS Pre-Code URML	SF_URM_1	Unreinforced Masonry – Wen and Li	SF_URM_41
Inventory 3 (I3)	Adapted HAZUS Pre-Code URML	SF_URM_1	Unreinforced Masonry – Wen and Li	SF_URM_41



### 2.1.1.2 Transportation Lifeline Inventory

#### **Algorithm**

**Inputs:** bridge structure type from bridge inventory database.

**Process:** Prompt user to map fragilities for bridge structure types based on descriptions in Table 2.1.1.2-1.

**Outputs:** modified bridge inventory database with each entity keyed to bridge fragility database

#### **Example**

Descriptions of bridge fragilities available from the MAE Center are shown in Table 2.1.1.2-1.

**Table 2.1.1.2-1 Available Bridge Fragility Descriptions**

MAE Center Fragility	Description	Retrofits
MSC_Concrete	Multi-Span Continuous Concrete Girder Bridge	None
MSC_Steel	Multi-Span Continuous Steel Girder Bridge	None
MSC_Slab	Multi-Span Continuous Concrete Slab	None
MSC_Conc Box	Multi-Span Continuous Concrete Box Girder	None
MSSS_Concrete	Multi-Span Simply Supported Concrete Girder Bridge	None
MSSS_Steel	Multi-Span Simply Supported Steel Girder Bridge	None
MSSS_Slab	Multi-Span Simply Supported Concrete Slab	None
MSSS_Conc Box	Multi-Span Simply Supported Concrete Box Girder	None
SS_Concrete	Single-Span Concrete Girder Bridge	None
SS_Steel	Single-Span Steel Girder Bridge	None
MSC_Concrete	Multi-Span Continuous Concrete Girder Bridge	Elastomeric Bearing
MSC_Steel	Multi-Span Continuous Steel Girder Bridge	Elastomeric Bearing
MSSS_Concrete	Multi-Span Simply Supported Concrete Girder Bridge	Elastomeric Bearing
MSSS_Steel	Multi-Span Simply Supported Steel Girder Bridge	Elastomeric Bearing
Other	Other	Elastomeric Bearing
SS_Concrete	Single-Span Concrete Girder Bridge	Elastomeric Bearing
SS_Steel	Single-Span Steel Girder Bridge	Elastomeric Bearing



MAE Center Fragility	Description	Retrofits
MSC_Concrete	Multi-Span Continuous Concrete Girder Bridge	Restrainer Cables
MSC_Steel	Multi-Span Continuous Steel Girder Bridge	Restrainer Cables
MSSS_Concrete	Multi-Span Simply Supported Concrete Girder Bridge	Restrainer Cables
MSSS_Steel	Multi-Span Simply Supported Steel Girder Bridge	Restrainer Cables
Other	Other	Restrainer Cables
SS_Concrete	Single-Span Concrete Girder Bridge	Restrainer Cables
SS_Steel	Single-Span Steel Girder Bridge	Restrainer Cables

Three bridges were selected at random from the available inventory for Memphis and Shelby County, TN. The example will use the following three bridges shown in Table 2.1.1.2-2.

**Table 2.1.1.2-2 Bridge Inventory Data**

	Classification	Spans	Structure Length (ft)	Deck Width (ft)	Latitude	Longitude
Bridge 1	SS-PSC	1	100.1	173.6	35.17167 N	89.84167 W
Bridge 2	MSC-PSC	2	236.9	34.4	35.26167 N	89.66500 W
Bridge 3	MSC-SG	3	974.1	36.4	35.25167 N	90.02500 W

The bridges can be mapped to appropriate fragilities as shown in Table 2.1.1.2-3. By default, bridges are not assumed to have retrofits installed.

**Table 2.1.1.2-3 Bridge Inventory to Fragility Mapping**

	Classification	Description	MAE Center Fragility
Bridge 1	SS-PSC	Single-Span Concrete Girder Bridge	SS_Concrete
Bridge 2	MSC-PSC	Multi-Span Continuous Concrete Girder Bridge	MSC_Concrete
Bridge 3	MSC-SG	Multi-Span Continuous Steel Girder Bridge	MSC_Steel



### 2.1.1.3 Utility Lifeline Inventory

#### Electric Power Plants

##### **Algorithm**

Inputs: electric power plant inventory database (no particular fields).

Process:

Prompt user to map fragilities for individual components in Table 2.1.1.3-1.

Provide user with option to add new component(s).

Outputs: modified electric power plant inventory database with each component of power plants keyed to electric utility fragility database(s). Modified inventory database has an entry for each component of each power plant, instead of a single entry for each power plant, as in the Input.

##### **Example**

A detailed roster of components can be listed and mapped to fragilities given in Tables 4.1.6-1 through 4.1.6-3, as shown in Table 2.1.1.3-1.

**Table 2.1.1.3-1 Default Mapping for Power Plant Components**

Component	Fragility	Fragility ID Code
Boilers + Steam Generators	Boilers and Pressure Vessels	EPP_MC_2
Turbines	Turbine	EPP_EC_7
Flat Bottom Tanks		N/A
Large Horizontal Tanks	Large horizontal vessels	EPP_MC_3
Small to medium Hz. tanks	Small to medium horizontal vessels	EPP_MC_4
Vertical pumps	Large vertical pumps	EPP_MC_5
Horizontal pumps	Motor Driven pumps	EPP_MC_6
Large motor operated valves	Large Motor Operated Valves	EPP_MC_7
Large hydraulic, air valves	Large Hydraulic and Air Actuated Valves	EPP_MC_8
Large relief, manual and relief valves	Large Relief, Manual and Check Valves	EPP_MC_9
Small valves	Small Motor Operated Valves	EPP_MC_10
Diesel Generators	Diesel Generators	EPP_EC_1



Component	Fragility	Fragility ID Code
Batteries	Battery Racks	EPP_EC_2
Instrument racks and panels	Instrument Racks and Panels	EPP_EC_4
Control Panels	Control Panels	EPP_EC_5
Switchgear	Switchgear	EPP_EC_3
Motor control centers	Aux. Relay Cabinets / MCCs / Circuit Breakers	EPP_EC_6
Inverters	Aux. Relay Cabinets / MCCs / Circuit Breakers	EPP_EC_6
Cable trays and raceways	Cable Trays	EPP_OTH_1
HVAC ducting	HVAC Ducting	EPP_OTH_2
HVAC equipment	HVAC Equipment – Fans	EPP_OTH_3
Switchyard		N/A
Miscellaneous		N/A

Three power plants were selected at random from the available inventory for Memphis and Shelby County, TN. The example will use the following three power plants shown in Table 2.1.1.3-2, where EPP is a generic name for Electric Power Plant.

**Table 2.1.1.3-2 Electric Power Plant Inventory Data**

	Capacity (MWe)	Fuel	Latitude	Longitude
EPP1	4.3	NG	35.0826 N	90.1364 W
EPP 2	72.3	NG	35.1996 N	89.9710 W
EPP 3	25.0	NG	35.2989 N	89.9629 W

All components will be mapped according to the defaults shown in Table 2.1.1.3-1.



*Electric Substations*

**Algorithm**

Inputs: Max Voltage electric substation inventory database.

Process:

Classify each substation as VHV, HV, or MHV, using Max Voltage and Table 2.1.1.3-3.

Prompt user to map fragilities for individual components in Tables 2.1.1.3-4 through 2.1.1.3-6.

Provide user with option to add new component(s).

Outputs: modified electric substation inventory database with each component of substations keyed to electric utility fragility database(s). Modified inventory database has an entry for each component of each substation, instead of a single entry for each substation, as in the Input.

**Example**

Substations are classified as Very High Voltage (VHV), High Voltage (HV), or Moderately High Voltage (MHV). The classifications correspond to a maximum voltage ranges shown in Table 2.1.1.3-3.

**Table 2.1.1.3-3 Electric Substation Classification**

Classification	Max Voltage (kV)
Moderately High Voltage (MHV)	$\leq 165$
High Voltage (HV)	$165 < \& \leq 350$
Very High Voltage (VHV)	$350 <$



A detailed roster of components can be listed and mapped to fragilities given in Tables 4.1.6-5 through 4.1.6-7 based on classification (VHV, HV, or MHV), as shown in Table 2.1.1.3-4 through Table 2.1.1.3-6.

**Table 2.1.1.3-4 Default Mapping for VHV Substation Components**

Component	Fragility	Fragility ID Code
Transformer - Anchored	Transformer - Anchored	ESS_VHV_1
Transformer - Unanchored	Transformer - Unanchored	ESS_VHV_2
Live Tank Circuit Breaker - Standard	Live Tank Circuit Breaker - Standard	ESS_VHV_3
Live Tank Circuit Breaker - Seismic	Live Tank Circuit Breaker - Seismic	ESS_VHV_4
Dead Tank Circuit Breaker - Standard	Dead Tank Circuit Breaker - Standard	ESS_VHV_5
Disconnect Switch - Rigid Bus	Disconnect Switch - Rigid Bus	ESS_VHV_6
Disconnect Switch - Flexible Bus	Disconnect Switch - Flexible Bus	ESS_VHV_7
Lightning Arrestor	Lightning Arrestor	ESS_VHV_8
CCVT - Cantilevered	CCVT - Cantilevered	ESS_VHV_9
CCVT - Suspended	CCVT - Suspended	ESS_VHV_10
Current Transformer (gasketed)	Current Transformer (gasketed)	ESS_VHV_11
Current Transformer (flanged)	Current Transformer (flanged)	ESS_VHV_12
Wave Trap - Cantilevered	Wave Trap - Cantilevered	ESS_VHV_13
Wave Trap - Suspended	Wave Trap - Suspended	ESS_VHV_14
Bus Structure - Rigid	Bus Structure - Rigid	ESS_VHV_15
Bus Structure - Flexible	Bus Structure - Flexible	ESS_VHV_16
Other Yard Equipment	Other Yard Equipment	ESS_VHV_17



**Table 2.1.1.3-5 Default Mapping for HV Substation Components**

Component	Fragility	Fragility ID Code
Transformer - Anchored	Transformer - Anchored	ESS_HV_1
Transformer - Unanchored	Transformer - Unanchored	ESS_HV_2
Live Tank Circuit Breaker - Standard	Live Tank Circuit Breaker - Standard	ESS_HV_3
Live Tank Circuit Breaker - Seismic	Live Tank Circuit Breaker - Seismic	ESS_HV_4
Dead Tank Circuit Breaker - Standard	Dead Tank Circuit Breaker - Standard	ESS_HV_5
Disconnect Switch - Rigid Bus	Disconnect Switch - Rigid Bus	ESS_HV_6
Disconnect Switch - Flexible Bus	Disconnect Switch - Flexible Bus	ESS_HV_7
Lightning Arrestor	Lightning Arrestor	ESS_HV_8
CCVT	CCVT	ESS_HV_9
Current Transformer (gasketed)	Current Transformer (gasketed)	ESS_HV_10
Wave Trap - Cantilevered	Wave Trap - Cantilevered	ESS_HV_11
Wave Trap - Suspended	Wave Trap - Suspended	ESS_HV_12
Bus Structure - Rigid	Bus Structure - Rigid	ESS_HV_13
Bus Structure - Flexible	Bus Structure - Flexible	ESS_HV_14
Other Yard Equipment	Other Yard Equipment	ESS_HV_15



**Table 2.1.1.3-6 Default Mapping for MHV Substation Components**

Component	Fragility	Fragility ID Code
Transformer - Anchored	Transformer - Anchored	ESS_MHV_1
Transformer - Unanchored	Transformer - Unanchored	ESS_MHV_2
Live Tank Circuit Breaker - Standard	Live Tank Circuit Breaker - Standard	ESS_MHV_3
Live Tank Circuit Breaker - Seismic	Live Tank Circuit Breaker - Seismic	ESS_MHV_4
Dead Tank Circuit Breaker - Standard	Dead Tank Circuit Breaker - Standard	ESS_MHV_5
Disconnect Switch - Rigid Bus	Disconnect Switch - Rigid Bus	ESS_MHV_6
Disconnect Switch - Flexible Bus	Disconnect Switch - Flexible Bus	ESS_MHV_7
Lightning Arrestor	Lightning Arrestor	ESS_MHV_8
CCVT	CCVT	ESS_MHV_9
Current Transformer (gasketed)	Current Transformer (gasketed)	ESS_MHV_10
Wave Trap - Cantilevered	Wave Trap - Cantilevered	ESS_MHV_11
Wave Trap - Suspended	Wave Trap - Suspended	ESS_MHV_12
Bus Structure - Rigid	Bus Structure - Rigid	ESS_MHV_13
Bus Structure - Flexible	Bus Structure - Flexible	ESS_MHV_14
Other Yard Equipment	Other Yard Equipment	ESS_MHV_15



Three electric substations were selected at random from the available inventory for Memphis and Shelby County, TN. The example will use the following three substations shown in Table 2.1.1.3-7, where ESS is a generic name for Electric Substation.

**Table 2.1.1.3-7 Electric Substation Inventory Data**

	Max Voltage (kV)	Latitude	Longitude
ESS1	161	35.0826 N	90.1364 W
ESS 2	0	35.1996 N	89.9710 W
ESS 3	500	35.2989 N	-89.9629 W

The sample substations will be classified according to Max Voltage and the scheme shown in Table 2.1.1.3-3 as shown in Table 2.1.1.3-8.

**Table 2.1.1.3-8 Electric Substation Inventory Classification**

	Max Voltage (kV)	Classification
ESS1	161	MHV
ESS 2	0	MHV
ESS 3	500	VHV

All components will be mapped to fragilities with the default mapping scheme in Tables 2.1.1.3-4 through 2.1.1.3-6.



## Water Tanks

### **Algorithm**

**Inputs:** Possibly (Fill, Anchorage, Height, Diameter, H/D).

**Process:**

Prompt user to choose between mappings based on Fill, Anchorage, or H/D ratio.

If user selects to map based on Fill, use default mapping as shown in Table 2.1.1.3-9.

If user selects to map based on Anchorage, use default mapping as shown in Table 2.1.1.3-10.

If user selects to map based on H/D ratio, use default mapping as shown in Table 2.1.1.3-11.

Assume the user will provide Height and Diameter data separately, and calculate H/D by default. Also provide an option for the user to specify H/D directly.

Provide user with to accept default mapping scheme or modify. Allow users to modify mapping parameters or map to new fragilities.

**Outputs:** modified water tank inventory database with each entity keyed to water tank fragility database.

### **Example**

If the user selects to map based on Fill, use the default mapping scheme shown in Table 2.1.1.3-9 to map to fragilities shown in Table 4.1.6-9. The “All Tanks” fragility is not intended to appear in the default mapping. Note that Default values shown are in percent fill. If Fill data is not provided, use the “Eidinger Fill  $\geq$  50%” fragility.

**Table 2.1.1.3-9 Water Tank Mapping Scheme for Fill**

Fill (percent)	Fragility
< 50	Eidinger Fill < 50%
50 $\leq$ & < 60	Eidinger Fill $\geq$ 50%
60 $\leq$ & < 90	Eidinger Fill $\geq$ 60%
90 $\leq$	Eidinger Fill $\geq$ 90%



If the user selects to map based on Anchorage, use the default mapping scheme shown in Table 2.1.1.3-10 to map to fragilities shown in Table 4.1.6-10.

**Table 2.1.1.3-10 Water Tank Mapping Scheme for Anchorage**

Anchored	Fragility
Y	Eidinger Anchored
N	Eidinger Unanchored
Unknown	Eidinger Anchorage Unknown

If the user selects to map based on H/D ratio, use the default mapping scheme shown in Table 2.1.1.3-11 to map to fragilities shown in Table 4.1.6-11. The “All Tanks” fragility is not intended to appear in the default mapping. Note that Default values shown are in percent fill.

**Table 2.1.1.3-11 Water Tank Mapping Scheme for H/D ratio**

Fill (percent)	H/D	Fragility
50 <		O’Rourke and So Fill > 50%
< 50	70 <=	O’Rourke and So H/D >= 0.7
< 50	< 70	O’Rourke and So H/D < 0.7

Sample water tank inventory data is listed in Table 2.1.1.3-12.

**Table 2.1.1.3-12 Sample Water Tank Inventory Data**

	Fill (percent)	Anchored	Height	Diameter	Latitude	Longitude
Water Tank 1	40	N	40	60	35.136 N	90.037 W
Water Tank 2	55	Y	60	30	35.221 N	89.907 W
Water Tank 3	80	Y	60	30	35.032 N	89.890 W

Users may provide all, some, or none of the data fields (location is always expected to be provided) specified in Table 2.1.1.3-12. As a default option if the user has no data other than locations of water tanks, the first fragility listed in Table 4.1.6-10 may be used.



## *Buried Pipelines*

### **Algorithm**

Inputs: Possibly (pipeline material, pipeline diameter, joint type, soil condition).

Process:

Prompt user to choose between mappings based on Researcher. The mapping of attributes from the pipeline dataset to MAEviz-recognized field types will depend on which Researcher is selected. Set the default Researcher to Eiding (2004).

Prompt the user to select default attributes, depending on which Researcher is selected.

If the user selects Eiding (2001) (or keeps the default), prompt the user for default pipe material, joint type, soils, and diameter mappings.

Set the defaults to Cast Iron, Cement, All, and Small, respectively.

Note that only certain combinations are available.

Check if the selected parameters are available and display an error if they are not. For example, if the user has selected Welded Steel, Lap – Arc Welded, Corrosive, Small, the parameters are valid. If the user then changes the diameter to Large, there is no soils parameter available besides All, so having Corrosive selected should generate an error.

If the user selects O'Rourke, M. and Ayala (1993), prompt the user for default pipe material mapping.

Set the default to Cast Iron.

If the user selects O'Rourke, T. and Jeon (1999), prompt the user for default pipe material and diameter mappings.

Set the defaults to Cast Iron and 8 inches, respectively.

Note that only certain combinations are available.

If the user selects Asbestos Cement Pipe, they must also choose between specifying PGV or diameter. By default, use PGV.

Outputs: modified pipeline inventory database with each entity keyed to pipeline fragility database.

### **Example**

Consider the pipe segment shown in Figure 2.1.1.3-1. Very little information is available to aid in assigning fragilities. If the user accepts the default Researcher, Eiding (2001), and selects a mapping for diameter -> DIAMETER, MAEviz should then assume that all pipes are Cast Iron material, have Cement joint types, and have an unknown soil type (ALL is appropriate).



MAEviz would then perform a check for each pipe segment to determine if the pipe diameter is Large (>12 inches) or Small (<= 12 inches), and assign fragilities appropriately. In this case, a fragility for Large pipes is not provided, so the default fragility for Small pipes would be used regardless of pipe diameter.

If the user selects the O'Rourke, M. and Ayala (1993) fragilities, the default fragility would be assigned for all pipes, depending on the default material selected by the user for pipe material. If the user selects O'Rourke, T. and Jeon (1999) fragilities, the default fragility will be assigned for all pipes.

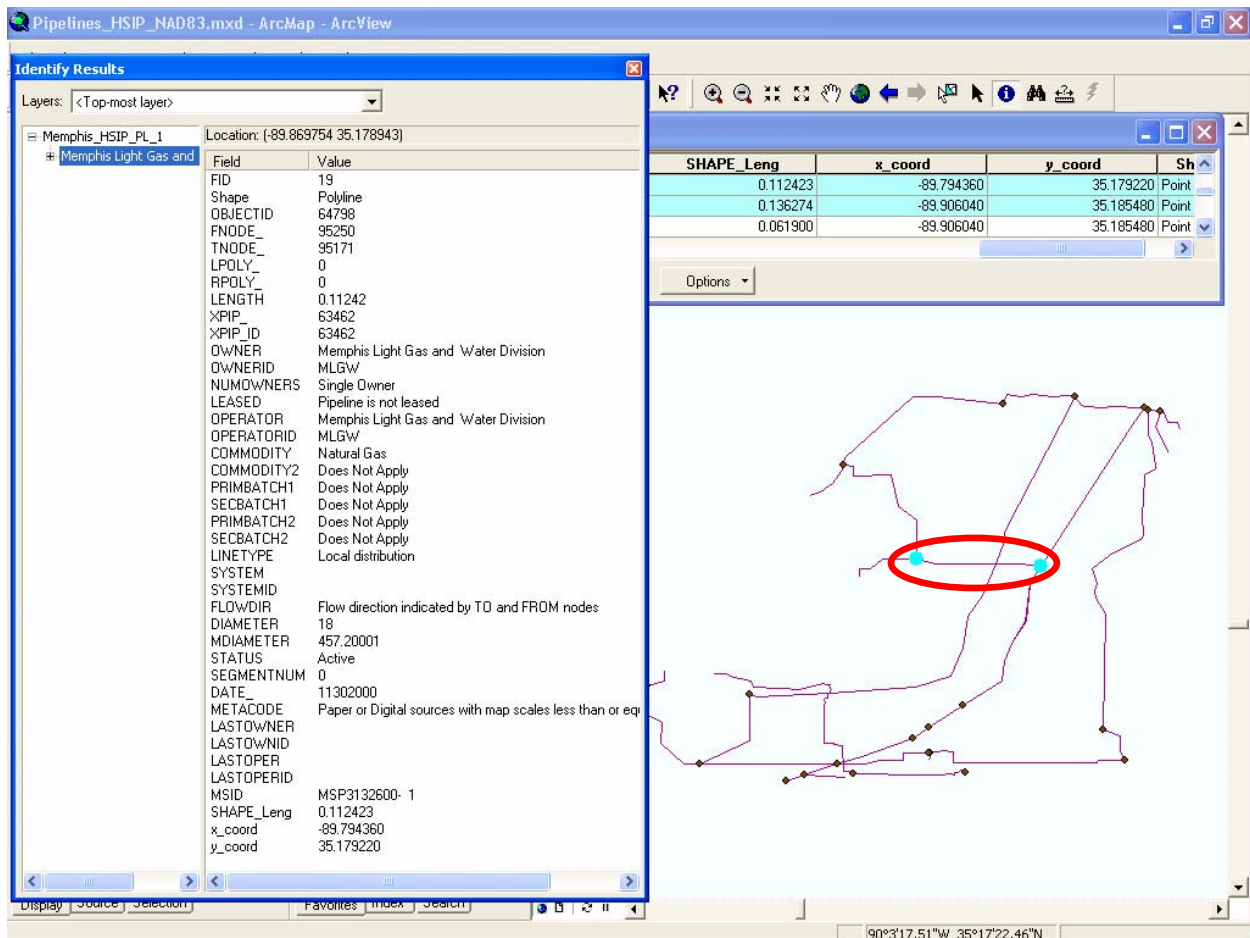


Figure 2.1.1.3-1. Sample Pipe Segment.



## 2.1.2 Modify inventory databases to store period for individual items after mapping to fragilities.

### 2.1.2.1 Building Stock Inventory

#### **Algorithm**

Inputs: Fragility associated with each entity in building stock inventory database. Go to fragility database for “T Eqn Type” and “T Eqn ParamX” parameters, where X can be 0, 1, and 2 (See *Fragility Database Documentation* in Appendix C.4.2.1). Number of stories from building stock inventory.

#### Process:

Apply equations given in the *Fragility Database Documentation* section of Appendix C.4.2.1 to evaluate periods based on fragilities and the number of stories obtained from the building stock inventory.

Provide user with option to accept default period calculations or modify. Allow users to modify mapping parameters or specify periods directly for particular fragilities.

NOTE: If structure type uncertainty is considered, allow users the option to calculate a period for each structure type available in the inventory. This is expected to be very computationally intensive and should NOT be performed by default.

Outputs: modified building stock inventory database with period calculated for each building.

#### **Example**

The default MAEViz building stock fragility database and accompanying documentation includes data to calculate approximate periods for each fragility set. The mapped fragility for the concrete frame building has “T Eqn Type” = 3. Using the equation supplied in the *Fragility Database Documentation* with the default values given in the fragility database yields a period of 0.95 seconds, as shown below, where the fragility database documentation indicates

when T Eqn Type = 3

$$T_1 = b * (a * NO\_STORIES)^c$$

And where

$$a = \text{T Eqn Param0} = 13$$

$$b = \text{T Eqn Param1} = 0.097$$

$$c = \text{T Eqn Param2} = 0.624$$

Therefore,

$$T_1 = 0.097 * (13 * 3)^{0.624} = 0.95 \text{ seconds}$$



Likewise, the fundamental period for URM structures may be estimated from data supplied in the fragility database and documentation. The inventory database within MAEViz would then be augmented to include the following data in Table 2.1.2.1-1.

**Table 2.1.2.1-1 Example Building Periods**

	Structural type	Period
Inventory 1 (11)	C1	0.95
Inventory 2 (12)	URM	0.6
Inventory 3 (13)	URM	0.6



### 2.1.2.2 Utility Lifeline Inventory

#### Electric Power Plants

##### **Algorithm**

Inputs: Component name in electric power plant database.

Process:

Assign periods to components listed in Tables 2.1.2.2-1 through 2.1.2.2-3 with Hazard Parameter of Sa.

Provide user with option to accept default periods or modify. Allow users to specify periods directly for particular fragilities.

Outputs: modified electric power plant inventory database with period assigned to each component, as required.

##### **Example**

Electric power plants typically include some components with fragilities calibrated to peak ground acceleration, and others calibrated to spectral acceleration. When components are calibrated to spectral acceleration, the inventory database should be modified to assign a period to the particular component, similar to the treatment of building inventory. The process for electric power plants is less complicated, though, because it is always a simple assignment, with no calculations required. The typical power plant components are shown in Tables 2.1.2.2-1 through 2.1.2.2-3, along with Component ID Codes to match with the data given in Table 2.1.1.3-1 for reference.

**Table 2.1.2.2-1 Electric Power Plant Equipment - Electrical Components - Well Anchored**

Component ID Code	Component	Hazard Parameter	Period (sec)
EPP_EC_1	Diesel Generators	Sa	0.045
EPP_EC_2	Battery Racks	Sa	0.030
EPP_EC_3	Switchgear	Sa	0.167
EPP_EC_4	Instrument Racks and Panels	Sa	0.200
EPP_EC_5	Control Panels	Sa	0.200
EPP_EC_6	Aux. Relay Cabinets / MCCs / Circuit Breakers	Sa	0.200
EPP_EC_7	Turbine	PGA	0.000



**Table 2.1.2.2-2 Electric Power Plant Equipment - Mechanical Equipment - Well Anchored**

Component ID Code	Component	Hazard Parameter	Period (sec)
EPP_MC_1	Large vertical vessels with formed heads	Sa	0.143
EPP_MC_2	Boilers and Pressure Vessels	Sa	0.100
EPP_MC_3	Large horizontal vessels	Sa	0.067
EPP_MC_4	Small to medium horizontal vessels	Sa	0.067
EPP_MC_5	Large vertical pumps	Sa	0.200
EPP_MC_6	Motor Driven pumps	Sa	0.143
EPP_MC_7	Large Motor Operated Valves	Sa	0.067
EPP_MC_8	Large Hydraulic and Air Actuated Valves	Sa	0.030
EPP_MC_9	Large Relief, Manual and Check Valves	Sa	0.030
EPP_MC_10	Small Motor Operated Valves	Sa	0.050

**Table 2.12.2-3 Electric Power Plant Equipment - Other Equipment**

Component ID Code	Component	Hazard Parameter	Period (sec)
EPP_OTH_1	Cable Trays	PGA	0.000
EPP_OTH_2	HVAC Ducting	Sa	0.125
EPP_OTH_3	HVAC Equipment – Fans	Sa	0.250



2.1.3 Partition total value of inventory items into component values.

2.1.3.1 Building Stock Inventory

**Algorithm**

Inputs: Appraised Value, Building Use, Essential Facility from building stock inventory database.

Process:

Use Table 2.2.1-3 to map Version 3 building use and essential facility status to HAZUS/Version 4 occupancy.

Allow users to modify parameters used for mapping or select alternate HAZUS/Version 4 mapped occupancies.

Use Table 2.2.1-6 to map HAZUS/Version 4 occupancy to percentages of component value for structural, acceleration-sensitive nonstructural, and drift-sensitive nonstructural components.

Allow users to specify alternate percentages of component values.

Multiply Appraised Value by the percentages obtained from Table 2.2.1-6 to obtain values for each component of each building stock entity.

Outputs: modified building stock inventory database with calculated values for components.

**Example**

Augment the inventory within MAEViz to partition total appraised value into structural, acceleration-sensitive nonstructural (AS NS), and drift-sensitive nonstructural (DS NS). The total appraised value of the sample buildings given in Table 2.1.1.1-1 is partitioned into structural, AS NS, and DS NS values as shown in Table 2.1.3.1-1.

**Table 2.1.3.1-1 Example Building Value Partitioning**

	Occupancy Class	Version 4 Occupancy	Appraised Value	% Struc Value, $\alpha^{SD}$	Structural Value	% AS NS Value, $\alpha^{NA}$	AS NS Value	% DS NS Value, $\alpha^{ND}$	DS NS Value
Inventory 1 (I1)	Industrial	IND1	\$136,400	15.7	\$21,415	72.5	\$98,890	11.8	\$16,095
Inventory 2 (I2)	Retail Trade	COM1	\$415,393	29.4	\$122,126	43.1	\$179,034	27.5	\$114,233
Inventory 3 (I3)	Industrial	IND1	\$811,346	15.7	\$127,381	72.5	\$588,226	11.8	\$95,739



### 2.1.3.2 Utility Lifeline Inventory

#### *Electric Power Plants*

#### **Algorithm**

**Inputs:** Value (directly in user supplied data) OR Fuel and Capacity from electric power plant inventory database.

#### **Process:**

IF Value is NOT obtained directly in user supplied data, use Table 2.1.3.2-1 to map value per unit output of power plants to inventory. Use values for “Gas Fired” for unknown Fuel types.

Allow users to modify parameters used for mapping or specify alternate values per unit output.

Multiply value per unit output times Capacity time inflation adjustment factor of 1.4 to obtain total power plant value.

Use Table 2.1.3.2-3 to partition total power plant value into component values.

Use Notes 1 and 2 given for Table 2.1.3.2-3 to estimate piping at each power plant.

Allow users to specify alternate percentages of component values or piping multipliers.

**Outputs:** modified electric power plant inventory database with calculated values for components and piping estimates.

#### **Example**

Default values of power plants per unit output are given in Table 2.1.3.2-1.



**Table 2.1.3.2-1 Default Electric Power Plant Value**

Fuel	Capacity (MWe)	Value per MWe
Coal Fired	0 - 200	\$1,250,000
	200 - 500	\$1,500,000
	500 +	\$1,750,000
Gas Fired	0 - 50	\$1,000,000
	50 - 200	\$1,500,000
	200 - 500	\$1,750,000
	500 +	\$1,750,000
Oil Fired	0 - 50	\$1,250,000
	50 - 200	\$1,500,000
	200 - 500	\$1,750,000
	500 +	\$1,750,000
Nuclear	All	\$2,500,000

Total value for the sample electric power plants given in Table 2.1.1.3-2 is presented in Table 2.1.3.2-2. The Fuel type, NG, corresponds to natural gas, so the Gas Fired values are used from Table 2.1.3.2-1.

**Table 2.1.3.2-2 Sample Electric Power Plant Values**

	Capacity (MWe)	Fuel	Mapped Fuel Type	1994 Value per MWe	1994 to 2006 inflation	Value
EPP1	4.3	NG	Gas Fired	\$ 1,000,000	1.40	\$ 6,020,000
EPP 2	72.3	NG	Gas Fired	\$ 1,500,000	1.40	\$ 151,830,000
EPP 3	25.0	NG	Gas Fired	\$ 1,000,000	1.40	\$ 35,000,000

The default partitioning scheme to break total value of power plants down into components is given in Table 2.1.3.2-3. Component names correspond to the names given in 2.1.1.3-1. Where ID Codes are marked “N/A”, either the loss is already assessed elsewhere in an analysis, or there is no data currently available to model damage to the particular component.



**Table 2.1.3.2-3 Default Mapping for Values of Power Plant Components**

Component	% of total value
Boiler Building	10
Turbine Building	8
Administration Building	2
Buried Pipe*	1
Elevated Pipe**	12
Boilers + Steam Generators	11
Turbines	5
Flat Bottom Tanks	3
Large Horizontal Tanks	4
Small to medium Hz. tanks	4
Vertical pumps	2
Horizontal pumps	3
Large motor operated valves	3
Large hydraulic, air valves	1
Large relief, manual and relief valves	1
Small valves	1
Diesel Generators	2
Batteries	2
Instrument racks and panels	1
Control Panels	1
Switchgear	1
Motor control centers	3
Inverters	1
Cable trays and raceways	3
HVAC ducting	1



Component	% of total value
HVAC equipment	2
Switchyard	n.a.
Miscellaneous	12

**Note 1:** 6,000 feet of buried pipe is assumed per 100 MWe.

**Note 2:** 40,000 feet of elevated pipe is assumed per 100 MWe.

Table 2.1.3.2-4 shows data for the estimated amounts of piping at each sample power plant, and also shows the sample value of boilers and steam generators as an example of partitioned component value.

**Table 2.1.3.2-4 Sample Electric Power Plant Component Data**

	Capacity (MWe)	Buried Pipe (thousands of feet)	Elevated Pipe (thousands of feet)	Boiler and Steam Generator Value (\$)
EPP1	4.3	0.258	1.72	662,200
EPP 2	72.3	4.338	28.92	16,701,300
EPP 3	25.0	1.5	10	3,850,000



*Electric Substations*

**Algorithm**

**Inputs:** Value (if available directly in user supplied data), substation classification (MHV, HV, VHV), and Seismic Zone design level (assume 0 as default if not specified) from electric substation inventory database.

**Process:**

IF Value is NOT obtained directly in user supplied data, use Table 2.1.3.2-5 to map total value to inventory for each substation.

Allow users to specify alternate values for substations.

Based on substation classification and Seismic Zone design level, use Table 2.1.3.2-6 or similar tables in Appendix A to partition total substation value into component values.

Allow users to specify alternate percentages of component values.

**Outputs:** modified electric substation inventory database with calculated values for components.

**Example**

Default values of substations are given in Table 2.1.3.2-5.

**Table 2.1.3.2-5 Assumed Values of Electric Substations**

Transformer Capacity (kV)	Transformers per Substation			Value per Transformer (1994)	Inflation Multiplier (2006)
	MHV	HV	VHV		
500	0	0	2	3000000	1.4
230	0	2	2	2000000	1.4
115	2	2	2	1000000	1.4
<b>Total Value (2006 \$)</b>	<b>2800000</b>	<b>8400000</b>	<b>16800000</b>		

For electric substations, partitioning total value into component value is a two-step process. First, the general type of component values are partitioned from total value, then more specific partitioning is applied to break down the general component values. Partitioning schemes are based on the substation classification (MHV, HV, VHV) and whether the substation specific components are likely to include elements designed to resist seismic effects. Mapping tables are provided in Appendix A.

A sample partitioning scheme from Appendix A is provided in Table 2.1.3.2-6 for a VHV substation which has elements that are not likely to have been designed for seismic effects



(Seismic Zone design level = 0 to 2). The Overall Multiplier should be applied directly to total value to calculate value for the specific component, i.e., anchored transformers account for 0.1 \* Total Value of the substation. This is equivalent to 40% (general component partitioning factor) \* 25% (specific component partitioning factor) = 10% = 0.1. The overall multipliers do not sum to 1 because either the damage is expected to be accounted for elsewhere in the analysis or damage estimation algorithms are not available for particular components.

**Table 2.1.3.2-6 Sample Electric Substation Subcomponent Value Partitioning  
(VHV Substation, not designed for seismic)**

Specific Component	Partitioning Factors (%)		Overall Multiplier	Component ID Code
	General	Specific		
Transformer - Anchored	40	25	0.100	ESS_VHV_1
Transformer - Unanchored	40	75	0.300	ESS_VHV_2
Live Tank Circuit Breaker - Standard	15	50	0.075	ESS_VHV_3
Live Tank Circuit Breaker - Seismic	15	0	0.000	ESS_VHV_4
Dead Tank Circuit Breaker - Standard	15	50	0.075	ESS_VHV_5
Disconnect Switch - Rigid Bus	2	50	0.010	ESS_VHV_6
Disconnect Switch - Flexible Bus	2	50	0.010	ESS_VHV_7
Lightning Arrestor	1	100	0.010	ESS_VHV_8
CCVT - Cantilevered	1	50	0.005	ESS_VHV_9
CCVT - Suspended	1	50	0.005	ESS_VHV_10
Current Transformer (gasketed)	2	50	0.010	ESS_VHV_11
Current Transformer (flanged)	2	50	0.010	ESS_VHV_12
Wave Trap - Cantilevered	1	50	0.005	ESS_VHV_13
Wave Trap - Suspended	1	50	0.005	ESS_VHV_14
Bus Structure - Rigid	7	50	0.035	ESS_VHV_15
Bus Structure - Flexible	7	50	0.035	ESS_VHV_16
Other Yard Equipment	11	100	0.110	ESS_VHV_17



Sample specific component data is provided for each of the sample substations in Table 2.1.3.2-7.

**Table 2.1.3.2-7 Electric Substation Sample Component Inventory Data**

	Classification	Total Value	Specific Component	Overall Multiplier	Component Value	Fragility ID Code
ESS1	MHV	2800000	Transformer - Anchored	0.100	280000	ESS_MHV_1
ESS 2	MHV	2800000	Transformer - Unanchored	0.300	840000	ESS_MHV_2
ESS 3	VHV	16800000	Live Tank Circuit Breaker - Standard	0.075	1260000	ESS_VHV_3



2.1.4 Prompt user for level of building stock structure type uncertainty to consider.

**Algorithm**

Inputs: None.

Process:

Prompt user to specify level of building stock structure type uncertainty.

Set default to 0% (perfect accuracy – no uncertainty).

Provide button to view metadata for building stock inventory (link to Excel spreadsheet provided by MAEC for inventory database).

If a non-zero uncertainty is specified, assign fragilities to each building based on the mapping for each type of structure in the inventory.

Outputs: User defined building stock structure type uncertainty.

**Example**

If a user were to use the button to view metadata for the building stock inventory database, they would have access to the confusion matrix shown in Table 2.2.1-1. They would also have access to building counts, and so they might make a somewhat arbitrary selection of uncertainty based on both the confusion matrix and knowledge of building counts as described in Section 2.2.1. Assume the user selects to consider a 15% overall uncertainty in the building stock. Also, for simplicity, the example will consider the three sample buildings to be the extents of the inventory. Therefore, the Concrete Frame building only needs to be assigned an alternate URM fragility, and the URM only needs to be assigned an alternate Concrete Frame fragility. For the full inventory of Memphis, an alternate fragility would need to be assigned for EACH available structure type.



## 2.2 Background

### 2.2.1 Building Stock

The majority of building stock data is generated by the MAE Center through use of census data, image synthesis data, and a series of regression and neural network algorithms (French and Muthukumar, 2006; French and Muthukumar, 2006). The process includes an initial data gathering exercise to acquire baseline data and subsequent calibration exercises to refine the model (French and Muthukumar, 2006). Inventory data for fire stations and schools have also been obtained independently (Patterson, 2006).

To produce reliable predictions of damage and potential losses, MAEViz should estimate hazard appropriately for each inventory item. For building stock, structural period must be known in order to estimate an appropriate spectral acceleration hazard. To estimate structural period, fragilities must be mapped to inventory items. Therefore, the first step in a MAEViz analysis (prior to hazard estimation) should be ingestion of inventory, immediately followed by mapping of inventory to fragilities, and their associated period expressions, based on particular data fields in the inventory database. For the present, consideration of period when estimating hazard for each structure should be available as a user option, but not required.

Validity of the model is not assured in geographical regions other than where data is gathered. Uncertainty exists for each inventory parameter, but the primary sources of uncertainty for building stock are in the predicted structure type and, to a lesser extent, the predicted occupancy type. Uncertainty in structure type can be represented by a confusion matrix for a particular sample of the building stock inventory, as shown in Table 2.2.1-1. The confusion matrix shows how many of each structure type are predicted by the neural network, and of those predicted for each structure type, how many actually belong to each structure type.

**Table 2.2.1-1 Sample Confusion Matrix for Memphis Building Stock**

STRUCTURE TYPE	CODE	PREDICTED									SURVEY TOTALS
		C1	C2	PC1	PC2	RM	S1	S3	URM	W	
Concrete Moment-resisting Frame	C1	27	9	0	2	0	2	1	3	0	44
Concrete Frame with Shear Wall	C2	1	6	0	0	0	0	0	0	0	7
Concrete Tilt-up	PC1	1	0	32	0	1	0	1	0	0	35
Precast Concrete Frame	PC2	2	1	0	9	1	2	0	0	0	15
Reinforced Masonry	RM	0	0	1	0	19	0	0	0	0	20
Steel Moment-resisting Frame	S1	7	1	0	0	5	26	2	1	0	42
Light Metal Frame	S3	4	2	4	0	1	9	61	2	0	83
Unreinforced Masonry	URM	9	1	2	2	1	1	8	60	0	84
Wood Frame	W	1	0	2	0	0	0	19	7	57	86
<b>TOTALS</b>		<b>52</b>	<b>20</b>	<b>41</b>	<b>13</b>	<b>28</b>	<b>40</b>	<b>92</b>	<b>73</b>	<b>57</b>	<b>416</b>
<b>PREDICTION ACCURACY</b>		<b>51.92%</b>	<b>30.00%</b>	<b>78.05%</b>	<b>69.23%</b>	<b>67.86%</b>	<b>65.00%</b>	<b>66.30%</b>	<b>82.19%</b>	<b>100.00%</b>	<b>71.39%</b>

There are two proposed methods intended to account for uncertainty in the structure type. For the first method, the confusion matrix will be used to develop adjusted probable damage factors for each structural type. The uncertainty has an effect on both the hazard and the fragility, since different structure types will have different natural periods, and therefore different demand



spectral accelerations. For a particular inventory item, therefore, the first step is to consider which structure types are likely, then compute appropriate hazard parameters at the location of the inventory item based on the natural periods of the probable structure types. Pending sensitivity analyses to analytically define a critical threshold, the effect of individual structure types which represent 5% or less of the actual structure types within each predicted structural type will be neglected. For the confusion matrix shown in Table 2.2.1-1, this approach takes into account a minimum of 85% of the actual structures contributing to the response of any given predicted structure type. The next step is to pass the hazard parameters into the appropriate fragility functions and obtain probable damage factors for each probable structure type. The final step is to compute a weighted average of probable damage factors, with the weights calculated based on the confusion matrix.

An alternate method, which may be useful when a confusion matrix is not available, is to assume all structure types have an equal probability of accuracy. Based on the confusion matrix shown for Memphis, this value may be taken as approximately 70%. Then, for the 30% inaccuracy, losses will be determined by a weighted average of expected losses for all structure types. The weighting of expected losses for each structure type is determined directly on the basis of how many of each structure type are believed to be in the inventory (that is, the more of a structure type there are, the more likely it will be inaccurately predicted to be some other building type, based on a random sampling approach). This alternate approach would use the information that is presumed to be inaccurate to develop a means of mitigating that same inaccuracy, but it also offers a method of approximately accounting for the fact that the structure type is uncertain in the event that a confusion matrix is not provided. It should also be noted that the selection of the value used for probability of accuracy is somewhat arbitrary, since using the value of 70% obtained from the surveys of 416 structures is only valid for that particular sample. Also, it should be noted that wood frame buildings only accounted for 86 of the 416 buildings that were surveyed, and each time a building was predicted to be wood frame, the prediction was correct. For the full set of building inventory in Shelby County, wood frame buildings will account for more than 90% of structures, and the probability of accuracy for the full building inventory will be significantly higher than 70%, probably closer to 85% at a minimum.

Two sets of databases have been provided by the MAE Center for Memphis inventory data. The sets are generally referred to as version 3 and version 4. Version 4 inventory data has been provided in a format that more closely matches HAZUS, primarily in terms of occupancy classifications. Most MAE Center researchers are expected to be more familiar with version 3 rather than version 4 format, so this document will focus on the use of version 3 data. The following is a list of the building stock inventory data that has been obtained within the MAE Center to date (version 3):

#### Data overview

Memphis Testbed building stock inventory data.



Location: Shelby County, Tennessee.

Source: Shelby county Tax Assessor’s database.

Database 1: Shelby\_Bldg\_ver3: 287,057 building records.

Database 2: Shelby\_noSF\_ver3: 21,903 building records (excluding single family residential structures).

These databases each have 16 parameters, as shown in Table 2.2.1-2.

**Table 2.2.1-2 Building Stock Inventory Parameters**

ID	Description	Categories*
STRUCT_TYP	Structure type	10 types
NO_STORIES	Number of stories in structure	
SQ_FOOT	Square footage of entire structure	
YEAR_BUILT	Year that the structure was constructed	
BLDG_USE	Occupancy class for the structure	9 classes
APPR_BLDG	Appraised value of the structure	
CONT_VAL	Value of contents contained with the structure	10 use-specific multipliers
DWELL_UNIT	Number of dwelling units in structure	
EFACILITY	Description of essential facility status of structure	6 statuses
BFOOTPRINT	Building footprint configuration	7 types
BMASSING	Building configuration in three-dimensions	
ADDRESS	Address of the parcel in which structure is contained	
SP_XCOORD	X-coordinate of structure location in feet	
SP_YCOORD	Y-coordinate of structure location in feet	
LAT	Latitude of structure location	
LON	Longitude of structure location	

\* See ‘Categories’ for details.

*The following category information is used in the building stock inventory of the MAE Center:*

Categories

a) Structure types (10)

Wood Frame (W)

Steel Moment Resisting Frame (S1)

Light Metal Frame (S3)

Concrete Moment Resisting Frame (C1)

Concrete Frame with Concrete Shear Wall (C2)

Concrete Tilt-Up (PC1)



- Precast Concrete Frame (PC2)
- Reinforced Masonry (RM)
- Unreinforced Masonry (URM)
- Unknown

Please note, as of version 4 of the building stock inventory database, the Unknown type is no longer used. Wood frames are also broken down into W1 and W2 subcategories, which now correspond to structure types found in HAZUS.

b) Occupancy classes (9)

- Residential\_SF (Single Family)
- Residential\_MF (Multi Family)
- Retail Trade
- Wholesale Trade
- Office
- Health Care
- Parking
- Industrial
- Light Industrial

Please note, as of version 4 of the building stock inventory database, occupancy classes are being assigned in a manner consistent with HAZUS. Based on documentation supplied for version 4 inventory data, a default mapping scheme has been established between Memphis version 3 inventory occupancy classes and HAZUS (and version 4) occupancy classes, as shown in Table 2.2.1-3. This mapping is expected to be accurate (to the greatest degree currently possible) for all occupancy classes except “Office.” According to the documentation provided with version 4, “Office” is comprised of COM3, COM4, COM5, and COM9 by about 42%, 12%, 32%, and 10%, respectively. Further refinement of the mapping scheme may be required if version 3 data will be used extensively in developing MAE Center algorithms.

**Table 2.2.1-3 Occupancy Mapping between Version 3 and HAZUS (Version 4)**

Version 3 Occupancy & Essential Facility	HAZUS (and Version 4) Occupancy
Building Use : Residential_SF	Single Family Dwelling (House) (RES1)
Building Use : Residential_MF	Multi Family Dwelling (Apt/Condominium) (RES3)
Building Use : Retail Trade	Retail Trade (Store) (COM1)
Building Use : Wholesale Trade	Wholesale Trade (Warehouse) (COM2)



Version 3 Occupancy & Essential Facility	HAZUS (and Version 4) Occupancy
Building Use : Office	Professional/Technical Services (Offices) (COM3)
Building Use : HealthCare	Hospital (COM6)
Building Use : Parking	Parking (Garages) (COM10)
Building Use : Industrial	Heavy (Factory) (IND1)
Building Use : Industrial_Light	Light (Factory) (IND2)
Essential Facility : School (EFS1)	Grade Schools (EDU1)
Essential Facility : Fire Station (EFFS)	Emergency Response (Police/Fire Station/EOC) (GOV2)
Essential Facility : Police Station (EFPS)	Emergency Response (Police/Fire Station/EOC) (GOV2)

c) Use-specific multipliers for value of contents (10)

**Table 2.2.1-4 Ratios of Contents to Appraised Value**

Occupancy or Essential Facility Status	Percent appraised value, $\alpha^{CL}$
Residential (SF and MF)	50%
Retail Trade	100%
Wholesale Trade	100%
Office	100%
Health Care	150%
Parking	50%
Industrial	150%
Light Industrial	150%
Schools (EFS1)	100%
Fire Stations and Police Stations (EFFS, EFPS)	150%

The values shown in Table 2.2.1-4 are identical to those given in the HAZUS Technical Manual, and have already been applied to the appraised values before the inventory databases are supplied from the MAE Center.

d) Essential facility status (6)

All inventory supplied by the MAE Center is provided with an accompanying essential facility flag, as shown in Table 2.2.1-5.

**Table 2.2.1-5 Essential facility types**



EFACILITY (String)	Facility
EFS1	Schools
EFHL	Low-rise hospitals
EFHM	Mid- and High-rise hospitals
EFFS	Fire stations
EFPS	Police stations
None	Not essential

The essential facility classifications given in Table 2.2.1-5 correlate closely to essential facility classifications used by HAZUS.

e) Building footprint configurations (7)

- Square
- Rectangular
- T-Shaped
- L-Shaped
- I- or H-Shaped
- C-Shaped
- Irregular

The appraised value of an inventory item is not the same as the replacement cost, but it can serve as a reasonable estimate of building value for a loss assessment (French, 2006). Building fragilities supplied by the MAE Center estimate damage to structural value only. There is no information currently available in the MAE Center regarding how to partition the total value of an inventory item into structural and nonstructural values. In lieu of such information, structural and nonstructural values will be partitioned from total value using HAZUS damage ratios given in Tables 15.2 through 15.4 of the HAZUS-MH MR2 Technical Manual (NIBS, 2006). According to those tables in the HAZUS Technical Manual, “Complete” damage corresponds to the following percentages of building total replacement cost, as shown in Table 2.2.1-6. The  $\alpha^{SD}$ ,  $\alpha^{NA}$ , and  $\alpha^{ND}$  headers for each column in Table 2.2.1-6 represent percentages of structural, acceleration-sensitive nonstructural, and drift-sensitive nonstructural values, respectively.

**Table 2.2.1-6 Percentages of component value based on HAZUS/Version 4 Occupancy**

Occupancy	$\alpha^{SD}$	$\alpha^{NA}$	$\alpha^{ND}$
RES1	23.4	26.6	50
RES2	24.4	37.8	37.8
RES3a-f	13.8	43.7	42.5



Occupancy	$\alpha^{SD}$	$\alpha^{NA}$	$\alpha^{ND}$
RES4	13.6	43.2	43.2
RES5	18.8	41.2	40
RES6	18.4	40.8	40.8
COM1	29.4	43.1	27.5
COM2	32.4	41.1	26.5
COM3	16.2	50	33.8
COM4	19.2	47.9	32.9
COM5	13.8	51.7	34.5
COM6	14	51.3	34.7
COM7	14.4	51.2	34.4
COM8	10	54.4	35.6
COM9	12.2	52.7	35.1
COM10	60.9	21.7	17.4
IND1	15.7	72.5	11.8
IND2	15.7	72.5	11.8
IND3	15.7	72.5	11.8
IND4	15.7	72.5	11.8
IND5	15.7	72.5	11.8
IND6	15.7	72.5	11.8
AGR1	46.2	46.1	7.7
REL1	19.8	47.6	32.6
GOV1	17.9	49.3	32.8
GOV2	15.3	50.5	34.2
EDU1	18.9	32.4	48.7
EDU2	11	29	60

Architectural and MEP (Nonstructural)

The MAE Center has provided nonstructural fragilities to estimate damage to specific nonstructural components for the MLGW Project, but the fragilities are only useful when inventory data for specific nonstructural components is also supplied. In most cases, specific nonstructural inventory data are not available, and a representation of nonstructural assets (value) will be adapted from HAZUS as an interim measure. HAZUS does not consider specific nonstructural inventory items, but rather breaks nonstructural inventory into two subsets: drift-sensitive and acceleration-sensitive. Fractions of total value for each subset of nonstructural inventory are shown in Table 2.2.1-6.

2.2.2 Transportation Systems



The MAE Center has provided bridge data obtained from the National Bridge Inventory for Memphis, Tennessee and Charleston, South Carolina (DesRoches, 2006; FHWA, 1995). Road data has been provided for both locations as well (French and Muthukumar, 2006; Patterson, 2006). Uncertainty is not characterized for the attributes of this inventory data.

### 2.2.3 Utility Systems

Water system inventory data, including pipelines and tanks, has been provided for Shelby County (French, 2006). Data for the cast iron pipe network carrying natural gas and the electric power network has been provided by municipal contacts (MLGW, 2005). Additional high fidelity Shelby County utility inventory data will also be made available to MAEViz developers as it is supplied by municipal contacts for other networks in addition to natural gas. An additional source of lifeline inventory is the Homeland Security Infrastructure Program (HSIP) GOLD Dataset (PMH, 2006). A small portion of the HSIP was made available to the MAE Center by FEMA through a sample HAZUS file for an eight state study region in Mid-America. The subset of HSIP utility inventory data was limited to natural gas and oil pipelines, and it had also been modified from its original form for use in HAZUS. The MAE Center has recently acquired the full release version of the HSIP and is currently investigating how the data might be used within MAEViz. Uncertainty is not characterized for the attributes of utility inventory data. The majority of data being used to estimate breakdowns of total value to component values for electric power plants and substations is based on the work of Eiding (G & E Engineering Systems, Inc., 1994).

### 2.2.4 HAZUS Inventory Data

HAZUS building stock inventory is aggregated to the census block level for default inventory. The data has been extracted directly from databases in HAZUS, but it has not yet been manipulated so that MAEViz could use it to perform analyses. In order for MAEViz to use the HAZUS building stock inventory data, the aggregated census tract inventory will need to be converted to equivalent buildings. This process will require the following steps for each census block:

- Compute total value of buildings for each specific occupancy using the approximate dollar exposure of each occupancy (\$/ft<sup>2</sup>) published in the HAZUS Technical Manual and the total floor area for each occupancy extracted from HAZUS databases.
- Partition building value for each occupancy into equivalent buildings by structure type (e.g., W1, S1, C1) by using occupancy mapping schemes in HAZUS.
- This approach will result in a maximum of (33 specific occupancies) x (36 specific structure types) = 1188 equivalent buildings for each census block. Assets other than general building stock are treated as point-wise entities by HAZUS.

Note that uncertainty is not characterized for the attributes of this inventory data.



### 3. HAZARD DEFINITION

#### 3.1 MAEViz Implementation

MAEViz can currently estimate seismic hazard in terms of spectral acceleration, peak ground acceleration, peak ground velocity, and peak ground displacement within the Mississippi Embayment using a collection of individual attenuation functions collectively referred to as the Rix-Fernandez attenuations (Fernandez and Rix, 2006). MAEViz can also estimate spectral acceleration and PGA outside of the Embayment by using the standard attenuations in use by USGS with NEHRP soil amplification factors, although MAEViz currently only evaluates one USGS attenuation for an analysis outside of the Embayment.

The following modifications are recommended for MAEViz hazard estimation:

- Within the Embayment, calculate hazard appropriate to specific inventory items (user option).
  - Building stock
  - Bridges
  - Utility lifelines
- In the Memphis area, implement the liquefaction hazard estimation algorithm provided by the MAE Center.
- When estimating hazard outside of the Embayment, but within the Central and Eastern United States (CEUS), use a weighted combination of USGS attenuation functions by default, where the weights are taken from Table 3.1.3-1.
- Implement Western United States (WUS) attenuation functions, with weights as shown in Table 3.1.4-1.
- Implement Toro and Silva soil amplification factors for use outside the Embayment but within the CEUS.



3.1.1 Within the Embayment, calculate hazard appropriate to specific inventory items (user option).

#### *3.1.1.1 Building Stock Hazard*

##### **Algorithm**

##### **Inputs:**

Fragility associated with each entity in building stock inventory database.

Go to fragility database for hazard type (typically  $S_a$ ) associated with fragility.

Period,  $T$ , for each building as calculated in Section 2.1.2.1.

Location of building from building inventory.

Underlying soil type and depth for each building based on location.

Seismic source magnitude and location.

##### **Process:**

Use Rix-Fernandez attenuations to estimate spectral acceleration at the appropriate period for each inventory item.

NOTE: If structure type uncertainty is considered, and users select the option to calculate a period for each structure type available in the inventory, compute appropriate hazard for each structure type in the inventory, based on period.

**Outputs:** mean and standard deviation of estimated hazard for each inventory item at appropriate period

##### **Example**

Hazard will be estimated for each of the three sample inventory items based on distances from a specified epicenter location and a magnitude assumed for the scenario. For this example, consider the default maximum magnitude event given for Memphis, TN in Table 3.2.2-1 ( $M_w = 7.9$  at Blytheville, AR). Note that the spectral accelerations shown in Table 3.1.1.1-1 were calculated for appropriate structural periods from Table 2.1.2.1-1.



**Table 3.1.1.1-1 Example Ground Shaking Hazard Data**

	Latitude	Longitude	Period	$\ln S_a$	
				Mean, $\lambda_{S_a}$	Standard deviation, $\beta_{S_a}$
Inventory 1 (I1)	35.13554 N	90.03732 W	0.95	-1.710	0.887
Inventory 2 (I2)	35.22057 N	89.90675 W	0.6	-1.463	0.827
Inventory 3 (I3)	35.03183 N	89.89023 W	0.6	-1.514	0.840



### 3.1.1.2 Transportation Lifeline Hazard

#### **Algorithm**

##### Inputs:

Fragility associated with each entity in bridge inventory database.

Go to fragility database for hazard type (typically PGA) associated with fragility.

Location of bridge from building inventory.

Underlying soil type and depth for each bridge based on location.

Seismic source magnitude and location.

##### Process:

Use Rix-Fernandez attenuations to estimate spectral acceleration at the appropriate period for each inventory item.

Outputs: mean and standard deviation of estimated hazard for each inventory item

#### **Example**

Bridge fragilities are calibrated to PGA. The calculated hazard for each of the three sample bridges is shown in Table 3.1.1.2-1.

**Table 3.1.1.2-1 Example Bridge Ground Shaking Hazard Data**

	Latitude	Longitude	$\ln PGA$	
			Mean, $\lambda_{PGA}$	Standard deviation, $\beta_{PGA}$
Bridge 1	35.17167 N	89.84167 W	-1.8494	0.3188
Bridge 2	35.26167 N	89.66500 W	-1.8529	0.3158
Bridge 3	35.25167 N	90.02500 W	-1.8548	0.3151



### 3.1.1.3 Utility Lifeline Hazard

#### Electric Power Plants

##### **Algorithm**

##### **Inputs:**

- Fragility associated with each entity in electric power plant inventory database.
- Go to fragility database for hazard type (typically Sa or PGA) associated with fragility.
- Period, T, for each component (from Section 2.1.2.2).
- Location of power plant from inventory database.
- Underlying soil type and depth for each power plant based on location.
- Seismic source magnitude and location.

##### **Process:**

- Use Rix-Fernandez attenuations to estimate spectral acceleration at the appropriate period or PGA for each component as appropriate, based on fragility.

**Outputs:** mean and standard deviation of estimated hazard for each component at appropriate period

##### **Example**

Hazard should be calculated for each component of electric power plants, based on component periods. Note that multiple components may have the same period, and therefore require only a single hazard calculation. Sample hazard data in terms of PGA and spectral acceleration are shown in Tables 3.1.1.3-1 and 3.1.1.3-2, respectively.

**Table 3.1.1.3-1 Example Electric Power Plant PGA Data**

	Latitude	Longitude	ln PGA	
			Mean, $\lambda_{PGA}$	Standard deviation, $\beta_{PGA}$
EPP 1	35.0826 N	90.1364 W	-1.8494	0.3188
EPP 2	35.1996 N	89.9710 W	-1.8529	0.3158
EPP 3	35.2989 N	89.9629 W	-1.8548	0.3151



**Table 3.1.1.3-2 Example Electric Power Plant Spectral Acceleration Data**

	Sample Component	Period	$\ln S_a$	
			Mean, $\lambda_{S_a}$	Standard deviation, $\beta_{S_a}$
EPP 1	Boilers + Steam Generators	0.100	-1.8144	0.4750
EPP 2	Boilers + Steam Generators	0.100	-1.5859	0.4750
EPP 3	Boilers + Steam Generators	0.100	-1.5831	0.4732



*Electric Substations*

**Algorithm**

Inputs:

- Fragility associated with each entity in electric substation inventory database.
- Go to fragility database for hazard type (typically PGA) associated with fragility.
- Period, T, for each component with fragility calibrated to Sa.
- Location of substation from inventory database.
- Underlying soil type and depth for each power plant based on location.
- Seismic source magnitude and location.

Process:

Use Rix-Fernandez attenuations to estimate spectral acceleration at the appropriate period or PGA for each component as appropriate, based on fragility.

Outputs: mean and standard deviation of estimated hazard for each component at appropriate period

**Example**

Hazard should be calculated for each component of electric substations, based on component periods. Currently, all components of substations are described by fragilities calibrated to PGA. Therefore, only PGA is currently required to be calculated for substations. Sample hazard data in terms of PGA is shown in Table 3.1.1.3-3.

**Table 3.1.1.3-3 Example Electric Substation PGA Data**

	Latitude	Longitude	ln PGA	
			Mean, $\lambda_{PGA}$	Standard deviation, $\beta_{PGA}$
ESS 1	35.0826 N	90.1364 W	-1.8494	0.3188
ESS 2	35.1996 N	89.9710 W	-1.8529	0.3158
ESS 3	35.2989 N	89.9629 W	-1.8548	0.3151



## Water Tanks

### Algorithm

#### Inputs:

Fragility associated with each entity in water tank inventory database.

Go to fragility database for hazard type (typically PGA) associated with fragility.

Period,  $T$ , for each component with fragility calibrated to  $S_a$ .

Location of water tank from inventory database.

Underlying soil type and depth for each power plant based on location.

Seismic source magnitude and location.

#### Process:

Use Rix-Fernandez attenuations to estimate spectral acceleration at the appropriate period or PGA for each component as appropriate, based on fragility.

Outputs: mean and standard deviation of estimated hazard for each component at appropriate period

### Example

Water tanks are described by fragilities calibrated to PGA. Sample hazard data in terms of PGA is shown in Table 3.1.1.3-4.

**Table 3.1.1.3-4 Example Ground Shaking Hazard Data**

	Latitude	Longitude	ln $PGA$	
			Mean, $\lambda_{PGA}$	Standard deviation, $\beta_{PGA}$
Water Tank 1	35.136 N	90.037 W	-1.850	0.566
Water Tank 2	35.221 N	89.907 W	-1.852	0.562
Water Tank 3	35.032 N	89.890 W	-1.859	0.572



## Buried Pipelines

### Algorithm

#### Inputs:

Location of end nodes (calculated internally or read from inventory database).

Underlying soil type and depth at the midpoint between end nodes for each pipeline based on location.

Seismic source magnitude and location.

#### Process:

Use Rix-Fernandez attenuations to estimate PGV for each pipeline.

Outputs: mean and standard deviation of estimated hazard for each pipeline

### Example

A representative hazard for a pipeline segment can be determined by evaluating the governing attenuation equations at the midpoint between the end nodes of the segment. For the example segment, the end nodes are located at (35.1792 °N, 89.7944 °W) and (35.1855 °N, 89.9060 °W). The Rix-Fernandez attenuations can then be applied to obtain the lognormal mean and standard deviation of peak ground velocity, PGV, at the average location of the two end nodes as shown in Table 3.1.1.3-5.

**Table 3.1.1.3-5 Example Buried Pipeline PGV Data**

	Approx. Latitude of Midpoint	Approx. Longitude of Midpoint	ln <i>PGV</i>	
			Mean, $\lambda_{PGV}$	Standard deviation, $\beta_{PGV}$
Segment 1	35.1824 N	89.8502 W	3.4434	0.5464



### 3.1.2 Implement MAEC liquefaction hazard estimation algorithm (Memphis).

#### **Algorithm**

##### Inputs:

Location of inventory.

Underlying soil type for each inventory item based on location (Note soil types for liquefaction are different than soil types for Rix-Fernandez attenuations).

Computed PGA for each item.

Seismic source magnitude and location.

##### Process:

Calculate magnitude scaling factor from Table B.3.2.6-2 based on magnitude of source event.

Then for each item:

Calculate duration-adjusted PGA from Equation (B.3.2.6-1).

Look up coefficients for LPI value of 15 in Table B.3.2.6-3 based on soil type.

Set  $w_1$  and  $w_2$  equal to 1/3 and 2/3 by default, unless all coefficients in a row of Table B.3.2.6-3 are zeros. When all coefficients for a row are zeros, set the weighting factor for the row populated with zeros equal to 0 and the weighting factor for the row with nonzero coefficients equal to 1.

Allow the user to adjust default weighting factors.

Substitute coefficients and weighting factors into Equation (B.3.2.6-3) to obtain probability of major liquefaction.

Outputs: probability of major liquefaction,  $P[LPI > 15]$

#### **Example**

To compute liquefaction hazard, PGA must be computed for inventory items. PGA values must also be scaled relative to the magnitude of the source event to account for duration effects. A Magnitude Scaling Factor (MSF) may be interpolated from Table B.3.2.6-2 as 0.95 for an  $M_w = 7.9$  source event. The maximum adjusted PGA is then checked to ensure it does not exceed a limiting value of 0.55 g.

$$PGA_{\max.adj} = \frac{PGA}{0.95} < 0.55g$$



**Table 3.1.2-1 Example Ground Failure Hazard Data**

	Structural type	Latitude	Longitude	Rix-Fernandez Output, ln(PGA)	PGA, g = exp(ln(PGA))	PGA <sub>maxadj</sub> , g
Inventory 1 (I1)	C1	35.13554 N	90.03732 W	-1.850	0.157	0.166
Inventory 2 (I2)	URM	35.22057 N	89.90675 W	-1.852	0.157	0.165
Inventory 3 (I3)	URM	35.03183 N	89.89023 W	-1.859	0.156	0.164

Using a shapefile supplied by the MAE Center (see Figure B.3.2.6-1 in Appendix B), the sample buildings may be determined to sit atop the geologic units noted in Table 3.1.2-2. Each soil unit has been mapped to coefficients as shown in Table B.3.2.6-3. The coefficients may then be used in an equation provided by the MAE Center to estimate probability of exceeding one of two LPI limits. Use the coefficients for evaluating probability of exceedence of LPI = 15 when estimating damage to inventory. The standard weighting factors of 1/3 for CPT coefficients and 2/3 for SPT coefficients were NOT used for the example because coefficients for CPT tests are all zeros for QI soil and coefficients for SPT tests are all zeros for af soil. Weighting factors of 0 for the CPT coefficients and 1 for the SPT coefficients were used for the URM sample buildings. Also, since inventory item I1 is in an artificial fill zone, weighting factors of 1 for the CPT coefficients and 0 for the SPT coefficients were used.

**Table 3.1.2-2 Soil Units and Coefficients**

	Soil Unit	w <sub>1</sub>	w <sub>2</sub>	Type of Test	a	b	c
Inventory 1 (I1)	af	1	0	CPT	0.998	39280.6	38.69
Inventory 2 (I2)	QI	0	1	SPT	0.193	122.12	15.89
Inventory 3 (I3)	QI	0	1	SPT	0.193	122.12	15.89

The general equation to evaluate liquefaction hazard is

$$P[LPI > x] = w_1 \frac{a_1}{\left[1 + b_1 \exp(-c_1 a_{\max.\text{adjusted}})\right]} + w_2 \frac{a_2}{\left[1 + b_2 \exp(-c_2 a_{\max.\text{adjusted}})\right]}$$

So the equation to estimate hazard for item I2, for example, becomes



$$P[LPI > 15] = (0) \frac{a_1}{[1 + b_1 \exp(-c_1 a_{\max. \text{adjusted}})]} + (1) \frac{0.193}{[1 + 122.12 \exp(-15.89 * 0.165)]}$$

$$P[LPI > 15] = 0.020$$

**Table 3.1.2-3 Probabilities of Ground Failure**

	Soil Unit	P[LPI>15]
Inventory 1 (I1)	af	0.0151
Inventory 2 (I2)	Ql	0.0196
Inventory 3 (I3)	Ql	0.0193



3.1.3 Implement typical USGS CEUS attenuation combinations.

**Algorithm**

Inputs:

Locations throughout study region where hazard must be estimated.

Underlying soil type (NEHRP) based on location (assume D by default).

Seismic source magnitude and location.

Process:

Prompt user to choose from a list (“Select Attenuation(s)”) including Characteristic Event (default), Non-Characteristic Event, or User Specified, for which the user manually enters weights.

Compute hazard for all attenuations required for combination as listed in Table 3.1.3-1.

For all attenuations EXCEPT Frankel et al. (1996), convert lognormal mean hazard values to standard mean values, multiply by the factors given in Table 3.1.3-2, then convert back to lognormal values.

Combine results using the weighting factors shown in Table 3.1.3-1.

Convert hazard from combined attenuations to standard mean values and multiply by NEHRP soil factors.

Outputs: mean of estimated hazard in terms of PGA, 0.2 sec Sa, and 1.0 sec Sa.

**Example**

**Table 3.1.3-1 Default CEUS Attenuation Functions and Weights  
(outside Mississippi Embayment)**

Applicable Region / Event	Attenuation Function	Weight
CEUS Characteristic Event (New Madrid and Charleston) outside Mississippi Embayment	Atkinson and Boore (1995)	0.250
	Toro et al (1997)	0.250
	Frankel et al (1996)	0.250
	Campbell (2002)	0.125
	Sommerville et al (2002)	0.125
CEUS source (not characteristic) outside Mississippi Embayment	Atkinson and Boore (1995)	0.286
	Toro et al (1997)	0.286
	Frankel et al (1996)	0.286
	Campbell (2002)	0.142



**Table 3.1.3-2 Correction Factors to Convert Site Class A Motions to B/C Motions**

Period	Factor
PGA	1.52
0.2 sec	1.76
0.3 sec	1.72
1 sec	1.34
> 1 sec	1.34

If a site is located at 35.294°N, 90.05°W, the expected ground motions resulting from an  $M_w=7.7$  CEUS Characteristic event may be determined as follows:

**Table 3.1.3-3 Initial Calculations of  $\ln Y$  (log10 for Atkinson and Boore)**

	PGA	0.2 sec Sa	1 sec Sa
Atkinson and Boore	2.43	2.60	2.06
Toro et al.	-1.34	-0.74	-1.58
Frankel et al.	-0.32	-0.04	-0.56
Campbell	-1.30	-0.92	-1.80
Sommerville et al.	-1.08	-0.52	-1.69

Next, convert all Y hazards from lognormal, except Frankel et al. Note that Atkinson and Boore values must be converted from base 10, and also from  $\text{cm/s}^2$  to  $\text{g}'\text{s}$ .

**Table 3.1.3-4 Values converted from lognormal**

	PGA	0.2 sec Sa	1 sec Sa
Atkinson and Boore	0.27	0.41	0.12
Toro et al.	0.26	0.48	0.21
Campbell	0.27	0.40	0.17
Sommerville et al.	0.34	0.59	0.18

Then, convert Site Class A motions to Site Class B/C motions, using values from Table 3.1.3-2.



**Table 3.1.3-5 Values converted from Site Class A to B/C**

	PGA	0.2 sec Sa	1 sec Sa
Atkinson and Boore	0.42	0.72	0.16
Toro et al.	0.40	0.84	0.27
Campbell	0.41	0.70	0.22
Sommerville et al.	0.52	1.04	0.25

Finally, convert values back to lognormal (all in terms of natural log)

**Table 3.1.3-6 Final values of lnY**

	PGA	0.2 sec Sa	1 sec Sa
Atkinson and Boore	-0.873	-0.329	-1.864
Toro et al.	-0.921	-0.177	-1.292
Frankel et al.	-0.319	-0.036	-0.561
Campbell	-0.882	-0.358	-1.503
Sommerville et al.	-0.659	0.041	-1.402

The values given in Table 3.1.3-6 can be used to determine median lognormal hazard and epistemic variance similarly to the Rix-Fernandez equations. Median PGA, 0.2 sec Sa, and 1 sec Sa are 0.486g, 0.840g, and 0.275g, respectively, for B/C motions. Fa and Fv can be determined in accordance with NEHRP to be 1.16 and 1.85 for Site Class D. 0.2 sec Sa then becomes 0.840 \* 1.16 = 0.977g, and 1 sec Sa becomes 0.275 \* 1.85 = 0.508g.

Lognormal median accelerations are -0.721, -0.175, -1.292 for PGA, 0.2 sec Sa, and 1 sec Sa. The epistemic standard deviations of lognormal accelerations are 0.245, 0.144, and 0.472. Aleatory standard deviations are fixed for all attenuations except Campbell. Campbell requires the coefficients given in Table 3.1.3-7.

**Table 3.1.3-7 Campbell Aleatory Standard Deviation Coefficients**

	C <sub>11</sub>	C <sub>12</sub>	C <sub>13</sub>
PGA	1.030	-0.0860	0.414
0.2 sec Sa	1.077	-0.0838	0.478
1 sec Sa	1.110	-0.0793	0.543

The values in Table 3.1.3-7 may then be used in Equations 3.1.3-1 and 3.1.3-2.

$$\sigma_{a,\ln Y} = c_{11} + c_{12}M_w \text{ when } M_w < M_1 \tag{3.1.3-1}$$



$$\sigma_{a,\ln Y} = c_{13} \text{ when } M_w \geq M_1 \quad (3.1.3-2)$$

where  $M_1 = 7.16$ . Lognormal aleatory standard deviations are given in Table 3.1.3-8.

**Table 3.1.3-8 Aleatory standard deviations of lnY**

	PGA	0.2 sec Sa	1 sec Sa
Atkinson and Boore	0.620	0.581	0.550
Toro et al.	0.750	0.750	0.800
Frankel et al.	0.750	0.750	0.800
Campbell	0.414	0.478	0.543
Sommerville et al.	0.587	0.611	0.693

The lognormal aleatory standard deviations can be squared to obtain variances, then combined with weighting factors similarly to the approach used for the Rix-Fernandez equations. Combined aleatory standard deviations are 0.665, 0.664, and 0.702 for PGA, 0.2 sec Sa, and 1 sec Sa, respectively.



3.1.4 Implement typical USGS WUS attenuation combinations.

**Algorithm**

Inputs:

Locations throughout study region where hazard must be estimated.

Underlying soil type (NEHRP) based on location (assume D by default).

Seismic source magnitude and location, type and orientation of fault rupture.

Process:

Prompt user to choose which combination shown in Table 3.1.4-1 is appropriate.

Compute hazard for all attenuations required for combination as listed in Table 3.1.4-1.

Combine results using the weighting factors shown in Table 3.1.4-1.

Convert hazard from combined attenuations to standard mean values and multiply by NEHRP soil factors.

Outputs: mean of estimated hazard in terms of PGA, 0.2 sec Sa, and 1.0 sec Sa.

**Example**

**Table 3.1.4-1 Default WUS Attenuation Functions and Weights**

Applicable Region / Event	Attenuation Function	Weight
WUS Shallow Crustal Event - Extensional	Abrahamson and Silva (1997): Hanging Wall	0.200
	Sadigh, Chang, Egan, Makdisi, and Young (1997)	0.200
	Boore, Joyner and Fumal (1997)	0.200
	Spudich et al. (1999)	0.200
	Campbell & Bozorgnia (2003)	0.200
WUS Shallow Crustal Event – Non-Extensional	Abrahamson and Silva (1997): Hanging Wall	0.250
	Sadigh, Chang, Egan, Makdisi, and Young (1997)	0.250
	Boore, Joyner and Fumal (1997)	0.250
	Campbell & Bozorgnia (2003)	0.250
WUS Cascadia Subduction Event	Youngs, Chiou, Silva and Humphrey (1997)	0.500
	Sadigh, Chang, Egan, Makdisi, and Young (1997)	0.500
WUS Deep Event (> 35 km in depth)	Youngs, Chiou, Silva and Humphrey (1997)	0.500
	Atkinson and Boore (2002) - Global	0.250



	Atkinson and Boore (2002) - Cascadia	0.250
--	--------------------------------------	-------

*[example data not currently available]*



### 3.1.5 Implement Toro and Silva soil amplification factors.

#### **Algorithm**

##### Inputs:

Locations throughout study region where hazard must be estimated.

Underlying soil type and depth based on location (only currently available between 84°W and 96°W, and between 36°N and 40°N).

Seismic source magnitude and location.

##### Process:

Prompt user to choose whether or not the seismic source is a Characteristic Event (default to yes).

Compute hazard for all attenuations required for combination as listed in Table 3.1.3-1.

For *only* the Frankel et al. (1996) attenuation, convert lognormal mean hazard values to standard mean values, *divide* by the factors given in Table 3.1.3-2, then convert back to lognormal values.

Combine results using the weighting factors shown in Table 3.1.3-1.

Convert hazard from combined attenuations to standard mean values.

Use PGA, soil type, and soil depth to determine Toro and Silva soil factors.

Multiply standard mean values of PGA, 0.2 sec Sa, and 1.0 sec Sa by Toro and Silva soil factors.

Outputs: mean of estimated hazard in terms of PGA, 0.2 sec Sa, and 1.0 sec Sa.

#### **Example**

Use Toro and Silva soil amplification factors rather than NEHRP soil factors for sites located between 84°W and 96°W, and between 36°N and 40°N where the soil is underlain by either Ozark Uplands or Glacial Till (e.g., St. Louis, MO), as shown in Figure 3.1.5-1.



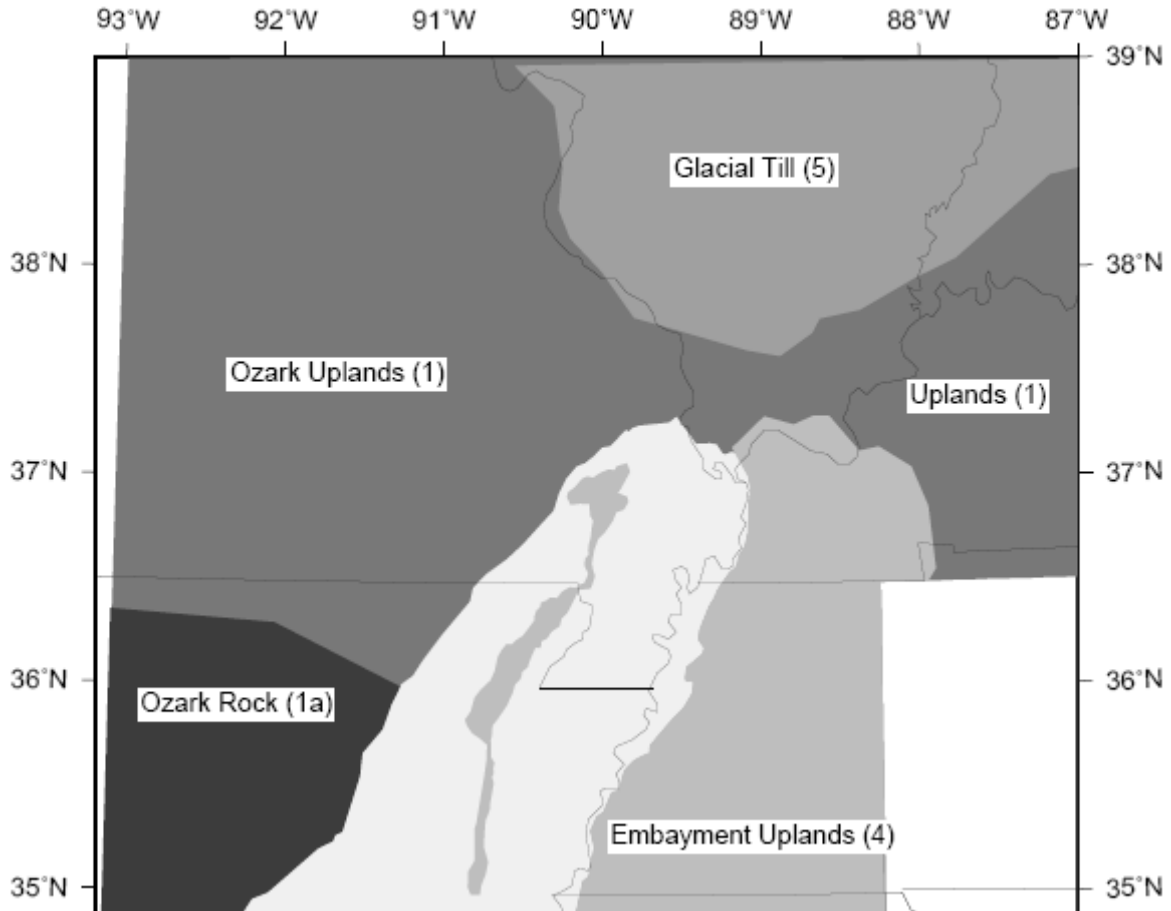


**Figure 3.1.5-1. Region of applicability for Toro and Silva amplification factors.**

Hazard estimation is identical to Section 3.1.4 except for two characteristics:

- Ground motions from attenuation functions must be calibrated to site A motions for Toro and Silva amplification factors, so divide the results of Frankel et al. (1996) by the factors shown in Table 3.1.4-2.
- Compute Toro and Silva amplification factors to be applied to standard normal mean of ground motion based on soil type, soil depth, and PGA. (Shape factors are available from the MAE Center for soil type and soil type in the region of applicability).

*[example data not currently available]*



### 3.1.6 Implement HAZUS liquefaction hazard estimation algorithms.

#### **Algorithm**

##### Inputs:

Map of liquefaction susceptibilities.

Map of PGA hazard.

Seismic source magnitude (if possible, record Mw used for generating PGA map and use as default value).

Map of groundwater depth (default to assumption of 5 ft).

##### Process:

Calculate probabilities of liquefaction throughout the study region using Equation (3.1.6-1).

Calculate expected value of lateral spreading using Equation (3.1.6-4).

Calculate expected value of ground settlement by multiplying the result of Equation (3.1.6-1) by the appropriate value in Table (3.1.6-4).

##### Outputs:

Probability of liquefaction for each building.

Expected lateral spreading for each building.

Expected ground settlement for each building.

#### **Example**

For use as a general approach when information is not sufficient to apply MAEC liquefaction algorithms (when soil conditions are significantly different than Memphis, TN), implement the HAZUS liquefaction hazard algorithms. The first step in the HAZUS liquefaction methodology is to quantitatively estimate liquefaction susceptibility using qualitative maps, according to Equation (3.1.6-1). The maps have six levels of liquefaction susceptibility, ranging from None to Very High.

$$P[Liquefaction_{SC}] = \frac{P[Liquefaction_{SC} | PGA = a]}{K_M \cdot K_w} \cdot P_{ml} \quad (3.1.6-1)$$

where

$P[Liquefaction_{SC} | PGA = a]$  is determined as a function of both PGA and liquefaction susceptibility category, according to Table 3.1.6-1.



**Table 3.1.6-1 Liquefaction probability functions**

Susceptibility Category	P [Liquefaction  PGA = a]
Very High	$0 \leq 9.09 a - 0.82 \leq 1.0$
High	$0 \leq 7.67a - 0.92 \leq 1.0$
Moderate	$0 \leq 6.67a - 1.0 \leq 1.0$
Low	$0 \leq 5.57a - 1.18 \leq 1.0$
Very Low	$0 \leq 4.16a - 1.08 \leq 1.0$
None	0.0

Assume a sample building sits on soil with a Very High Susceptibility Category, and a PGA of 0.3g. Substituting  $a = 0.3$  into the equation shown in Table 3.1.6-1 for Very High results in the maximum value of 1.0.

The terms in the denominator of Equation (3.1.6-1) calibrate the susceptibility function to account for the magnitude of the seismic source event and the influence of the groundwater table. They can be determined according to

$$K_M = 0.0027M^3 - 0.0267M^2 - 0.2055M + 2.9188 \quad (3.1.6-2)$$

and

$$K_w = 0.022d_w + 0.93 \quad (3.1.6-3)$$

where  $M$  is the moment magnitude of the seismic source and  $d_w$  is the depth of the groundwater table. If the moment magnitude of the source event is 7.9,  $K_M = 0.96$ . If the groundwater depth is 5 ft,  $K_w = 1.04$ .

Finally, the  $P_{ml}$  coefficients may be obtained from Table 3.1.6-2.

**Table 3.1.6-2 Map calibration factors**

Mapped Relative Susceptibility	Proportion of Map Unit
Very High	0.25
High	0.20
Moderate	0.10
Low	0.05
Very Low	0.02
None	0.00

The  $P_{ml}$  coefficient for Very High is 0.25. Probability of liquefaction can then be calculated as

$$P[Liquefaction_{sc}] = \frac{1}{0.96 \cdot 1.04} \cdot 0.25 = 0.250 \quad (3.1.6-1)$$

Next, calculate expected lateral spreading using Equation (3.1.6-4).



$$E[PGD_{SC}] = K_{\Delta} \cdot E \left[ PGD \mid \left( \frac{PGA}{PL_{SC}} \right) = a \right] \quad (3.1.6-4)$$

Where  $E \left[ PGD \mid \left( \frac{PGA}{PL_{SC}} \right) = a \right]$  is determined using a normalized PGA accounting for the threshold value of PGA required to induce liquefaction, as shown in Figure 3.1.6-1.

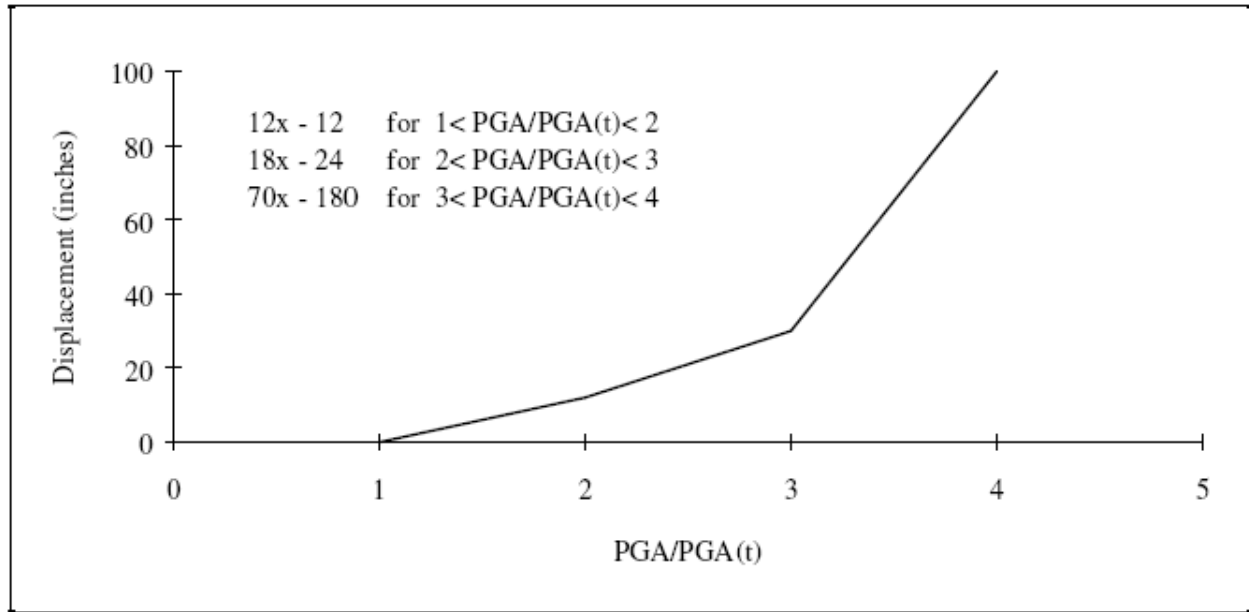


Figure 3.1.6-1 Expected lateral spreading with respect to normalized PGA [from NIBS (2006)]

The values of  $PGA(t)$  may be obtained from Table 3.1.6-3.

Table 3.1.6-3 Threshold PGA required to induce liquefaction

Susceptibility Category	PGA(t)
Very High	0.09g
High	0.12g
Moderate	0.15g
Low	0.21g
Very Low	0.26g
None	N/A

The normalized  $PGA/PGA(t)$  for the sample building is  $0.3/0.09 = 3.33$ . Using this value in Figure 3.1.6-1 yields an unadjusted expected lateral spreading of  $70 \cdot 3.33 - 180 = 53$  inches.

The  $K_{\Delta}$  term can be evaluated using Equation (3.1.6-5).

$$K_{\Delta} = 0.0086M^3 - 0.0914M^2 + 0.4698M - 0.9835 \quad (3.1.6-5)$$



where M is the moment magnitude of the source event. Using  $M = 7.9$  as before,  $K_{\Delta} = 1.26$ . The adjusted expected lateral spreading is then  $1.26 * 53 = 67$  inches.

Ground settlement can be calculated by multiplying the result of (3.1.6-1) by the appropriate value from Table 3.1.6-4 depending on mapped susceptibility category.

**Table 3.1.6-4 Expected ground settlement**

<b>Relative Susceptibility</b>	<b>Settlement (inches)</b>
Very High	12
High	6
Moderate	2
Low	1
Very Low	0
None	0

For the sample building, the expected ground settlement is  $0.25 * 12 = 3$  inches.



## 3.2 Background

### 3.2.1 Hazard Definition Overview

The seismic hazard models of MAEViz will be primarily based on project HD-1<sup>1</sup> on synthetic ground motions for ‘regional hazard analyses’ (with epistemic uncertainties quantified) (Fernandez and Rix, 2006; Romero and Rix, 2005; Park and Hashash, 2005). Project HD-3 on seismic path modeling of earthquakes in mid-America has provided results that are already incorporated into project HD-1. Project HD-4 on site modeling established procedures for conducting ‘site-specific hazard analyses’ when detailed knowledge of local site conditions are available. Projects HD-2 on intraplate ground motion and HD-5 on verification of site response paradigms do not have results to be implemented now, but the upcoming findings in these projects may improve the hazard models in MAEViz in the future. Project HD-2 has started to yield critical information that will help constrain recurrence intervals for large earthquakes in the New Madrid Seismic Zone (NMSZ). Project HD-5 is intended to validate the ground motion models used for the Mississippi Embayment region.

### 3.2.2 Seismic Source Definition

The New Madrid fault is roughly composed of three primary segments: New Madrid North, Reelfoot, and Cottonwood Grove, also called the Blytheville Arch. Primary (i.e., default) seismic sources for the New Madrid Seismic Zone have been defined by the Hazard Definition (HD) thrust for use in MAEViz with paired data indicating the magnitude and location of scenario events. The source events originate on the Blytheville Arch for Memphis, Tennessee, and on the New Madrid North fault for St. Louis, Missouri and Cairo, Illinois. The Memphis source events are located with a maximum magnitude event near the center of the Blytheville Arch (at Blytheville, Arkansas) and with a lesser magnitude event near the southern tip of the Blytheville Arch, at Marked Tree, Arkansas. The source events that are considered critical for St. Louis and Cairo happen to be the same location, and are both located at Cairo, Illinois. The Wabash Valley Seismic Zone also poses a significant threat to Mid-America, and St. Louis, Missouri in particular. A Wabash Valley seismic source was proposed by the team working on a project for the Illinois Emergency Management Agency within the MAE Center, including members of the HD thrust. MAEViz will include these sources as default choices for Mid-America. Default magnitude and location data are shown in Table 3.2.2-1.

**Table 3.2.2-1 Default Scenario Event Seismic Sources for Mid-America**

Seismic Zone	Critical City	Magnitude	Latitude	Longitude
New Madrid	Memphis, TN	7.9	35.927N	89.919W
New Madrid	Memphis, TN	6.2	35.535N	90.430W

---

<sup>1</sup> Throughout the report, specific projects within the MAE Center are identified while highlighting specific contributions from those projects.



New Madrid	St. Louis, MO	7.7	37.06N	89.12W
New Madrid	St. Louis, MO	6.2	37.06N	89.12W
New Madrid	Cairo, IL	7.7	37.06N	89.12W
New Madrid	Cairo, IL	6.2	37.06N	89.12W
Wabash Valley	St. Louis, MO	7.1	38.20N	88.17W

The sources provided by the HD thrust represent deaggregation of USGS probabilistic seismic hazard maps to determine likely combinations of earthquake magnitude and location, but also incorporate expert opinion of multiple team members in establishing the final locations. MAEViz also offer users the option of specifying a magnitude and location of their choosing. For a scenario event, there is a presumption of the occurrence of a particular event, and thus there is no quantified uncertainty associated with the choice of the source event. Similarly, the description of a source event cannot be framed within the context of a constant recurrence interval.

### 3.2.3 Ground Motion Attenuation

Ground motion is determined at inventory locations as a function of the magnitude and distance of a seismic event and soil data. Multiple attenuation functions process this data and output local ground motions, which are then weighted and combined to arrive at a singular set of ground motion data (PGA, PGV, PGD,  $S_a$ ,  $S_v$ ,  $S_d$ ).

#### *3.2.3.1 Attenuation to Locations Inside the Mississippi Embayment*

Part of the HD thrust was devoted to developing more appropriate attenuation models for the Mississippi Embayment than those currently in use by USGS. Memphis, TN and Cairo, IL are both located within the Mississippi Embayment. Figure 3.2.3.1-1, from Fernandez and Rix (2006), shows the extents of the Embayment.



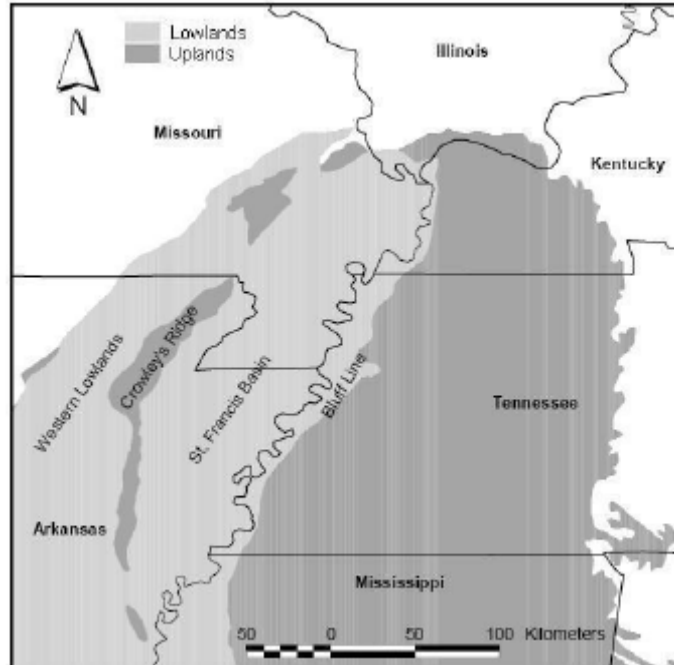


**Figure 3.2.3.1-1. Extents of Mississippi Embayment [from Fernandez and Rix (2006)]**

Fernandez and Rix (2006) used one-corner-frequency (Frankel et al. 1996 and Silva et al. 2003) and two-corner frequency (Atkinson and Boore, 1995) ‘point’ source models for establishing the attenuation relations associated with point epicenters. Three values of median stress drop are used for each of the one-corner-frequency models, resulting in a total of seven attenuation relations (see Table B.3.2.3.1-1). The effects of nonlinear soil were also included in each attenuation relation, using the equivalent linear method (separate from the work conducted for Project HD-4 on response of inelastic soil). Each attenuation relationship predicts ground motions and spectral values as a function of magnitude, distance, soil type (Uplands or Lowlands), and soil depth. See Appendix section B.3.2.3.1 for more information.

Soil maps containing default data (soil type and depth) for the Mississippi Embayment have been incorporated into MAEViz. The default soil values can be modified by the user to adjust soil type (Uplands vs. Lowlands) or soil depth in accordance with more detailed site information, when available, by substituting a revised shape file when MAEViz reads in soil data (all terrain and hazard information are typically to be stored within a GIS database). Magnitude, distance to epicenter, and soil data are passed into the seven Mississippi Embayment attenuation functions, and the function outputs are weighted and combined to arrive at final peak ground motions and spectral values. The attenuation functions are also capable of providing spectral values for 298 periods between 0.01 and 10 seconds.

Aleatory uncertainty was included by the HD team with respect to source (e.g. stress drop, depth), path, and site response parameters, as well as random modeling errors, when developing the attenuation functions for the Mississippi Embayment. See Appendix B 3.2.3.1 for more information.



### *3.2.3.2 USGS Attenuation to Locations Inside the CEUS but Outside the Mississippi Embayment*

When the region of interest is outside of the Mississippi Embayment, the attenuation functions used by USGS in developing its probabilistic maps are more appropriate than those developed within the MAE Center specifically to address the geology of the Mississippi Embayment. The USGS attenuation functions, unlike those developed within the MAE Center for the Mississippi Embayment, do not include the effects of local soil amplification. Therefore, obtaining ground motions outside of the Mississippi Embayment is a two-step process. Probabilistic bedrock motion is determined at a location of interest based on the typical USGS CEUS attenuation functions in the first step, and deterministic site-specific soil amplification effects from NEHRP are included in the second step to determine peak ground surface response and spectral values. MAEViz currently assumes site class D at all locations outside the Mississippi Embayment, unless the user provides more detailed information.

Most USGS CEUS attenuation relations are for site class A (hard rock) site motions, but the site amplification factors in NEHRP are for B/C motions. Wherever the approach of using the deterministic NEHRP factors is employed, correction factors are required to provide more accurate hazard results. Only the Frankel et al. (1996) model provides B/C motions. The spectral acceleration results of the remaining four CEUS attenuation relations must be corrected by the following factors listed in Table 3.1.4-2 (Fernandez, 2006). Values may be linearly interpolated for periods between those listed in the Table. Note that these factors should be applied to actual acceleration values, not the lognormal outputs that are commonly obtained as direct outputs from the attenuation functions. Functions describing the uncertainty associated with the CEUS relations used by USGS are available and ready for implementation in MAEViz.

### *3.2.3.3 Toro and Silva site factors (84°W to 96°W, 36°N to 40°N)*

The NEHRP site factors were developed for the geology of the WUS (see Borchardt, 1994 and Dobry et al., 2000 for discussion on NEHRP soil factors). Hazard estimation for the CEUS outside of the Mississippi Embayment can be improved by using generalized soil amplification factors developed by Toro and Silva (2001) for the Central U.S. rather than the NEHRP soil factors. This method provides a more accurate hazard estimate for the CEUS outside of the Mississippi Embayment, relative to using NEHRP factors, both in terms of geologic effects on seismic response and also in terms of providing insight into the range of uncertainty that should be expected for soil amplification.

### *3.2.3.4 MAEC Attenuation to Locations Inside the CEUS but Outside the Mississippi Embayment*



For the long term future, an approach to computing weighted attenuation in the CEUS outside the Mississippi Embayment is being developed for implementation similar to the approach used within the Mississippi Embayment as described in Section 3.2.3.1.

### 3.2.3.5 USGS Attenuation to WUS Locations

See Section 3.1 and Table 3.1.5-1. The MAEC is not currently developing attenuation models for the WUS.

### 3.2.3.6 Attenuation to Locations outside the US

The MAEC is not currently developing attenuation models outside the US.

## 3.2.4 Implementation of Scenario-Based Ground Shaking Hazard Models

Scenario-based ground shaking hazard models are appropriate for loss assessment studies of many inventory items and interconnected systems over a broad region. In order to obtain the ground shaking hazard for a particular scenario, a magnitude and location of the source event must be specified, as outlined in Section 3.2.2, and appropriate attenuation functions must be selected, as outlined in Section 3.2.3. To improve the accuracy of the hazard estimation, soil data may be updated to better reflect actual conditions when they are known. Weighting factors on attenuation functions may also be adjusted to emphasize certain features of the study region.

The epistemic uncertainty associated with the use of attenuation functions can be quantified by calculating the variance of the function outputs about the mean. For example, the attenuation functions provided by the HD thrust output the natural logarithm of hazard parameters (e.g.,  $\ln(\text{PGA})$ ,  $\ln(S_a)$ ), and the weighting factors provided for the functions used in the Mississippi Embayment are applicable to the natural logarithm values. Epistemic uncertainty is computed as follows:

$$\overline{\ln(y)} = \sum_{i=1}^{n=7} w_i \ln(y_i) \quad (3.2.4-1)$$

$$\beta_e^2 = \sum_{i=1}^{n=7} w_i (\ln(y_i) - \overline{\ln(y)})^2 \quad (3.2.4-2)$$

$$\sum_{i=1}^{n=7} w_i = 1.0 \quad (3.2.4-3)$$

Where  $\ln(y_i)$  is expected value of a ground motion hazard parameter for attenuation function “*i*” based on Monte Carlo simulations considering aleatory uncertainties. The weighting factor,  $w_i$ ,



is the weighting factor associated with attenuation relationship  $i$ , and there are  $n=7$  attenuation relationships used inside the Mississippi Embayment, as shown in Table B.3.2.3.1-1.

The aleatory uncertainty for each attenuation function is computed along with seismic hazard parameters using equations provided by the HD team (see Equation (B.3.2.3.1-3)). The expressions used to compute aleatory uncertainty were derived based on performing Monte Carlo simulations varying the aleatory parameters, such as stress drop, depth to source, path to site, and site response parameters like shear wave velocity profile. Aleatory uncertainty for multiple attenuation functions can be combined mathematically by using the following formula:

$$\beta_a^2 = \sum_{i=1}^{n=7} w_i \beta_{a,i}^2 \quad (3.2.4-4)$$

Where  $\beta_{a,i}$  is the standard deviation representing aleatory uncertainty for an individual attenuation relationship and the weighting factors,  $w_i$ , sum to 1.0 as they did when calculating epistemic uncertainty. Note that the expressions provided for calculating  $\beta_{a,i}$  actually provide the natural log of hazard parameters. Finally, aleatory and epistemic uncertainties can be combined to find the total uncertainty using

$$\beta_{total}^2 = \beta_e^2 + \beta_a^2 \quad (3.2.4-5)$$

### 3.2.5 Implementation of Probabilistic Ground Shaking Hazard Models

Probabilistic hazard maps are appropriate for estimating risk, framed within a time interval, across a study region. The probabilistic hazard represents the consideration of the effects of multiple possible events, and as such, provides an estimation of the probability of exceeding a specified hazard within a certain period of time at a particular location. Since the effects of all considered events are represented for each mapped location, evaluations of system interdependencies will produce unrealistically high risk estimates. Considerations of system interdependencies for probabilistic scenarios must incorporate a deaggregation of the probabilistic hazard into the original source events to obtain realistic results.

Quantifiable uncertainty in probabilistic hazard supplied by the MAE Center is limited to epistemic uncertainties. Aleatory uncertainties are incorporated directly in calculations of the probabilistic seismic hazard curve plotting hazard magnitude versus probability of exceedence. Epistemic uncertainties may be computed as follows:

$$\overline{\ln \lambda} = \sum_{i=1}^n w_i \ln \lambda_i \quad (3.2.5-1)$$

$$\sigma_{total}^2 = \sigma_e^2 = \sum_{i=1}^n w_i (\ln \lambda_i - \overline{\ln \lambda})^2 \quad (3.2.5-2)$$



where  $\lambda_i$  is the annual frequency of exceedance for a given level of ground motion derived using the  $i^{\text{th}}$  attenuation relationship. Mean, mean + sigma, and mean – sigma maps for the Mississippi Embayment have been provided by the HD thrust. If hazard at some fraction of sigma other than +/- 1 is desired, it may be determined as follows.

Note that “sigma” is actually a logarithmic standard deviation. So, to find probabilistic hazard for cases other than mean and mean +/- sigma, use the following steps:

1. Isolate the logstandard deviation of ground motion. This may be done by taking  $\ln(\text{sigma}) = \ln(\text{mean} + \text{sigma}) - \ln(\text{mean})$ .
2. Apply whatever fraction of sigma is desired, x, to the value that was calculated in step 1.
3. Sum  $\ln(\text{mean})$  and x times  $\ln(\text{sigma})$  (from step 2).
4. Obtain hazard in terms of g by raising e, the base of a natural logarithm, to the power of the value calculated in step 3.

As an example, consider hazard level at 3 logstandard deviations (i.e., x = 3 in step 2). The spectral acceleration, Sa, for “mean + 3 sigma” would be  $e^{(\ln(\text{mean Sa}) + 3*\ln(\text{sigma}))}$ , where e is the base of a natural logarithm.

### 3.2.6 Ground Failure Hazard (Liquefaction)

The development of liquefaction maps within the MAE Center for Memphis, Tennessee was coordinated by USGS as part of their Memphis Hazards Mapping Project. As a result of the research conducted during the Memphis Hazards Mapping Project, the MAE Center has been able to develop a generalized approach for estimating liquefaction potential at Memphis, TN (see Appendix B.3.2.6 for a description of the algorithm and the background that influenced its development). Probabilities of liquefaction induced damage are estimated as a function of duration adjusted PGA and regression coefficients correlated to soil types. The ground failure hazard metric used by the MAE Center is liquefaction potential index (LPI). Coefficients are provided to estimate probabilities of  $LPI \geq 5$  and  $LPI \geq 15$ , which correspond to the formation of sand boils and lateral spreading, respectively. See Appendix section B.3.2.6 for further details.

Uncertainty is introduced into LPI (and therefore ground failure hazard estimation) by the limited standard penetration test (SPT) and cone penetration test (CPT) data available, both in terms of the limited number of sampling points and also the lack of a complete set of data for particular samples (many samples do not extend the full depth preferred for LPI determination), the way in which SPT and CPT data are implemented (using all, none, or some weighted portion of each data set), groundwater table elevation, assumed homogeneity of geologic units, and the selection of seismic sources and attenuation functions. However, uncertainty in the liquefaction hazard is not currently characterized quantitatively for the liquefaction hazard algorithm supplied by the MAE Center.



## 4. ENGINEERING ENGINES (FRAGILITY CURVES)

### 4.1 MAEViz Implementation

MAEViz can currently estimate structural damage to buildings and bridges based on ground shaking hazard. Bridge fragilities are functions of PGA, but building fragilities are typically functions of spectral acceleration, and are therefore dependent on period of the structure.

The following modifications are recommended for MAEViz hazard estimation:

- Implement Parametric Fragilities.
- Propagate hazard uncertainty effects through evaluation of vulnerability.
- Implement generalized (HAZUS) nonstructural building fragilities.
- Combine ground shaking and ground failure probabilities of damage.
- Implement transportation lifeline fragilities.
- Implement utility lifeline fragilities.



4.1.1 Implement Parametric Fragilities.

**Algorithm**

Inputs:

Hazard in terms of PGA, 0.2 sec Sa, or 1.0 sec Sa, depending on which fragility sets are being used (hazard is given in master building fragility database).

Three median and lognormal standard deviation pairs for each fragility set (e.g., 3 pairs of  $\lambda$  and  $\beta$  for a low-rise concrete shear wall structure, one pair for each limit state).

Process:

Prompt user to choose whether or not to use MAE Center parametric fragilities.

If user chooses to use parametric fragilities, use mapped fragilities (see Appendix C).

Evaluate probability of exceeding each limit state using Equation (4.1.2-4).

Outputs: probabilities of exceeding limit states at lower bounds of Moderate, Heavy, and Complete damage.

**Example**

Parametric fragilities offer an alternative method of estimating structural damage. Data for mapping of parametric fragilities is provided in Appendix C. These fragilities may be used instead of HAZUS fragilities when the MAE Center has not performed research for a specific building type.

During the preparation of this document, only data for the Lowlands soil profile and 84<sup>th</sup> percentile ground motions were available. In the future, data will be provided for both Uplands and Lowlands at 50<sup>th</sup> and 84<sup>th</sup> percentile ground motions. The choice of included ground motion uncertainty will be a user option, but MAEviz should determine whether Uplands or Lowlands soil underlies a particular building. For the mapping shown below, it is assumed that the user selected to use parametric fragilities keyed to 0.2 second Sa hazard.

**Table 4.1.1-1 Example Building Mapping for Parametric Fragilities  
(Lowlands soil profile, 84<sup>th</sup> percentile ground motions)**

	Default Mapped Parametric Fragility	Default Fragility ID Code
Inventory 1 (I1)	Parametric Pre-Code Low Rise Concrete Frame	SF_C1_42
Inventory 2 (I2)	Parametric Pre-Code Low Rise Unreinforced Masonry	SF_URM_9
Inventory 3 (I3)	Parametric Pre-Code Low Rise Unreinforced Masonry	SF_URM_9



Damage can be estimated using a lognormal standard deviation,

$$P(LS_i | \lambda_{S_a}) = \Phi\left(\frac{\lambda_{S_a} - \lambda_i}{\beta_i}\right) \quad (4.1.1-1)$$

If parametric fragilities were selected for use, then hazard would be calculated based on the hazard parameter appropriate for a specific parametric fragility database, which would be 0.2 second  $S_a$  in this case. In Table 4.1.1-1, the Period column entries are all “N/A (0.2)” because a 0.2 second period is used to estimate hazard, regardless of what the actual period of the structure is.

**Table 4.1.1-1 Example Ground Shaking Hazard Data**

	Latitude	Longitude	Period	$\ln S_a$	
				Mean, $\lambda_{S_a}$	Standard deviation, $\beta_{S_a}$
Inventory 1 (I1)	35.13554 N	90.03732 W	N/A (0.2)	-1.721	0.724
Inventory 2 (I2)	35.22057 N	89.90675 W	N/A (0.2)	-1.714	0.720
Inventory 3 (I3)	35.03183 N	89.89023 W	N/A (0.2)	-1.735	0.729



Structural damage can be estimated by using the hazard data in Table 4.1.1-1 with appropriate fragility parameters in Equation (4.1.1-1), resulting in the probability of exceedence data shown in Table 4.1.1-2.

**Table 4.1.1-2 Sample Structural Fragility Calculations with Parametric Fragilities**

Inventory items		Limit states, $LS_i$		
		PL1	PL2	PL3
I1	$\lambda_i$	-1.0795	-0.3579	0.36233
Concrete Bracci (3-story)	$\beta_i$ $P(LS_i   \lambda_{S_a})$	0.73886 0.193	0.70742 0.027	0.76244 0.003
I2	$\lambda_i$	-1.1881	-0.4848	0.16767
URM Wen (2-story)	$\beta_i$ $P(LS_i   \lambda_{S_a})$	0.9164 0.283	0.9241 0.092	0.9087 0.019
I3	$\lambda_i$	-1.1881	-0.4848	0.16767
URM Wen (2-story)	$\beta_i$ $P(LS_i   \lambda_{S_a})$	0.9164 0.275	0.9241 0.088	0.9087 0.018



#### 4.1.2 Propagate hazard uncertainty effects through evaluation of vulnerability.

##### **Algorithm**

###### Inputs:

Median and lognormal standard deviation of hazard in terms of PGA or Sa.

Three median and lognormal standard deviation pairs for each fragility set.

###### Process:

Compute equivalent lognormal uncertainty using Equation (4.1.2-1).

Use equivalent lognormal uncertainty from Equation (4.1.2-1) in Equation (4.1.1-1).

NOTE: If structure type uncertainty is considered, calculate damage for each structure type in the inventory.

Outputs: probabilities of exceeding limit states at lower bounds of Moderate, Heavy, and Complete damage, adjusted for hazard uncertainty.

##### **Example**

When hazard uncertainty is quantified (see Table 3.1.1-1), that effect can be reflected in the estimation of vulnerability. A closed form approach has been developed by J. Song within the MAE Center to reflect hazard uncertainty in damage estimation (see Appendix D for more information). The first step is to evaluate an equivalent lognormal standard deviation, as shown in Equation (4.1.2-1).

$$\beta_{i,equiv} = \sqrt{(\beta_i)^2 + (\beta_{S_a})^2} \quad (4.1.2-1)$$

Where  $\beta_{S_a}$  is the standard deviation of hazard (obtained directly from attenuation functions), and  $\beta_i$  is the lognormal standard deviation used in defining a fragility. The calculation generally has the effect of flattening the fragility curve, reflecting a greater degree of uncertainty in damage estimation. MAEViz calculations to date have assumed that hazard estimation is perfect, i.e., has no uncertainty. Table 4.1.2-1 shows the  $\lambda$  and  $\beta$  terms used to evaluate damage for the sample buildings, as well as the estimations of probability of exceedence when considering the effects of hazard uncertainty.



**Table 4.1.2-1 Sample Structural Fragility Calculations**

Inventory items		Limit states, $LS_i$		
		PL1	PL2	PL3
I1	$\lambda_i$	-1.99	-1.52	-1.17
Concrete	$\beta_i$	0.51	0.39	0.43
Bracci (3-story)	$P(LS_i)$	0.608	0.423	0.293
I2	$\lambda_i$	-1.89	-1.20	-0.69
URM	$\beta_i$	0.30	0.30	0.33
Wen (2-story)	$P(LS_i)$	0.686	0.382	0.194
I3	$\lambda_i$	-1.89	-1.20	-0.69
URM	$\beta_i$	0.30	0.30	0.33
Wen (2-story)	$P(LS_i)$	0.663	0.362	0.182

If uncertainty is considered for the inventory, then these same fragility calculations would need to be performed for each building type for each building. In this small example, considering only the three given buildings to be the entirety of the inventory, calculations would have to be performed for a URM structure subjected to the I1 hazard and for a concrete structure subjected to the I2 and I3 hazards.



### 4.1.3 Implement generalized (HAZUS) nonstructural building fragilities.

#### **Algorithm**

##### Inputs:

Hazard in terms of  $S_a$ .

Building period obtained from inventory database.

Three median and lognormal standard deviation pairs for each fragility set, for each type of nonstructural assets (acceleration-sensitive (AS NS) and drift-sensitive (DS NS)).

##### Process:

Calculate equivalent lognormal spectral displacement using lognormal spectral acceleration and building period, as shown in Equation (4.1.3-2).

Compute equivalent lognormal uncertainty using Equation (4.1.2-1).

Evaluate AS NS and DS NS fragilities similarly to building structural fragilities, using equivalent lognormal uncertainty from Equation (4.1.2-1) in Equation (4.1.1-1) for each limit state.

NOTE: If structure type uncertainty is considered, calculate damage for each structure type in the inventory.

Outputs: probabilities of exceeding limit states at lower bounds of Moderate, Heavy, and Complete damage, adjusted for hazard uncertainty, for AS NS and DS AS components.

#### **Example**

Most buildings will not have data to define specific nonstructural entity attributes, so a generalized approach will be implemented in the interim, pending more refined data and algorithms.  $\lambda$  and  $\beta$  parameters to define two generalized types of nonstructural assets, drift-sensitive and acceleration-sensitive, have been provided in the master fragility database. The analysis approach is similar to that used for structural vulnerability. The only significant difference being that drift-sensitive fragilities use spectral displacement rather than spectral acceleration as a hazard parameter. To evaluate drift-sensitive damage, the typical fragility expression in terms of spectral acceleration (see Equation 4.1.2-4) will need to be adjusted to use spectral displacements, as shown in Equation (4.1.3-1).

$$P(LS_i) = \Phi\left(\frac{\lambda_{S_d} - \lambda_i}{\beta_i}\right) \quad (4.1.3-1)$$

where  $\lambda_i$  and  $\beta_i$  are median and lognormal standard deviation of capacity in terms of spectral displacement, and the mean demand in terms of lognormal spectral displacement may be related to the mean demand in terms of spectral acceleration (that is, the typical direct output of attenuation functions) using



$$\lambda_{S_d} = \lambda_{S_a} + \ln(9.78 \cdot T^2) \quad (4.1.3-2)$$

The natural period, T, is obtained for each structure from the inventory database (see Section 2.1.2). In accordance with the mapping shown in Appendix C, nonstructural fragilities used for I1 correlate to pre-code, low-rise concrete frame buildings in HAZUS, and nonstructural fragilities used for I2 and I3 correlate to pre-code, low-rise unreinforced masonry. Sample fragility calculations for nonstructural inventory are provided in Tables 4.1.3-1 and 4.1.3-2.

**Table 4.1.3-1 Sample Acceleration-Sensitive Nonstructural Fragility Calculations**

Inventory items		Limit states, $LS_i$		
		PL1	PL2	PL3
I1	$\lambda_i$	-0.92	-0.22	0.47
Concrete Bracci (3-story)	$\beta_i$	0.68	0.68	0.68
	$P(LS_i)$	0.239	0.092	0.026
I2	$\lambda_i$	-0.92	-0.22	0.47
URM Wen (2-story)	$\beta_i$	0.65	0.65	0.65
	$P(LS_i)$	0.302	0.119	0.033
I3	$\lambda_i$	-0.92	-0.22	0.47
URM Wen (2-story)	$\beta_i$	0.65	0.65	0.65
	$P(LS_i)$	0.287	0.112	0.031



**Table 4.1.3-2 Sample Drift-Sensitive Nonstructural Fragility Calculations**

Inventory items		Limit states, $LS_i$		
		PL1	PL2	PL3
I1	$\lambda_i$	0.36	1.50	2.20
Concrete Bracci (3-story)	$\beta_i$	0.98	0.93	1.03
	$P(LS_i)$	0.532	0.210	0.102
I2	$\lambda_i$	0.08	1.22	1.91
URM Wen (2-story)	$\beta_i$	1.23	1.23	1.03
	$P(LS_i)$	0.425	0.169	0.055
I3	$\lambda_i$	0.08	1.22	1.91
URM Wen (2-story)	$\beta_i$	1.23	1.23	1.03
	$P(LS_i)$	0.412	0.162	0.052



4.1.4 Combine ground shaking and ground failure probabilities of damage.

**Algorithm**

Inputs:

Probability of exceeding each limit state for structural, AS NS, and DS NS components, as described in Sections 4.1.2 and 4.1.3 (ground shaking hazard).

Probability of major liquefaction, from Section 3.1.2 (ground failure hazard).

Process:

Compute probabilities of exceeding limit states based solely on liquefaction, as shown in Equations (4.1.4-1) through (4.1.4-4).

Compute combined probabilities of exceeding limit states based on both ground shaking and liquefaction, as shown in Equations (4.1.4-5) through (4.1.4-7). Repeat this process three times, once each for structural, AS NS, and DS NS damage.

Compute discrete combined probabilities of damage states, as shown in Equations (4.1.4-8) through (4.1.4-11). Repeat this process three times, once each for structural, AS NS, and DS NS damage.

NOTE: If structure type uncertainty is considered, calculate discrete damage state probabilities for each component of each structure type in the inventory.

Outputs: discrete probabilities of damage states resulting from both ground shaking and ground failure hazard, for structural, AS NS, and DS AS components.

**Example**

Ground failure (liquefaction) is considered to cause complete damage when  $LPI > 15$ , and to not cause appreciable damage otherwise. The calculation to estimate the probability of  $LPI > 15$  was shown in Section 3.1.2. Table 4.1.4-1 shows the interpretation of ground failure hazard calculations relative to damage states.

**Table 4.1.4-1 Probabilities of Exceeding Damage State Thresholds caused by Ground Failure**

	P(LPI>15)	Limit states, $LS_i$		
		PL1	PL2	PL3
Inventory 1 (I1)	0.0151	0.0151	0.0151	0.0151
Inventory 2 (I2)	0.0196	0.0196	0.0196	0.0196
Inventory 3 (I3)	0.0193	0.0193	0.0193	0.0193



The data shown in Table 4.1.4-1 can be written in equation form as follows

$$P_{GF}(PL1) = P(LPI \geq 15) \quad (4.1.4-1)$$

$$P_{GF}(PL2) = P(LPI \geq 15) \quad (4.1.4-2)$$

$$P_{GF}(PL3) = P(LPI \geq 15) \quad (4.1.4-3)$$

Where the GF subscript indicates that the probability is based on ground failure. Next, the probabilities of damage states resulting from combinations of ground shaking (GS) and ground failure (GF) hazard types are calculated by:

$$P_{COMB}(DS \geq C) = P_{GS}(PL3) + P_{GF}(PL3) - P_{GS}(PL3) \times P_{GF}(PL3) \quad (4.1.4-4)$$

$$P_{COMB}(DS \geq H) = P_{GS}(PL2) + P_{GF}(PL2) - P_{GS}(PL2) \times P_{GF}(PL2) \quad (4.1.4-5)$$

$$P_{COMB}(DS \geq M) = P_{GS}(PL1) + P_{GF}(PL1) - P_{GS}(PL1) \times P_{GF}(PL1) \quad (4.1.4-6)$$

$$P_{GF}(DS \geq I) = 1 \text{ in all cases by definition} \quad (4.1.4-7)$$

Where the probabilities of exceedence based on ground shaking were calculated as shown in Sections 4.1.2 and 4.1.3. The damage states in Equations (4.1.4-4) through (4.1.4-7) correspond to Complete (C), Heavy (H), Moderate (M), and Insignificant (I). This process is carried out for structural, acceleration-sensitive nonstructural, and drift-sensitive nonstructural probabilities of exceeding damage states. For this example, the combined probabilities of exceeding damage states are given in Table 4.1.4-2, where AS NS indicates acceleration-sensitive nonstructural, and DS NS indicates drift-sensitive nonstructural.

As an example, to calculate the combined probability of exceedence of Moderate damage (probability that damage will be at least “Moderate”) for structural damage to item I1, the probability of ground shaking damage causing at least Moderate damage is 0.608 (from Table 4.1.2-1) and the probability of ground failure damage causing at least Moderate damage is 0.0151 (from Table 4.1.4-1). Equation (4.1.4-6) can then be used to obtain

$$P_{COMB}(DS \geq M) = 0.608 + 0.0151 - 0.608 \times 0.0151$$

$$P_{COMB}(DS \geq M) = 0.614$$

For another example calculation, combined probability of exceedence of Heavy acceleration-sensitive nonstructural damage for item I2 can be calculated using the probability of ground shaking damage causing at least Heavy damage, 0.119 from Table 4.1.3-1, and the probability of



ground failure damage causing at least Heavy damage, 0.0196 from Table 4.1.4-1, in Equation (4.1.4-5) to obtain

$$P_{COMB}(DS \geq H) = 0.119 + 0.0196 - 0.119 \times 0.0196$$

$$P_{COMB}(DS \geq H) = 0.137$$

**Table 4.1.4-2 Sample Combined Probabilities of Exceedence**

Inventory items		Damage states, $DS_i$		
		Moderate (M)	Heavy (H)	Complete (C)
I1 Concrete Bracci (3-story)	Structural	0.614	0.432	0.304
	AS NS	0.250	0.105	0.040
	DS NS	0.539	0.222	0.115
I2 URM Wen (2-story)	Structural	0.692	0.395	0.209
	AS NS	0.315	0.137	0.052
	DS NS	0.437	0.185	0.073
I3 URM Wen (2-story)	Structural	0.670	0.375	0.197
	AS NS	0.301	0.129	0.050
	DS NS	0.424	0.178	0.070

Finally, the discrete probabilities of occurrence for each damage state are:

$$P_{COMB}(DS = C) = P_{COMB}(DS \geq C) \quad (4.1.4-8)$$

$$P_{COMB}(DS = H) = P_{COMB}(DS \geq H) - P_{COMB}(DS \geq C) \quad (4.1.4-9)$$

$$P_{COMB}(DS = M) = P_{COMB}(DS \geq M) - P_{COMB}(DS \geq H) \quad (4.1.4-10)$$

$$P_{COMB}(DS = I) = 1 - P_{COMB}(DS \geq M) \quad (4.1.4-11)$$

For example, the probability of the Insignificant damage state, based on combined ground shaking and ground failure hazards, for acceleration-sensitive nonstructural assets in item I2 is determined using the probability of at least Moderate damage, 0.315 in Table 4.1.4-2, and Equation (4.1.4-11).



$$P_{COMB}[DS = I] = 1 - 0.315$$

$$P_{COMB}[DS = I] = 0.685$$

**Table 4.1.4-3 Sample Discrete Probabilities of Damage States for Combined Hazard**

Inventory items		Damage states, $DS_i$			
		Insignificant (I)	Moderate (M)	Heavy (H)	Complete (C)
I1 Concrete Bracci (3-story)	Structural	0.386	0.182	0.128	0.304
	AS NS	0.750	0.145	0.065	0.040
	DS NS	0.461	0.317	0.107	0.115
I2 URM Wen (2-story)	Structural	0.308	0.297	0.186	0.209
	AS NS	0.685	0.178	0.085	0.052
	DS NS	0.563	0.252	0.112	0.073
I3 URM Wen (2-story)	Structural	0.330	0.295	0.178	0.197
	AS NS	0.699	0.172	0.079	0.050
	DS NS	0.576	0.246	0.108	0.070



#### 4.1.5 Implement transportation lifeline fragilities.

##### Algorithm

##### Inputs:

Hazard in terms of PGA.

Four median and lognormal standard deviation pairs for each fragility set.

##### Process:

Evaluate probability of exceeding each limit state using Equation (4.1.5-1).

Compute discrete probabilities of damage states, as shown in Equations (4.1.5-2) through (4.1.5-6).

Outputs: discrete probabilities of None, Slight, Moderate, Extreme, and Complete damage states.

##### Example

Bridge damage may be estimated by applying Equation (4.1.5-1) to obtain the results shown in Table 4.1.5-1. Note that  $\lambda_i = \text{LN}(\text{Median PGA})$  for each fragility curve.

$$P(LS_i | \lambda_{PGA}) = \Phi\left(\frac{\lambda_{PGA} - \lambda_i}{\beta_i}\right) \quad (4.1.5-1)$$

**Table 4.1.5-1 Sample Bridge Fragility Calculations**

Parameters	Damage States, DS <sub>i</sub>			
	Slight	Moderate	Extensive	Complete
Bridge 1				
$\lambda_i$	-1.050	0.285	0.604	0.916
$\beta_i$	0.9	0.9	0.9	0.9
$P(LS_i   \lambda_{PGA})$	0.1872	0.0089	0.0032	0.0011
Bridge 2				
$\lambda_i$	-1.833	-0.635	-0.288	0.010
$\beta_i$	0.7	0.7	0.7	0.7
$P(LS_i   \lambda_{PGA})$	0.4884	0.0409	0.0127	0.0039
Bridge 3				
$\lambda_i$	-1.661	-1.139	-0.892	-0.673
$\beta_i$	0.5	0.5	0.5	0.5
$P(LS_i   \lambda_{PGA})$	0.3490	0.0763	0.0270	0.0091



To obtain discrete probabilities of damage states, use equations (4.1.5-2) through (4.1.5-6), where N corresponds to a None damage state.

$$P(DS = C) = P(DS \geq C) \quad (4.1.5-2)$$

$$P(DS = E) = P(DS \geq E) - P(DS \geq C) \quad (4.1.5-3)$$

$$P(DS = M) = P(DS \geq M) - P(DS \geq E) \quad (4.1.5-4)$$

$$P(DS = S) = P(DS \geq S) - P(DS \geq M) \quad (4.1.5-5)$$

$$P(DS = N) = 1 - P(DS \geq S) \quad (4.1.5-6)$$

The discrete probabilities of damage states for the sample bridges are shown in Table 4.1.5-2.

**Table 4.1.5-2 Sample Bridge Probabilities of Damage**

	Probabilities of Damage States, DS <sub>i</sub>				
	None	Slight	Moderate	Extensive	Complete
Bridge 1	0.8128	0.1783	0.0056	0.0021	0.0011
Bridge 2	0.5116	0.4475	0.0283	0.0088	0.0039
Bridge 3	0.6510	0.2727	0.0492	0.0180	0.0091



#### 4.1.6 Implement utility lifeline fragilities.

##### *Electric Power Plants*

##### **Algorithm**

##### Inputs:

Hazard in terms of PGA and Sa.

One median and lognormal standard deviation pair for each fragility set, one set for each component, as shown in Tables 4.1.6-1 through 4.1.6-3.

##### Process:

Evaluate probability of exceeding the limit state for each component using Equation (4.1.2-4) for Sa or Equation (4.1.5-1) for PGA, depending on particular component (see Tables 2.1.2.3-1 through 2.1.2.3-3).

Outputs: probabilities of damaged component for each component.

##### **Example**

Tables 4.1.6-1 through 4.1.6-3 present the fragility curve information for electric power plant components. Note that  $\lambda_i = \text{LN}(\text{Median PGA})$  for each fragility curve. The fragilities are calibrated to use either PGA or Sa, as noted in the Tables 2.1.2.3-1 through 2.1.2.3-3, in a logstandard CDF (similar to buildings with Sa and bridges with PGA).

**Table 4.1.6-1 Electric Power Plant Equipment - Electrical Components - Well Anchored**

Component ID Code	Component	Median A (g)	$\beta$
EPP_EC_1	Diesel Generators	0.65	0.40
EPP_EC_2	Battery Racks	2.29	0.50
EPP_EC_3	Switchgear	2.33	0.81
EPP_EC_4	Instrument Racks and Panels	1.15	0.82
EPP_EC_5	Control Panels	11.50	0.88
EPP_EC_6	Aux. Relay Cabinets / MCCs / Circuit Breakers	7.63	0.88
EPP_EC_7	Turbine	0.30	0.40



**Table 4.1.6-2 Electric Power Plant Equipment - Mechanical Equipment - Well Anchored**

Component ID Code	Component	Median A (g)	$\beta$
EPP_MC_1	Large vertical vessels with formed heads	1.46	0.40
EPP_MC_2	Boilers and Pressure Vessels	1.30	0.70
EPP_MC_3	Large horizontal vessels	3.91	0.61
EPP_MC_4	Small to medium horizontal vessels	1.84	0.51
EPP_MC_5	Large vertical pumps	2.21	0.39
EPP_MC_6	Motor Driven pumps	3.19	0.34
EPP_MC_7	Large Motor Operated Valves	4.83	0.65
EPP_MC_8	Large Hydraulic and Air Actuated Valves	7.61	0.46
EPP_MC_9	Large Relief, Manual and Check Valves	8.90	0.40
EPP_MC_10	Small Motor Operated Valves	9.84	0.65

**Table 4.1.6-3 Electric Power Plant Equipment - Other Equipment**

Component ID Code	Component	Median A (g)	$\beta$
EPP_OTH_1	Cable Trays	2.23	0.39
EPP_OTH_2	HVAC Ducting	3.97	0.54
EPP_OTH_3	HVAC Equipment – Fans	2.24	0.34



Applying the fragility parameters given above to the sample power plant inventory, probability of damage may be estimated as shown in Table 4.1.6-4. Note the power plant component fragilities estimate the probability of damage occurring to a particular component, not the probability of falling into one of several damage states, as was the case with buildings and bridges.

**Table 4.1.6-4 Sample Electric Power Plant Fragility Calculations**

	Component	Component ID Code	$\lambda_i$	$\beta_i$	P(damage   $\mu$ )
EPP 1	Boilers + Steam Generators	EPP_MC_2	0.2624	0.70	0.0015
EPP 2	Boilers + Steam Generators	EPP_MC_2	0.2624	0.70	0.0041
EPP 3	Boilers + Steam Generators	EPP_MC_2	0.2624	0.70	0.0042



## *Electric Substations*

### **Algorithm**

#### **Inputs:**

Hazard in terms of PGA.

One median and lognormal standard deviation pair for each fragility set, one set for each component, as shown in Tables 4.1.6-5 through 4.1.6-7.

#### **Process:**

Evaluate probability of exceeding the limit state for each component using Equation (4.1.2-4) for  $S_a$  or Equation (4.1.5-1) for PGA, depending on particular component (see Tables 2.1.2.3-1 through 2.1.2.3-3).

**Outputs:** probabilities of damaged component for each component.

### **Example**

Tables 4.1.6-5 through 4.1.6-7 present the fragility curve information for electric substation components. The fragilities are calibrated to use PGA in a logstandard CDF (similar to bridges). Note that  $\lambda_i = \text{LN}(\text{Median PGA})$  for each fragility curve.



**Table 4.1.6-5 VHV Substation Components (500 kV and Higher)**

Component ID Code	Component	Median A (g)	$\beta$
ESS_VHV_1	Transformer - Anchored	0.40	0.70
ESS_VHV_2	Transformer - Unanchored	0.25	0.70
ESS_VHV_3	Live Tank Circuit Breaker - Standard	0.30	0.70
ESS_VHV_4	Live Tank Circuit Breaker - Seismic	0.40	0.70
ESS_VHV_5	Dead Tank Circuit Breaker - Standard	0.70	0.70
ESS_VHV_6	Disconnect Switch - Rigid Bus	0.40	0.70
ESS_VHV_7	Disconnect Switch - Flexible Bus	0.60	0.70
ESS_VHV_8	Lightning Arrestor	0.40	0.70
ESS_VHV_9	CCVT - Cantilevered	0.90	0.60
ESS_VHV_10	CCVT - Suspended	0.30	0.70
ESS_VHV_11	Current Transformer (gasketed)	0.30	0.70
ESS_VHV_12	Current Transformer (flanged)	0.80	0.70
ESS_VHV_13	Wave Trap - Cantilevered	0.50	0.70
ESS_VHV_14	Wave Trap - Suspended	1.30	0.60
ESS_VHV_15	Bus Structure - Rigid	0.40	0.70
ESS_VHV_16	Bus Structure - Flexible	2.00	0.70
ESS_VHV_17	Other Yard Equipment	0.40	0.70



**Table 4.1.6-6 HV Substation Components (165kV - 350 kV)**

Component ID Code	Component	Median A (g)	$\beta$
ESS_HV_1	Transformer - Anchored	0.60	0.70
ESS_HV_2	Transformer - Unanchored	0.30	0.70
ESS_HV_3	Live Tank Circuit Breaker - Standard	0.50	0.70
ESS_HV_4	Live Tank Circuit Breaker - Seismic	0.70	0.70
ESS_HV_5	Dead Tank Circuit Breaker - Standard	1.60	0.70
ESS_HV_6	Disconnect Switch - Rigid Bus	0.50	0.70
ESS_HV_7	Disconnect Switch - Flexible Bus	0.75	0.70
ESS_HV_8	Lightning Arrestor	0.60	0.70
ESS_HV_9	CCVT	0.60	0.70
ESS_HV_10	Current Transformer (gasketed)	0.50	0.70
ESS_HV_11	Wave Trap - Cantilevered	0.60	0.70
ESS_HV_12	Wave Trap - Suspended	1.40	0.60
ESS_HV_13	Bus Structure - Rigid	0.60	0.70
ESS_HV_14	Bus Structure - Flexible	2.00	0.70
ESS_HV_15	Other Yard Equipment	0.60	0.70



**Table 4.1.6-7 MHV Substation Components (100 kV - 165kV)**

Component ID Code	Component	Median A (g)	$\beta$
ESS_MHV_1	Transformer - Anchored	0.75	0.70
ESS_MHV_2	Transformer - Unanchored	0.50	0.70
ESS_MHV_3	Live Tank Circuit Breaker - Standard	0.60	0.70
ESS_MHV_4	Live Tank Circuit Breaker - Seismic	1.00	0.70
ESS_MHV_5	Dead Tank Circuit Breaker - Standard	2.00	0.70
ESS_MHV_6	Disconnect Switch - Rigid Bus	0.90	0.70
ESS_MHV_7	Disconnect Switch - Flexible Bus	1.20	0.70
ESS_MHV_8	Lightning Arrestor	1.00	0.70
ESS_MHV_9	CCVT	1.00	0.70
ESS_MHV_10	Current Transformer (gasketed)	0.75	0.70
ESS_MHV_11	Wave Trap - Cantilevered	1.00	0.70
ESS_MHV_12	Wave Trap - Suspended	1.60	0.60
ESS_MHV_13	Bus Structure - Rigid	1.00	0.70
ESS_MHV_14	Bus Structure - Flexible	2.00	0.70
ESS_MHV_15	Other Yard Equipment	1.00	0.70



Applying the fragility parameters given above to the sample substation inventory, probability of damage may be estimated as shown in Table 4.1.6-8. Note the substation component fragilities estimate the probability of damage occurring to a particular component, not the probability of falling into one of several damage states, as was the case with buildings and bridges.

**Table 4.1.6-8 Sample Electric Substation Fragility Calculations**

	Component	Component ID Code	$\lambda_i$	$\beta_i$	P(damage   $\lambda_{Sa}$ or $\lambda_{PGA}$ )
ESS 1	Transformer - Anchored	ESS_MHV_1	-0.2877	0.70	0.0093
ESS 2	Transformer - Unanchored	ESS_MHV_2	-0.6931	0.70	0.0472
ESS 3	Live Tank Circuit Breaker - Standard	ESS_VHV_3	-1.2040	0.70	0.1780



## Water Tanks

### Algorithm

#### Inputs:

Hazard in terms of PGA.

Four median and lognormal standard deviation pairs for each fragility set, as shown in Tables 4.1.6-9 through 4.1.6-11. Particular  $\lambda$ ,  $\beta$  pairs used for any given water tank depend on the mapping scheme chosen in 2.1.1.3 (Tables 2.1.1.3-9 through 2.1.1.3-11).

#### Process:

Evaluate probability of exceeding each limit state using Equation (4.1.5-1).

Compute discrete probabilities of damage states, as shown in Equations (4.1.5-2) through (4.1.5-6).

Outputs: discrete probabilities of None, Slight, Moderate, Extreme, and Complete damage states.

### Example

The following Tables provide data for water tank fragilities. All water tank fragilities are calibrated to use PGA as the hazard parameter in a logstandard CDF (similar to bridges). If no data is supplied to allow mapping, use the first fragility given in Table 4.1.6-10 (Fill  $\geq$  50%, N=251) as a default. Table 4.1.6-9 shows fragilities dependant upon the amount of fluid in the tank, and Table 4.1.6-10 presents fragility information dependant upon the anchorage of the tank. These parameters can be used to map appropriate fragilities to inventory, assuming the user has the required data. Note that  $\lambda_i = \text{LN}(\text{Median PGA})$  for each fragility curve.

**Table 4.1.6-9 Water Tank Fragility Curves from Eiding (2001) by % Fill**

Damage State	All Tanks, N=531		Fill < 50%, N=95		Fill $\geq$ 50%, N=251		Fill $\geq$ 60%, N=209		Fill $\geq$ 90%, N=120	
	Median	$\beta$	Median	$\beta$	Median	$\beta$	Median	$\beta$	Median	$\beta$
Slight Damage	0.38	0.80	0.56	0.80	0.18	0.80	0.22	0.80	0.13	0.07
Moderate Damage	0.86	0.80	>2.0	0.40	0.73	0.80	0.70	0.80	0.67	0.80
Extensive Damage	1.18	0.61			1.14	0.80	1.09	0.80	1.01	0.80
Complete Damage	1.16	0.07			1.16	0.40	1.16	0.41	1.15	0.10

**Table 4.1.6-10 Water Tank Fragility Curves from Eiding (2001) by Anchorage**

Damage State	Fill $\geq$ 50%, N=251		Fill $\geq$ 50%, Anchored N=46		Fill $\geq$ 50%, Unanchored N=205	
	Median	$\beta$	Median	$\beta$	Median	$\beta$
Slight Damage	0.18	0.80	0.71	0.80	0.15	0.12
Moderate Damage	0.73	0.80	2.36	0.80	0.62	0.80
Extensive Damage	1.14	0.80	3.72	0.80	1.06	0.80
Complete Damage	1.16	0.80	4.26	0.80	1.13	0.10



Table 4.1.6-11 presents water tank fragility curves separated by the height to diameter ratio (H/D) and by the percentage of fluid in the tank. Median values given in the tables are values of PGA with units of g. Note that  $\lambda_i = \text{LN}(\text{Median PGA})$  for each fragility curve.

**Table 4.1.6-11 Water Tank Fragility Curves from O'Rourke and So (1999)**

Damage State	All Tanks		H/D < 0.70		H/D >= 0.70		% Full > 50%	
	Median	$\beta$	Median	$\beta$	Median	$\beta$	Median	$\beta$
Slight	0.70	0.48	0.67	0.50	0.45	0.47	0.49	0.55
Moderate	1.10	0.35	1.18	0.34	0.69	0.32	0.86	0.39
Extensive	1.29	0.28	1.56	0.35	0.89	0.21	0.99	0.27
Complete	1.35	0.22	1.79	0.29	1.07	0.15	1.17	0.21

Damage States (O'Rourke, M and So 1999)

- None No Damage
- Slight Damage to roof, minor loss of content, minor shell damage, no elephant foot failure
- Moderate Elephant foot bucking with no leak or minor loss of contents
- Extensive Elephant foot buckling with major loss of content, severe damage
- Complete Total failure, tank collapse



The fragility curves applied to inventory and resulting probabilities of damage will vary depending on how the user chooses to map inventory to fragilities. If the user chooses to map to fragilities based on fill, the data shown in Table 4.1.6-12 is obtained, assuming the user has provided fill data for all tanks. The “All Tanks” fragility is not used unless the user specifically maps to it. Note that the probabilities shown are probabilities of exceedence.

**Table 4.1.6-12 Sample Water Tank Fragility Calculations when Mapping by Fill  
(assumes user provides fill data)**

	Fill	Fragility	Parameters	Damage States, DS <sub>i</sub>			
				Slight	Moderate	Extensive	Complete
Water Tank 1	40	Fill < 50%	$\lambda_i$	-0.57982	0.693147	2.302585	2.302585
			$\beta_i$	0.80	0.40	0.00	0.00
			$P(LS_i   \lambda_{PGA})$	0.056	0.000	0.000	0.000
Water Tank 2	55	50% ≤ Fill < 60%	$\lambda_i$	-1.7148	-0.31471	0.131028	0.14842
			$\beta_i$	0.80	0.80	0.80	0.40
			$P(LS_i   \lambda_{PGA})$	0.432	0.027	0.007	0.000
Water Tank 3	80	60% ≤ Fill < 90%	$\lambda_i$	-1.51413	-0.35667	0.086178	0.14842
			$\beta_i$	0.80	0.80	0.80	0.41
			$P(LS_i   \lambda_{PGA})$	0.333	0.030	0.008	0.000



Alternatively, if the user chooses to map based on fill, but does not provide fill data for some or all of the tanks, use the fragility for fill greater than or equal to 50% and less than 60%. Using that mapping, the data shown in Figure 4.1.6-13 is obtained.

**Table 4.1.6-13 Sample Water Tank Fragility Calculations when Mapping by Fill  
(assumes user does NOT provide fill data)**

	Fill	Fragility	Parameters	Damage States, DS <sub>i</sub>			
				Slight	Moderate	Extensive	Complete
Water Tank 1		50% <=	$\lambda_i$	-1.7148	-0.31471	0.131028	0.14842
		Fill	$\beta_i$	0.80	0.80	0.80	0.40
		< 60%	$P(LS_i   \lambda_{PGA})$	0.433	0.027	0.007	0.000
Water Tank 2		50% <=	$\lambda_i$	-1.7148	-0.31471	0.131028	0.14842
		Fill	$\beta_i$	0.80	0.80	0.80	0.40
		< 60%	$P(LS_i   \lambda_{PGA})$	0.432	0.027	0.007	0.000
Water Tank 3		50% <=	$\lambda_i$	-1.7148	-0.31471	0.131028	0.14842
		Fill	$\beta_i$	0.80	0.80	0.80	0.40
		< 60%	$P(LS_i   \lambda_{PGA})$	0.429	0.027	0.006	0.000



If the user chooses to map to fragilities based on anchorage, the data shown in Table 4.1.6-14 is obtained, assuming the user has provided fill data for all tanks. Note that the probabilities shown are probabilities of exceedence.

**Table 4.1.6-14 Sample Water Tank Fragility Calculations when Mapping by Anchorage  
(assumes user provides anchorage data)**

	Anchored	Fragility	Parameters	Damage States, $DS_i$			
				Slight	Moderate	Extensive	Complete
Water Tank 1	N	Unanchored	$\lambda_i$	-1.89712	-0.47804	0.058269	0.122218
			$\beta_i$	0.12	0.80	0.80	0.10
			$P(LS_i   \lambda_{PGA})$	0.653	0.043	0.009	0.000
Water Tank 2	Y	Anchored	$\lambda_i$	-0.34249	0.858662	1.313724	1.449269
			$\beta_i$	0.80	0.80	0.80	0.80
			$P(LS_i   \lambda_{PGA})$	0.030	0.000	0.000	0.000
Water Tank 3	Y	Anchored	$\lambda_i$	-0.34249	0.858662	1.313724	1.449269
			$\beta_i$	0.80	0.80	0.80	0.80
			$P(LS_i   \lambda_{PGA})$	0.029	0.000	0.000	0.000



Alternatively, if the user chooses to map based on anchorage, but does not provide anchorage data for some or all of the tanks, use the fragility which represents an average of the anchored and unanchored water tank fragilities. Using that mapping, the data shown in Figure 4.1.6-15 is obtained.

**Table 4.1.6-15 Sample Water Tank Fragility Calculations when Mapping by Anchorage  
(assumes user does NOT provide anchorage data)**

Anchored	Fragility	Parameters	Damage States, DS <sub>i</sub>			
			Slight	Moderate	Extensive	Complete
Water Tank 1	Anchorage Unknown	$\lambda_i$	-1.7148	-0.31471	0.131028	0.14842
		$\beta_i$	0.80	0.80	0.80	0.80
		$P(LS_i   \lambda_{PGA})$	0.433	0.027	0.007	0.000
Water Tank 2	Anchorage Unknown	$\lambda_i$	-1.7148	-0.31471	0.131028	0.14842
		$\beta_i$	0.80	0.80	0.80	0.80
		$P(LS_i   \lambda_{PGA})$	0.432	0.027	0.007	0.000
Water Tank 3	Anchorage Unknown	$\lambda_i$	-1.7148	-0.31471	0.131028	0.14842
		$\beta_i$	0.80	0.80	0.80	0.80
		$P(LS_i   \lambda_{PGA})$	0.429	0.027	0.006	0.000



If the user chooses to map to fragilities based on H/D ratio, the data shown in Table 4.1.6-16 is obtained, assuming the user has provided H/D data and fill level for all tanks. The H/D ratio only enters the mapping if the fill level of the water tank is less than or equal to 50%. The “All Tanks” fragility based on H/D is not used unless the user specifically maps to it. Note that the probabilities shown are probabilities of exceedence.

**Table 4.1.6-16 Sample Water Tank Fragility Calculations when Mapping by H/D and Fill**  
(assumes user provides H, D, and fill data)

	H/D	% Fill > 50 ?	Fragility	Parameters	Damage States, DS <sub>i</sub>			
					Slight	Moderate	Extensive	Complete
Water Tank 1	0.67	False	H/D < 0.7	$\lambda_i$	-0.40048	0.165514	0.444686	0.582216
				$\beta_i$	0.50	0.34	0.35	0.29
				$P(LS_i   \lambda_{PGA})$	0.002	0.000	0.000	0.000
Water Tank 2	2.00	True	Fill > 50%, H/D is N/A	$\lambda_i$	-0.71335	-0.15082	-0.01005	0.157004
				$\beta_i$	0.55	0.39	0.27	0.21
				$P(LS_i   \lambda_{PGA})$	0.019	0.000	0.000	0.000
Water Tank 3	2.00	True	Fill > 50%, H/D is N/A	$\lambda_i$	-0.71335	-0.15082	-0.01005	0.157004
				$\beta_i$	0.55	0.39	0.27	0.21
				$P(LS_i   \lambda_{PGA})$	0.019	0.000	0.000	0.000



Alternatively, if the user chooses to map based on H/D ratio, but does not provide either H/D data, fill data, or both, for some or all of the tanks, use the fragility which represents an average of the water tank fragilities based on H/D ratios. Using that mapping, the data shown in Figure 4.1.6-17 is obtained.

**Table 4.1.6-17 Sample Water Tank Fragility Calculations when Mapping by H/D and Fill  
(assumes user does NOT provide H, D, and fill data)**

H/D	Fill	Fragility	Parameters	Damage States, DS <sub>i</sub>			
				Slight	Moderate	Extensive	Complete
Water Tank 1		All H/D and fill	$\lambda_i$	-0.35667	0.09531	0.254642	0.300105
			$\beta_i$	0.48	0.35	0.28	0.22
			$P(LS_i   \lambda_{PGA})$	0.001	0.000	0.000	0.000
Water Tank 2		All H/D and fill	$\lambda_i$	-0.35667	0.09531	0.254642	0.300105
			$\beta_i$	0.48	0.35	0.28	0.22
			$P(LS_i   \lambda_{PGA})$	0.001	0.000	0.000	0.000
Water Tank 3		All H/D and fill	$\lambda_i$	-0.35667	0.09531	0.254642	0.300105
			$\beta_i$	0.48	0.35	0.28	0.22
			$P(LS_i   \lambda_{PGA})$	0.001	0.000	0.000	0.000



Finally, to obtain discrete probabilities of damage states, use equations (4.1.5-2) through (4.1.5-6), where N corresponds to a None damage state, as for bridges. The discrete probabilities for the water tanks are shown in Table 4.1.6-18 resulting from various mapping schemes.

**Table 4.1.6-18 Sample Water Tank Probabilities of Damage for all Mapping schemes**

Fragility	Probabilities of Damage States, DS <sub>i</sub>					
	None	Slight	Moderate	Extensive	Complete	
Water Tank 1	Fill < 50%	0.944	0.056	0.000	0.000	0.000
	50% <= Fill < 60%	0.567	0.405	0.021	0.007	0.000
	Unanchored	0.347	0.610	0.035	0.009	0.000
	Anchorage Unknown	0.567	0.405	0.021	0.007	0.000
	H/D < 0.7	0.998	0.002	0.000	0.000	0.000
	All H/D and fill	0.999	0.001	0.000	0.000	0.000
Water Tank 2	50% <= Fill < 60%	0.568	0.405	0.021	0.007	0.000
	50% <= Fill < 60%	0.568	0.405	0.021	0.007	0.000
	Anchored	0.970	0.029	0.000	0.000	0.000
	Anchorage Unknown	0.568	0.405	0.021	0.007	0.000
	Fill > 50%, H/D is N/A	0.981	0.019	0.000	0.000	0.000
	All H/D and fill	0.999	0.001	0.000	0.000	0.000
Water Tank 3	60% <= Fill < 90%	0.667	0.303	0.023	0.008	0.000
	50% <= Fill < 60%	0.571	0.402	0.020	0.006	0.000
	Anchored	0.971	0.029	0.000	0.000	0.000
	Anchorage Unknown	0.571	0.402	0.020	0.006	0.000
	Fill > 50%, H/D is N/A	0.981	0.019	0.000	0.000	0.000
	All H/D and fill	0.999	0.001	0.000	0.000	0.000



## *Buried Pipelines*

### **Algorithm**

#### Inputs:

Mapped fragility set to use for pipes.

Hazard in terms of PGV.

Pipe material required for any pipe fragility.

Pipe diameter, joint type, and soil data may be required, depending on which fragilities were selected by the user.

Pipe segment lengths.

#### Process:

Evaluate repair rate using inputs and backbone fragility curves corresponding to the Researcher and fragility mapping.

Multiply repair rate by the lengths of pipes to obtain expected number of repairs.

Outputs: expected number of repairs for each pipe.

### **Example**

Fragility curves for buried pipelines use PGV and pipe diameter inputs, and output repairs per length of pipe. Table 4.1.6-19 displays fragility curves from three separate analyses for varying types of buried pipelines. The fragilities are listed in order of preference in Table 4.1.6-19. Required mapping data is also listed in Table 4.1.6-19. Table 4.1.6-20 shows the K coefficients to be used with the algorithm developed by Eiding (2001) presented in Table 4.1.6-19 to determine pipe damage.



**Table 4.1.6-19 Fragility curves for Buried Pipelines**

Material	Researcher	Backbone Fragility Curve	Non-dimensional Coefficient (K)	Source Earthquakes	Req'd Mapping Data	NOTES:
Cast-Iron Pipe		$RR=0.050*(PGV/D)^{1.138*0.865}$			Pipe material, diameter	RR: Repairs / Km
Ductile Iron Pipe	O'Rourke, T and Jeon (1999)	$RR=0.004*(PGV/D)^{0.468*1.378}$	N/A	Northridge Earthquake	Pipe material, diameter	PGV: cm / sec
Asbestos Cement Pipe		$\text{Log}(RR) = -4.59*\text{Log}(D)+8.96$		(1994)	Pipe material, diameter	D: cm
Asbestos Cement Pipe		$\text{Log}(RR) = 2.26*\text{Log}(PGV) - 11.01$			Pipe material	PGV: cm / sec
Buried Pipeline	O'Rourke, M and Ayala (1993)	$RR=K \times 0.00003 (PGV)^{2.65}$	1.0 - Cast-Iron, Asbestos, Cement, Concrete	11 data points from 4 US and 2 Mexican Earthquakes	Pipe material	RR: Repairs / Km PGV: cm / sec
Buried Pipeline	Eidinger (2001)	$RR=K*0.00187*PGV$	0.3 - Steel, Ductile Iron, PVC Depends on Composition, Joint Type, Soil Condition, and Diameter	81 data points from 18 Earthquakes (B: 1.15)	Pipe material, diameter, joint type, soils (see Table 2)	PGV: in / sec RR: Repairs / 1000 ft

**Table 4.1.6-20 K Coefficients from Eidinger (2001)**

Pipe Material	Joint Type	Soils	Diameter	K
Cast Iron	Cement	All	Small	1.0
Cast Iron	Cement	Corrosive	Small	1.4
Cast Iron	Cement	Non-Corrosive	Small	0.7
Cast Iron	Rubber Gasket	All	Small	0.8
Welded Steel	Lap - Arc Welded	All	Small	0.6
Welded Steel	Lap - Arc Welded	Corrosive	Small	0.9
Welded Steel	Lap - Arc Welded	Non-Corrosive	Small	0.3
Welded Steel	Lap - Arc Welded	All	Large	0.2
Welded Steel	Rubber Gasket	All	Small	0.7
Welded Steel	Screwed	All	Small	1.3



Pipe Material	Joint Type	Soils	Diameter	K
Welded Steel	Riveted	All	Small	1.3
Asbestos Cement	Rubber Gasket	All	Small	0.5
Asbestos Cement	Cement	All	Small	1.0
Concrete w/ Steel Cylinder	Lap - Arc Welded	All	Large	0.7
Concrete w/ Steel Cylinder	Rubber Gasket	All	Large	1.0
Concrete w/ Steel Cylinder	Rubber Gasket	All	Large	0.8
PVC	Rubber Gasket	All	Small	0.5
Ductile Iron	Rubber Gasket	All	Small	0.5

For the sample pipeline, the length may be extracted from the shapefile data or calculated by MAEviz. A calculation using the Great Circle method results in an approximate distance between the end nodes of 10.1695 km. Also, from Table 3.1.1.3-5, the lognormal mean PGV for the segment is 3.4434. This value is the natural log of PGV with units of cm/sec, so the expected mean of PGV is  $\exp(3.4434) = 31.29 \text{ cm/sec} = 12.32 \text{ in/sec}$ .

Using the default mappings described in Section 2.1.1.3 will provide the following results. For Eidinger (2001), the K term will be taken as 1.0 to match the fragility (Cast Iron, Cement, All, Small). Then

$$RR = K \cdot 0.00187 \cdot PGV = 1.0 \cdot 0.00187 \cdot 12.32 = 0.023 \frac{\text{repairs}}{1000 \text{ ft}} \cdot \frac{1000 \text{ ft}}{0.3048 \text{ km}} = 0.0756 \frac{\text{repairs}}{\text{km}}$$

And the total number of expected repairs is

$$E[\text{repairs}] = 0.0756 \frac{\text{repairs}}{\text{km}} \cdot 10.1695 \text{ km} = 0.77 \text{ repairs}$$

For O'Rourke, M. and Ayala (1993), the K term will be taken as 1.0 to match the fragility (Cast Iron). Then

$$RR = K \cdot 0.00003 \cdot PGV^{2.65} = 1.0 \cdot 0.00003 \cdot (31.29 \text{ cm/sec})^{2.65} = 0.2754 \frac{\text{repairs}}{\text{km}}$$

And the total number of expected repairs is

$$E[\text{repairs}] = 0.2754 \frac{\text{repairs}}{\text{km}} \cdot 10.1695 \text{ km} = 2.8 \text{ repairs}$$

For O'Rourke, T. and Jeon (1999), the diameter must be converted from 18 inches to 45.72 cm. Then, for Cast Iron material,



$$RR = 0.050 \cdot \left( \frac{PGV}{D^{1.138}} \right)^{0.865} = 0.050 \cdot \left( \frac{31.29 \text{ cm/sec}}{(45.72 \text{ cm})^{1.138}} \right)^{0.865} = 0.0228 \frac{\text{repairs}}{\text{km}}$$

And the total number of expected repairs is

$$E[\text{repairs}] = 0.0228 \frac{\text{repairs}}{\text{km}} \cdot 10.1695 \text{ km} = 0.23 \text{ repairs}$$



#### 4.1.7 Implement HAZUS liquefaction damage estimation for buildings.

##### **Algorithm**

###### Inputs:

Probability of liquefaction for each building.

Expected lateral spreading for each building.

Expected ground settlement for each building.

Foundation type for each structure (shallow or deep foundation, assume shallow by default if no data is provided).

###### Process:

Calculate probabilities of exceedence for damage states as shown in Equations (4.1.7-1) through (4.1.7-6) and adjust for deep foundations, if applicable.

Use the maximum probabilities of exceedence between lateral spreading and settlement.

Outputs: Probabilities of exceedence for damage states resulting from ground failure.

##### **Example**

To calculate probability of exceeding the Moderate and Heavy damage states for both lateral spreading and ground settlement, use the typical lognormal cumulative distribution function (the same as for building fragilities) multiplied by probability of liquefaction, Equation (3.1.6-1). For shallow foundations, the  $\lambda$  value is **ln(60)** for lateral spreading and **ln(10)** for settlement when estimating probability of exceeding Moderate damage. The  $\beta$  value is 1.2 in both cases. The probability of exceeding Heavy damage is taken as 20% of the probability of exceeding Moderate damage. That is, for lateral spreading,

$$P_{GF}(PL1) = \Phi\left(\frac{\ln(E[lateral\_spreading]) - \ln(60)}{1.2}\right) \cdot P[liquefaction] \quad (4.1.7-1)$$

$$P_{GF}(PL2) = \Phi\left(\frac{\ln(E[lateral\_spreading]) - \ln(60)}{1.2}\right) \cdot P[liquefaction] \quad (4.1.7-2)$$

$$P_{GF}(PL3) = 0.2 \cdot \Phi\left(\frac{\ln(E[lateral\_spreading]) - \ln(60)}{1.2}\right) \cdot P[liquefaction] \quad (4.1.7-3)$$

and for settlement,

$$P_{GF}(PL1) = \Phi\left(\frac{\ln(E[settlement]) - \ln(10)}{1.2}\right) \cdot P[liquefaction] \quad (4.1.7-4)$$

$$P_{GF}(PL2) = \Phi\left(\frac{\ln(E[settlement]) - \ln(10)}{1.2}\right) \cdot P[liquefaction] \quad (4.1.7-5)$$



$$P_{GF}(PL3) = 0.2 \cdot \Phi\left(\frac{\ln(E[\textit{settlement}]) - \ln(10)}{1.2}\right) \cdot P[\textit{liquefaction}] \quad (4.1.7-6)$$

For buildings with deep foundations, the probabilities evaluated in Equations (4.1.7-4) through (4.1.7-6) are divided by 10, and the probabilities evaluated in Equations (4.1.7-1) through (4.1.7-3) are divided by 2. Probabilities of ground failure damage are then combined with probabilities ground shaking failure as indicated in Section 4.1.4.

From Section 3.1.6,

$$P[\textit{liquefaction}] = 0.25$$

$$E[\textit{lateral\_spreading}] = 67\textit{in}$$

$$E[\textit{settlement}] = 3\textit{in}$$

Then for lateral spreading of shallow foundations

$$P_{GF}(PL1) = \Phi\left(\frac{\ln(67) - \ln(60)}{1.2}\right) \cdot 0.25 = 0.539$$

$$P_{GF}(PL2) = \Phi\left(\frac{\ln(67) - \ln(60)}{1.2}\right) \cdot 0.25 = 0.539$$

$$P_{GF}(PL3) = 0.2 \cdot \Phi\left(\frac{\ln(67) - \ln(60)}{1.2}\right) \cdot 0.25 = 0.108$$

and for ground settlement of shallow foundations

$$P_{GF}(PL1) = \Phi\left(\frac{\ln(3) - \ln(10)}{1.2}\right) \cdot 0.25 = 0.158$$

$$P_{GF}(PL2) = \Phi\left(\frac{\ln(3) - \ln(10)}{1.2}\right) \cdot 0.25 = 0.158$$

$$P_{GF}(PL3) = 0.2 \cdot \Phi\left(\frac{\ln(3) - \ln(10)}{1.2}\right) \cdot 0.25 = 0.032$$

The maximum exceedence probabilities are used, so the quantities used for combination with ground shaking hazard are

$$P_{GF}(PL1) = \textit{MAX}(0.539, 0.158) = 0.539$$

$$P_{GF}(PL2) = \textit{MAX}(0.539, 0.158) = 0.539$$

$$P_{GF}(PL3) = \textit{MAX}(0.108, 0.032) = 0.108$$

Calculations for lateral spreading with deep foundations are similar to those performed for shallow foundations, except with simple multipliers.



$$P_{GF}(PL1) = \Phi\left(\frac{\ln(67) - \ln(60)}{1.2}\right) \cdot 0.25 \cdot \frac{1}{2} = 0.269$$

$$P_{GF}(PL2) = \Phi\left(\frac{\ln(67) - \ln(60)}{1.2}\right) \cdot 0.25 \cdot \frac{1}{2} = 0.269$$

$$P_{GF}(PL3) = 0.2 \cdot \Phi\left(\frac{\ln(67) - \ln(60)}{1.2}\right) \cdot 0.25 \cdot \frac{1}{2} = 0.054$$

and for ground settlement of deep foundations

$$P_{GF}(PL1) = \Phi\left(\frac{\ln(3) - \ln(10)}{1.2}\right) \cdot 0.25 \cdot \frac{1}{10} = 0.0158$$

$$P_{GF}(PL2) = \Phi\left(\frac{\ln(3) - \ln(10)}{1.2}\right) \cdot 0.25 \cdot \frac{1}{10} = 0.0158$$

$$P_{GF}(PL3) = 0.2 \cdot \Phi\left(\frac{\ln(3) - \ln(10)}{1.2}\right) \cdot 0.25 \cdot \frac{1}{10} = 0.0032$$

Again, the maximum exceedence probabilities are used, so the quantities used for combination with ground shaking hazard are

$$P_{GF}(PL1) = \text{MAX}(0.269, 0.0158) = 0.269$$

$$P_{GF}(PL2) = \text{MAX}(0.269, 0.0158) = 0.269$$

$$P_{GF}(PL3) = \text{MAX}(0.054, 0.0032) = 0.054$$



#### 4.1.8 Implement Capacity Spectrum Method (CSM) for HAZUS fragilities.

##### **Algorithm**

###### Inputs:

Spectral acceleration at 0.3 and 1 second periods, including soil effects. (If 0.2 second  $S_a$  is available instead of 0.3 second for USGS CEUS attenuations, divide by 1.4 to obtain approximate 0.3 second hazard for CEUS.)

Spectral acceleration and displacement at yield, and spectral acceleration at ultimate for building type and code level (from NIBS (2006)).

Lognormal median and standard deviation for building type and code level (from NIBS (2006)).

###### Process:

Determine demand for a given structure using the CSM.

Evaluate structural, drift- and acceleration-sensitive damage using cumulative lognormal distribution and demand from CSM.

Calculate discrete probabilities of damage states (adjust for liquefaction if appropriate).

User option: adjust probabilities of damage states so that nonstructural damage is at least as likely to experience complete damage as structural damage.

###### Outputs:

Discrete probabilities of damage states using CSM.

##### **Example**

Consider the I1 example building (3-story, Pre-Code C1 structure) subjected to CEUS ground motions from an  $M_w = 7.9$  event at Blytheville, AR. Using Site Class D for NEHRP factors,  $S_a$  at 0.2 seconds is 0.703g and  $S_a$  at 1 second is 0.374g. The first step in this case is to calculate an approximate  $S_a$  at 0.3 seconds using the 0.2 seconds value,  $0.703 / 1.4 = 0.502g$ . The  $S_a$  value at 0.3 seconds will be referred to as  $S_s$ , and the  $S_a$  value at 1 second will be referred to as  $S_1$ . Compute spectral displacement at the end of the constant spectral acceleration range using Equation (4.1.8-1)

$$S_{dlh} = 9.8 \cdot \left( \frac{S_1^2}{S_s} \right) \quad (4.1.8-1)$$

For the sample building,  $S_{dlh} = 2.73$  inches.

The capacity spectrum will be a bilinear function, linearly increasing from  $S_a$  and  $S_d = 0$ , and having constant  $S_a$  with increasing  $S_d$  at the ultimate spectral acceleration capacity of the structure,  $A_u$ . The slope of the linear portion is defined by the spectral acceleration and displacement at yield,  $A_y$  and  $D_y$ . These three parameters are available in the HAZUS Technical



Manual (NIBS, 2006). For the sample building, NIBS (2006) lists  $D_y = 0.1$  inches,  $A_y = 0.062g$ , and  $A_u = 0.187g$ .

There are three possible scenarios for the CSM: the inclined portion of the capacity curve intersects the constant portion of the demand curve, the inclined portion of the capacity curve intersects the decreasing portion of the demand curve, or the inclined portion of the capacity curve ends before reaching the demand curve. To determine which of these cases controls, and calculate CSM demand parameters, use the following method:

$$\text{If } \frac{A_y}{D_y} \geq \frac{S_s}{S_{dlh}} \text{ AND } S_s \leq A_u$$

Then

$$S_a = S_s \tag{4.1.8-2}$$

$$S_d = S_s \cdot \left( \frac{D_y}{A_y} \right) \tag{4.1.8-3}$$

If  $A_u = 0.55g$  rather than  $0.187g$ , this case would apply. The CSM would provide results as shown in Figure 4.1.8-1, with  $S_a = 0.502g$  and  $S_d = 0.810$  inches.

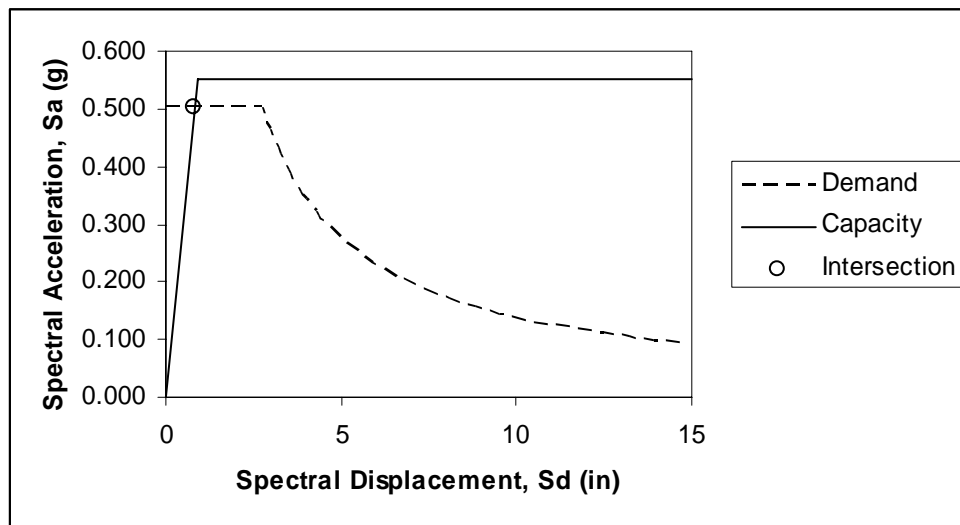


Figure 4.1.8-1 Example CSM result for Case 1

$$\text{Else If } \frac{A_y}{D_y} < \frac{S_s}{S_{dlh}} \text{ AND } S_1 \sqrt{\frac{9.8 \cdot A_y}{D_y}} \leq A_u$$

Then



$$S_a = S_1 \sqrt{\frac{9.8 \cdot A_y}{D_y}} \quad (4.1.8-4)$$

$$S_d = S_1 \sqrt{\frac{9.8 \cdot D_y}{A_y}} \quad (4.1.8-5)$$

If  $A_u = 0.55g$  rather than  $0.187g$  and  $D_y = 0.5$  inches rather than  $0.1$  inches, this case would apply. The CSM would provide results as shown in Figure 4.1.8-2, with  $S_a = 0.412g$  and  $S_d = 3.324$  inches.

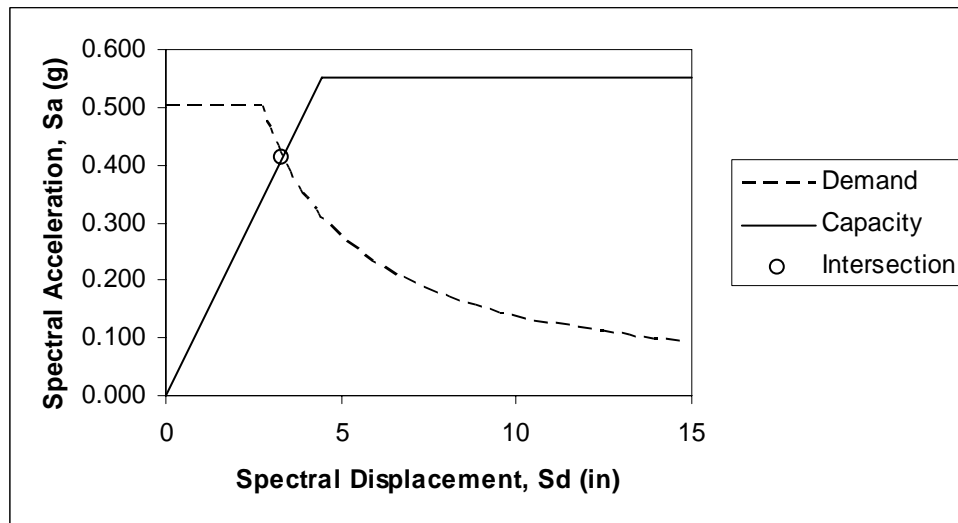


Figure 4.1.8-2 Example CSM result for Case 2

Else

$$S_a = A_u \quad (4.1.8-6)$$

$$S_d = 9.8 \cdot \frac{S_1^2}{A_u} \quad (4.1.8-7)$$

This is the case that applies to the sample structure with the parameters given in NIBS (2006). The CSM provides results as shown in Figure 4.1.8-3, with  $S_a = 0.187g$  and  $S_d = 7.327$  inches.



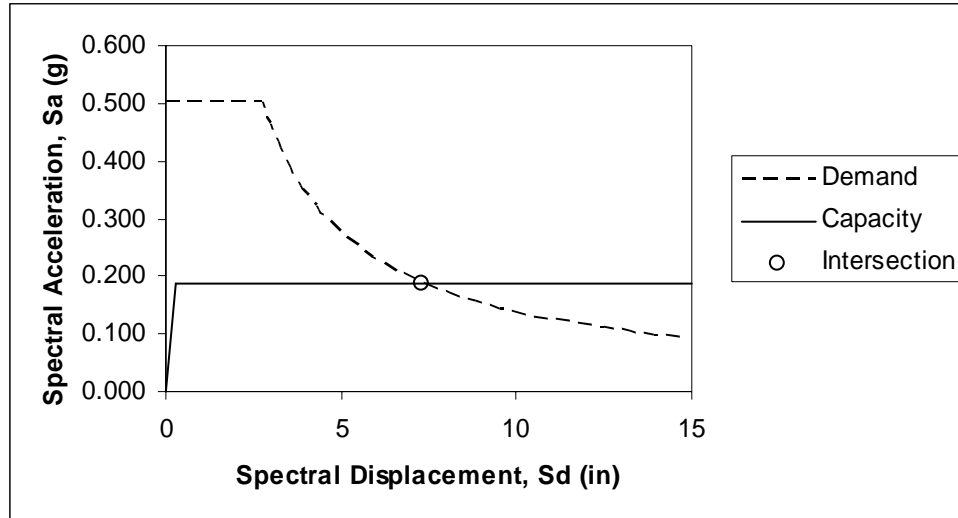


Figure 4.1.8-3 Example CSM result for Case 3

With the  $S_a$  and  $S_d$  hazard parameters obtained from the CSM, evaluation of building structural and nonstructural damage may be carried out using cumulative lognormal distribution functions, as currently implemented.

Using the  $\lambda$  and  $\beta$  parameters for Pre-Code C1L structures in NIBS (2006), probabilities of exceedence for performance limits may be determined, and discrete probabilities of individual damage states may then be computed, as shown in Table 4.1.8-1 (these calculations assume liquefaction is negligible).

Table 4.1.8-1 Sample Base Calculations for HAZUS fragilities with CSM

		Damage States, $DS_i$			
		I	M	H	C
II C1L HAZUS (3-story)	Structural	0.024	0.125	0.343	0.507
	Drift-Sensitive Nonstructural	0.048	0.252	0.279	0.421
	Acceleration-Sensitive Nonstructural	0.868	0.115	0.015	0.001

These damage state probabilities may be used as they are to compute expected losses, or if the user elects, they may be adjusted to ensure that nonstructural components have at least the same probability of Complete damage as the structure itself. To make this adjustment, use Equations (4.1.8-8) and (4.1.8-9) for both drift- and acceleration-sensitive nonstructural damage state probabilities.

$$P(DS = C)_{adj}^{NS} = P(DS = C)_{base}^{NS} + P(DS = C)^{str} \cdot (1 - P(DS = C)_{base}^{NS}) \quad (4.1.8-8)$$



Where  $P(DS = C)_{adj}^{NS}$  is the adjusted probability of complete damage for nonstructural components,  $P(DS = C)_{base}^{NS}$  is the base probability of complete damage for nonstructural components as shown in Table 4.1.8-1, and  $P(DS = C)^{str}$  is the probability of complete damage for the structural components. This equation should be applied once for each of drift- and acceleration-sensitive nonstructural components. Then, use

$$P(DS_i)_{adj}^{NS} = P(DS_i)_{base}^{NS} \cdot (1 - P(DS = C)^{str}) \quad (4.1.8-9)$$

to adjust other nonstructural damage state probabilities, where  $P(DS_i)_{adj}^{NS}$  are the adjusted probabilities of damage states for nonstructural components, and  $P(DS_i)_{base}^{NS}$  are the base probabilities of damage states for nonstructural components as shown in Table 4.1.8-1.  $DS_i$  ranges from Insignificant to Heavy, for a total of six applications of Equation (4.1.8-9) per building (2 types of nonstructural components times 3 damage states). Sample calculations for adjusted damage state probabilities are given in Table 4.1.8-2.

**Table 4.1.8-2 Sample Adjusted Calculations for HAZUS fragilities with CSM**

		Damage States, $DS_i$			
		I	M	H	C
II C1L HAZUS (3-story)	Structural	0.024	0.125	0.343	0.507
	Drift-Sensitive Nonstructural	0.024	0.124	0.138	0.715
	Acceleration-Sensitive Nonstructural	0.428	0.057	0.008	0.508



## 4.2 Background

### 4.2.1. Building structures

#### 4.2.1.1 Building Structural Damage

Building fragilities have been developed by the MAE Center for construction typical of the Mid-America region (e.g., Erberik and Elnashai, 2006; Kwon and Elnashai, 2006; Bai and Hueste, 2006; Bai and Hueste, 2007; Celik and Ellingwood, 2006; Ellingwood, 2005; Hueste and Bai, 2007; Hueste and Bai, 2007; Ramamoorthy et al., 2006; Ramamoorthy et al., 2006). These vulnerability functions were derived by conducting structural analyses that accounted for aleatory uncertainty related to both structural characteristics and excitation uncertainty. Structural uncertainties are introduced by variations in material and geometric properties. Excitation uncertainty is introduced by including various synthetic ground motions with different frequency contents and durations. Uncertainty in seismic intensity is obtained from the hazard model. Table 4.2.1.1-1 lists the fragility curves that have been derived for buildings within the MAE Center. See Appendix C for a proposed mapping scheme relating inventory to fragilities, as well as supplementary fragility metadata.

**Table 4.2.1.1-1 MAE Center Building Fragility Curves**

PI	Hueste (TAMU)
Structure	5 Story flat-slab with perimeter RC moment frame (1980s central U.S. office buildings)
Retrofits	(1) Shear wall-perimeter frames, (2) Column jacketing, (3) Confining with steel plates at column ends. (Seismic/Nonseismic)
Seismicity	Sa at fundamental building periods (from given number of stories). (Ground motions by (1) Wen & Wu and (2) Rix & Fernandez-Leon.)
Limit states	FEMA356 (Based on interstory drift ratios) (1) IO (immediate occupancy: global/member), (2) LS (life safety: global/member), (3) CP (collapse prevention: global/member), (4) FY (first yield), (5) PMI (plastic mechanism initiation), (6) SD (strength degradation).
Parameters	$\lambda$ and $\beta$ of lognormal CDF. See Equation (4.2.1.1-1).
Fundamental Period	As-built $T_1 = 0.32 * NO\_STORIES$ , 1.62 seconds for model building Retrofit (1) $T_1 = 0.13 * NO\_STORIES$ , 0.66 seconds for model building Retrofit (2) $T_1 = 0.28 * NO\_STORIES$ , 1.38 seconds for model building Retrofit (3) $T_1 = 0.32 * NO\_STORIES$ , 1.62 seconds for model building
PI	Bracci & Gardoni (TAMU)
Structure	RC moment frame systems (designed primarily for gravity loads) story heights 1-10 (fragility surfaces)
Retrofits	Low-rise RC frames retrofitted by column strengthening (ACI 318 requirements).
Seismicity	Sa at fundamental building periods (from given number of stories).



Limit states	From FEMA 356: Immediate Occupancy (0.5% IDR), Life Safety (1% IDR), Collapse Prevention (2% IDR)
Parameters	lognormal CDF using $\alpha_{11}$ $\alpha_{12}$ $\alpha_{13}$ $\alpha_{14}$ $\alpha_{21}$ $\alpha_{22}$ . See Equations (4.2.1.1-2) and (4.2.1.1-3).
Fundamental Period	$T_1 = \eta_1 (h)^{\eta_2}$ , where $\eta_1 = 0.097$ , $\eta_2 = 0.624$ , and h = height of building frame from base (ft). Typically assume 13 ft story height.

PI	Ellingwood (GT) & Rosowsky (TAMU)
Structure	Low-rise steel frames, wood shear walls Selected story heights
Retrofits	N/A
Seismicity	Sa at selected fundamental building periods.
Limit states	Steel: Elastic Limit (varies), 2%, Collapse Prevention based on IDA Wood: 0.5%, 1%, 2% Interstory Drift
Parameters	Median Sa ( $= \overline{S_a}$ ) and $\beta$ of lognormal CDF. See Equation (4.2.1.1-1).
Fundamental Period	2-story PR steel frame, $T_1 = 1.07$ seconds for model building 3-story FR steel frame, $T_1 = 2.01$ seconds for model building 4-story PR steel frame, $T_1 = 1.34$ seconds for model building 6-story X-braced steel frame, $T_1 = 1.04$ seconds for model building 1-story wood frame on slab-on-grade, $T_1 = 0.24$ seconds for model building 1-story wood frame on cripple wall/crawl space, $T_1 = 0.22$ seconds for model building 2-story wood frame on slab-on-grade, $T_1 = 0.38$ seconds for model building

PI	Wen (UIUC)
Structure	Unreinforced masonry buildings Selected story heights
Retrofits	N/A
Seismicity	Sa at selected fundamental building periods.
Limit states	Un-reinforced masonry: IO (0.3% FEMA), LS (0.6% FEMA), IC (1.5% IDA)
Parameters	Median Sa ( $= \overline{S_a}$ ) and $\beta$ of lognormal CDF. See Equation (4.2.1.1-1).
Fundamental Period	$T_1 = 0.3 * NO\_STORIES$ , 0.55 seconds for model building

PI	Elnashai (UIUC)
Structure	5-story 3-bay flat slab moment frame with masonry infill walls
Retrofits	N/A
Seismicity	Sa at selected fundamental building periods.
Limit states	HAZUS Limit States, based on Interstory Drift Ratio (IDR) Slight (0.1% IDR), Moderate (1% IDR), Extensive (2% IDR), Complete (3.5% IDR)



Parameters	$\lambda$ and $\beta$ of lognormal CDF. See Equation (4.2.1.1-1).
Fundamental Period	$T_1 = 0.2 * \text{NO\_STORIES}$ , 0.98 seconds for model building
PI	Elnashai (UIUC) & Kuchma (UIUC)
Structure	Frame – Core wall coupled system (high-rise)
Retrofits	N/A
Seismicity	Sa at selected fundamental building periods.
Limit states	Serviceability (0.2% IDR), Damage Control (0.2% IDR), Collapse Prevention (0.2% IDR)
Parameters	$\lambda$ and $\beta$ of lognormal CDF. See Equation (4.2.1.1-1).
Fundamental Period	$T_1 = 0.08 * \text{NO\_STORIES}$ , 3.05 seconds for model building

Most fragilities developed within the MAE Center to estimate structural damage use lognormal median and standard deviation parameters  $\lambda$  and  $\beta$ . The equation describing the probability of exceeding a certain limit state, given a spectral acceleration is

$$P(LS | S_a) = \Phi\left(\frac{\ln(S_a) - \lambda}{\beta}\right) \quad (4.2.1.1-1)$$

Where  $S_a$  is the demand spectral acceleration, obtained from attenuation functions for a scenario event or from a map for a probabilistic hazard analysis.  $\Phi$  represents the standard normal cumulative distribution function. In some cases, MAE Center PIs report median spectral acceleration values for limit states. Equation (4.2.1.1-1) may still be used in those cases, except that  $\lambda$  must be taken as  $\lambda = \ln(\text{median } S_a) = \ln(\overline{S_a})$ .

An alternative form is also included in the MAE Center fragilities for fragility surfaces which apply to several story heights (Ramamoorthy et al., 2006). The MAE Center fragility surface equations have the form

$$P(LS | S_a) = \Phi\left(\frac{\ln(S_a) - (\alpha_{11} + \alpha_{12}T)}{(\alpha_{13} + \alpha_{14}T)}\right) \quad (4.2.1.1-2)$$

when  $0.87 \leq T(\text{sec})$

and

$$P(LS | S_a) = \Phi\left(\frac{\ln(S_a) - (\alpha_{11} + \alpha_{12}0.87)}{(\alpha_{13} + \alpha_{14}0.87)} + (0.87 - T)\frac{\ln(S_a) - \alpha_{21}}{\alpha_{22}}\right) \quad (4.2.1.1-3)$$

when  $0 < T < 0.87(\text{sec})$



where  $S_a$  and  $\Phi$  are the same as in Equation (4.2.1.1-1), and the  $\alpha$  terms are specified for each limit state by the MAE Center PI providing the fragilities.

For MAE Center building fragilities, there are consistently four damage states (DS): Insignificant (I), Moderate (M), Heavy (H), and Complete (C). HAZUS uses five damage states: None, Slight, Moderate, Extensive, and Complete. MAE Center damage states Complete, Heavy, and Moderate map approximately to HAZUS Complete, Extensive, and Moderate. The MAE Center Insignificant damage state is approximately equivalent to the combination of HAZUS None and Slight damage states. Therefore, when comparing results between MAE Center fragilities and HAZUS fragilities, or when adapting HAZUS fragilities for use in MAEViz, the three heaviest damage states will be considered to map directly to each other, while the combination of the two lightest HAZUS damage states will be considered to map to the Insignificant MAE Center damage state.

MAE Center fragility curves set the thresholds for probabilities of exceeding these limit states, therefore

$$P(DS > I) = P(PL1 | S_a) \quad (4.2.1.1-4)$$

$$P(DS > M) = P(PL2 | S_a) \quad (4.2.1.1-5)$$

$$P(DS > H) = P(PL3 | S_a) \quad (4.2.1.1-6)$$

Where the numbers following “PL” correlate to the use of fragility parameters for appropriate limit states (given by MAE Center PIs). For the HAZUS fragilities, the limit state numbers would increase by 1 in each case. For example, PL4 for HAZUS corresponds to the probability of having damage heavier than Extensive, and the HAZUS Extensive damage state is approximately equivalent to the Heavy damage state in the MAE Center. This can also be stated as the probability of having damage *greater than or equal to* Complete damage. For clarity, expressions have been provided in (4.2.1.1-7) through (4.2.1.1-9) to define equivalent MAE Center damage states from HAZUS damage states.

$$P(DS > I) = P(DS \geq M_{HAZUS}) = P(PL2_{HAZUS} | S_d) \quad (4.2.1.1-7)$$

$$P(DS > M) = P(DS \geq E_{HAZUS}) = P(PL3_{HAZUS} | S_d) \quad (4.2.1.1-8)$$

$$P(DS > H) = P(DS \geq C_{HAZUS}) = P(PL3_{HAZUS} | S_d) \quad (4.2.1.1-9)$$

Discrete probabilities of damage states may then be computed by

$$P(DS = C) = P(DS > H) \quad (4.2.1.1-10)$$

$$P(DS = H) = P(DS > M) - P(DS > H) \quad (4.2.1.1-11)$$

$$P(DS = M) = P(DS > I) - P(DS > M) \quad (4.2.1.1-12)$$

$$P(DS = I) = 1 - P(DS > I) \quad (4.2.1.1-13)$$



#### 4.2.1.2 Building Nonstructural and Contents Damage

The MAE Center has provided nonstructural fragilities to describe specific nonstructural components for the MLGW project. When available, specific nonstructural inventory data will be used for loss assessments and paired with appropriate fragilities for specific components. In most cases, specific nonstructural inventory data are not available, and nonstructural damage algorithms will need to be adapted from HAZUS-MH as an interim measure pending the implementation of MAE Center algorithms for estimating damage to general nonstructural and contents. HAZUS-MH does not consider specific nonstructural inventory items, but rather breaks nonstructural inventory into two subsets: drift-sensitive and acceleration-sensitive. Values of each subset of nonstructural inventory can be partitioned from the total building value using the percentages shown in Table 2.2.1-6.

The HAZUS drift sensitive non-structural fragilities are based on global building displacement, which may be estimated as the spectral displacement,  $S_d$ , related to spectral acceleration,  $S_a$ , as shown in Equation (4.1.3-1). According to the HAZUS Technical Manual (NIBS, 2006), uncertainty for each non-structural drift sensitive damage state is assumed to originate from one of three contributors: uncertainty in the damage state threshold of non-structural components, variability in capacity of the model building type that contains the non-structural components (i.e., displacements determined by Capacity Spectrum Method), and variability in response of the model building type due to the spatial variability of ground motion demand. These uncertainties are combined to arrive at a single  $\beta$  term, which is coupled with a median spectral displacement,  $\overline{S_d}$ , to define a lognormal fragility formulation.

Values of  $\overline{S_d}$  and  $\beta$  from the HAZUS Technical Manual are provided in Appendix C. Note that HAZUS damage states Complete, Extensive, and Moderate correlate approximately to MAE Center damage states Complete, Heavy, and Moderate, respectively. The MAE Center damage state Insignificant is approximately equivalent to the combination of HAZUS Slight and None damage states.

Fragilities for acceleration-sensitive nonstructural assets are based on spectral acceleration. According to the HAZUS Technical Manual, nonstructural acceleration-sensitive components are divided into two subpopulations: (1) components at or near ground level and (2) components at upper floors or on the roof. Also, according to the HAZUS Technical Manual, PGA, rather than spectral acceleration, is a more appropriate hazard input for components at or near ground level. Fragility curves used by HAZUS for nonstructural acceleration-sensitive components assume 50% (low-rise), 33% (mid-rise) or 20% (high-rise) of nonstructural components are located at, or near, the ground floor, and represent a weighted combination of the probability of damage to components located at, or near, ground level and components located at upper-floor levels of the building. Variability of each non-structural acceleration sensitive damage state is considered to originate from the same three contributors mentioned previously with regard to



drift-sensitive fragilities. The general form of the fragility equation for acceleration-sensitive nonstructural components is similar to Equation (4.2.1.1-1), except that the HAZUS Technical Manual provides median  $S_a$  values instead of  $\lambda$  values. Equation (4.2.1.1-1) can be used to describe acceleration-sensitive nonstructural damage if  $\ln(\text{median } S_a)$  is substituted for  $\lambda$ . Nonstructural acceleration sensitive median  $S_a$  and lognormal  $\beta$  fragility parameters from the HAZUS Technical Manual are provided in Appendix C. Note that HAZUS uses acceleration-sensitive nonstructural fragilities to estimate damage to contents, as well.

#### 4.2.1.3. Parametric fragility curves

A methodology has been developed within the MAE Center whereby fragilities can be generated in a relatively short amount of time based on five key structural parameters: period, strength, ductility, damping and post-to-preyield stiffness ratio. Additional information is provided in Table 4.2.1.3-1. Finding the parameters that correspond to the structure types in the inventory data will be essential for this methodology's use in a CBE framework. Databases have currently been developed based on using parameters obtained from the HAZUS Technical Manual which describe particular structure types, and modeling the parameterized structures under time history analysis with synthetic ground motions.

**Table 4.2.1.3-1 MAE Center Parameterized Building Fragility Curves**

PI	Amr Elnashai
Structure	Generic buildings characterized by (1) period, (2) strength (as ratio to weight), (3) ductility (4) damping and (5) post-to-pre-yield stiffness ratio // For inventory items, these parameters can be determined by push-over analyses or more simply determined in the following way: (1) period estimated from the height or equations available in the literature, (2) ratio of strength to weight; 1-1.5% for no lateral force design, 2-3% for wind-design, 3-5% low seismic design, 5-9% medium, 10-12% full (3) damping: 2-8% depending on the level of ductility, (4) post-yield stiffness ratio: 10% full seismic, 5% for medium, 2% for low, 0% for wind, -2~-4% for no lateral load design, etc.
Retrofits	Flexible, reflected in parameters used for modeling
Seismicity	Currently PGA, 0.2 second $S_a$ , 1.0 second $S_a$ (g) future versions may also use PGV, PGD, $S_v$ , and $S_d$
Limit states	Drift of an SDOF system; e.g., 0.8% serviceability, 1.5% damage control, 3% collapse.
Parameters	median $S_a$ and $\beta$ of lognormal CDF.

#### 4.2.2 Transportation systems

The MAE Center has developed fragilities for common bridge types found in the Central and Eastern U.S., as well as fragilities describing the performance of bridges after installation of retrofits (Choi et al., 2004; DesRoches, 2003). The fragilities consider uncertainties from material (e.g., steel grade, concrete strength), geometry (e.g., height of columns, length of deck),



and ground motion (duration, frequency content). Similar to the building fragility curves, uncertainty in seismic intensity is obtained from the hazard model. Table 4.2.2-1 lists the fragility curves that have been derived for buildings within the MAE Center.

**Table 4.2.2-1 MAE Center Bridge Fragility Curves**

PI	Reginald DesRoches
Structure	Nine bridge classes (# of Spans): Continuous Concrete (3), Continuous Slab (3), Continuous Steel Girder (3), Simply Supported Concrete Girder (3), Simply Supported Concrete Box Girder (3), Simply Supported Slab (3), Simply Supported Steel Girder (3) Concrete Girder (1), Steel Girder (1)
Retrofits	Steel restrainer cables, elastomeric bearings, seat extenders, steel jackets
Seismicity	PGA (g)
Limit states	Slight, Moderate, Extensive, Complete * Percent functional after 0, 1, 3, 7 and 30 days Slight: 50-100-100-100-100 Moderate: 0-50-50-100-100 Extensive: 0-0-0-50-50 Complete: 0-0-0-0-0
Parameters	$\lambda$ and $\beta$ of lognormal CDF, see Equation (4.2.1.1-1). Substitute PGA for $S_a$ in Eq (4.2.1.1-1)

The fragility equation for bridges is identical to Equation (4.2.1.1-1), except that bridge fragilities are based on PGA instead of spectral acceleration. Evaluation of bridge direct damage or loss of functionality follows the same general procedure as in Equations (4-4) through (4-10), except that there is an additional damage state. The MAE Center currently does not have fragility data to represent bridges constructed to resist earthquakes in high seismic zones, although, in the future, modifiers are expected to be developed to adjust the non-seismic fragility curves to represent the influence of seismic design.

### 4.2.3 Utility Lifeline Fragilities

#### *4.2.3.1 Buried Pipelines*

The development of fragility curves for buried pipelines has been largely based upon empirical evidence and engineering judgment. Typically, fragility curves are expressed in terms of pipe damage versus demand intensity, such as peak ground acceleration (PGA) or peak ground velocity (PGV). However, pipe fragility curves are expressed as a repair rate per length of pipe versus the demand parameter. Due to the susceptibility of buried pipelines to wave propagation, peak ground velocity will be used as the demand parameter for the pipeline



fragilities. A pipe repair can either be due to a complete fracture of the pipe, a leak in the pipe, or damage to an appurtenance of the pipe. A break takes longer to repair; however, the type of repair is the same for both states. Therefore, to estimate the cost of repairs, one must make an engineering judgment concerning the average time it takes a crew to repair a break or leak.

Barenberg (1988) conducted a study to compute the relationship between buried cast iron pipe damage in breaks/km, observed in four past earthquakes, and PGV experienced at the associated sites. This study was the first to adopt PGV rather than the Modified Mercalli Intensity levels to determine damage. This switch was important because there are mathematical models which relate the PGV to the strains induced in the pipes, which has been deemed the actual cause of damage. Then, O'Rourke, M. and Ayala (1993) provided additional empirical data for pipe damage versus peak ground velocity.

This study plotted damage rate versus PGV for cast iron, concrete, prestressed, and asbestos cement pipes. This was based on single data points from the 1965 Puget Sound, 1969 Santa Rosa, and 1989 Mexico events; two data points from the 1971 San Fernando and 1983 Coalinga events; and four data points from the 1985 Michoacán event in Mexico. This database is significant because it was the first to include large diameter asbestos cement pipes (20" and 48" diameters), with mostly cemented joints.

Eidinger (1998) then conducted a study of the East Bay Municipal Utility District after the 1989 Loma Prieta earthquake. Upon analysis of the database, the question arose concerning which of the following two formats to use to represent the pipe fragility:

- $RR=K * a (PGV)^b$ , where a and b are constants developed by the entire empirical pipe database and k is some set of pipe-specific constants, or
- $RR=a (PGV)^b$ , where a and b are pipe-specific constants which depend on all factors such as joinery, material, age, etc.

A GIS-based analysis of the pipeline damage from 1994 Northridge to the Los Angeles Department of Water and Power was conducted by O'Rourke, T. and Jeon (1999). The data used cast iron, ductile iron, asbestos cement, and steel pipes up to 24" in diameter. To ensure that each data point had an equal influence for the length of pipe it represents, O'Rourke, T. and Jeon (1999) weighted each data point to normalize the results. The results of this study show that the smaller samples of pipes at higher PGV levels have a small influence on the regression coefficients, and the regression curve with weighting is almost linear (power coefficient = 0.99). The results suggested that cast iron pipes were 30% more vulnerable than average, asbestos cement pipes were 30% less vulnerable than average, and ductile iron pipes were 10% less vulnerable than average.

Eidinger (2001) organized the available damage to buried pipelines from 18 previous earthquake events into a set of fragility curves. Most of the empirical evidence prior to 1989 shows only the performance of small diameter pipes (< 12 inches) because this was the most



prevalent pipe size in use in water systems at that time. The inclusion of more modern earthquakes has expanded the database to include pipes composed of asbestos cement, ductile iron, and welded steel pipe; however, a complete empirical database for all pipe materials under all levels of shaking still does not exist.

Analyses show that pipe material, pipe diameter, and earthquake magnitude all affect pipeline performance. Thus, using the existing database and the O'Rourke and Jeon (1999) results, which indicate a linear regression curve to be adequate, Eiding (2001) selected the following form for the pipeline fragility:

$RR = K * a (PGV)$ , where  $a$  is a constant developed from the entire empirical pipeline database.

The  $K$  values were developed to account for specific pipe materials, pipe diameters, soil conditions, and pipe joint type. Eiding (2001) found ductile iron and steel pipe to be less vulnerable than cast iron by less than a factor of two, and asbestos cement has exhibited the best performance. This trend is inconsistent with the conventional thinking that brittle materials, such as cast iron or asbestos cement, are more vulnerable than ductile materials, such as steel or ductile iron, by more than a factor of three, as assumed in HAZUS. Further, the empirical data from Loma Prieta, 1989, and Northridge, 1994, differs significantly from the previously reported data for asbestos cement pipe in Haicheng or Mexico City as observed by O'Rourke and Ayala (1993). A possible explanation for this is that the asbestos cement pipe damage in Mexico City and Haicheng were often the result of inflexible cemented joints rather than the more flexible rubber gasketed joints. Thus, the  $K$  factor for rubber gasketed joints is  $\frac{1}{2}$  the value for cemented joints, and cemented joints more closely resemble cast iron pipes.

Also, evidence has shown that large diameter pipes have lower damage rates than small diameter pipes. This assumption is reasonable because large diameter pipes typically have fewer service connections, fewer bends, and thicker walls to contain an equal amount of pressure. For Eiding (2001), the most common material in the database was cast iron (38 points) followed by steel (13), asbestos cement (10), ductile iron (9), and concrete (2). Another 9 points have both cast and ductile iron pipe combined. The database mostly contains pipes sizes associated with distribution main systems; in fact, only 8 points were identified as being specifically for large diameter pipes (> 12 inches). Additional analyses were conducted, and it has been determined that the sample size of 8 data points was not enough to show a marked difference in the relative vulnerability between a distribution pipe and a small diameter pipe. Therefore, Eiding (2001) has  $K$  factors which reflect the size of the pipe diameter, but they are mostly the result of engineering judgment.

#### 4.2.3.2 Water Tanks

To predict the damage to water tanks, one must know the PGA or response spectrum at a particular damping level, or if liquefaction is possible, PGD. One also needs the fragility curves for each damage state, the replacement value of the tank, and the correlation between the damage



state and economic losses. The most common form of damage is the outward buckling of the bottom shell courses, or “elephant foot” buckling. Other important failure mechanisms include damage due to sloshing of the contents, anchorage failure, tank support system failure, and foundation failure.

Eidinger (2001) identified several trends from the empirical data for 531 tanks over 22 earthquakes. It was observed that tanks with fill levels below 50% have a much higher median acceleration; therefore, they typically experience less damage. Also, the lognormal standard deviations are typically around 0.80, which indicates a large uncertainty involved in the tank database. When compared to the HAZUS fragility curves, it was noted that the unanchored tanks were in the same range as the empirical curves. Also, the HAZUS curves indicate an increase in capacity for anchored tanks compared to unanchored tanks, and the empirical database shows an even larger increase. O’Rourke and So (1999) also constructed fragility curves from a database of 422 tanks over 9 earthquakes. Most of the fragility curves align well with Eidinger (2001), and the discrepancies observed can be attributed to the fact that O’Rourke and So excluded all damage from an Alaskan earthquake, during which 32 of 39 tanks were damaged. Thus, the O’Rourke and So analysis has a higher median PGA for the slight damage state.

#### *4.2.3.3 Tunnels*

Dowding and Rozen (1978) created fragility curves from 68 post earthquake tunnels. The three damage states identified were none, slight – minor cracking of the tunnel liner, and moderate damage – moderate cracking of the tunnel liner and rock falls. However, this database made no delineation among the types of tunnel liner and the material through which the tunnel was constructed. Power et al. (1998) constructed a database of 217 bored tunnels that had experienced strong ground motions due to prior earthquakes. Since most damage occurs to the tunnel liner, the fragility curves provided by Power were presented as a function of the liner system. This database was also used by HAZUS; however, HAZUS also considers the quality of construction.

#### *4.2.3.4 Electric System*

Eidinger (1994) developed the damage algorithms for substation equipment based upon empirical evidence strongly tempered with engineering judgment. There are currently no known publicly available databases of damage algorithms for major substation equipment. Given this limitation, the damage algorithms were developed from the limited results of 10 earthquakes and engineering judgment. Information used to develop the fragility curves for mechanical and electrical equipment was obtained from the US Army Corps of Engineers SAFEGUARD program, while the distribution circuit damage algorithms were developed from the 1994 Northridge earthquake.



#### 4.2.4 Combined Damage from Ground Shaking and Ground Failure

Damage is expected to be strongly correlated to lateral spreading, so the probability of  $LPI \geq 15$  is taken equal to the probability of Complete damage caused by ground failure. When ground failure influences damage, the actual damage must be estimated as a combination of ground failure and ground shaking. The conceptual process of assigning damage states to structures based on a combination of the two hazard types assumes the damage from each type to be statistically independent. Currently, ground failure damage is defined as causing either no damage or Complete damage.



## 5. SOCIAL AND ECONOMIC LOSSES

### 5.1 MAEViz Implementation

The following upgrades are recommended for MAEViz hazard estimation:

- Implement Building Structural Damage Factors.
- Implement Building Nonstructural and Contents Damage Factors.
- Implement Bridge Repair Factors.
- Implement utility lifeline damage factors.
- Adjust Loss Calculations to Consider Inventory Uncertainty.
- Aggregate Losses of Inventory within Study Region.



### 5.1.1 Implement Building Structural Damage Factors and Compute Loss of Structural Value.

#### **Algorithm**

##### Inputs:

- Discrete probabilities of damage states for structural components from Section 4.1.4.
- Mean and standard deviation of damage factors from Table 5.1.1-1.
- Value of structural components from building stock inventory database (see Section 2.1.3.1).

##### Process:

- Compute expected loss ratio for each building's structural loss from discrete probabilities of damage states and mean damage factors, as shown in Equation (5.1.1-1).
- Compute variance of expected loss of building's structural components using standard deviation and mean damage factor for each damage state, discrete probabilities of damage states, and the expected loss ratio, as shown in Equation (5.1.1-2).
- Compute mean expected loss for each building by multiplying expected loss ratio for structural components and value of structural components.

##### Outputs:

- Mean and variance of expected loss ratio for structural components of each building.
- Mean of expected loss of structural value for each building.

#### **Example**

The MAE Center has provided damage factors representing the fraction of value lost as a result of damage to structural elements, as shown in Table 5.1.1-1.

**Table 5.1.1-1 MAE Center Structural Damage Factors**

MAE Center Damage State	Range of Beta Distribution (%)	Mean of Damage Factor, $\mu_{D DS_i}$ (%)	Standard Deviation of Damage Factor, $\sigma_{D DS_i}$ (%)
Insignificant (I)	[0, 1]	0.5	0.333
Moderate (M)	[1, 30]	15.5	9.67
Heavy (H)	[30, 80]	55	16.7
Complete (C)	[80, 100]	90	6.67

For both the MAEC and HAZUS building fragility sets, for each fragility set, three fragility curves are given. These demarcate between the four damage states listed in the first column above. Each damage state has an expected proportion of loss, as well as some measure of



uncertainty about that proportion. An overall expected loss ratio and loss ratio variance can be computed using Equations (5.1.1-1) and (5.1.1-2), respectively.

$$\mu_D = \sum_{i=1}^4 [P(DS_i) \cdot \mu_{D|DS_i}] \quad (5.1.1-1)$$

$$\sigma_D^2 = \sum_{i=1}^4 [P(DS_i) \cdot (\sigma_{D|DS_i}^2 + \mu_{D|DS_i}^2)] - \mu_D^2 \quad (5.1.1-2)$$

Equations (5.1.1-1) and (5.1.1-2) may be applied to I2 to obtain

$$\mu_D = 0.308 \cdot 0.5\% + 0.297 \cdot 15.5\% + 0.186 \cdot 55\% + 0.209 \cdot 90\% = 33.80\%$$

$$(\sigma_I^2 + \mu_I^2) = (0.333^2 + 0.5^2) = 0.361$$

$$(\sigma_M^2 + \mu_M^2) = (9.67^2 + 15.5^2) = 334$$

$$(\sigma_H^2 + \mu_H^2) = (16.7^2 + 55^2) = 3304$$

$$(\sigma_C^2 + \mu_C^2) = (6.67^2 + 90^2) = 8144$$

$$\sigma_D^2 = 0.308 \cdot 0.361 + 0.297 \cdot 334 + 0.186 \cdot 3304 + 0.209 \cdot 8144 - (33.80\%)^2 = 1274\%^2$$

The mean expected structural loss ratios and variance of expected structural loss ratios for all three sample structures is shown in Table 5.1.1-2.

**Table 5.1.1-2 MAE Center Sample Structural Damage Ratio Mean and Variance**

	$\mu_D$ (%)	$\sigma_D^2$ (% <sup>2</sup> )
I1 Concrete Bracci (3-story)	37.41	1560
I2 URM Wen (2-story)	33.80	1274
I3 URM Wen (2-story)	32.26	1251

The mean of expected structural loss for each building may then be computed by multiplying structural value by expected structural loss ratio (note the expected loss ratio is shown as a percentage), resulting in the data shown in Table 5.1.1-3.

**Table 5.1.1-3 MAE Center Sample Mean Structural Loss**

	$\mu_D$ (%)	Structural Value (\$)	Expected Loss of Structural Value (\$)
I1 Concrete Bracci (3-story)	37.41	21,415	8,012
I2 URM Wen (2-story)	33.80	122,126	41,276
I3 URM Wen (2-story)	32.26	127,381	41,090



5.1.2 Implement Damage Factors and Compute Losses of Building Nonstructural and Contents.

**Algorithm**

Inputs:

Discrete probabilities of damage states for nonstructural components from Section 4.1.4.

Mean and standard deviation of damage factors from Tables 5.1.2-1 through 5.1.2-3.

Value of nonstructural components and contents from building stock inventory database (see Section 2.1.3.1).

Process:

Compute expected loss ratio for each building’s nonstructural and contents loss from discrete probabilities of damage states and mean damage factors, as shown in Equation (5.1.1-1). Use acceleration sensitive probabilities of damage states when evaluating contents losses.

Compute variance of expected loss of building’s nonstructural and contents losses using standard deviation and mean damage factor for each damage state, discrete probabilities of damage states, and the expected loss ratio, as shown in Equation (5.1.1-2).

Compute mean expected nonstructural and contents losses for each building by multiplying respective expected loss ratios and values of components.

Outputs:

Mean and variance of expected loss ratio for AS NS, DS NS, and contents for each building.

Mean of expected loss of value for AS NS, DS NS, and contents for each building.

**Example**

Damage factors similar to structural damage are also available for nonstructural and contents loss estimation, as shown in Tables 5.1.2-1 through 5.1.2-3.

**Table 5.1.2-1 Acceleration-Sensitive Nonstructural Damage Factors**

MAE Center Damage State	Range of Beta Distribution (%)	Mean of Damage Factor, $\mu_{D DSi}$ (%)	Standard Deviation of Damage Factor, $\sigma_{D DSi}$ (%)
Insignificant (I)	[0, 6]	3	2
Moderate (M)	[6, 20]	13	4.67
Heavy (H)	[20, 65]	42.5	15
Complete (C)	[65, 100]	82.5	11.7



**Table 5.1.2-2 Drift-Sensitive Nonstructural Damage Factors**

MAE Center Damage State	Range of Beta Distribution (%)	Mean of Damage Factor, $\mu_{D DSi}$ (%)	Standard Deviation of Damage Factor, $\sigma_{D DSi}$ (%)
Insignificant (I)	[0, 6]	3	2
Moderate (M)	[6, 30]	18	8
Heavy (H)	[30, 75]	52.5	15
Complete (C)	[75, 100]	87.5	8.33

**Table 5.1.2-3 Contents Damage Factors**

MAE Center Damage State	Range of Beta Distribution (%)	Mean of Damage Factor, $\mu_{D DSi}$ (%)	Standard Deviation of Damage Factor, $\sigma_{D DSi}$ (%)
Insignificant (I)	[0, 3]	1.5	1
Moderate (M)	[3, 15]	9	4
Heavy (H)	[15, 37.5]	26.25	7.5
Complete (C)	[37.5, 50]	43.75	4.17

Equations (5.1.1-1) and (5.1.1-2) are also applicable to nonstructural and contents losses. Note that the probabilities of acceleration-sensitive nonstructural damage are used to determine contents losses. Mean and variance of expected damage factors for the sample buildings are shown in Table 5.1.2-4.

**Table 5.1.2-4 MAE Center Sample Nonstructural and Contents Damage Mean and Variance**

	Acceleration-Sensitive Nonstructural		Drift-Sensitive Nonstructural		Contents	
	$\mu_D$ (%)	$\sigma_D^2$ (% <sup>2</sup> )	$\mu_D$ (%)	$\sigma_D^2$ (% <sup>2</sup> )	$\mu_D$ (%)	$\sigma_D^2$ (% <sup>2</sup> )
I1 Concrete Bracci (3-story)	10.20	343	22.77	818	5.89	108
I2 URM Wen (2-story)	12.27	426	18.49	661	7.14	132
I3 URM Wen (2-story)	11.82	410	17.95	643	6.86	127



The mean of expected AS NS, DS NS, and contents loss for each building may then be computed by multiplying the value of the each component by its respective expected loss ratio (note the expected loss ratio is shown as a percentage), resulting in the data shown in Tables 5.1.2-5 through 5.1.2-7.

**Table 5.1.2-5 MAE Center Sample Mean Acceleration-Sensitive Nonstructural Loss**

	$\mu_D$ (%)	AS NS Value (\$)	Expected Loss of AS NS Value (\$)
I1 Concrete Bracci (3-story)	10.20	98,890	10,084
I2 URM Wen (2-story)	12.27	179,034	21,970
I3 URM Wen (2-story)	11.82	588,226	69,502

**Table 5.1.2-6 MAE Center Sample Mean Drift-Sensitive Nonstructural Loss**

	$\mu_D$ (%)	DS NS Value (\$)	Expected Loss of DS NS Value (\$)
I1 Concrete Bracci (3-story)	22.77	16,095	3,665
I2 URM Wen (2-story)	18.49	114,233	21,125
I3 URM Wen (2-story)	17.95	95,739	17,186

**Table 5.1.2-7 MAE Center Sample Mean Contents Loss**

	$\mu_D$ (%)	Contents Value (\$)	Expected Loss of Contents Value (\$)
I1 Concrete Bracci (3-story)	5.89	204,600	12,043
I2 URM Wen (2-story)	7.14	415,393	29,641
I3 URM Wen (2-story)	6.86	1,217,019	83,460



### 5.1.3 Implement Bridge Repair Factors and Calculate Expected Economic Loss for Bridges.

#### **Algorithm**

##### Inputs:

- Discrete probabilities of damage states for bridges from Section 4.1.5.
- Mean and standard deviation of damage factors from Tables 5.1.3-1.
- Number of spans from bridge inventory data (required to estimate damage from Complete damage state).
- Bridge structure type and total length and width from inventory.
- Replacement cost data from Table 5.1.3-3.

##### Process:

- Compute expected loss ratio for each bridge from discrete probabilities of damage states and mean damage factors, as shown in Equation (5.1.1-1).
- Compute variance of expected loss of each bridge using standard deviation and mean damage factor for each damage state, discrete probabilities of damage states, and the expected loss ratio, as shown in Equation (5.1.1-2).
- Compute expected loss for each bridge from the expected loss ratio, the mean replacement cost in Table 5.1.3-3, and the total surface area of the bridge, as shown in Equation (5.1.3-1).

Outputs: mean and variance of expected loss ratio and mean of expected loss for each bridge.

#### **Example**

Damage factors are available for bridges, as shown in Table 5.1.3-1. The damage factors are generally applicable to bridges throughout the US and are very similar to values used by HAZUS-MH (NIBS, 2006). The bridge damage factors represent the fraction of value which must be repaired as a result of earthquake damage. The “n” shown in the Complete damage row refers to the number of spans.



**Table 5.1.3-1 Bridge Damage Factors**

MAE Center Damage State	Mean of Damage Factor, $\mu_{SLi}$ (%)	Standard Deviation of Damage Factor, $\sigma_{SLi}$ (%)	Range of Beta Distribution (%)
None (N)	0.5	0.333	[0, 1]
Slight (S)	2	0.667	[1, 3]
Moderate (M)	8	4.33	[2, 15]
Extensive (E)	25	10.0	[10, 40]
Complete (C)	65 (n <= 2)	23.3	[30, 100]
	130/n (n > 2)	(200/3n)-10	

Equations (5.1.1-1) and (5.1.1-2) are again applicable to evaluating bridge damage, similarly to building damage. Applying the equations to the sample bridges damage state probabilities in Table 4.1.5-2 yields the results shown in Table 5.1.3-2.

**Table 5.1.3-2 Sample Bridge Damage Mean and Variance**

	$\mu_{BrD_i}$	$\sigma_{BrD_i}^2$
Bridge 1	0.931	7.29
Bridge 2	1.85	26.02
Bridge 3	2.11	32.48



Approximate replacement values are given in Table 5.1.3-3. The values were specifically developed for South Carolina, but provide a reasonable estimation of damage in Memphis in lieu of factors developed specifically for Tennessee.

**Table 5.1.3-3 Bridge Mean and Standard Deviation of Replacement Cost**

	$\mu_{replace}$	$\sigma_{replace}$
MSC_Concrete	67.71	16.57
MSSS_Concrete	67.71	16.57
SS_Concrete	67.71	16.57
MSC_Steel	94.37	18.36
MSSS_Steel	94.37	18.36
SS_Steel	94.37	18.36
MSC_Conc Box	67.98	14.03
MSSS_Conc Box	67.98	14.03
MSC_Slab	60.04	6.64
MSSS_Slab	60.04	6.64

The table values carry units of dollars per square foot, so mean expected damage to a particular bridge can be determined by Equation (5.1.3-1).

$$\mu_{Loss} = \mu_{BrD_i} \cdot L_{bridge} \cdot W_{bridge} \cdot \mu_{replace} \quad (5.1.3-1)$$

Mean damage for each of the sample bridges is shown in Table 5.1.3-4.

**Table 5.1.3-4 Sample Bridge Mean Damage**

	$\mu_{Loss}$ (\$)
Bridge 1	10944
Bridge 2	10218
Bridge 3	70522



5.1.4 Implement utility lifeline damage factors.

*Electric Power Plants*

**Algorithm**

Inputs:

Probabilities of damage for each component from Section 4.1.6.

Mean damage factors from Table 5.1.4-1 through 5.1.4-3.

Process:

Compute expected loss ratio for each component from probabilities of damage and mean damage factors, as shown in Equation (5.1.1-1).

Compute expected loss for each component by multiplying expected loss ratio and value for each component.

Outputs: mean of expected loss ratio and dollar value of expected loss for each component of each power plant.

**Example**

Tables 5.1.4-1 through 5.1.4-3 present the damage factors for electric system power plant components. The damage factors shown in the tables are the ratio of the repair cost to the replacement value of the component. Note that the probability of damage obtained from the fragilities is also the probability of loss of function.

**Table 5.1.4-1 Electric Power Plant Equipment - Electrical Components - Well Anchored**

Component ID Code	Component	Damage Description	Damage Factor
EPP_EC_1	Diesel Generators		0.00
EPP_EC_2	Battery Racks	failure of batteries	0.05
EPP_EC_3	Switchgear	spurious actuation of relays	0.00
EPP_EC_4	Instrument Racks and Panels	relay chatter	0.00
EPP_EC_5	Control Panels	malfunctioning equip.	0.05
EPP_EC_6	Aux. Relay Cabinets / MCCs / Circuit Breakers		0.00
EPP_EC_7	Turbine	Turbine Trip	0.00

\*Damage Factor is the ratio of the repair cost of the component / replacement value of component

NOTE: The probability of exceedence computed from the fragility for each component is also the probability of loss of function.



**Table 5.1.4-2 Electric Power Plant Equipment - Mechanical Equipment - Well Anchored**

Component ID Code	Component	Damage Factor
EPP_MC_1	Large vertical vessels with formed heads	0.25
EPP_MC_2	Boilers and Pressure Vessels	0.40
EPP_MC_3	Large horizontal vessels	0.25
EPP_MC_4	Small to medium horizontal vessels	0.25
EPP_MC_5	Large vertical pumps	0.50
EPP_MC_6	Motor Driven pumps	0.50
EPP_MC_7	Large Motor Operated Valves	0.25
EPP_MC_8	Large Hydraulic and Air Actuated Valves	0.25
EPP_MC_9	Large Relief, Manual and Check Valves	0.25
EPP_MC_10	Small Motor Operated Valves	0.25

**Table 5.1.4-3 Electric Power Plant Equipment - Other Equipment**

Component ID Code	Component	Damage Description	Damage Factor
EPP_OTH_1	Cable Trays		0.25
EPP_OTH_2	HVAC Ducting	Support System Failure	0.12
EPP_OTH_3	HVAC Equipment – Fans		0.25



Losses for the sample components are shown in Table 5.1.4-4.

**Table 5.1.4-4 Sample Electric Power Plant Component Losses**

	Component	Component ID Code	Mean Expected Loss (\$)
EPP 1	Boilers + Steam Generators	EPP_MC_2	399
EPP 2	Boilers + Steam Generators	EPP_MC_2	27666
EPP 3	Boilers + Steam Generators	EPP_MC_2	6453



## *Electric Substations*

### **Algorithm**

#### Inputs:

Probabilities of damage for each component from Section 4.1.6.

Mean damage factors from Table 5.1.4-5 through 5.1.4-7.

#### Process:

Compute expected loss ratio for each component from probabilities of damage and mean damage factors, as shown in Equation (5.1.1-1).

Compute expected loss for each component by multiplying expected loss ratio and value for each component.

Outputs: mean of expected loss ratio and dollar value of expected loss for each component of each power plant.

### **Example**

Tables 5.1.4-5 through 5.1.4-7 present the damage factors for electric system substation components. The damage factors shown in the tables are the ratio of the repair cost to the replacement value of the component. Note that the probability of damage obtained from the fragilities is also the probability of loss of function.

**Table 5.1.4-5 VHV Substation Components (500 kV and Higher)**

Component ID Code	Component	Damage Factor
ESS_VHV_1	Transformer - Anchored	0.40
ESS_VHV_2	Transformer - Unanchored	0.60
ESS_VHV_3	Live Tank Circuit Breaker - Standard	0.60
ESS_VHV_4	Live Tank Circuit Breaker - Seismic	0.10
ESS_VHV_5	Dead Tank Circuit Breaker - Standard	0.40
ESS_VHV_6	Disconnect Switch - Rigid Bus	0.50
ESS_VHV_7	Disconnect Switch - Flexible Bus	0.10
ESS_VHV_8	Lightning Arrestor	1.00
ESS_VHV_9	CCVT - Cantilevered	1.00
ESS_VHV_10	CCVT - Suspended	1.00



---

ESS_VHV_11	Current Transformer (gasketed)	0.60
ESS_VHV_12	Current Transformer (flanged)	0.40
ESS_VHV_13	Wave Trap - Cantilevered	1.00
ESS_VHV_14	Wave Trap - Suspended	0.50
ESS_VHV_15	Bus Structure - Rigid	0.15
ESS_VHV_16	Bus Structure - Flexible	0.05
ESS_VHV_17	Other Yard Equipment	0.50

---



**Table 5.1.4-6 HV Substation Components (165kV - 350 kV)**

Component ID Code	Component	Damage Factor
ESS_HV_1	Transformer - Anchored	0.40
ESS_HV_2	Transformer - Unanchored	0.60
ESS_HV_3	Live Tank Circuit Breaker - Standard	0.60
ESS_HV_4	Live Tank Circuit Breaker - Seismic	0.10
ESS_HV_5	Dead Tank Circuit Breaker - Standard	0.40
ESS_HV_6	Disconnect Switch - Rigid Bus	0.50
ESS_HV_7	Disconnect Switch - Flexible Bus	0.10
ESS_HV_8	Lightning Arrestor	1.00
ESS_HV_9	CCVT	1.00
ESS_HV_10	Current Transformer (gasketed)	0.50
ESS_HV_11	Wave Trap - Cantilevered	1.00
ESS_HV_12	Wave Trap - Suspended	0.50
ESS_HV_13	Bus Structure - Rigid	0.15
ESS_HV_14	Bus Structure - Flexible	0.05
ESS_HV_15	Other Yard Equipment	0.50



**Table 5.1.4-7 MHV Substation Components (100 kV - 165kV)**

Component ID Code	Component	Damage Factor
ESS_MHV_1	Transformer - Anchored	0.40
ESS_MHV_2	Transformer - Unanchored	0.60
ESS_MHV_3	Live Tank Circuit Breaker - Standard	0.60
ESS_MHV_4	Live Tank Circuit Breaker - Seismic	0.10
ESS_MHV_5	Dead Tank Circuit Breaker - Standard	0.40
ESS_MHV_6	Disconnect Switch - Rigid Bus	0.50
ESS_MHV_7	Disconnect Switch - Flexible Bus	0.10
ESS_MHV_8	Lightning Arrestor	1.00
ESS_MHV_9	CCVT	1.00
ESS_MHV_10	Current Transformer (gasketed)	0.50
ESS_MHV_11	Wave Trap - Cantilevered	1.00
ESS_MHV_12	Wave Trap - Suspended	0.50
ESS_MHV_13	Bus Structure - Rigid	0.15
ESS_MHV_14	Bus Structure - Flexible	0.05
ESS_MHV_15	Other Yard Equipment	0.50



Losses for the sample components are shown in Table 5.1.4-8.

**Table 5.1.4-8 Sample Electric Substation Component Losses**

	Component	Component ID Code	Mean Expected Loss (\$)
ESS 1	Transformer - Anchored	ESS_MHV_1	1042
ESS 2	Transformer - Unanchored	ESS_MHV_2	23810
ESS 3	Live Tank Circuit Breaker - Standard	ESS_VHV_3	134596



### 5.1.5 Adjust Loss Calculations to Consider Inventory Uncertainty.

#### **Algorithm**

##### Inputs:

Mean and variance of expected loss ratio for each possible structure type for each inventory item. If there are 10 structure types available for a given set of inventory, then there would be 9 additional sets of analyses for each building similar to those performed in the previous sections. The following steps will be required for each building:

Iterate through possible building types other than the expected type (e.g., for I1 in the full Memphis inventory, RM, URM, Wood frame, and all other building types *except* concrete moment frame would be considered).

Assign structural and nonstructural fragilities appropriate to each possible building type.

Allow users to decide if they want to calculate hazard at an appropriate period for each building type. Set the default setting to NO. If the user adjusts this option to YES, calculate appropriate hazard for each building type based on approximate period as described previously.

Calculate probabilities of damage states for structural and nonstructural components, as described previously, for each possible building type.

Calculate mean and variance of loss ratio, as previously discussed, for each possible building type.

User specified level of inventory uncertainty.

##### Process:

Define probability of accurate identification.

Compute a weighted average of expected loss, with weights based on the user specified inventory uncertainty and the relative number of each structure type believed to exist in the inventory.

##### Outputs:

Mean and variance of expected loss ratio adjusted for inventory uncertainty.

#### **Example**

For a general case, the probability of accurate identification, denoted by  $p_{id}$ , will be defined by the user. This means there is  $(1 - p_{id})$  probability that the structure belongs to any of the *other* structural types in the inventory. Then, the mean of the damage ratio is calculated as

$$\mu_{\bar{D}} = p_{id}\mu_D + (1 - p_{id})\mu_{D_r} \quad (5.1.5-1)$$



where  $\mu_{\tilde{D}}$  is the mean damage ratio with the inventory uncertainty considered,  $\mu_D$  is the mean damage ratio based on the identified structure type, as calculated in previous sections, and  $\mu_{D_r}$  is the “representative” mean damage ratio assuming an inaccurate prediction of structure type. The “representative” mean damage ratio is estimated as the weighted average of the mean damage ratios based on all the identified structural types except for the originally predicted type, that is,

$$\mu_{D_r} = \frac{1}{N} \sum_{j=1}^{N_{id}} n_j \cdot \mu_D^j \quad (5.1.5-2)$$

where  $N_{id}$  is the number of the structure types identified in the inventory minus one (for the originally predicted type);  $n_j$  is the number of the inventory items identified as the  $j$ -th structural type,  $j = 1, \dots, N_{id}$ ;  $N = \sum_j^{N_{id}} n_j$  is the total number of inventory items excluding those identified as the originally predicted type; and  $\mu_D^j$  is the mean damage ratio estimated based on the  $j$ -th structural type at the given site.

Note that for this example, the hazard will be assumed constant with respect to structure type. In fact, each structure type can have its own period, and a calculation should be performed for each period to estimate an appropriate spectral acceleration to maximize the accuracy of the predictions. When the hazard is *transformed* from spectral acceleration to spectral displacement for drift-sensitive damage estimation, the period corresponding to the particular structure type is used, regardless of whether the spectral acceleration hazard has been recalculated for the appropriate period.

Variance can be adjusted to account for inventory uncertainty by calculating

$$\sigma_{\tilde{D}}^2 = E[\tilde{D}^2] - \mu_{\tilde{D}}^2 = [p_{id}(\mu_D^2 + \sigma_D^2) + (1 - p_{id})(\mu_{D_r}^2 + \sigma_{D_r}^2)] - \mu_{\tilde{D}}^2 \quad (5.1.5-3)$$

and

$$(\mu_{D_r}^2 + \sigma_{D_r}^2) = \frac{1}{N} \sum_{j=1}^{N_{id}} n_j \cdot (\mu_D^2 + \sigma_D^2)^j \quad (5.1.5-4)$$

where terms are defined similarly to those used in Equations (5.1.5-1) and (5.1.5-2). Note that in Equations 5.1.5-1 through 5.1.5-4, the “ $j$ ” superscripts are counters for structural types, *not* exponents.

Consider that the user specifies a level of inventory uncertainty of 15%. For computational simplicity, assume that the buildings could only be assigned concrete moment frame or URM building types (*for purposes of this example, it is impossible that the buildings could have been classified as wood or steel frame or any other building type*). As a result, the building that was identified as a concrete frame has a 15% probability of being something else, which for this example could only be URM. Likewise, the URM buildings each have a 15% probability of actually being a concrete frame building instead of URM. Using Equation (5.1.5-1) with an inventory uncertainty of 15%, the mean of the damage factors can be calculated with the formula given below:



$$\mu_{\bar{D}} = 0.85\mu_D + 0.15\mu_{D_r} \quad (5.1.5-5)$$

The  $\mu_{D_r}$  term will vary in general, depending on what the expected type of building was. In this example,  $\mu_{D_r} = \mu_D^{URM}$  for the concrete frame building, and  $\mu_{D_r} = \mu_D^{concrete}$  for the URMs. For a general case, the “representative” would be based on a weighted average of how many of each building are expected in the total inventory *excluding* the predicted type (see Table 5.1.5-2).

The updated mean of damage factors can be written as

$$\mu_{\bar{D}} = 0.85\mu_D^{concrete} + 0.15\mu_D^{URM} \quad (5.1.5-6)$$

for inventory item I1, and

$$\mu_{\bar{D}} = 0.15\mu_D^{concrete} + 0.85\mu_D^{URM} \quad (5.1.5-7)$$

for inventory items I2 and I3.

Also, the variance for the concrete building can be calculated as

$$\sigma_{\bar{D}}^2 = \left[ 0.85(\mu_D^2 + \sigma_D^2)^{concrete} + 0.15(\mu_D^2 + \sigma_D^2)^{URM} \right] - \mu_{\bar{D}}^2 \quad (5.1.5-8)$$

where the  $\mu_D^2$  term is calculated in Equation (5.1.5-6) for the concrete frame building.

Likewise, the variance for each of the URM buildings can be calculated as

$$\sigma_{\bar{D}}^2 = \left[ 0.15(\mu_D^2 + \sigma_D^2)^{concrete} + 0.85(\mu_D^2 + \sigma_D^2)^{URM} \right] - \mu_{\bar{D}}^2 \quad (5.1.5-9)$$

where the  $\mu_D^2$  term is calculated in Equation (5.1.5-7) for each URM building.

With Eqs. (5.1.5-6) through (5.1.5-9), the mean and variance for the example inventory can be updated with 15% inventory uncertainty as shown in Table 5.1.5-1.

**Table 5.1.5-1 Updating with Inventory Uncertainty**

Inventory Buildings			Without Inventory Uncertainty	With 15% Inventory Uncertainty
Concrete Building	Structural damage	$\mu$	0.374	0.358
		var	0.156	0.151
	Non-structural damage	$\mu$	0.102	0.102



Inventory Buildings		Without Inventory Uncertainty	With 15% Inventory Uncertainty	
I2 URM 1	(acceleration-sensitive)	var	0.034	0.034
	Contents loss	$\mu$	0.228	0.217
		var	0.082	0.079
	Non-structural damage (drift-sensitive)	$\mu$	0.059	0.059
		var	0.011	0.011
	Structural damage	$\mu$	0.338	0.356
		var	0.127	0.134
	Non-structural damage (acceleration-sensitive)	$\mu$	0.123	0.123
		var	0.043	0.043
	Contents loss	$\mu$	0.185	0.198
		var	0.066	0.071
	Non-structural damage (drift-sensitive)	$\mu$	0.071	0.072
var		0.013	0.013	
I3 URM 2	Structural damage	$\mu$	0.323	0.340
		var	0.125	0.132
	Non-structural damage (acceleration-sensitive)	$\mu$	0.118	0.118
		var	0.041	0.041
	Contents loss	$\mu$	0.180	0.192
		var	0.064	0.069
	Non-structural damage (drift-sensitive)	$\mu$	0.069	0.069
		var	0.013	0.013



The small sample of buildings used in the example is not fully descriptive of the process. If the buildings were considered to be part of the full Memphis building inventory (version 4), expected mean and variance of loss ratios would need to be evaluated considering several other building types, and weighting factors would need to be applied to those calculated values to obtain a “representative” value for inaccurate structure type prediction, as shown in Table 5.1.5-2. Weighting factors are calculated as the number of buildings in the entire inventory with a certain predicted structure type divided by the total number of buildings excluding the predicted structure type of the inventory item under consideration.

For example, item I1 was classified as a concrete moment frame, so the cell for concrete moment frame building count under I1 is left blank. The total number of buildings in the inventory, excluding those predicted to be concrete moment frames, is 291,910. The weighting factor for Light Wood Frame is  $( 269,725 / 291,910 ) = 0.924$ . When computing the representative damage ratio for an inaccurate prediction of I1 structure type, the damage ratio calculated assuming a Light Wood Frame structure type would be multiplied by 0.924 to obtain its contribution to the total representative damage ratio.

**Table 5.1.5-2 Inventory Uncertainty Weighting Factors for Full v4 MTB Inventory**

Structure Types	I1 Inventory Uncertainty		I2 and I3 Inventory Uncertainty	
	Building Count	Weighting Factor	Building Count	Weighting Factor
Concrete Moment Resisting Frame		0.000	528	0.002
Concrete Frame with Concrete Shear Wall	114	0.000	114	0.000
Concrete Tilt-up	1,078	0.004	1,078	0.004
Precast Concrete Frame	167	0.001	167	0.001
Reinforced Masonry	2,586	0.009	2,586	0.009
Steel Frame	612	0.002	612	0.002
Light Metal Frame	6,668	0.023	6,668	0.023
Unreinforced Masonry	6,302	0.022		0.000
Light Wood Frame	269,725	0.924	269,725	0.943
Commercial Wood Frame	4,658	0.016	4,658	0.016
<b>TOTALS</b>	<b>291,910</b>	<b>1</b>	<b>286,136</b>	<b>1</b>



*5.1.6 Scale losses to account for inflation.*

**Algorithm**

Inputs:

Table of inflation factors.

Estimated direct economic losses for inventory items.

Data for each inventory item identifying year of appraisal.

Process:

Lookup appropriate inflation factor from supplied table based on year of appraisal for each inventory item.

Multiply estimated losses by appropriate inflation factors for each inventory item.

Outputs:

Adjusted direct economic loss accounting for inflation.

**Example**

*[Example data not currently available]*



### 5.1.7 Aggregate Losses of Inventory within Study Region.

#### **Algorithm**

##### Inputs:

Mean and variance of expected loss ratio for items to be aggregated (e.g., building structural, bridges).

Value of items (and components, as appropriate) for which losses are being aggregated.

User specified confidence level for loss ratio.

##### Process:

Calculate mean of loss for each item and sum per Equation 5.1.7-4.

Calculate variance of aggregated loss per Equation 5.1.7-5.

Calculate mean and standard deviation of the loss ratio per Equations 5.1.7-8 and 5.1.7-9.

Calculate  $\lambda$  and  $\beta$  for a lognormal distribution of loss ratio per Equations 5.1.7-10 and 5.1.7-11.

##### Outputs:

Plot of probability density function with respect to loss ratio using Equation 5.1.7-12.

Plot of probability of exceedence as a function of loss ratio using Equation 5.1.7-13.

Confidence bounds for loss ratio using Equation 5.1.7-14.

#### **Example**

The general form of the equation for total direct economic loss for a building is given by

$$Loss_i = M_i (\alpha_i^{SD} \mu_{\tilde{D}_i^{SD}} + \alpha_i^{NA} \mu_{\tilde{D}_i^{NA}} + \alpha_i^{ND} \mu_{\tilde{D}_i^{ND}} + \alpha_i^{CL} \mu_{\tilde{D}_i^{CL}}) \quad (5.1.7-1)$$

where  $M_i$  is the total assessed value of the i-th inventory item;  $\alpha_i^{SD}$ ,  $\alpha_i^{NA}$  and  $\alpha_i^{ND}$  are the fractions of the values of structural and non-structural (acceleration- and drift-sensitive) components;  $\alpha_i^{CL}$  is the ratio of the contents value to the total assessed value;  $\mu_{\tilde{D}_i^{SD}}$ ,  $\mu_{\tilde{D}_i^{NA}}$  and  $\mu_{\tilde{D}_i^{ND}}$  are the damage ratios of the i-th inventory item adjusted by the inventory uncertainty; and  $\mu_{\tilde{D}_i^{CL}}$  is the adjusted content loss ratio. Values of  $M_i \cdot \alpha_i$  were calculated for structural, acceleration-sensitive nonstructural, and drift-sensitive nonstructural assets in Section 2.1.3.1. Currently, the MAEC inventory data includes a pre-calculation of  $M_i \cdot \alpha_i^{CL}$  in their own data field prior to ingestion into MAEviz, so the  $\alpha_i^{CL}$  coefficients are not visible. The value of the various components may be represented in equation form as

$$M_i^{SD} = M_i \cdot \alpha_i^{SD} \text{ is the structural component value} \quad (5.1.7-2a)$$



$$M_i^{NA} = M_i \cdot \alpha_i^{NA} \text{ is the acceleration-sensitive nonstructural component value} \quad (5.1.7-2b)$$

$$M_i^{ND} = M_i \cdot \alpha_i^{ND} \text{ is the drift-sensitive nonstructural component value} \quad (5.1.7-2c)$$

$$M_i^{CL} = M_i \cdot \alpha_i^{CL} \text{ is the contents value} \quad (5.1.7-2d)$$

The total loss of the inventory is obtained by aggregating the losses of the inventory items, that is,

$$Loss = \sum_{i=1}^N Loss_i \quad (5.1.7-3)$$

Then mean of the total loss is estimated as

$$\mu_{Loss} = \sum_{i=1}^N \left( M_i^{SD} \mu_{\tilde{D}_i^{SD}} + M_i^{NA} \mu_{\tilde{D}_i^{NA}} + M_i^{ND} \mu_{\tilde{D}_i^{ND}} + M_i^{CL} \mu_{\tilde{D}_i^{CL}} \right) \quad (5.1.7-4)$$

Assuming the damage ratios of different inventory items are conditionally independent given a seismic intensity, the variance of the total loss is computed as

$$\sigma_{Loss}^2 = \sum_{i=1}^N \left( (M_i^{SD})^2 \sigma_{\tilde{D}_i^{SD}}^2 + (M_i^{NA})^2 \sigma_{\tilde{D}_i^{NA}}^2 + (M_i^{ND})^2 \sigma_{\tilde{D}_i^{ND}}^2 + (M_i^{CL})^2 \sigma_{\tilde{D}_i^{CL}}^2 \right) \quad (5.1.7-5)$$

The coefficient of variation (c.o.v.) of the total loss is

$$\delta_{Loss} = \frac{\sigma_{Loss}}{\mu_{Loss}} \quad (5.1.7-6)$$

The mean, standard deviation and c.o.v. of the total loss of the example inventory are estimated as 0.366 (million US\$), 0.208 (million US\$) and 56.92%, respectively.

Loss Ratio ( $L_r$ ) may be defined as the total loss normalized by the sum of structural, non-structural and content values in a region, that is,

$$L_r = \frac{Loss}{\sum_{i=1}^N M_i (\alpha_i^{SD} + \alpha_i^{NA} + \alpha_i^{ND} + \alpha_i^{CL})} = \frac{Loss}{\sum_{i=1}^N M_i + M_i^{CL}} = \frac{Loss}{M_{total}} \quad (5.1.7-7)$$

Then, mean and standard deviation of the loss ratio are, respectively,

$$\mu_{L_r} = \frac{\mu_{Loss}}{M_{total}} \quad (5.1.7-8)$$

and

$$\sigma_{L_r} = \frac{\sigma_{Loss}}{M_{total}} \quad (5.1.7-9)$$

The c.o.v. of the loss ratio is the same as that of the total loss. For the example inventory, the mean and standard deviation of the loss ratio are estimated as 11.4 % and 6.51 %, respectively.



The probability distribution of the loss ratio can be determined, given the estimated mean and standard deviation, and an assumed distribution type.

It is assumed that the loss ratio follows the lognormal distribution. The lognormal distribution requires two parameters  $\lambda$  and  $\beta$ , which are the mean and standard deviation of the natural logarithm of the quantity. These parameters are obtained from the estimated mean and standard deviation of the loss ratio as follows.

$$\beta = \sqrt{\ln \left[ 1 + \left( \frac{\sigma_{L_r}}{\mu_{L_r}} \right)^2 \right]} \quad (5.1.7-10)$$

$$\lambda = \ln \mu_{L_r} - 0.5\beta^2 \quad (5.1.7-11)$$

The lognormal parameters of the loss ratio in the example are  $\lambda = -2.308$  and  $\beta = 0.530$ . The probability density function (PDF) of the loss ratio is defined as

$$f_{L_r}(l_r) = \frac{1}{\sqrt{2\pi}\beta l_r} \exp \left[ -\frac{1}{2} \left( \frac{\ln l_r - \lambda}{\beta} \right)^2 \right] \quad (5.1.7-12)$$

The plot of this function for the sample data is shown in Figure 5.1.7-1.

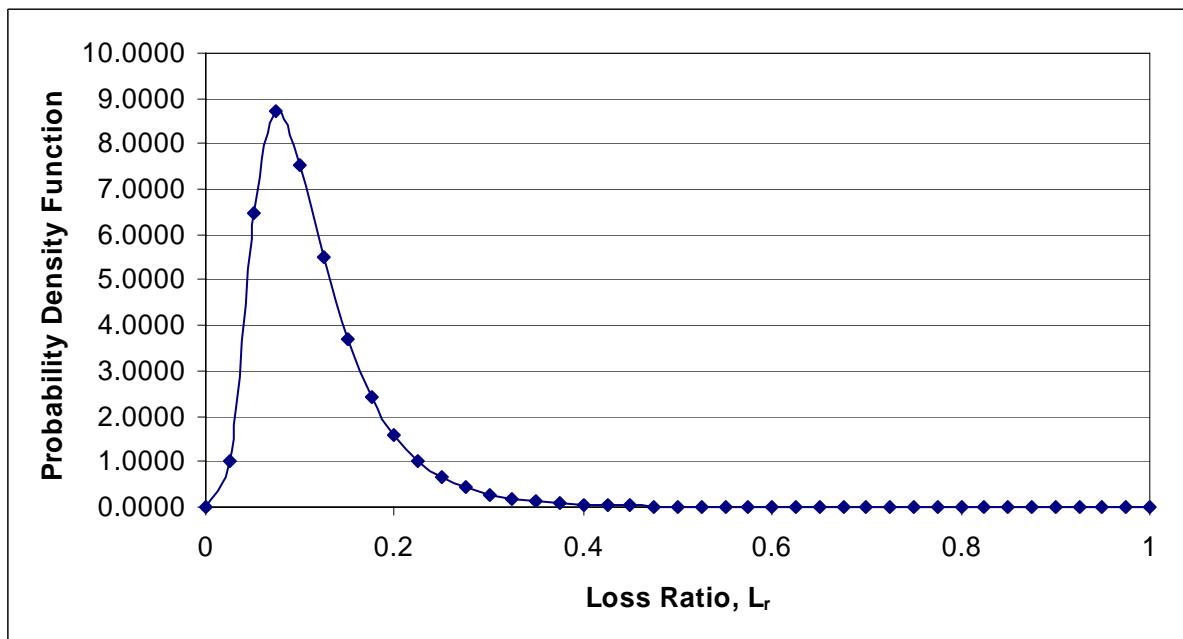


Figure 5.1.7-1. Probability Density Function for Loss Ratio.

The complementary cumulative density function (CCDF) can also be plotted to show probabilities of exceedence for various levels of loss ratio. The CCDF is defined by



$$C_{L_r}(l_r) = 1 - \Phi \left[ \frac{\ln(l_r) - \lambda}{\beta} \right] \quad (5.1.7-13)$$

which can be plotted as shown in Figure 5.1.7-2. Table 5.1.7-1 lists the exceedance probabilities at selected thresholds of loss ratio.

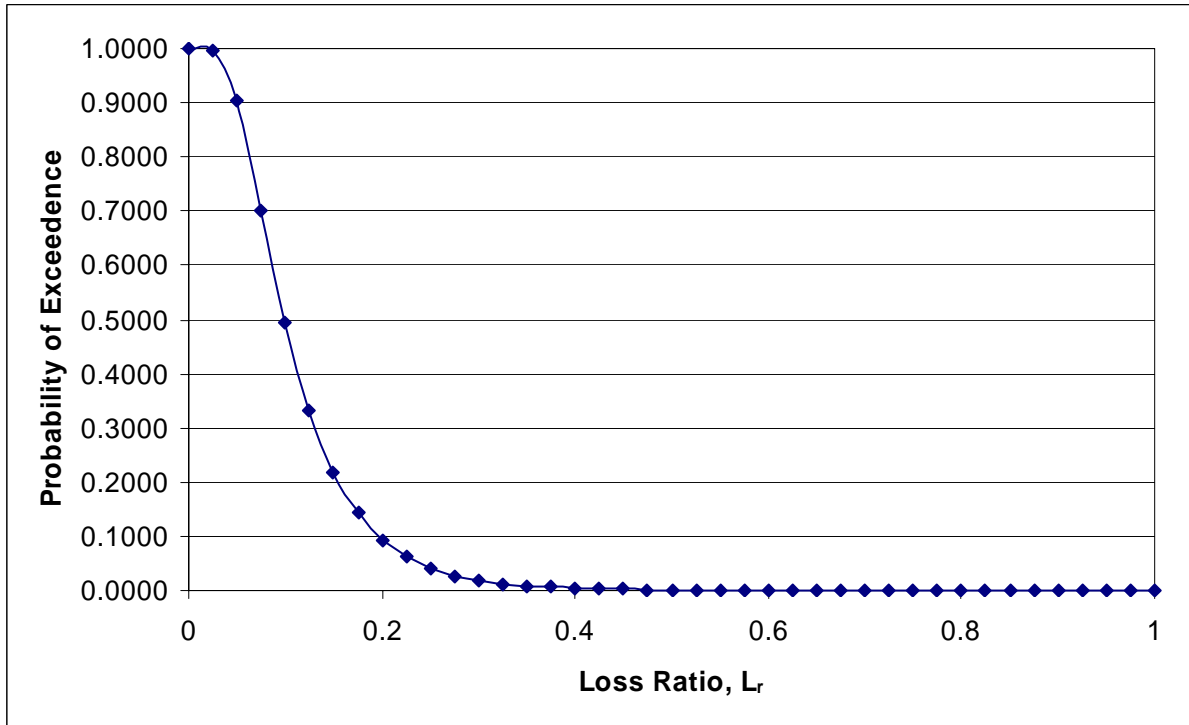


Figure 5.1.7-2. Probability of Exceedence in terms of Loss Ratio.

Table 5.1.7-1. Selected Probabilities of Exceedance

Loss ratio (%)	Probability of exceedence, % (lognormal distribution)
0	100.00
1	100.00
5	90.29
10	49.58
20	9.36



Loss ratio (%)	Probability of exceedence, % (lognormal distribution)
30	1.86
40	0.43
50	0.11

Based on the estimated uncertainty in the loss ratio, we can predict the loss ratio by an interval with a certain level of confidence. An interval that encloses the true loss ratio with probability  $1 - \alpha$  (or an interval with ‘confidence level’  $1 - \alpha$ ) is

$$[\exp(\lambda - k_{\alpha/2}\beta), \exp(\lambda + k_{\alpha/2}\beta)] \quad (5.1.7-14)$$

where  $k_{\alpha/2} = \Phi^{-1}(1 - \alpha/2)$ . Table 5.1.7-2 shows the coefficient values for selected confidence levels and the corresponding confidence intervals.

**Table 5.1.7-2. Confidence intervals for loss ratio**

Confidence level, $1 - \alpha$ (%)	$k_{\alpha/2}$	Confidence interval (%)
60	0.8416	[6.37, 15.53]
70	1.0364	[5.74, 17.22]
80	1.2816	[5.04, 19.61]
90	1.6449	[4.16, 23.77]
95	1.9600	[3.52, 28.09]
99	2.5758	[2.54, 38.92]



### 5.1.8 Calculate Fiscal Losses (Property Tax Revenue).

#### **Algorithm**

##### Inputs:

Mean damage factors for structural, acceleration-sensitive nonstructural, and drift-sensitive nonstructural building components for each building.

Value for each set of building components for each building.

Property Tax rate applicable to each building (based on jurisdiction). This will likely be determined internally by MAEviz by comparing building locations to polygons in a shapefile with an associated attribute of Property Tax.

##### Process:

Calculate Direct Economic Damage for building components only (do NOT include contents losses) by multiplying building component values by mean loss factors, as shown in Equation 5.1.8-1.

$$\mu_{DED} = M_i^{SD} \mu_{\tilde{D}_i^{SD}} + M_i^{NA} \mu_{\tilde{D}_i^{NA}} + M_i^{ND} \mu_{\tilde{D}_i^{ND}} \quad (5.1.8-1)$$

Calculate Loss Ratio for Direct Economic Damage as shown in Equation 5.1.8-2, where  $M_i$  is the assessed building value originally supplied in the inventory database.

$$\mu_{L_r-DED} = \frac{\mu_{DED}}{M_i} \quad (5.1.8-2)$$

If the Loss Ratio for Direct Economic Damage is greater than 0.1 (10%), then calculate Property Tax loss as shown in Equation 5.1.8-3,  $TR_j$  is the property tax rate for jurisdiction “j”, determined by comparing a building’s location to a map of property tax rates for various jurisdictions.

$$\text{if } \mu_{L_r-DED} > 0.1 \text{ then } PTL_i = \mu_{DED} \cdot TR_j \quad (5.1.8-3)$$

Repeat these steps for each building in the inventory.

Allow the user to select a group of items for aggregation (offer summation by jurisdiction as a default) and sum  $PTL_i$  to obtain fiscal losses.

##### Outputs:

Fiscal losses for individual buildings and groups of buildings as selected by the user.

#### **Example**

*[Example data not currently available]*



## 5.2 Background

### 5.2.1. Economic Loss for Building structures

#### *5.2.1.1 Building Structural Damage*

A framework has been advanced within the MAE Center to establish correlations between structural damage states and direct economic losses (i.e., repair and replacement), as shown in Table 5.1.1-1 (Bai et al., 2006). The damage factors,  $\mu_{Li}$ , form a bridge between the engineering engine outputs (i.e., probabilities of exceeding limit states defined by analytical thresholds, such as interstory drift ratio) and economic losses in terms of monetary values.

#### *5.2.1.2 Building Nonstructural and Contents losses*

There is not currently any MAE Center research addressing direct economic losses from nonstructural and contents. In the absence of MAE Center research, nonstructural and contents damage factors may be adapted from HAZUS. HAZUS provides deterministic damage factors for discrete damage states, with no stated ranges or uncertainties. The deterministic damage factors may be converted to approximate ranges by assuming that ranges extend to the midpoints between adjacent damage factors. Damage factors and uncertainties presented similarly to the values in Table 5.1.1-1 are provided in Tables 5.1.2-1 through 5.1.2-3.

### 5.2.2. Social Impacts

The MAEC is actively developing social impact algorithms (Peacock and Zhang, 2005; Prater et al., 2005; French, 2005; French, 2005; French et al., 2005), but the algorithms are not yet ready for inclusion in the MAEC CRM framework and MAEviz.



## 6. NETWORK MODELING

The MAE Center is presently engaged in developing network models for transportation and utility lifeline functionality. The transportation models are currently more advanced than utility network models, and are being implemented for a transportation testbed at Charleston, SC (DesRoches et al., 2006; Duthie et al., 2006; Karoonsoontawong and Waller, 2005; Kim et al., 2006). Transportation network models include two phases. The first phase considers the original traffic flow pattern and how that pattern can be expected to be perturbed by a major earthquake. The second phase examines how the modified flow pattern will be affected by damage to transportation network components (i.e., bridges) and what economic consequences can be expected as an end result of perturbed traffic flow in terms of costs to commuters resulting from time lost in transit. Models for loss effects of utility networks are still in development, and are not yet ready for implementation.

## 7. SYSTEM INTERDEPENDENCIES

The MAE Center is currently developing a methodology for predicting losses in utility networks resulting from failures in other networks (e.g., water network functionality impacted by loss of electric power to pump stations). A general framework has been developed within the MAE Center (Duenas-Osorio et al., 2004; Duenas-Osorio, 2005) but is not currently ready for implementation.

## 8. DECISION SUPPORT

The overarching view of decision support seeks to provide tools for decision makers to maximize the benefit of capital investments. This effort is generally facilitated using one of three approaches:

- (1) Equivalent cost analysis (ECA): convert all losses to monetary values
- (2) Multi-attribute utility theory (MAUT): value-measuring theory incorporating risk-attitude of decision makers.
- (3) Joint probability decision making (JPDM): probability that criteria will be satisfied.

Another capability of decision support is sensitivity analysis, which allows the user to investigate the sensitivity of the above results with respect to changes in various parameters.

Decision support currently relies on a methodology developed by Park (2004). Park (2004) focuses primarily on retrofit of general building stock, and draws an approximate correlation between “code level” in HAZUS and retrofit performance objectives. There is a basic presumption that the building under consideration is appropriately modeled with Pre-Code



fragilities in HAZUS, and that fragility data for higher code levels can be mapped to performance objectives as follows:

Low Code → Life Safety (LS)

Moderate Code → Immediate Occupancy (IO)

High Code → New Construction

The Park (2004) methodology is rigid, requiring the use of HAZUS fragilities to approximately represent the installation of retrofits. The methodology has been adjusted to now consider MAEC parametric fragilities based on physical parameters stated in the HAZUS technical manual. A promising option which will be explored in the near future will seek to make retrofit objectives more flexible by targeting code levels as objectives, and allowing the user to have greater freedom to influence the exact level of performance desired. The MAEC parametric fragility curves have far greater flexibility in representing various retrofit schemes relative to the published “code-level” parameters for HAZUS, and specific behaviors could be modeled, such as increasing stiffness independently with respect to force capacity and ductility to represent the installation of shear walls.

Decision support will also build on increasingly sophisticated loss models and consider a broader scope of analysis including traffic flow, lifeline network models, and system interdependencies.

## 9. CONCLUSIONS

This document presents an overview of the current knowledge base available within the MAE Center for use in the Consequence-based Risk Management framework, as well as an overview of the currently implemented and proposed features for MAEviz. While the knowledge base is quite extensive and detailed for inventory collection, hazard definition, and vulnerability estimation, several issues are still outstanding which should be addressed to make the MAE Center CRM framework truly comprehensive and as accurate as possible.

Social and economic impact algorithms are currently in development by many researchers within the MAE Center, and the results of their efforts will play a key role in bridging the gap between engineering damage estimation and social and economic losses affecting society. Further investigation is also warranted for building stock nonstructural loss estimation. Nonstructural and contents losses can often far exceed losses in structural value, but the MAE Center is currently forced to adapt the approximate methodologies used by HAZUS for valuation, damage estimation, and losses caused by nonstructural damage due to a lack of research in this key area. Network modeling, system interdependencies, and decision support capabilities are all developing rapidly and will soon be able to be fully integrated into the MAE Center CRM framework and MAEviz.



## REFERENCES

- Atkinson, G. M., and Boore, D. M. (1995). "Ground Motion Relations for Eastern North America." *Bulletin of the Seismological Society of America*, 85(1), 17 - 30.
- Bai, J.-W. and Hueste, M. D. (2006). "Seismic Fragility of a Tilt-Up Concrete Building in the Central United States," Proceedings of the 8th U.S. National Conference on Earthquake Engineering, San Francisco, California, April 18-22, 2006, Earthquake Engineering Research Institute, Oakland, California.
- Bai, J.-W. and Hueste, M. D. (2007). "Deterministic and Probabilistic Evaluation of Retrofit Alternatives for a Five-Story Flat-Slab RC Building," Mid-America Earthquake (MAE) Center Technical Report, 06-01.
- Bai, J.-W., Hueste, M. D., and Gardoni, P. (2006). "A Probabilistic Framework for the Assessment of Structural Losses due to Seismic Events," Limited distribution in preparation for publication, June 30, 2006.
- Borcherdt, R. D. (1994). "Estimates of Site-Dependent Response Spectra for Design (Methodology and Justification)," *Earthquake Spectra*, Vol. 10, pp. 617-653.
- Celik, O. C. and Ellingwood, B. R. (2006). "Fragility Assessment of Reinforced Concrete Frames Designed for Regions of Moderate Seismicity," Proceedings of the 1st European Conference on Earthquake Engineering and Seismology, Geneva, Switzerland, September 3-8, 2006, Symporg SA, Geneva, Switzerland (ISBN 10:2 8399-0190-0).
- Choi, E., DesRoches, R., and Nielson, B., (2004), "Seismic Fragility of Typical Bridges in Moderate Seismic Zones," *Engineering Structures*, Vol. 26, No. 2, pp. 187-199, January.
- DesRoches, R. (2006). "Memphis Testbed Bridge Inventory from National Bridge Inventory," personal communication.
- DesRoches, R., Leon, R. T., and Dyke, S., (2003), "Response Modification of Bridges," Internal Report, CD Release 03-08, Mid-America Earthquake Center, Urbana, Illinois, December.
- DesRoches, R., Padgett, J. E., Elnashai, A. S., Kin, Y. S., and Reed, D. (2006) "MAE Center Transportation Test Bed," Proceedings of the 8<sup>th</sup> U. S. National Conference on Earthquake Engineering, San Francisco, California, 2006, Earthquake Engineering Research Institute, Oakland, California.
- Dobry, R., Borcherdt, R. D., Crouse, C. B., Idriss, I. M., Joyner, W. B., Martin, G. R., Power, M. S., Rinne, E. E., and Seed, R. B. (2000). "New Site Coefficients and Site Classification System Used in Recent Building Seismic Code Provisions," *Earthquake Spectra*, Vol. 16, pp. 41-67.



- Dowding, C. H. and Rozen, A. (1978). "Damage to Rock Tunnels from Earthquake Shaking," *Journal of the Geotechnical Engineering Division*, American Society of Civil Engineers, New York, New York, February.
- Duenas-Osorio, L., (2005), "Interdependent Response of Networked Systems to Natural Hazards and Intentional Disruptions," Ph.D. Dissertation, Georgia Institute of Technology, Atlanta, Georgia.
- Duenas-Osorio, L., Craig, J. I., and Goodno, B. J., (2004), "Probabilistic Response of Interdependent Infrastructure Networks," 2004 ANCER Annual Meeting, Honolulu, HI, July 28-30, 2004.
- Duthie, J., Unnikrishnan, A., and Waller, S. T. (2006). "Network Evaluation with Uncertain and Correlated Long-Term Demand," Proceedings of the 85th Annual Meeting of the Transportation Research Board, Washington, DC.
- Eidinger, J. (2001). "Seismic Fragility Formulations for Water Systems," sponsored by the American Lifelines Alliance, G&E Engineering Systems Inc., web site. <<http://homepage.mac.com/eidinger>>.
- Ellingwood, B. R. (2005). "Seismic Fragility Assessment of Light-Frame Wood Residential Construction," Proceedings of the Luis Esteva Symposium Earthquake Engineering, Challenges and Tendencies, Mexico City, Mexico, September 7-11, 2005, Universidad Nacional Autonoma de Mexico, Mexico, DF.
- Erberik, M. A., and Elnashai, A. S. (2006). "Loss Estimation Analysis of Flat-Slab Structures," *Natural Hazards Review*, Vol. 7, No. 1, pp. 26-37, February.
- Federal Highway Administration (FHWA) (1995). "Recording and Coding Guide for the Structure Inventory and Appraisal of the Nation's Bridges," U.S. Department of Transportation, Office of Engineering, Bridge Division, Report No. FHWA-PD-96-001, December, 1995.
- Fernandez, J. A. (2006). "Hard Rock Attenuation Correction Factors." Personal communication.
- Fernandez, J. A., and Rix, G. J. (2006). "Soil Attenuation Relationships and Seismic Hazard Analyses in the Upper Mississippi Embayment". Proceedings of the 8<sup>th</sup> U.S. National Conference on Earthquake Engineering San Francisco, California, April 18-22, 2006, Earthquake Engineering Research Institute, Oakland, California.
- Frankel, A., Mueller, C., Barnhard, T., Perkins, D., Leyendecker, E. V., Dickman, N., Hanson, S., and Hopper, M. (1996). "National Seismic Hazard Maps: Documentation." *OFR 96-532*, U.S. Geological Survey.
- French, S. P. (2005). "Conceptualizing the Social and Economic Consequences of Natural Hazards," Presentation at the 46th Annual Conference of the Association of Collegiate Schools of Planning, Kansas City, Missouri, October 27-30, 2005.



- French, S. P. (2006). "Memphis Water Pipeline and Water Tank Databases," Personal communication.
- French, S. P. (2006). "Valuation of Building Stock," Personal communication.
- French, S. P. (2005). "Social Science Research in the Mid-America Earthquake Center," Internal Report, Mid-America Earthquake Center, Urbana, Illinois
- French, S. P., Lee, D., and Rees, J. (2005). "Estimating the Social and Economic Consequences of Earthquakes and Other Natural Hazards," Presentation at the 46th Annual Conference of the Association of Collegiate Schools of Planning, Kansas City, Missouri, October 27-30, 2005.
- French, S.P., and Muthukumar, S. (2006). "MTB Inventory Summary, version 3." Personal communication.
- French, S. P., and Muthukumar, S. (2006). "Memphis Building Stock Inventory Shapefiles and Databases, Version 4." Personal communication.
- French, S. P., and Muthukumar, S. (2006). "Advanced Technologies for Earthquake Risk Inventories," *Journal of Earthquake Engineering*, Vol. 10, No. 2, pp. 207-236.
- French, S. P., and Muthukumar, S. (2006). "MTB roadway inventory." Personal communication.
- G & E Engineering Systems, Inc. (1994). "Earthquake Loss Estimation Methods, Technical Manual, Electric Power Utilities," National Institute of Building Sciences, Washington, D.C.
- Hueste, M. D. and Bai, J.-W. (2007). "Seismic Retrofit of a Reinforced Concrete Flat-Slab Structure: Part I – Seismic Performance Evaluation." *Engineering Structures*, in press.
- Hueste, M. D. and Bai, J.-W. (2007). "Seismic Retrofit of a Reinforced Concrete Flat-Slab Structure: Part II – Seismic Fragility Analysis." *Engineering Structures*, in press..
- Karoonsoontawong, A., and Waller, S. T. (2005). "Comparison of System and User-Optimal Stochastic Dynamic Network Design Models Using Monte Carlo Bounding Techniques," *Journal of the Transportation Research Board*, No. 1923, Transportation Research Board, Washington, D.C.
- Kim, Y. S., Elnashai, A. S., Spencer, B. F., Ukkusuri, S., and Waller, S. T. (2006) "Seismic Performance Assessment of Highway Networks," Proceedings of the 8<sup>th</sup> U. S. National Conference on Earthquake Engineering, San Francisco, CA, April 18-22, 2006, Earthquake Engineering Research Institute, Oakland, California.
- Kwon, O.-S., and Elnashai, A. (2006). "The Effect of Material and Ground Motion Uncertainty on the Seismic Vulnerability Curves of RC Structure," *Engineering Structures*, Vol. 28, No. 2, pp. 289-303, February.
- Memphis Light, Gas & Water (MLGW) (2005). "Memphis Cast-Iron Pipeline Database," Personal communication.



- National Institute of Building Sciences (NIBS) (2006). "HAZUS-MH MR2 Users Manual," Federal Emergency Management Agency, Washington, D.C.
- O'Rourke, M. J., and Ayala, G. (1993). "Pipeline Damage due to Wave Propagation," *Journal of Geotechnical Engineering*, ASCE, Vol. 119, No. 9, pp 1490-1498, September.
- O'Rourke, T. D., and Jeon, S-S. (1999). "Factors Affecting the Earthquake Damage of Water Distribution Systems," *TCLÉE Monograph No. 16*, ASCE.
- O'Rourke, M. J., and So, P. (1999). "Seismic Behavior of On-Grade Steel Tanks; Fragility Curves," *TCLÉE Monograph No. 16*, ASCE.
- Park, D., and Hashash, Y. M. A. (2005). "Evaluation of Seismic Factors in the Mississippi Embayment: I. Estimation of Dynamic Properties," *Soil Dynamics and Earthquake Engineering*, Vol. 25, pp. 133-144, February.
- Park, J. (2004). "Development and Application of Probabilistic Decision Support Framework for Seismic Rehabilitation of Structural Systems," Ph.D. Thesis, Georgia Institute of Technology, Atlanta, Georgia.
- Patterson, G. (2006). "Memphis School, Fire Station, and Bridge Databases," personal communication.
- Peacock, W. G., and Zhang, Y. (2005). "Single Family Housing Recovery after Hurricane Andrew," Proceedings of the CASA/NCAR Decision Sciences Workshop, Boulder, Colorado, December 12, 2005, Proceedings of the Southern Sociological Society Meetings, Charlotte, North Carolina, April 14-17, 2005, National Center for Atmospheric Research, Boulder, Colorado.
- (PMH) Office of Americas/North America & Homeland Security Division (2006). Homeland Security Infrastructure Program (HSIP) GOLD Dataset, Washington, D.C., (2) DVD set.
- Prater, C., Peacock, W. G., Lindell, M. K., Lu, J. C., and Zhang, Y. (2005). "DS-8: A Social Vulnerability Approach to Estimating Potential Socioeconomic Impacts of Earthquakes," Internal Report, Mid-America Earthquake Center, University of Illinois, Urbana, Illinois.
- Ramamoorthy, S.K., Gardoni, P., and Bracci, J.M. (2006) "Probabilistic Demand Models and Fragility Curves for Reinforced Concrete Frames," *Journal of Structural Engineering*, October 2006.
- Ramamoorthy, S.K., Gardoni, P., and Bracci, J.M. (2006) "Seismic Fragility and Confidence Bounds for Gravity Load Designed Reinforced Concrete Frame of Varying Height," Submitted to *Journal of Structural Engineering*, May 2006.
- Romero, S. and Rix, G. J. (2005). "Ground Motion Amplification of Soils in the Upper Mississippi Embayment," Internal Report, CD Release 05-01, Mid-America Earthquake Center, Urbana, Illinois, March.



Silva, W., Gregor, N., and Darragh, R. (2003). "Development of Regional Hard Rock Attenuation Relations for Central and Eastern North America, Mid-Continent and Gulf Coast Areas." Pacific Engineering and Analysis, El Cerrito, CA.

Toro, G. and Silva W. (2001). "Scenario Earthquakes for St. Louis, MO, and Memphis, TN, and Seismic Hazard Maps for the Central United States Region Including the Effect of Site Conditions," Internal Report, U. S. Geological Survey, Department of the Interior, Washington, D.C.



## APPENDIX A – SUPPLEMENTARY INVENTORY INFORMATION

### A.2.1.3.2 Utility Component Mapping Data

Default component value mapping data for electric substations may be obtained from Tables A.2.1.3.2-1 through A.2.1.3.2-7.

**Table A.2.1.3.2-1 Electric Substation General Subcomponent Value Partitioning Factors**

General Component	Partitioning Factor (%)
Transformers	40
Circuit Breakers	15
Disconnect Switches	2
Lightning (Surge) Arrestors	1
CCVTs	1
Current Transformers	2
Wave Traps	1
Bus Structures	7
Control Building	10
Batteries	1
Electrical Control Equipment	9
Other Yard Equipment	11



**Table A.2.1.3.2-2 Electric Substation Subcomponent Value Partitioning  
For VHV Substations, Seismic Zones 0/1/2**

Specific Component	Partitioning Factors (%)		Overall Multiplier	Component ID Code
	General	Specific		
Transformer - Anchored	40	25	0.100	ESS_VHV_1
Transformer - Unanchored	40	75	0.300	ESS_VHV_2
Live Tank Circuit Breaker - Standard	15	50	0.075	ESS_VHV_3
Live Tank Circuit Breaker - Seismic	15	0	0.000	ESS_VHV_4
Dead Tank Circuit Breaker - Standard	15	50	0.075	ESS_VHV_5
Disconnect Switch - Rigid Bus	2	50	0.010	ESS_VHV_6
Disconnect Switch - Flexible Bus	2	50	0.010	ESS_VHV_7
Lightning Arrestor	1	100	0.010	ESS_VHV_8
CCVT - Cantilevered	1	50	0.005	ESS_VHV_9
CCVT - Suspended	1	50	0.005	ESS_VHV_10
Current Transformer (gasketed)	2	50	0.010	ESS_VHV_11
Current Transformer (flanged)	2	50	0.010	ESS_VHV_12
Wave Trap - Cantilevered	1	50	0.005	ESS_VHV_13
Wave Trap - Suspended	1	50	0.005	ESS_VHV_14
Bus Structure - Rigid	7	50	0.035	ESS_VHV_15
Bus Structure - Flexible	7	50	0.035	ESS_VHV_16
Other Yard Equipment	11	100	0.110	ESS_VHV_17



**Table A.2.1.3.2-3 Electric Substation Subcomponent Value Partitioning  
For VHV Substations, Seismic Zones 3/4**

Specific Component	Partitioning Factors (%)		Overall Multiplier	Component ID Code
	General	Specific		
Transformer - Anchored	40	90	0.360	ESS_VHV_1
Transformer - Unanchored	40	10	0.040	ESS_VHV_2
Live Tank Circuit Breaker - Standard	15	15	0.023	ESS_VHV_3
Live Tank Circuit Breaker - Seismic	15	5	0.008	ESS_VHV_4
Dead Tank Circuit Breaker - Standard	15	80	0.120	ESS_VHV_5
Disconnect Switch - Rigid Bus	2	50	0.010	ESS_VHV_6
Disconnect Switch - Flexible Bus	2	50	0.010	ESS_VHV_7
Lightning Arrestor	1	100	0.010	ESS_VHV_8
CCVT - Cantilevered	1	50	0.005	ESS_VHV_9
CCVT - Suspended	1	50	0.005	ESS_VHV_10
Current Transformer (gasketed)	2	50	0.010	ESS_VHV_11
Current Transformer (flanged)	2	50	0.010	ESS_VHV_12
Wave Trap - Cantilevered	1	50	0.005	ESS_VHV_13
Wave Trap - Suspended	1	50	0.005	ESS_VHV_14
Bus Structure - Rigid	7	50	0.035	ESS_VHV_15
Bus Structure - Flexible	7	50	0.035	ESS_VHV_16
Other Yard Equipment	11	100	0.110	ESS_VHV_17



**Table A.2.1.3.2-4 Electric Substation Subcomponent Value Partitioning  
For HV Substations, Seismic Zones 0/1/2**

Specific Component	Partitioning Factors (%)		Overall Multiplier	Component ID Code
	General	Specific		
Transformer - Anchored	40	25	0.100	ESS_HV_1
Transformer - Unanchored	40	75	0.300	ESS_HV_2
Live Tank Circuit Breaker - Standard	15	50	0.075	ESS_HV_3
Live Tank Circuit Breaker - Seismic	15	0	0.000	ESS_HV_4
Dead Tank Circuit Breaker - Standard	15	50	0.075	ESS_HV_5
Disconnect Switch - Rigid Bus	2	50	0.010	ESS_HV_6
Disconnect Switch - Flexible Bus	2	50	0.010	ESS_HV_7
Lightning Arrestor	1	100	0.010	ESS_HV_8
CCVT	1	100	0.010	ESS_HV_9
Current Transformer (gasketed)	2	100	0.020	ESS_HV_10
Wave Trap - Cantilevered	1	50	0.005	ESS_HV_11
Wave Trap - Suspended	1	50	0.005	ESS_HV_12
Bus Structure - Rigid	7	50	0.035	ESS_HV_13
Bus Structure - Flexible	7	50	0.035	ESS_HV_14
Other Yard Equipment	11	100	0.110	ESS_HV_15



**Table A.2.1.3.2-5 Electric Substation Subcomponent Value Partitioning  
For HV Substations, Seismic Zones 3/4**

Specific Component	Partitioning Factors (%)		Overall Multiplier	Component ID Code
	General	Specific		
Transformer - Anchored	40	90	0.360	ESS_HV_1
Transformer - Unanchored	40	10	0.040	ESS_HV_2
Live Tank Circuit Breaker - Standard	15	15	0.023	ESS_HV_3
Live Tank Circuit Breaker - Seismic	15	5	0.008	ESS_HV_4
Dead Tank Circuit Breaker - Standard	15	80	0.120	ESS_HV_5
Disconnect Switch - Rigid Bus	2	50	0.010	ESS_HV_6
Disconnect Switch - Flexible Bus	2	50	0.010	ESS_HV_7
Lightning Arrestor	1	100	0.010	ESS_HV_8
CCVT	1	100	0.010	ESS_HV_9
Current Transformer (gasketed)	2	100	0.020	ESS_HV_10
Wave Trap - Cantilevered	1	50	0.005	ESS_HV_11
Wave Trap - Suspended	1	50	0.005	ESS_HV_12
Bus Structure - Rigid	7	50	0.035	ESS_HV_13
Bus Structure - Flexible	7	50	0.035	ESS_HV_14
Other Yard Equipment	11	100	0.110	ESS_HV_15



**Table A.2.1.3.2-6 Electric Substation Subcomponent Value Partitioning  
For MHV Substations, Seismic Zones 0/1/2**

Specific Component	Partitioning Factors (%)		Overall Multiplier	Component ID Code
	General	Specific		
Transformer - Anchored	40	25	0.100	ESS_MHV_1
Transformer - Unanchored	40	75	0.300	ESS_MHV_2
Live Tank Circuit Breaker - Standard	15	50	0.075	ESS_MHV_3
Live Tank Circuit Breaker - Seismic	15	0	0.000	ESS_MHV_4
Dead Tank Circuit Breaker - Standard	15	50	0.075	ESS_MHV_5
Disconnect Switch - Rigid Bus	2	50	0.010	ESS_MHV_6
Disconnect Switch - Flexible Bus	2	50	0.010	ESS_MHV_7
Lightning Arrestor	1	100	0.010	ESS_MHV_8
CCVT	1	100	0.010	ESS_MHV_9
Current Transformer (gasketed)	2	100	0.020	ESS_MHV_10
Wave Trap - Cantilevered	1	50	0.005	ESS_MHV_11
Wave Trap - Suspended	1	50	0.005	ESS_MHV_12
Bus Structure - Rigid	7	50	0.035	ESS_MHV_13
Bus Structure - Flexible	7	50	0.035	ESS_MHV_14
Other Yard Equipment	11	100	0.110	ESS_MHV_15



**Table A.2.1.3.2-7 Electric Substation Subcomponent Value Partitioning  
For MHV Substations, Seismic Zones 3/4**

Specific Component	Partitioning Factors (%)		Overall Multiplier	Component ID Code
	General	Specific		
Transformer - Anchored	40	90	0.360	ESS_MHV_1
Transformer - Unanchored	40	10	0.040	ESS_MHV_2
Live Tank Circuit Breaker - Standard	15	15	0.023	ESS_MHV_3
Live Tank Circuit Breaker - Seismic	15	5	0.008	ESS_MHV_4
Dead Tank Circuit Breaker - Standard	15	80	0.120	ESS_MHV_5
Disconnect Switch - Rigid Bus	2	50	0.010	ESS_MHV_6
Disconnect Switch - Flexible Bus	2	50	0.010	ESS_MHV_7
Lightning Arrestor	1	100	0.010	ESS_MHV_8
CCVT	1	100	0.010	ESS_MHV_9
Current Transformer (gasketed)	2	100	0.020	ESS_MHV_10
Wave Trap - Cantilevered	1	50	0.005	ESS_MHV_11
Wave Trap - Suspended	1	50	0.005	ESS_MHV_12
Bus Structure - Rigid	7	50	0.035	ESS_MHV_13
Bus Structure - Flexible	7	50	0.035	ESS_MHV_14
Other Yard Equipment	11	100	0.110	ESS_MHV_15



## APPENDIX B – SUPPLEMENTARY HAZARD INFORMATION

### B.3.2.3.1 Attenuation to Locations Inside the Mississippi Embayment

The seven attenuation functions and default weights, as proposed by Fernandez and Rix (2006), are shown in Table B.3.2.3.1-1.

**Table B.3.2.3.1-1 Default Attenuation Functions and Weights for the Mississippi Embayment**

Applicable Event	Region /	Attenuation Function	Weight
New Madrid Seismic Zone within Mississippi Embayment		Atkinson and Boore (1995)	0.333
		Frankel et al (1996) – High Median Stress Drop	0.056
		Frankel et al (1996) – Med Median Stress Drop	0.222
		Frankel et al (1996) – Low Median Stress Drop	0.056
		Silva et al (2003) – High Median Stress Drop	0.056
		Silva et al (2003) – Med Median Stress Drop	0.222
		Silva et al (2003) – Low Median Stress Drop	0.056

The attenuation functions of Fernandez and Rix (2006) take the following general form,

$$\ln(y) = c_1 + c_2 \cdot M + c_3 \cdot (M - 6)^2 + c_4 \cdot \ln(R_M) + c_5 \cdot \max\left[\ln\left(\frac{R}{70}\right), 0\right] + c_6 \cdot R_M \quad (\text{B.3.2.3.1-1})$$

where  $R_M$  is defined as

$$R_M = R + c_7 \cdot \exp(c_8 \cdot M) \quad (\text{B.3.2.3.1-2})$$

In Equations (B.3.2.3.1-1) and (B.3.2.3.1-2),  $y$  can be peak ground displacement in centimeters, peak ground velocity in centimeters/second, or 5% damped spectral acceleration in units of  $g$ .  $R$  is the epicentral distance in kilometers, which is taken as the shortest distance traveling along the curved surface of the Earth assuming the average radius of the Earth to be approximately 6373 km.  $M$  is the moment magnitude of the source event, and  $c_1$  through  $c_8$  are regression coefficients which may be obtained from

[www.ce.gatech.edu/~geosys/soil\\_dynamics/research/soilattenuations](http://www.ce.gatech.edu/~geosys/soil_dynamics/research/soilattenuations).

Regression coefficients are selected based on whether ground motions are being calculated at a location with Upland or Lowland soil (see Figure 3.2.3.1-1), and also what the depth of soil is expected to be.

The general form of the equation used to compute the aleatory standard deviation of the natural logarithm of hazard parameters is (Fernandez and Rix, 2006),

$$\sigma_{\ln(y)} = c_9 \cdot M + c_{10} \quad (\text{B.3.2.3.1-3})$$



where  $M$  is moment magnitude and  $c_9$  and  $c_{10}$  are regression coefficients, similar to Equations (B.3.2.3.1-1) and (B.3.2.3.1-2).

#### B.3.2.6 Estimating Probability of Liquefaction-Induced Ground Failure

[ The following text in Section B.3.2.6 was supplied by Dr. Glenn Rix, unless noted otherwise. Figures, Tables, and Equations have been renumbered to be consistent with the numbering scheme of the overall document.]

The purpose of this algorithm is to estimate the probability of “moderate” or “major” liquefaction-induced ground failures given an earthquake magnitude  $M_w$  and a resulting peak ground acceleration  $a_{max}$  defined at the ground surface at location  $P(x,y)$ .

The algorithm described herein is based on the liquefaction potential index (LPI) proposed by Iwasaki et al. (1978; 1982). Iwasaki et al. (1982) identified LPI values of 5 and 15 as the lower bounds of “moderate” and “major” liquefaction, respectively, from SPT measurements at 85 Japanese sites subjected to six earthquakes. Toprak and Holzer (2003) correlated LPI with surface manifestations of liquefaction using 50 CPT soundings at 20 sites affected by the 1989 Loma Prieta ( $M_w = 6.9$ ) earthquake. They found that median values of LPI equal to 5 and 12 corresponded to the occurrence of sand boils and lateral spreading, respectively. Analyses of liquefaction features from the 2003  $M_w = 6.5$  San Simeon earthquake also support the use of  $LPI=5$  as the threshold for surface manifestations of liquefaction (Holzer et al., 2005). LPI is potentially of great use for spatial analysis of liquefaction hazards because it allows one to develop a two-dimensional representation of a three-dimensional phenomenon (i.e., FS vs. depth), which is ideal for mapping (Luna and Frost, 1998), and it correlates well with liquefaction effects (Toprak and Holzer, 2003).

Rix and Romero-Hudock (2006) developed the methodology described herein to map liquefaction hazards in the Memphis/Shelby County, Tennessee area. The method is similar to that used by Holzer et al. (2002; 2006a) to develop liquefaction potential maps for the Oakland, CA area for scenario earthquakes on the Hayward Fault and by Holzer et al. (2006b) to predict the extent of liquefaction in East Bay fills due to a repeat of the 1906 San Francisco earthquake. Application of the method to areas other than Memphis/Shelby County should be done with caution because soil conditions (and thus susceptibility to liquefaction) may vary significantly. Furthermore, the method is intended as a screening method; site-specific studies are needed to better estimate the magnitude of resulting permanent ground deformations and other liquefaction-related ground failures.

#### Step 1. Determine the soil unit in which $P(x,y)$ lies

The liquefaction susceptibility of the soil units listed in Table B.3.2.6-1 and shown in Figure B.3.2.6-1 was evaluated by Rix and Romero-Hudock (2006). Step 1 consists of determining which soil unit the location  $P(x,y)$  lies in.



**Table B.3.2.6-1 Surficial geology of the Memphis/Shelby County, Tennessee area  
(Van Arsdale and Cox, 2003).**

Surficial Geology	Description
Qal	Holocene alluvium; sand, clayey silt, and minor gravel; sand is very fine to coarse grained quartz with chert; thick-bedded basal point bar sands are overlain by alternating thin beds of sand and silt and capped by overbank clayey silt.
Qa	Holocene alluvium; silt with minor mixed sand and clay; dispersed sand is very fine to very coarse grained quartz and minor chert; floodplain of Nonconnah Creek and tributaries to Wolf River and Nonconnah Creek consist of reworked loess; channel bars are covered with sand and gravel.
Ql	Late Pleistocene loess; silt with < 10 percent sand and < 10 percent clay; loess is dominantly quartz; thickness ranges from 2 to 20 m.
Qtl	Pleistocene loess-covered terrace; dense, cross-bedded, medium-grained sand capped by loess silt.
Artificial Fill (af)	Holocene, man-made; mostly silt, sand, and chert gravel locally derived from loess, alluvium, and the Lafayette gravel.



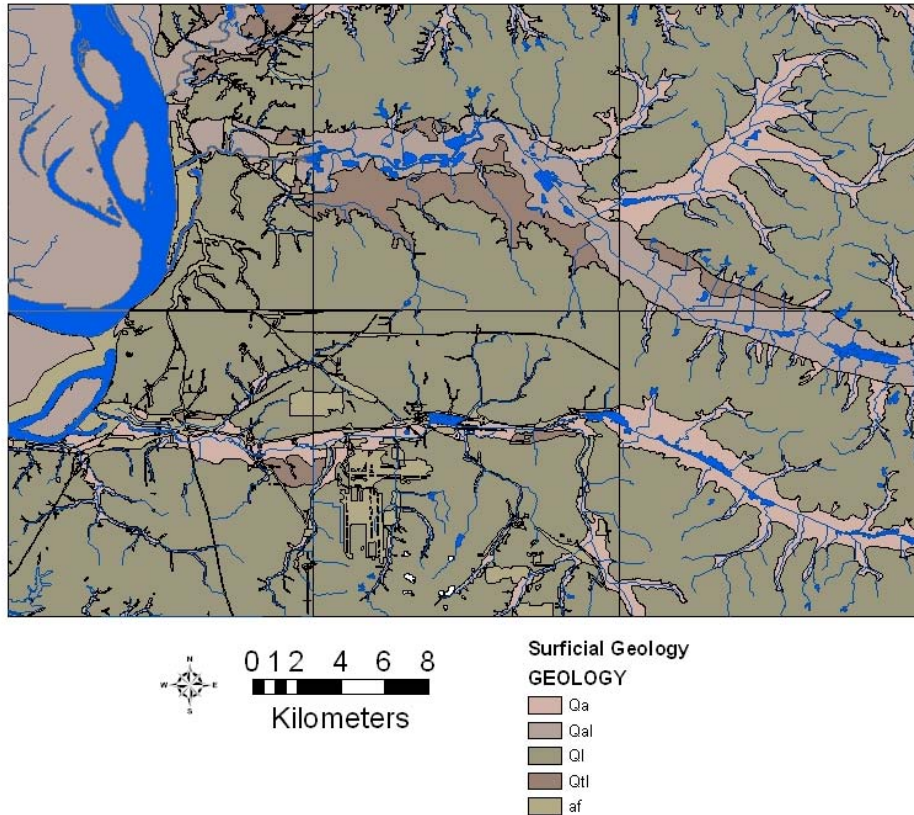


**Figure B.3.2.6-1. Surface Geology of Memphis/Shelby County, Tennessee**  
 (Broughton and Van Arsdale, 2004; Cox, 2004, Moore and Diehl, 2004a; 2004b; Van Arsdale, 2004a; 2004b)

*Step 2. Determine the Magnitude Scaling Factor*

For the scenario earthquake being analyzed, determine the Magnitude Scaling Factor (MSF) by interpolating linearly between values given in Table B.3.2.6-2.

**Table B.3.2.6-2 Magnitude Scaling Factors**

Moment Magnitude	Magnitude Scaling Factor
5.5	1.43
6.0	1.32
6.5	1.19
7.0	1.08
7.5	1.00
8.0	0.94
8.5	0.89

*Step 3. Calculate the Duration-Adjusted Peak Ground Acceleration*



For the peak ground acceleration  $a_{\max}$  calculated (independently) for the location  $P(x,y)$ , calculate the duration-adjusted peak ground acceleration:

$$a_{\max \text{ .adjusted}} = \frac{a_{\max}}{\text{MSF}} < 0.55g \quad (\text{B.3.2.6-1})$$

Note that the duration-adjusted peak ground acceleration may not exceed 0.55 g.

Step 4. Estimate the probability of “moderate” or “major” liquefaction-induced ground failures

Using the soil unit identified in Step 1 and the desired severity of liquefaction-induced ground failures (“moderate” corresponds to LPI = 5; “major” corresponds to LPI = 15), estimate the probability of liquefaction-induced ground failures of that severity by calculating a weighted average of results determined by Cone Penetration Test (CPT) and Standard Penetration Test (SPT) techniques:

$$P[\text{LPI} > x] = w_1 \frac{a_1}{\left[1 + b_1 \exp(-c_1 a_{\max \text{ .adjusted}})\right]} + w_2 \frac{a_2}{\left[1 + b_2 \exp(-c_2 a_{\max \text{ .adjusted}})\right]} \quad (\text{B.3.2.6-2})$$

where  $a_1$ ,  $b_1$ , and  $c_1$  are coefficients selected from Table B.3.2.6-3 for the CPT results for a given soil unit and severity;  $a_2$ ,  $b_2$ , and  $c_2$  are coefficients selected from Table B.3.2.6-3 for the SPT results for the same soil unit and severity;  $w_1$  and  $w_2$  are factors to weight the relative contributions from CPT and SPT tests, respectively. The factors  $w_1$  and  $w_2$  must sum to 1.0. Rix and Romero-Hudock (2006) used  $w_1 = 0.333$  and  $w_2 = 0.667$ .



**Table B.3.2.6-3 Coefficients for Each Soil Unit, Test Type, and LPI Value.**

Soil Unit	Type of Test	LPI Value	a	b	c
Qa	CPT	5	0.890	16219.4	29.81
	SPT	5	0.669	59.63	14.19
	CPT	15	1.183	1539.9	12.92
	SPT	15	0.232	639.31	21.12
Qal	CPT	5	NA [0]	NA [0]	NA [0]
	SPT	5	0.782	78.15	17.34
	CPT	15	NA [0]	NA [0]	NA [0]
	SPT	15	0.388	74.66	13.06
Ql	CPT	5	0	0	0
	SPT	5	0.535	50.98	13.74
	CPT	15	0	0	0
	SPT	15	0.193	122.12	15.89
Qtl	CPT	5	1.000	$2.453 \times 10^6$	44.98
	SPT	5	0.769	68.88	18.98
	CPT	15	0	0	0
	SPT	15	0.468	101.50	13.28
af	CPT	5	0.996	$6.632 \times 10^6$	81.97
	SPT	5	0	0	0
	CPT	15	0.998	39280.6	38.69
	SPT	15	0	0	0



## APPENDIX C – SUPPLEMENTARY FRAGILITY INFORMATION

### C4.2.1 Supplementary Fragility Data

Table 4.2.1-1 provides a proposed mapping scheme between inventory and fragilities for Shelby County, TN, using Fragility ID Codes to condense the table. Descriptive data for the mapped fragilities has been excerpted from the master building fragility database and provided in Table 4.2.1-2. In cases where MAE Center research does not provide fragility data, fragility curves may be adapted from HAZUS. For structural damage, HAZUS fragilities for Moderate, Extensive, and Complete damage states map approximately to the typical PL1, PL2, and PL3 limits used by the MAE Center. Fragility ID Codes correspond to rows in the master building fragility database.

Mappings are also provided to parametric fragilities developed by Jeong and Elnashai, which may be used as alternates to the typical MAE Center and HAZUS fragilities. Note that parametric fragilities, unlike fragilities from the MAE Center and HAZUS, must be evaluated with specific hazards (i.e., PGA, 0.2 sec Sa, 1.0 sec Sa) which may not correspond to expected seismic loads for the structure (based on structure period). The  $\lambda$ ,  $\beta$  pairs for parametric fragilities provided in the attached spreadsheet must be evaluated with the appropriate hazard parameter, as noted in the spreadsheet. In the following table, Fragility ID Codes for parametric fragilities correspond to curves which must be evaluated with 0.2 sec Sa.

General mapping checks are broken down into two categories: height and age.

Building heights are generally broken down into three categories:

1. Low-Rise (1-3 stories)
2. Mid-Rise (4-7 stories)
3. High-Rise (8+ stories)

Building age is generally broken down into two categories, with the following code level implications:

1. Pre-Code (before 1992, when Memphis first adopted a seismic building code)
2. Low-Code (1992 - present, after Memphis adopted the SBC)



**Table C4.2.1-1 Default Inventory-to-Fragility Mapping Scheme**

MAEC Structural Type	v3 Mapping Check(s)	v4 Mapping Check(s)	Non-Retrofit Period (seconds)	Non-Retrofit Fragility	Non-Retrofit Fragility ID Code	Retrofit Period (seconds)	Retrofit Fragility	Retrofit Fragility ID Code	Parametric Non-Retrofit Fragility ID Code	Parametric Retrofit Fragility ID Code	Drift-Sensitive Fragility ID Code	Acceleration-Sensitive Fragility ID Code
Concrete Moment Frame (C1)	NO_STORIES >= 4 & NO_STORIES <= 7 & OCC_TYPE = Office & YEAR_BLT >= 1977 & YEAR_BLT <= 1992	NO_STORIES >= 4 & NO_STORIES <= 7 & OCC_TYPE = COM4 & YEAR_BLT >= 1977 & YEAR_BLT <= 1992	T <sub>1</sub> = 0.32 * NO_STORIES	Hueste 5-story flat plate w/ perimeter moment frame	SF_C1_1	T <sub>1</sub> = 0.13 * NO_STORIES	Hueste shear walls	SF_C1_2	SF_C1_43	SF_C1_52	NSF_DS_C1_2	NSF_AS_C1_2
Concrete Moment Frame (C1)	NO_STORIES >= 4 & NO_STORIES <= 7 & OCC_TYPE = Office & YEAR_BLT >= 1977 & YEAR_BLT <= 1992	NO_STORIES >= 4 & NO_STORIES <= 7 & OCC_TYPE = COM4 & YEAR_BLT >= 1977 & YEAR_BLT <= 1992	T <sub>1</sub> = 0.32 * NO_STORIES	Hueste 5-story flat plate w/ perimeter moment frame	SF_C1_1	T <sub>1</sub> = 0.28 * NO_STORIES	Hueste column jackets	SF_C1_3	SF_C1_43	SF_C1_52	NSF_DS_C1_2	NSF_AS_C1_2



MAEC Structural Type	v3 Mapping Check(s)	v4 Mapping Check(s)	Non-Retrofit Period (seconds)	Non-Retrofit Fragility	Non-Retrofit Fragility ID Code	Retrofit Period (seconds)	Retrofit Fragility	Retrofit Fragility ID Code	Parametric Non-Retrofit Fragility ID Code	Parametric Retrofit Fragility ID Code	Drift-Sensitive Fragility ID Code	Acceleration-Sensitive Fragility ID Code
Concrete Moment Frame (C1)	NO_STORIES >= 4 & NO_STORIES <= 7 & OCC_TYPE = Office & YEAR_BLT >= 1977 & YEAR_BLT <= 1992	NO_STORIES >= 4 & NO_STORIES <= 7 & OCC_TYPE = COM4 & YEAR_BLT >= 1977 & YEAR_BLT <= 1992	$T_1 = 0.32 *$ NO_STORIES	Hueste 5-story flat plate w/ perimeter moment frame	SF_C1_1	$T_1 = 0.32 *$ NO_STORIES	Hueste confining plates at column ends	SF_C1_4	SF_C1_43	SF_C1_52	NSF_DS_C1_2	NSF_AS_C1_2
Concrete Moment Frame (C1)	NO_STORIES >= 4 & NO_STORIES <= 7 & OCC_TYPE = Residential_MF (Multi Family) & YEAR_BLT >= 1992	NO_STORIES >= 4 & NO_STORIES <= 7 & OCC_TYPE = RES3 & YEAR_BLT >= 1992	$T_1 = 0.2 *$ NO_STORIES	Erberik and Elnashai 5-story flat plate w/ masonry infill walls	SF_C1_9	$T_1 = 0.75$	HAZUS C1M High Code	SF_C1_28	SF_C1_46	SF_C1_55	NSF_DS_C1_5	NSF_AS_C1_5



MAEC Structural Type	v3 Mapping Check(s)	v4 Mapping Check(s)	Non-Retrofit Period (seconds)	Non-Retrofit Fragility	Non-Retrofit Fragility ID Code	Retrofit Period (seconds)	Retrofit Fragility	Retrofit Fragility ID Code	Parametric Non-Retrofit Fragility ID Code	Parametric Retrofit Fragility ID Code	Drift-Sensitive Fragility ID Code	Acceleration-Sensitive Fragility ID Code
Concrete Moment Frame (C1)	NO_STORIES >= 1 & NO_STORIES <= 3 & YEAR_BLT <= 1976	NO_STORIES >= 1 & NO_STORIES <= 3 & YEAR_BLT <= 1976	$T_1 = \eta_1(h)^{\eta_2}$ , where $\eta_1 = 0.097$ , $\eta_2 = 0.624$ , and h = height of building frame from base (ft). Typically assume 13 ft story height.	Bracci Gravity Load Designed (GLD) of buildings	SF_C1_10	$T_1 = 0.40$	HAZUS CIL High Code	SF_C1_27	SF_C1_42	SF_C1_51	NSF_DS_C1_1	NSF_AS_C1_1
Concrete Moment Frame (C1)	NO_STORIES >= 4 & NO_STORIES <= 7 & YEAR_BLT <= 1976	NO_STORIES >= 4 & NO_STORIES <= 7 & YEAR_BLT <= 1976	$T_1 = \eta_1(h)^{\eta_2}$ , where $\eta_1 = 0.097$ , $\eta_2 = 0.624$ , and h = height of building frame from base (ft). Typically assume 13 ft story height.	Bracci Gravity Load Designed (GLD) of buildings	SF_C1_10	$T_1 = 0.75$	HAZUS CIM High Code	SF_C1_28	SF_C1_43	SF_C1_52	NSF_DS_C1_2	NSF_AS_C1_2



MAEC Structural Type	v3 Mapping Check(s)	v4 Mapping Check(s)	Non-Retrofit Period (seconds)	Non-Retrofit Fragility	Non-Retrofit Fragility ID Code	Retrofit Period (seconds)	Retrofit Fragility	Retrofit Fragility ID Code	Parametric Non-Retrofit Fragility ID Code	Parametric Retrofit Fragility ID Code	Drift-Sensitive Fragility ID Code	Acceleration-Sensitive Fragility ID Code
Concrete Moment Frame (C1)	NO_STORIES >= 8 & YEAR_BLT <= 1976	NO_STORIES >= 8 & YEAR_BLT <= 1976	$T_1 = \frac{0.097}{0.624} \eta_1 (h)^{\eta_2}$ , where $\eta_1 = 0.097$ , $\eta_2 = 0.624$ , and h = height of building frame from base (ft). Typically assume 13 ft story height.	Bracci Gravity Load Designed (GLD) buildings	SF_C1_10	$T_1 = 1.45$	HAZUS C1H High Code	SF_C1_29	SF_C1_44	SF_C1_53	NSF_DS_C1_3	NSF_AS_C1_3
Concrete Moment Frame (C1)	NO_STORIES >= 20	NO_STORIES >= 20	$T_1 = 0.08 * NO\_STORIES$	Concrete frame with shear wall core	SF_C1_15	$T_1 = 1.45$	HAZUS C1H High Code	SF_C1_29	SF_C1_47	SF_C1_53	NSF_DS_C1_6	NSF_AS_C1_6
Concrete Moment Frame (C1)	NO_STORIES >= 1 & NO_STORIES <= 3 & YEAR_BLT >= 1992	NO_STORIES >= 1 & NO_STORIES <= 3 & YEAR_BLT >= 1992	$T_1 = 0.4$	Adapted HAZUS Low Code CIL	SF_C1_21	$T_1 = 0.4$	HAZUS CIL High Code	SF_C1_27	SF_C1_45	SF_C1_51	NSF_DS_C1_4	NSF_AS_C1_4



MAEC Structural Type	v3 Mapping Check(s)	v4 Mapping Check(s)	Non-Retrofit Period (seconds)	Non-Retrofit Fragility	Non-Retrofit Fragility ID Code	Retrofit Period (seconds)	Retrofit Fragility	Retrofit Fragility ID Code	Parametric Non-Retrofit Fragility ID Code	Parametric Retrofit Fragility ID Code	Drift-Sensitive Fragility ID Code	Acceleration-Sensitive Fragility ID Code
Concrete Moment Frame (C1)	NO_STORIES >= 1 & NO_STORIES <= 3 & YEAR_BLT < 1992	NO_STORIES >= 1 & NO_STORIES <= 3 & YEAR_BLT < 1992	T <sub>1</sub> = 0.4	Adapted HAZUS Pre-Code C1L	SF_C1_18	T <sub>1</sub> = 0.4	HAZUS C1L High Code	SF_C1_27	SF_C1_42	SF_C1_51	NSF_DS_C1_1	NSF_AS_C1_1
Concrete Moment Frame (C1)	NO_STORIES >= 4 & NO_STORIES <= 7 & YEAR_BLT >= 1992	NO_STORIES >= 4 & NO_STORIES <= 7 & YEAR_BLT >= 1992	T <sub>1</sub> = 0.75	Adapted HAZUS Low Code C1M	SF_C1_22	T <sub>1</sub> = 0.75	HAZUS C1M High Code	SF_C1_28	SF_C1_46	SF_C1_52	NSF_DS_C1_5	NSF_AS_C1_5
Concrete Moment Frame (C1)	NO_STORIES >= 4 & NO_STORIES <= 7 & YEAR_BLT < 1992	NO_STORIES >= 4 & NO_STORIES <= 7 & YEAR_BLT < 1992	T <sub>1</sub> = 0.75	Adapted HAZUS Pre-Code C1M	SF_C1_19	T <sub>1</sub> = 0.75	HAZUS C1M High Code	SF_C1_28	SF_C1_43	SF_C1_52	NSF_DS_C1_2	NSF_AS_C1_2
Concrete Moment Frame (C1)	NO_STORIES >= 8 & YEAR_BLT >= 1992	NO_STORIES >= 8 & YEAR_BLT >= 1992	T <sub>1</sub> = 1.45	Adapted HAZUS Low-Code C1H	SF_C1_23	T <sub>1</sub> = 1.45	HAZUS C1H High Code	SF_C1_29	SF_C1_47	SF_C1_53	NSF_DS_C1_6	NSF_AS_C1_6



MAEC Structural Type	v3 Mapping Check(s)	v4 Mapping Check(s)	Non-Retrofit Period (seconds)	Non-Retrofit Fragility	Non-Retrofit Fragility ID Code	Retrofit Period (seconds)	Retrofit Fragility	Retrofit Fragility ID Code	Parametric Non-Retrofit Fragility ID Code	Parametric Retrofit Fragility ID Code	Drift-Sensitive Fragility ID Code	Acceleration-Sensitive Fragility ID Code
Concrete Moment Frame (C1)	NO_STORIES >= 8 & YEAR_BLT < 1992	NO_STORIES >= 8 & YEAR_BLT < 1992	T <sub>1</sub> = 1.45	Adapted HAZUS Pre-Code C1H	SF_C1_20	T <sub>1</sub> = 1.45	HAZUS C1H High Code	SF_C1_29	SF_C1_44	SF_C1_53	NSF_DS_C1_3	NSF_AS_C1_3
Concrete Frame with Concrete Shear Walls (C2)	NO_STORIES >= 20	NO_STORIES >= 20	T <sub>1</sub> = 0.08 * NO_STORIES	Concrete frame with shear wall core	SF_C1_15	T <sub>1</sub> = 1.09	HAZUS C2H High Code	SF_C1_29	SF_C1_47	SF_C1_53	NSF_DS_C2_6	NSF_AS_C2_6
Concrete Frame with Concrete Shear Walls (C2)	NO_STORIES >= 1 & NO_STORIES <= 3 & YEAR_BLT >= 1992	NO_STORIES >= 1 & NO_STORIES <= 3 & YEAR_BLT >= 1992	T <sub>1</sub> = 0.35	Adapted HAZUS Low Code C2L	SF_C2_4	T <sub>1</sub> = 0.35	HAZUS C2L High Code	SF_C2_10	SF_C2_28	SF_C2_34	NSF_DS_C2_4	NSF_AS_C2_4
Concrete Frame with Concrete Shear Walls (C2)	NO_STORIES >= 1 & NO_STORIES <= 3 & YEAR_BLT < 1992	NO_STORIES >= 1 & NO_STORIES <= 3 & YEAR_BLT < 1992	T <sub>1</sub> = 0.35	Adapted HAZUS Pre-Code C2L	SF_C2_1	T <sub>1</sub> = 0.35	HAZUS C2L High Code	SF_C2_10	SF_C2_25	SF_C2_34	NSF_DS_C2_1	NSF_AS_C2_1



MAEC Structural Type	v3 Mapping Check(s)	v4 Mapping Check(s)	Non-Retrofit Period (seconds)	Non-Retrofit Fragility	Non-Retrofit Fragility ID Code	Retrofit Period (seconds)	Retrofit Fragility	Retrofit Fragility ID Code	Parametric Non-Retrofit Fragility ID Code	Parametric Retrofit Fragility ID Code	Drift-Sensitive Fragility ID Code	Acceleration-Sensitive Fragility ID Code
Concrete Frame with Concrete Shear Walls (C2)	NO_STORIES >= 4 & NO_STORIES <= 7 & YEAR_BLT >= 1992	NO_STORIES >= 4 & NO_STORIES <= 7 & YEAR_BLT >= 1992	T <sub>1</sub> = 0.56	Adapted HAZUS Low Code C2M	SF_C2_5	T <sub>1</sub> = 0.56	HAZUS C2M High Code	SF_C2_11	SF_C2_29	SF_C2_35	NSF_DS_C2_5	NSF_AS_C2_5
Concrete Frame with Concrete Shear Walls (C2)	NO_STORIES >= 4 & NO_STORIES <= 7 & YEAR_BLT < 1992	NO_STORIES >= 4 & NO_STORIES <= 7 & YEAR_BLT < 1992	T <sub>1</sub> = 0.56	Adapted HAZUS Pre-Code C2M	SF_C2_2	T <sub>1</sub> = 0.56	HAZUS C2M High Code	SF_C2_11	SF_C2_26	SF_C2_35	NSF_DS_C2_2	NSF_AS_C2_2
Concrete Frame with Concrete Shear Walls (C2)	NO_STORIES >= 8 & YEAR_BLT >= 1992	NO_STORIES >= 8 & YEAR_BLT >= 1992	T <sub>1</sub> = 1.09	Adapted HAZUS Low Code C2H	SF_C2_6	T <sub>1</sub> = 1.09	HAZUS C2H High Code	SF_C2_12	SF_C2_30	SF_C2_36	NSF_DS_C2_6	NSF_AS_C2_6
Concrete Frame with Concrete Shear Walls (C2)	NO_STORIES >= 8 & YEAR_BLT < 1992	NO_STORIES >= 8 & YEAR_BLT < 1992	T <sub>1</sub> = 1.09	Adapted HAZUS Pre-Code C2H	SF_C2_3	T <sub>1</sub> = 1.09	HAZUS C2H High Code	SF_C2_12	SF_C2_27	SF_C2_36	NSF_DS_C2_3	NSF_AS_C2_3



MAEC Structural Type	v3 Mapping Check(s)	v4 Mapping Check(s)	Non-Retrofit Period (seconds)	Non-Retrofit Fragility	Non-Retrofit Fragility ID Code	Retrofit Period (seconds)	Retrofit Fragility	Retrofit Fragility ID Code	Parametric Non-Retrofit Fragility ID Code	Parametric Retrofit Fragility ID Code	Drift-Sensitive Fragility ID Code	Acceleration-Sensitive Fragility ID Code
Concrete Tilt-Up (PC1)	YEAR_BLT >= 1992	YEAR_BLT >= 1992	T <sub>1</sub> = 0.35	Adapted HAZUS Low Code PC1	SF_PC1_2	T <sub>1</sub> = 0.35	Adapted HAZUS High Code PC1	SF_PC1_4	SF_PC1_10	SF_PC1_12	NSF_DS_PC1_2	NSF_AS_PC1_2
Concrete Tilt-Up (PC1)	YEAR_BLT < 1992	YEAR_BLT < 1992	T <sub>1</sub> = 0.35	Adapted HAZUS Pre-Code PC1	SF_PC1_1	T <sub>1</sub> = 0.35	Adapted HAZUS High Code PC1	SF_PC1_4	SF_PC1_9	SF_PC1_12	NSF_DS_PC1_1	NSF_AS_PC1_1
Precast Concrete Frame (PC2)	NO_STORIES >= 1 & NO_STORIES <= 3 & YEAR_BLT >= 1992	NO_STORIES >= 1 & NO_STORIES <= 3 & YEAR_BLT >= 1992	T <sub>1</sub> = 0.35	Adapted HAZUS Low Code PC2L	SF_PC2_4	T <sub>1</sub> = 0.35	Adapted HAZUS High Code PC2L	SF_PC2_10	SF_PC2_28	SF_PC2_34	NSF_DS_PC2_4	NSF_AS_PC2_4
Precast Concrete Frame (PC2)	NO_STORIES >= 1 & NO_STORIES <= 3 & YEAR_BLT < 1992	NO_STORIES >= 1 & NO_STORIES <= 3 & YEAR_BLT < 1992	T <sub>1</sub> = 0.35	Adapted HAZUS Pre-Code PC2L	SF_PC2_1	T <sub>1</sub> = 0.35	Adapted HAZUS High Code PC2L	SF_PC2_10	SF_PC2_25	SF_PC2_34	NSF_DS_PC2_1	NSF_AS_PC2_1



MAEC Structural Type	v3 Mapping Check(s)	v4 Mapping Check(s)	Non-Retrofit Period (seconds)	Non-Retrofit Fragility	Non-Retrofit Fragility ID Code	Retrofit Period (seconds)	Retrofit Fragility	Retrofit Fragility ID Code	Parametric Non-Retrofit Fragility ID Code	Parametric Retrofit Fragility ID Code	Drift-Sensitive Fragility ID Code	Acceleration-Sensitive Fragility ID Code
Precast Concrete Frame (PC2)	NO_STORIES >= 4 & NO_STORIES <= 7 & YEAR_BLT >= 1992	NO_STORIES >= 4 & NO_STORIES <= 7 & YEAR_BLT >= 1992	T <sub>1</sub> = 0.56	Adapted HAZUS Low Code PC2M	SF_PC2_5	T <sub>1</sub> = 0.56	Adapted HAZUS High Code PC2M	SF_PC2_11	SF_PC2_29	SF_PC2_35	NSF_DS_PC2_5	NSF_AS_PC2_5
Precast Concrete Frame (PC2)	NO_STORIES >= 4 & NO_STORIES <= 7 & YEAR_BLT < 1992	NO_STORIES >= 4 & NO_STORIES <= 7 & YEAR_BLT < 1992	T <sub>1</sub> = 0.56	Adapted HAZUS Pre-Code PC2M	SF_PC2_2	T <sub>1</sub> = 0.56	Adapted HAZUS High Code PC2M	SF_PC2_11	SF_PC2_26	SF_PC2_35	NSF_DS_PC2_2	NSF_AS_PC2_2
Precast Concrete Frame (PC2)	NO_STORIES >= 8 & YEAR_BLT >= 1992	NO_STORIES >= 8 & YEAR_BLT >= 1992	T <sub>1</sub> = 1.09	Adapted HAZUS Low Code PC2H	SF_PC2_6	T <sub>1</sub> = 1.09	Adapted HAZUS High Code PC2H	SF_PC2_12	SF_PC2_30	SF_PC2_36	NSF_DS_PC2_6	NSF_AS_PC2_6
Precast Concrete Frame (PC2)	NO_STORIES >= 8 & YEAR_BLT < 1992	NO_STORIES >= 8 & YEAR_BLT < 1992	T <sub>1</sub> = 1.09	Adapted HAZUS Pre-Code PC2H	SF_PC2_3	T <sub>1</sub> = 1.09	Adapted HAZUS High Code PC2H	SF_PC2_12	SF_PC2_27	SF_PC2_36	NSF_DS_PC2_3	NSF_AS_PC2_3



MAEC Structural Type	v3 Mapping Check(s)	v4 Mapping Check(s)	Non-Retrofit Period (seconds)	Non-Retrofit Fragility	Non-Retrofit Fragility ID Code	Retrofit Period (seconds)	Retrofit Fragility	Retrofit Fragility ID Code	Parametric Non-Retrofit Fragility ID Code	Parametric Retrofit Fragility ID Code	Drift-Sensitive Fragility ID Code	Acceleration-Sensitive Fragility ID Code
Reinforced Masonry (RM)	NO_STORIES >= 1 & NO_STORIES <= 3 & YEAR_BLT >= 1992 & EF = EFS1	NO_STORIES >= 1 & NO_STORIES <= 3 & YEAR_BLT >= 1992 & EF = EFS1	T <sub>1</sub> = 0.35	Adapted HAZUS Low Code RM2L	SF_RM_8	T <sub>1</sub> = 0.35	Adapted HAZUS High Code RM2L	SF_RM_18	SF_RM_48	SF_RM_58	NSF_DS_RM_8	NSF_AS_RM_8
Reinforced Masonry (RM)	NO_STORIES >= 1 & NO_STORIES <= 3 & YEAR_BLT < 1992 & EF = EFS1	NO_STORIES >= 1 & NO_STORIES <= 3 & YEAR_BLT < 1992 & EF = EFS1	T <sub>1</sub> = 0.35	Adapted HAZUS Pre-Code RM2L	SF_RM_3	T <sub>1</sub> = 0.35	Adapted HAZUS High Code RM2L	SF_RM_18	SF_RM_43	SF_RM_58	NSF_DS_RM_3	NSF_AS_RM_3
Reinforced Masonry (RM)	NO_STORIES >= 1 & NO_STORIES <= 3 & YEAR_BLT >= 1992	NO_STORIES >= 1 & NO_STORIES <= 3 & YEAR_BLT >= 1992	T <sub>1</sub> = 0.35	Adapted HAZUS Low Code RM1L	SF_RM_6	T <sub>1</sub> = 0.35	Adapted HAZUS High Code RM1L	SF_RM_16	SF_RM_46	SF_RM_56	NSF_DS_RM_6	NSF_AS_RM_6



MAEC Structural Type	v3 Mapping Check(s)	v4 Mapping Check(s)	Non-Retrofit Period (seconds)	Non-Retrofit Fragility	Non-Retrofit Fragility ID Code	Retrofit Period (seconds)	Retrofit Fragility	Retrofit Fragility ID Code	Parametric Non-Retrofit Fragility ID Code	Parametric Retrofit Fragility ID Code	Drift-Sensitive Fragility ID Code	Acceleration-Sensitive Fragility ID Code
Reinforced Masonry (RM)	NO_STORIES >= 1 & NO_STORIES <= 3 & YEAR_BLT < 1992	NO_STORIES >= 1 & NO_STORIES <= 3 & YEAR_BLT < 1992	T <sub>1</sub> = 0.35	Adapted HAZUS Pre-Code RM1L	SF_RM_1	T <sub>1</sub> = 0.35	Adapted HAZUS High Code RM1L	SF_RM_16	SF_RM_41	SF_RM_56	NSF_DS_RM_1	NSF_AS_RM_1
Reinforced Masonry (RM)	NO_STORIES >= 4 & NO_STORIES <= 7 & YEAR_BLT >= 1992 & EF = EFS1	NO_STORIES >= 4 & NO_STORIES <= 7 & YEAR_BLT >= 1992 & EF = EFS1	T <sub>1</sub> = 0.56	Adapted HAZUS Low Code RM2M	SF_RM_9	T <sub>1</sub> = 0.56	Adapted HAZUS High Code RM2M	SF_RM_19	SF_RM_49	SF_RM_59	NSF_DS_RM_9	NSF_AS_RM_9
Reinforced Masonry (RM)	NO_STORIES >= 4 & NO_STORIES <= 7 & YEAR_BLT < 1992 & EF = EFS1	NO_STORIES >= 4 & NO_STORIES <= 7 & YEAR_BLT < 1992 & EF = EFS1	T <sub>1</sub> = 0.56	Adapted HAZUS Pre-Code RM2M	SF_RM_4	T <sub>1</sub> = 0.56	Adapted HAZUS High Code RM2M	SF_RM_19	SF_RM_44	SF_RM_59	NSF_DS_RM_4	NSF_AS_RM_4



MAEC Structural Type	v3 Mapping Check(s)	v4 Mapping Check(s)	Non-Retrofit Period (seconds)	Non-Retrofit Fragility	Non-Retrofit Fragility ID Code	Retrofit Period (seconds)	Retrofit Fragility	Retrofit Fragility ID Code	Parametric Non-Retrofit Fragility ID Code	Parametric Retrofit Fragility ID Code	Drift-Sensitive Fragility ID Code	Acceleration-Sensitive Fragility ID Code
Reinforced Masonry (RM)	NO_STORIES >= 4 & NO_STORIES <= 7 & YEAR_BLT >= 1992	NO_STORIES >= 4 & NO_STORIES <= 7 & YEAR_BLT >= 1992	T <sub>1</sub> = 0.56	Adapted HAZUS Low Code RM1M	SF_RM_7	T <sub>1</sub> = 0.56	Adapted HAZUS High Code RM1M	SF_RM_17	SF_RM_47	SF_RM_57	NSF_DS_RM_7	NSF_AS_RM_7
Reinforced Masonry (RM)	NO_STORIES >= 4 & NO_STORIES <= 7 & YEAR_BLT < 1992	NO_STORIES >= 4 & NO_STORIES <= 7 & YEAR_BLT < 1992	T <sub>1</sub> = 0.56	Adapted HAZUS Pre-Code RM1M	SF_RM_2	T <sub>1</sub> = 0.56	Adapted HAZUS High Code RM1M	SF_RM_17	SF_RM_42	SF_RM_57	NSF_DS_RM_2	NSF_AS_RM_2
Reinforced Masonry (RM)	NO_STORIES >= 8 & YEAR_BLT >= 1992	NO_STORIES >= 8 & YEAR_BLT >= 1992	T <sub>1</sub> = 1.09	Adapted HAZUS Low Code RM2H	SF_RM_10	T <sub>1</sub> = 1.09	Adapted HAZUS High Code RM2H	SF_RM_20	SF_RM_50	SF_RM_60	NSF_DS_RM_10	NSF_AS_RM_10
Reinforced Masonry (RM)	NO_STORIES >= 8 & YEAR_BLT < 1992	NO_STORIES >= 8 & YEAR_BLT < 1992	T <sub>1</sub> = 1.09	Adapted HAZUS Pre-Code RM2H	SF_RM_5	T <sub>1</sub> = 1.09	Adapted HAZUS High Code RM2H	SF_RM_20	SF_RM_45	SF_RM_60	NSF_DS_RM_5	NSF_AS_RM_5



MAEC Structural Type	v3 Mapping Check(s)	v4 Mapping Check(s)	Non-Retrofit Period (seconds)	Non-Retrofit Fragility	Non-Retrofit Fragility ID Code	Retrofit Period (seconds)	Retrofit Fragility	Retrofit Fragility ID Code	Parametric Non-Retrofit Fragility ID Code	Parametric Retrofit Fragility ID Code	Drift-Sensitive Fragility ID Code	Acceleration-Sensitive Fragility ID Code
Unreinforced Masonry (URM)	NO_STORIES >= 1 & NO_STORIES <= 2 & YEAR_BLT >= 1992	NO_STORIES >= 1 & NO_STORIES <= 2 & YEAR_BLT >= 1992	T <sub>1</sub> = 0.35	Adapted HAZUS Low Code URML	SF_URM_3	T <sub>1</sub> = 0.35	Adapted HAZUS High Code RM1L	SF_RM_16	SF_URM_11	SF_RM_56	NSF_DS_URM_3	NSF_AS_URM_3
Unreinforced Masonry (URM)	NO_STORIES >= 1 & NO_STORIES <= 2 & YEAR_BLT < 1992	NO_STORIES >= 1 & NO_STORIES <= 2 & YEAR_BLT < 1992	T <sub>1</sub> = 0.35	Adapted HAZUS Pre-Code URML	SF_URM_1	T <sub>1</sub> = 0.35	Adapted HAZUS High Code RM1L	SF_RM_16	SF_URM_9	SF_RM_56	NSF_DS_URM_1	NSF_AS_URM_1
Unreinforced Masonry (URM)	NO_STORIES >= 3 & YEAR_BLT >= 1992	NO_STORIES >= 3 & YEAR_BLT >= 1992	T <sub>1</sub> = 0.50	Adapted HAZUS Low Code URMM	SF_URM_4	T <sub>1</sub> = 0.50	Adapted HAZUS High Code RM1M	SF_RM_17	SF_URM_12	SF_RM_57	NSF_DS_URM_4	NSF_AS_URM_4
Unreinforced Masonry (URM)	NO_STORIES >= 3 & YEAR_BLT < 1992	NO_STORIES >= 3 & YEAR_BLT < 1992	T <sub>1</sub> = 0.50	Adapted HAZUS Pre-Code URMM	SF_URM_2	T <sub>1</sub> = 0.50	Adapted HAZUS High Code RM1M	SF_RM_17	SF_URM_10	SF_RM_57	NSF_DS_URM_2	NSF_AS_URM_2



MAEC Structural Type	v3 Mapping Check(s)	v4 Mapping Check(s)	Non-Retrofit Period (seconds)	Non-Retrofit Fragility	Non-Retrofit Fragility ID Code	Retrofit Period (seconds)	Retrofit Fragility	Retrofit Fragility ID Code	Parametric Non-Retrofit Fragility ID Code	Parametric Retrofit Fragility ID Code	Drift-Sensitive Fragility ID Code	Acceleration-Sensitive Fragility ID Code
Steel Moment Resisting Frame (S1)	NO_STORIES >= 1 & NO_STORIES <= 3 & YEAR_BLT < 1992	NO_STORIES >= 1 & NO_STORIES <= 3 & YEAR_BLT < 1992	T <sub>1</sub> = 1.07	Ellingwood 2 story PR	SF_S1_1	T <sub>1</sub> = 0.50	Adapted HAZUS High Code S1L	SF_S1_13	SF_S1_16	SF_S1_25	NSF_DS_S1_1	NSF_AS_S1_1
Steel Moment Resisting Frame (S1)	NO_STORIES >= 4 & NO_STORIES <= 7 & YEAR_BLT >= 1992	NO_STORIES >= 4 & NO_STORIES <= 7 & YEAR_BLT >= 1992	T <sub>1</sub> = 1.04	Ellingwood 6 story X-braced	SF_S2_1	T <sub>1</sub> = 0.86	Adapted HAZUS High Code S2M	SF_S2_12	SF_S2_30	SF_S2_36	NSF_DS_S2_5	NSF_AS_S2_5
Steel Moment Resisting Frame (S1)	NO_STORIES >= 1 & NO_STORIES <= 3 & YEAR_BLT >= 1992	NO_STORIES >= 1 & NO_STORIES <= 3 & YEAR_BLT >= 1992	T <sub>1</sub> = 0.50	Adapted HAZUS Low Code S1L	SF_S1_7	T <sub>1</sub> = 0.50	Adapted HAZUS High Code S1L	SF_S1_13	SF_S1_19	SF_S1_25	NSF_DS_S1_4	NSF_AS_S1_4
Steel Moment Resisting Frame (S1)	NO_STORIES >= 4 & NO_STORIES <= 7 & YEAR_BLT < 1992	NO_STORIES >= 4 & NO_STORIES <= 7 & YEAR_BLT < 1992	T <sub>1</sub> = 0.86	Adapted HAZUS Pre-Code S2M	SF_S2_3	T <sub>1</sub> = 0.86	Adapted HAZUS High Code S2M	SF_S2_12	SF_S2_27	SF_S2_36	NSF_DS_S2_2	NSF_AS_S2_2



MAEC Structural Type	v3 Mapping Check(s)	v4 Mapping Check(s)	Non-Retrofit Period (seconds)	Non-Retrofit Fragility	Non-Retrofit Fragility ID Code	Retrofit Period (seconds)	Retrofit Fragility	Retrofit Fragility ID Code	Parametric Non-Retrofit Fragility ID Code	Parametric Retrofit Fragility ID Code	Drift-Sensitive Fragility ID Code	Acceleration-Sensitive Fragility ID Code
Steel Moment Resisting Frame (S1)	NO_STORIES >= 8 & YEAR_BLT >= 1992	NO_STORIES >= 8 & YEAR_BLT >= 1992	T <sub>1</sub> = 1.77	Adapted HAZUS Low Code S2H	SF_S2_7	T <sub>1</sub> = 1.77	Adapted HAZUS High Code S2H	SF_S2_13	SF_S2_31	SF_S2_37	NSF_DS_S2_6	NSF_AS_S2_6
Steel Moment Resisting Frame (S1)	NO_STORIES >= 8 & YEAR_BLT < 1992	NO_STORIES >= 8 & YEAR_BLT < 1992	T <sub>1</sub> = 1.77	Adapted HAZUS Pre-Code S2H	SF_S2_4	T <sub>1</sub> = 1.77	Adapted HAZUS High Code S2H	SF_S2_13	SF_S2_28	SF_S2_37	NSF_DS_S2_3	NSF_AS_S2_3
Light Metal Frame (S3)	YEAR_BLT >= 1992	YEAR_BLT >= 1992	T <sub>1</sub> = 0.40	Adapted HAZUS Low Code S3	SF_S3_2	T <sub>1</sub> = 0.40	Adapted HAZUS High Code S3	SF_S3_4	SF_S3_10	SF_S3_12	NSF_DS_S3_2	NSF_AS_S3_2
Light Metal Frame (S3)	YEAR_BLT < 1992	YEAR_BLT < 1992	T <sub>1</sub> = 0.40	Adapted HAZUS Pre-Code S3	SF_S3_1	T <sub>1</sub> = 0.40	Adapted HAZUS High Code S3	SF_S3_4	SF_S3_9	SF_S3_12	NSF_DS_S3_1	NSF_AS_S3_1
Wood Frame (W)	NO_STORIES = 1 & YEAR_BLT < 1992	NO_STORIES = 1 & YEAR_BLT < 1992	T <sub>1</sub> = 0.24	Ellingwood 1 story Slab-on-grade	SF_W1_1	T <sub>1</sub> = 0.35	Adapted HAZUS High Code W1	SF_W1_6	SF_W1_11	SF_W1_14	NSF_DS_W1_1	NSF_AS_W1_1



MAEC Structural Type	v3 Mapping Check(s)	v4 Mapping Check(s)	Non-Retrofit Period (seconds)	Non-Retrofit Fragility	Non-Retrofit Fragility ID Code	Retrofit Period (seconds)	Retrofit Fragility	Retrofit Fragility ID Code	Parametric Non-Retrofit Fragility ID Code	Parametric Retrofit Fragility ID Code	Drift-Sensitive Fragility ID Code	Acceleration-Sensitive Fragility ID Code
Wood Frame (W)	NO_STORIES = 1 & YEAR_BLT >= 1992	NO_STORIES = 1 & YEAR_BLT >= 1992	T <sub>1</sub> = 0.35	Adapted HAZUS Low Code W1	SF_W1_4	T <sub>1</sub> = 0.35	Adapted HAZUS High Code W1	SF_W1_6	SF_W1_12	SF_W1_14	NSF_DS_W1_2	NSF_AS_W1_2
Wood Frame (W)	NO_STORIES = 2 & YEAR_BLT < 1992	NO_STORIES = 2 & YEAR_BLT < 1992	T <sub>1</sub> = 0.38	Ellingwood 2 story Slab-on-grade	SF_W2_1	T <sub>1</sub> = 0.40	Adapted HAZUS High Code W2	SF_W2_5	SF_W2_10	SF_W2_13	NSF_DS_W2_1	NSF_AS_W2_1
Wood Frame (W)	NO_STORIES = 2 & YEAR_BLT >= 1992	NO_STORIES = 2 & YEAR_BLT >= 1992	T <sub>1</sub> = 0.40	Adapted HAZUS Low Code W2	SF_W2_3	T <sub>1</sub> = 0.40	Adapted HAZUS High Code W2	SF_W2_5	SF_W2_11	SF_W2_13	NSF_DS_W2_2	NSF_AS_W2_2
Unknown	EF = (EFS OR EFS1) & NO_STORIES <= 2 & YEAR_BLT >= 1992	EF = (EFS OR EFS1) & NO_STORIES <= 2 & YEAR_BLT >= 1992	T <sub>1</sub> = 0.35	Adapted HAZUS Low Code URML	SF_URM_3	T <sub>1</sub> = 0.35	Adapted HAZUS High Code RM1L	SF_RM_16	SF_URM_11	SF_RM_56	NSF_DS_URM_3	NSF_AS_URM_3



MAEC Structural Type	v3 Mapping Check(s)	v4 Mapping Check(s)	Non-Retrofit Period (seconds)	Non-Retrofit Fragility	Non-Retrofit Fragility ID Code	Retrofit Period (seconds)	Retrofit Fragility	Retrofit Fragility ID Code	Parametric Non-Retrofit Fragility ID Code	Parametric Retrofit Fragility ID Code	Drift-Sensitive Fragility ID Code	Acceleration-Sensitive Fragility ID Code
Unknown	EF = (EFFS OR EFPS OR EFS1) & NO_STORIES <= 2 & YEAR_BLT < 1992	EF = (EFFS OR EFPS OR EFS1) & NO_STORIES <= 2 & YEAR_BLT < 1992	$T_1 = 0.35$	Adapted HAZUS Pre-Code URML	SF_URM_1	$T_1 = 0.35$	Adapted HAZUS High Code RM1L	SF_RM_16	SF_URM_9	SF_RM_56	NSF_DS_URM_1	NSF_AS_URM_1
Unknown	EF = (EFFS OR EFPS OR EFS1) & NO_STORIES > 2 & YEAR_BLT >= 1992	EF = (EFFS OR EFPS OR EFS1) & NO_STORIES > 2 & YEAR_BLT >= 1992	$T_1 = 0.50$	Adapted HAZUS Low Code URMM	SF_URM_4	$T_1 = 0.50$	Adapted HAZUS High Code RM1M	SF_RM_17	SF_URM_12	SF_RM_57	NSF_DS_URM_4	NSF_AS_URM_4
Unknown	EF = (EFFS OR EFPS OR EFS1) & NO_STORIES > 2 & YEAR_BLT < 1992	EF = (EFFS OR EFPS OR EFS1) & NO_STORIES > 2 & YEAR_BLT < 1992	$T_1 = 0.50$	Adapted HAZUS Pre-Code URMM	SF_URM_2	$T_1 = 0.50$	Adapted HAZUS High Code RM1M	SF_RM_17	SF_URM_10	SF_RM_57	NSF_DS_URM_2	NSF_AS_URM_2



MAEC Structural Type	v3 Mapping Check(s)	v4 Mapping Check(s)	Non-Retrofit Period (seconds)	Non-Retrofit Fragility	Non-Retrofit Fragility ID Code	Retrofit Period (seconds)	Retrofit Fragility	Retrofit Fragility ID Code	Parametric Non-Retrofit Fragility ID Code	Parametric Retrofit Fragility ID Code	Drift-Sensitive Fragility ID Code	Acceleration-Sensitive Fragility ID Code
Unknown	EF = EFHL & YEAR_BLT >= 1992	EF = EFHL & YEAR_BLT >= 1992	T <sub>1</sub> = 0.4	Adapted HAZUS Moderate Code CIL	SF_C1_24	T <sub>1</sub> = 0.4	HAZUS CIL High Code	SF_C1_27	SF_C1_48	SF_C1_51	NSF_DS_C1_7	NSF_AS_C1_7
Unknown	EF = EFHL & YEAR_BLT < 1992	EF = EFHL & YEAR_BLT < 1992	T <sub>1</sub> = $\eta_1(h)^{\eta_2}$ , where $\eta_1 = 0.097$ , $\eta_2 = 0.624$ , and h = height of building frame from base (ft). Typically assume 13 ft story height.	Bracci Gravity Load (GLD) of buildings	SF_C1_10	T <sub>1</sub> = 0.40	HAZUS CIL High Code	SF_C1_27	SF_C1_42	SF_C1_51	NSF_DS_C1_1	NSF_AS_C1_1



**Table C4.2.1-2 Descriptive Data for Fragilities in Default Mapping Scheme**

<b>Fragility ID Code</b>	<b>Author</b>	<b>Structure Type</b>	<b>Stories</b>	<b>Description</b>	<b>Ground Motions</b>	<b>Code</b>	<b>Demand Type</b>	<b>Demand Units</b>
SF_C1_1	Hueste	Concrete Moment Frame	5	Flat Slab with Perimeter Moment Frame	Rix and Fernandez	Low-Code	Sa	g
SF_C1_2	Hueste	Concrete Moment Frame	5	Flat Slab with Perimeter Moment Frame with shear walls	Rix and Fernandez	High-Code	Sa	g
SF_C1_3	Hueste	Concrete Moment Frame	5	Flat Slab with Perimeter Moment Frame with column jackets	Rix and Fernandez	Moderate-Code	Sa	g
SF_C1_4	Hueste	Concrete Moment Frame	5	Flat Slab with Perimeter Moment Frame with confining plates at column ends	Rix and Fernandez	Low-Code	Sa	g
SF_C1_9	Elnashai and Erberik	Concrete Moment Frame	5	Flat Slab with Masonry Infill Walls	10 actual records (worldwide)	Low-Code	Sa	g
SF_C1_10	Bracci	Concrete Moment Frame	0	Gravity Load Designed Concrete Frames	Rix and Fernandez, Wen	Pre-Code	Sa	g
SF_C1_15	Elnashai, Kuchma, Ji	Concrete Moment Frame	54	High-rise with dual-core wall system	30 actual records (worldwide)	Low-Code	Sa	g
SF_C1_18	HAZUS	Concrete Moment Frame	2	Low-Rise Concrete Moment Frame	Unknown	Pre-Code	Sd	in
SF_C1_19	HAZUS	Concrete Moment Frame	5	Mid-Rise Concrete Moment Frame	Unknown	Pre-Code	Sd	in
SF_C1_20	HAZUS	Concrete Moment Frame	12	High-Rise Concrete Moment Frame	Unknown	Pre-Code	Sd	in
SF_C1_21	HAZUS	Concrete Moment Frame	2	Low-Rise Concrete Moment Frame	Unknown	Low-Code	Sd	in
SF_C1_22	HAZUS	Concrete Moment Frame	5	Mid-Rise Concrete Moment Frame	Unknown	Low-Code	Sd	in
SF_C1_23	HAZUS	Concrete Moment Frame	12	High-Rise Concrete Moment Frame	Unknown	Low-Code	Sd	in



<b>Fragility ID Code</b>	<b>Author</b>	<b>Structure Type</b>	<b>Stories</b>	<b>Description</b>	<b>Ground Motions</b>	<b>Code</b>	<b>Demand Type</b>	<b>Demand Units</b>
SF_C1_24	HAZUS	Concrete Moment Frame	2	Low-Rise Concrete Moment Frame	Unknown	Moderate -Code	Sd	in
SF_C1_27	HAZUS	Concrete Moment Frame	2	Low-Rise Concrete Moment Frame	Unknown	High-Code	Sd	in
SF_C1_28	HAZUS	Concrete Moment Frame	5	Mid-Rise Concrete Moment Frame	Unknown	High-Code	Sd	in
SF_C1_29	HAZUS	Concrete Moment Frame	12	High-Rise Concrete Moment Frame	Unknown	High-Code	Sd	in
SF_C1_42	Elnashai and Jeong	Concrete Moment Frame	2	Low-Rise Concrete Moment Frame	84th percentile, Memphis Lowlands, 7.5 @ Blytheville, AR	Pre-Code	0.2 sec Sa	g
SF_C1_43	Elnashai and Jeong	Concrete Moment Frame	5	Mid-Rise Concrete Moment Frame	84th percentile, Memphis Lowlands, 7.5 @ Blytheville, AR	Pre-Code	0.2 sec Sa	g
SF_C1_44	Elnashai and Jeong	Concrete Moment Frame	12	High-Rise Concrete Moment Frame	84th percentile, Memphis Lowlands, 7.5 @ Blytheville, AR	Pre-Code	0.2 sec Sa	g
SF_C1_45	Elnashai and Jeong	Concrete Moment Frame	2	Low-Rise Concrete Moment Frame	84th percentile, Memphis Lowlands, 7.5 @ Blytheville, AR	Low-Code	0.2 sec Sa	g
SF_C1_46	Elnashai and Jeong	Concrete Moment Frame	5	Mid-Rise Concrete Moment Frame	84th percentile, Memphis Lowlands, 7.5 @ Blytheville, AR	Low-Code	0.2 sec Sa	g
SF_C1_47	Elnashai and Jeong	Concrete Moment Frame	12	High-Rise Concrete Moment Frame	84th percentile, Memphis Lowlands, 7.5 @ Blytheville, AR	Low-Code	0.2 sec Sa	g
SF_C1_48	Elnashai and Jeong	Concrete Moment Frame	2	Low-Rise Concrete Moment Frame	84th percentile, Memphis Lowlands, 7.5 @ Blytheville, AR	Moderate -Code	0.2 sec Sa	g
SF_C1_51	Elnashai and Jeong	Concrete Moment Frame	2	Low-Rise Concrete Moment Frame	84th percentile, Memphis Lowlands, 7.5 @ Blytheville, AR	High-Code	0.2 sec Sa	g
SF_C1_52	Elnashai and Jeong	Concrete Moment Frame	5	Mid-Rise Concrete Moment Frame	84th percentile, Memphis Lowlands, 7.5 @ Blytheville, AR	High-Code	0.2 sec Sa	g
SF_C1_53	Elnashai and Jeong	Concrete Moment Frame	12	High-Rise Concrete Moment Frame	84th percentile, Memphis Lowlands, 7.5 @ Blytheville, AR	High-Code	0.2 sec Sa	g



<b>Fragility ID Code</b>	<b>Author</b>	<b>Structure Type</b>	<b>Stories</b>	<b>Description</b>	<b>Ground Motions</b>	<b>Code</b>	<b>Demand Type</b>	<b>Demand Units</b>
SF_C1_55	Elnashai and Jeong	Concrete Moment Frame	5	Mid-Rise Concrete Moment Frame	84th percentile, Memphis Lowlands, 7.5 @ Blytheville, AR	Pre-Code	1.0 sec Sa	g
SF_C2_1	HAZUS	Concrete Frame w/ Shear Walls	2	Low-Rise Concrete Frame w/ Shear Walls	Unknown	Pre-Code	Sd	in
SF_C2_2	HAZUS	Concrete Frame w/ Shear Walls	5	Mid-Rise Concrete Frame w/ Shear Walls	Unknown	Pre-Code	Sd	in
SF_C2_3	HAZUS	Concrete Frame w/ Shear Walls	12	High-Rise Concrete Frame w/ Shear Walls	Unknown	Pre-Code	Sd	in
SF_C2_4	HAZUS	Concrete Frame w/ Shear Walls	2	Low-Rise Concrete Frame w/ Shear Walls	Unknown	Low-Code	Sd	in
SF_C2_5	HAZUS	Concrete Frame w/ Shear Walls	5	Mid-Rise Concrete Frame w/ Shear Walls	Unknown	Low-Code	Sd	in
SF_C2_6	HAZUS	Concrete Frame w/ Shear Walls	12	High-Rise Concrete Frame w/ Shear Walls	Unknown	Low-Code	Sd	in
SF_C2_10	HAZUS	Concrete Frame w/ Shear Walls	2	Low-Rise Concrete Frame w/ Shear Walls	Unknown	High-Code	Sd	in
SF_C2_11	HAZUS	Concrete Frame w/ Shear Walls	5	Mid-Rise Concrete Frame w/ Shear Walls	Unknown	High-Code	Sd	in
SF_C2_12	HAZUS	Concrete Frame w/ Shear Walls	12	High-Rise Concrete Frame w/ Shear Walls	Unknown	High-Code	Sd	in
SF_C2_25	Elnashai and Jeong	Concrete Frame w/ Shear Walls	2	Low-Rise Concrete Frame w/ Shear Walls	84th percentile, Memphis Lowlands, 7.5 @ Blytheville, AR	Pre-Code	0.2 sec Sa	g
SF_C2_26	Elnashai and Jeong	Concrete Frame w/ Shear Walls	5	Mid-Rise Concrete Frame w/ Shear Walls	84th percentile, Memphis Lowlands, 7.5 @ Blytheville, AR	Pre-Code	0.2 sec Sa	g
SF_C2_27	Elnashai and Jeong	Concrete Frame w/ Shear Walls	12	High-Rise Concrete Frame w/ Shear Walls	84th percentile, Memphis Lowlands, 7.5 @ Blytheville, AR	Pre-Code	0.2 sec Sa	g
SF_C2_28	Elnashai and Jeong	Concrete Frame w/ Shear Walls	2	Low-Rise Concrete Frame w/ Shear Walls	84th percentile, Memphis Lowlands, 7.5 @ Blytheville, AR	Low-Code	0.2 sec Sa	g



<b>Fragility ID Code</b>	<b>Author</b>	<b>Structure Type</b>	<b>Stories</b>	<b>Description</b>	<b>Ground Motions</b>	<b>Code</b>	<b>Demand Type</b>	<b>Demand Units</b>
SF_C2_29	Elnashai and Jeong	Concrete Frame w/ Shear Walls	5	Mid-Rise Concrete Frame w/ Shear Walls	84th percentile, Memphis Lowlands, 7.5 @ Blytheville, AR	Low-Code	0.2 sec Sa	g
SF_C2_30	Elnashai and Jeong	Concrete Frame w/ Shear Walls	12	High-Rise Concrete Frame w/ Shear Walls	84th percentile, Memphis Lowlands, 7.5 @ Blytheville, AR	Low-Code	0.2 sec Sa	g
SF_C2_34	Elnashai and Jeong	Concrete Frame w/ Shear Walls	2	Low-Rise Concrete Frame w/ Shear Walls	84th percentile, Memphis Lowlands, 7.5 @ Blytheville, AR	High-Code	0.2 sec Sa	g
SF_C2_35	Elnashai and Jeong	Concrete Frame w/ Shear Walls	5	Mid-Rise Concrete Frame w/ Shear Walls	84th percentile, Memphis Lowlands, 7.5 @ Blytheville, AR	High-Code	0.2 sec Sa	g
SF_C2_36	Elnashai and Jeong	Concrete Frame w/ Shear Walls	12	High-Rise Concrete Frame w/ Shear Walls	84th percentile, Memphis Lowlands, 7.5 @ Blytheville, AR	High-Code	0.2 sec Sa	g
SF_PC1_1	HAZUS	Concrete Tilt-Up	1	Concrete Tilt-Up	Unknown	Pre-Code	Sd	in
SF_PC1_2	HAZUS	Concrete Tilt-Up	1	Concrete Tilt-Up	Unknown	Low-Code	Sd	in
SF_PC1_4	HAZUS	Concrete Tilt-Up	1	Concrete Tilt-Up	Unknown	High-Code	Sd	in
SF_PC1_9	Elnashai and Jeong	Concrete Tilt-Up	1	Concrete Tilt-Up	84th percentile, Memphis Lowlands, 7.5 @ Blytheville, AR	Pre-Code	0.2 sec Sa	g
SF_PC1_10	Elnashai and Jeong	Concrete Tilt-Up	1	Concrete Tilt-Up	84th percentile, Memphis Lowlands, 7.5 @ Blytheville, AR	Low-Code	0.2 sec Sa	g
SF_PC1_12	Elnashai and Jeong	Concrete Tilt-Up	1	Concrete Tilt-Up	84th percentile, Memphis Lowlands, 7.5 @ Blytheville, AR	High-Code	0.2 sec Sa	g
SF_PC2_1	HAZUS	Precast Concrete Frame	2	Low-Rise Precast Concrete Frame	Unknown	Pre-Code	Sd	in
SF_PC2_2	HAZUS	Precast Concrete Frame	5	Mid-Rise Precast Concrete Frame	Unknown	Pre-Code	Sd	in
SF_PC2_3	HAZUS	Precast Concrete Frame	12	High-Rise Precast Concrete Frame	Unknown	Pre-Code	Sd	in



<b>Fragility ID Code</b>	<b>Author</b>	<b>Structure Type</b>	<b>Stories</b>	<b>Description</b>	<b>Ground Motions</b>	<b>Code</b>	<b>Demand Type</b>	<b>Demand Units</b>
SF_PC2_4	HAZUS	Precast Concrete Frame	2	Low-Rise Precast Concrete Frame	Unknown	Low-Code	Sd	in
SF_PC2_5	HAZUS	Precast Concrete Frame	5	Mid-Rise Precast Concrete Frame	Unknown	Low-Code	Sd	in
SF_PC2_6	HAZUS	Precast Concrete Frame	12	High-Rise Precast Concrete Frame	Unknown	Low-Code	Sd	in
SF_PC2_9	HAZUS	Precast Concrete Frame	12	High-Rise Precast Concrete Frame	Unknown	Moderate-Code	Sd	in
SF_PC2_10	HAZUS	Precast Concrete Frame	2	Low-Rise Precast Concrete Frame	Unknown	High-Code	Sd	in
SF_PC2_11	HAZUS	Precast Concrete Frame	5	Mid-Rise Precast Concrete Frame	Unknown	High-Code	Sd	in
SF_PC2_25	Elnashai and Jeong	Precast Concrete Frame	2	Low-Rise Precast Concrete Frame	84th percentile, Memphis Lowlands, 7.5 @ Blytheville, AR	Pre-Code	0.2 sec Sa	g
SF_PC2_26	Elnashai and Jeong	Precast Concrete Frame	5	Mid-Rise Precast Concrete Frame	84th percentile, Memphis Lowlands, 7.5 @ Blytheville, AR	Pre-Code	0.2 sec Sa	g
SF_PC2_27	Elnashai and Jeong	Precast Concrete Frame	12	High-Rise Precast Concrete Frame	84th percentile, Memphis Lowlands, 7.5 @ Blytheville, AR	Pre-Code	0.2 sec Sa	g
SF_PC2_28	Elnashai and Jeong	Precast Concrete Frame	2	Low-Rise Precast Concrete Frame	84th percentile, Memphis Lowlands, 7.5 @ Blytheville, AR	Low-Code	0.2 sec Sa	g
SF_PC2_29	Elnashai and Jeong	Precast Concrete Frame	5	Mid-Rise Precast Concrete Frame	84th percentile, Memphis Lowlands, 7.5 @ Blytheville, AR	Low-Code	0.2 sec Sa	g
SF_PC2_30	Elnashai and Jeong	Precast Concrete Frame	12	High-Rise Precast Concrete Frame	84th percentile, Memphis Lowlands, 7.5 @ Blytheville, AR	Low-Code	0.2 sec Sa	g
SF_PC2_34	Elnashai and Jeong	Precast Concrete Frame	2	Low-Rise Precast Concrete Frame	84th percentile, Memphis Lowlands, 7.5 @ Blytheville, AR	High-Code	0.2 sec Sa	g
SF_PC2_35	Elnashai and Jeong	Precast Concrete Frame	5	Mid-Rise Precast Concrete Frame	84th percentile, Memphis Lowlands, 7.5 @ Blytheville, AR	High-Code	0.2 sec Sa	g



<b>Fragility ID Code</b>	<b>Author</b>	<b>Structure Type</b>	<b>Stories</b>	<b>Description</b>	<b>Ground Motions</b>	<b>Code</b>	<b>Demand Type</b>	<b>Demand Units</b>
SF_PC2_3 6	Elnashai and Jeong	Precast Concrete Frame	12	High-Rise Precast Concrete Frame	84th percentile, Memphis Lowlands, 7.5 @ Blytheville, AR	High- Code	0.2 sec Sa	g
SF_RM_1	HAZUS	Reinforced Masonry	2	Low-Rise Reinforced Masonry Bearing Walls with Wood or Metal Deck Diaphragms	Unknown	Pre- Code	Sd	in
SF_RM_2	HAZUS	Reinforced Masonry	5	Mid-Rise Reinforced Masonry Bearing Walls with Wood or Metal Deck Diaphragms	Unknown	Pre- Code	Sd	in
SF_RM_3	HAZUS	Reinforced Masonry	2	Low-Rise Reinforced Masonry Bearing Walls with Precast Concrete Diaphragms	Unknown	Pre- Code	Sd	in
SF_RM_4	HAZUS	Reinforced Masonry	5	Mid-Rise Reinforced Masonry Bearing Walls with Precast Concrete Diaphragms	Unknown	Pre- Code	Sd	in
SF_RM_5	HAZUS	Reinforced Masonry	12	High-Rise Reinforced Masonry Bearing Walls with Precast Concrete Diaphragms	Unknown	Pre- Code	Sd	in
SF_RM_6	HAZUS	Reinforced Masonry	2	Low-Rise Reinforced Masonry Bearing Walls with Wood or Metal Deck Diaphragms	Unknown	Low- Code	Sd	in
SF_RM_7	HAZUS	Reinforced Masonry	5	Mid-Rise Reinforced Masonry Bearing Walls with Wood or Metal Deck Diaphragms	Unknown	Low- Code	Sd	in
SF_RM_8	HAZUS	Reinforced Masonry	2	Low-Rise Reinforced Masonry Bearing Walls with Precast Concrete Diaphragms	Unknown	Low- Code	Sd	in
SF_RM_9	HAZUS	Reinforced Masonry	5	Mid-Rise Reinforced Masonry Bearing Walls with Precast Concrete Diaphragms	Unknown	Low- Code	Sd	in
SF_RM_1 0	HAZUS	Reinforced Masonry	12	High-Rise Reinforced Masonry Bearing Walls with Precast Concrete Diaphragms	Unknown	Low- Code	Sd	in
SF_RM_1 6	HAZUS	Reinforced Masonry	2	Low-Rise Reinforced Masonry Bearing Walls with Wood or Metal Deck Diaphragms	Unknown	High- Code	Sd	in
SF_RM_1 7	HAZUS	Reinforced Masonry	5	Mid-Rise Reinforced Masonry Bearing Walls with Wood or Metal Deck Diaphragms	Unknown	High- Code	Sd	in
SF_RM_1 8	HAZUS	Reinforced Masonry	2	Low-Rise Reinforced Masonry Bearing Walls with Precast Concrete Diaphragms	Unknown	High- Code	Sd	in



<b>Fragility ID Code</b>	<b>Author</b>	<b>Structure Type</b>	<b>Stories</b>	<b>Description</b>	<b>Ground Motions</b>	<b>Code</b>	<b>Demand Type</b>	<b>Demand Units</b>
SF_RM_19	HAZUS	Reinforced Masonry	5	Mid-Rise Reinforced Masonry Bearing Walls with Precast Concrete Diaphragms	Unknown	High-Code	Sd	in
SF_RM_20	HAZUS	Reinforced Masonry	12	High-Rise Reinforced Masonry Bearing Walls with Precast Concrete Diaphragms	Unknown	High-Code	Sd	in
SF_RM_41	Elnashai and Jeong	Reinforced Masonry	2	Low-Rise Reinforced Masonry Bearing Walls with Wood or Metal Deck Diaphragms	84th percentile, Memphis Lowlands, 7.5 @ Blytheville, AR	Pre-Code	0.2 sec Sa	g
SF_RM_42	Elnashai and Jeong	Reinforced Masonry	5	Mid-Rise Reinforced Masonry Bearing Walls with Wood or Metal Deck Diaphragms	84th percentile, Memphis Lowlands, 7.5 @ Blytheville, AR	Pre-Code	0.2 sec Sa	g
SF_RM_43	Elnashai and Jeong	Reinforced Masonry	2	Low-Rise Reinforced Masonry Bearing Walls with Precast Concrete Diaphragms	84th percentile, Memphis Lowlands, 7.5 @ Blytheville, AR	Pre-Code	0.2 sec Sa	in
SF_RM_44	Elnashai and Jeong	Reinforced Masonry	5	Mid-Rise Reinforced Masonry Bearing Walls with Precast Concrete Diaphragms	84th percentile, Memphis Lowlands, 7.5 @ Blytheville, AR	Pre-Code	0.2 sec Sa	in
SF_RM_45	Elnashai and Jeong	Reinforced Masonry	12	High-Rise Reinforced Masonry Bearing Walls with Precast Concrete Diaphragms	84th percentile, Memphis Lowlands, 7.5 @ Blytheville, AR	Pre-Code	0.2 sec Sa	in
SF_RM_46	Elnashai and Jeong	Reinforced Masonry	2	Low-Rise Reinforced Masonry Bearing Walls with Wood or Metal Deck Diaphragms	84th percentile, Memphis Lowlands, 7.5 @ Blytheville, AR	Low-Code	0.2 sec Sa	in
SF_RM_47	Elnashai and Jeong	Reinforced Masonry	5	Mid-Rise Reinforced Masonry Bearing Walls with Wood or Metal Deck Diaphragms	84th percentile, Memphis Lowlands, 7.5 @ Blytheville, AR	Low-Code	0.2 sec Sa	in
SF_RM_48	Elnashai and Jeong	Reinforced Masonry	2	Low-Rise Reinforced Masonry Bearing Walls with Precast Concrete Diaphragms	84th percentile, Memphis Lowlands, 7.5 @ Blytheville, AR	Low-Code	0.2 sec Sa	in
SF_RM_49	Elnashai and Jeong	Reinforced Masonry	5	Mid-Rise Reinforced Masonry Bearing Walls with Precast Concrete Diaphragms	84th percentile, Memphis Lowlands, 7.5 @ Blytheville, AR	Low-Code	0.2 sec Sa	in
SF_RM_50	Elnashai and Jeong	Reinforced Masonry	12	High-Rise Reinforced Masonry Bearing Walls with Precast Concrete Diaphragms	84th percentile, Memphis Lowlands, 7.5 @ Blytheville, AR	Low-Code	0.2 sec Sa	in
SF_RM_56	Elnashai and Jeong	Reinforced Masonry	2	Low-Rise Reinforced Masonry Bearing Walls with Wood or Metal Deck Diaphragms	84th percentile, Memphis Lowlands, 7.5 @ Blytheville, AR	High-Code	0.2 sec Sa	in
SF_RM_57	Elnashai and Jeong	Reinforced Masonry	5	Mid-Rise Reinforced Masonry Bearing Walls with Wood or Metal Deck Diaphragms	84th percentile, Memphis Lowlands, 7.5 @ Blytheville, AR	High-Code	0.2 sec Sa	in



<b>Fragility ID Code</b>	<b>Author</b>	<b>Structure Type</b>	<b>Stories</b>	<b>Description</b>	<b>Ground Motions</b>	<b>Code</b>	<b>Demand Type</b>	<b>Demand Units</b>
SF_RM_58	Elnashai and Jeong	Reinforced Masonry	2	Low-Rise Reinforced Masonry Bearing Walls with Precast Concrete Diaphragms	84th percentile, Memphis Lowlands, 7.5 @ Blytheville, AR	High-Code	0.2 sec Sa	in
SF_RM_59	Elnashai and Jeong	Reinforced Masonry	5	Mid-Rise Reinforced Masonry Bearing Walls with Precast Concrete Diaphragms	84th percentile, Memphis Lowlands, 7.5 @ Blytheville, AR	High-Code	0.2 sec Sa	in
SF_RM_60	Elnashai and Jeong	Reinforced Masonry	12	High-Rise Reinforced Masonry Bearing Walls with Precast Concrete Diaphragms	84th percentile, Memphis Lowlands, 7.5 @ Blytheville, AR	High-Code	0.2 sec Sa	in
SF_URM_1	HAZUS	Unreinforced Masonry	2	Low-Rise Unreinforced Masonry Bearing Walls	Unknown	Pre-Code	Sd	in
SF_URM_2	HAZUS	Unreinforced Masonry	5	Mid-Rise Unreinforced Masonry Bearing Walls	Unknown	Pre-Code	Sd	in
SF_URM_3	HAZUS	Unreinforced Masonry	2	Low-Rise Unreinforced Masonry Bearing Walls	Unknown	Low-Code	Sd	in
SF_URM_4	HAZUS	Unreinforced Masonry	5	Mid-Rise Unreinforced Masonry Bearing Walls	Unknown	Low-Code	Sd	in
SF_URM_9	Elnashai and Jeong	Unreinforced Masonry	2	Low-Rise Unreinforced Masonry Bearing Walls	84th percentile, Memphis Lowlands, 7.5 @ Blytheville, AR	Pre-Code	0.2 sec Sa	g
SF_URM_10	Elnashai and Jeong	Unreinforced Masonry	5	Mid-Rise Unreinforced Masonry Bearing Walls	84th percentile, Memphis Lowlands, 7.5 @ Blytheville, AR	Pre-Code	0.2 sec Sa	g
SF_URM_11	Elnashai and Jeong	Unreinforced Masonry	2	Low-Rise Unreinforced Masonry Bearing Walls	84th percentile, Memphis Lowlands, 7.5 @ Blytheville, AR	Low-Code	0.2 sec Sa	g
SF_URM_12	Elnashai and Jeong	Unreinforced Masonry	5	Mid-Rise Unreinforced Masonry Bearing Walls	84th percentile, Memphis Lowlands, 7.5 @ Blytheville, AR	Low-Code	0.2 sec Sa	g
SF_S1_1	Ellingwood	Steel Moment Resisting Frame	2	2-story Partially Restrained Steel Frame	Unknown	Pre-Code	Sa	g
SF_S1_7	HAZUS	Steel Moment Resisting Frame	2	Low-Rise Steel Moment Frame	Unknown	Low-Code	Sd	in
SF_S1_13	HAZUS	Steel Moment Resisting Frame	2	Low-Rise Steel Moment Frame	Unknown	High-Code	Sd	in



<b>Fragility ID Code</b>	<b>Author</b>	<b>Structure Type</b>	<b>Stories</b>	<b>Description</b>	<b>Ground Motions</b>	<b>Code</b>	<b>Demand Type</b>	<b>Demand Units</b>
SF_S1_16	Elnashai and Jeong	Steel Moment Resisting Frame	2	Low-Rise Steel Moment Frame	84th percentile, Memphis Lowlands, 7.5 @ Blytheville, AR	Pre-Code	PGA	g
SF_S1_19	Elnashai and Jeong	Steel Moment Resisting Frame	2	Low-Rise Steel Moment Frame	84th percentile, Memphis Lowlands, 7.5 @ Blytheville, AR	Low-Code	PGA	g
SF_S1_25	Elnashai and Jeong	Steel Moment Resisting Frame	2	Low-Rise Steel Moment Frame	84th percentile, Memphis Lowlands, 7.5 @ Blytheville, AR	High-Code	PGA	g
SF_S2_1	Ellingwood	Steel Braced Frame	6	6-story X-braced Steel Frame	Unknown	Low-Code	Sa	g
SF_S2_3	HAZUS	Steel Braced Frame	5	Mid-Rise Steel Braced Frame	Unknown	Pre-Code	Sd	in
SF_S2_4	HAZUS	Steel Braced Frame	13	High-Rise Steel Braced Frame	Unknown	Pre-Code	Sd	in
SF_S2_7	HAZUS	Steel Braced Frame	13	High-Rise Steel Braced Frame	Unknown	Low-Code	Sd	in
SF_S2_12	HAZUS	Steel Braced Frame	5	Mid-Rise Steel Braced Frame	Unknown	High-Code	Sd	in
SF_S2_13	HAZUS	Steel Braced Frame	13	High-Rise Steel Braced Frame	Unknown	High-Code	Sd	in
SF_S2_27	Elnashai and Jeong	Steel Braced Frame	5	Mid-Rise Steel Braced Frame	84th percentile, Memphis Lowlands, 7.5 @ Blytheville, AR	Pre-Code	0.2 sec Sa	g
SF_S2_28	Elnashai and Jeong	Steel Braced Frame	13	High-Rise Steel Braced Frame	84th percentile, Memphis Lowlands, 7.5 @ Blytheville, AR	Pre-Code	0.2 sec Sa	g
SF_S2_30	Elnashai and Jeong	Steel Braced Frame	5	Mid-Rise Steel Braced Frame	84th percentile, Memphis Lowlands, 7.5 @ Blytheville, AR	Low-Code	0.2 sec Sa	g
SF_S2_31	Elnashai and Jeong	Steel Braced Frame	13	High-Rise Steel Braced Frame	84th percentile, Memphis Lowlands, 7.5 @ Blytheville, AR	Low-Code	0.2 sec Sa	g
SF_S2_36	Elnashai and Jeong	Steel Braced Frame	5	Mid-Rise Steel Braced Frame	84th percentile, Memphis Lowlands, 7.5 @ Blytheville, AR	High-Code	0.2 sec Sa	g



<b>Fragility ID Code</b>	<b>Author</b>	<b>Structure Type</b>	<b>Stories</b>	<b>Description</b>	<b>Ground Motions</b>	<b>Code</b>	<b>Demand Type</b>	<b>Demand Units</b>
SF_S2_37	Elnashai and Jeong	Steel Braced Frame	13	High-Rise Steel Braced Frame	84th percentile, Memphis Lowlands, 7.5 @ Blytheville, AR	High-Code	0.2 sec Sa	g
SF_S3_1	HAZUS	Light Metal Frame	1	Steel Light Frame	Unknown	Pre-Code	Sd	in
SF_S3_2	HAZUS	Light Metal Frame	1	Steel Light Frame	Unknown	Low-Code	Sd	in
SF_S3_4	HAZUS	Light Metal Frame	1	Steel Light Frame	Unknown	High-Code	Sd	in
SF_S3_9	Elnashai and Jeong	Light Metal Frame	1	Steel Light Frame	84th percentile, Memphis Lowlands, 7.5 @ Blytheville, AR	Pre-Code	0.2 sec Sa	g
SF_S3_10	Elnashai and Jeong	Light Metal Frame	1	Steel Light Frame	84th percentile, Memphis Lowlands, 7.5 @ Blytheville, AR	Low-Code	0.2 sec Sa	g
SF_S3_12	Elnashai and Jeong	Light Metal Frame	1	Steel Light Frame	84th percentile, Memphis Lowlands, 7.5 @ Blytheville, AR	High-Code	0.2 sec Sa	g
SF_W1_1	Ellingwood	Wood Frame	1	1-story Wood Frame on slab-on-grade	Unknown	Pre-Code	Sa	g
SF_W1_4	HAZUS	Wood Frame	1	Light Wood Frame	Unknown	Low-Code	Sd	in
SF_W1_6	HAZUS	Wood Frame	1	Light Wood Frame	Unknown	High-Code	Sd	in
SF_W1_1 1	Elnashai and Jeong	Wood Frame	1	Light Wood Frame	84th percentile, Memphis Lowlands, 7.5 @ Blytheville, AR	Pre-Code	0.2 sec Sa	g
SF_W1_1 2	Elnashai and Jeong	Wood Frame	1	Light Wood Frame	84th percentile, Memphis Lowlands, 7.5 @ Blytheville, AR	Low-Code	0.2 sec Sa	g
SF_W1_1 4	Elnashai and Jeong	Wood Frame	1	Light Wood Frame	84th percentile, Memphis Lowlands, 7.5 @ Blytheville, AR	High-Code	0.2 sec Sa	g
SF_W2_1	Ellingwood	Wood Frame	2	2-story Wood Frame on slab-on-grade	Unknown	Pre-Code	Sa	g



<b>Fragility ID Code</b>	<b>Author</b>	<b>Structure Type</b>	<b>Stories</b>	<b>Description</b>	<b>Ground Motions</b>	<b>Code</b>	<b>Demand Type</b>	<b>Demand Units</b>
SF_W2_3	HAZUS	Wood Frame	2	Commercial and Industrial Wood Frame	Unknown	Low-Code	Sd	in
SF_W2_5	HAZUS	Wood Frame	2	Commercial and Industrial Wood Frame	Unknown	High-Code	Sd	in
SF_W2_1 0	Elnashai and Jeong	Wood Frame	2	Commercial and Industrial Wood Frame	84th percentile, Memphis Lowlands, 7.5 @ Blytheville, AR	Pre-Code	0.2 sec Sa	g
SF_W2_1 1	Elnashai and Jeong	Wood Frame	2	Commercial and Industrial Wood Frame	84th percentile, Memphis Lowlands, 7.5 @ Blytheville, AR	Low-Code	0.2 sec Sa	g
SF_W2_1 3	Elnashai and Jeong	Wood Frame	2	Commercial and Industrial Wood Frame	84th percentile, Memphis Lowlands, 7.5 @ Blytheville, AR	High-Code	0.2 sec Sa	g
NSF_DS_ C1_1	HAZUS	Concrete Moment Frame	2	Low-Rise Concrete Moment Frame	Unknown	Pre-Code	Sd	in
NSF_DS_ C1_2	HAZUS	Concrete Moment Frame	5	Mid-Rise Concrete Moment Frame	Unknown	Pre-Code	Sd	in
NSF_DS_ C1_3	HAZUS	Concrete Moment Frame	12	High-Rise Concrete Moment Frame	Unknown	Pre-Code	Sd	in
NSF_DS_ C1_4	HAZUS	Concrete Moment Frame	2	Low-Rise Concrete Moment Frame	Unknown	Low-Code	Sd	in
NSF_DS_ C1_5	HAZUS	Concrete Moment Frame	5	Mid-Rise Concrete Moment Frame	Unknown	Low-Code	Sd	in
NSF_DS_ C1_6	HAZUS	Concrete Moment Frame	12	High-Rise Concrete Moment Frame	Unknown	Low-Code	Sd	in
NSF_DS_ C1_7	HAZUS	Concrete Moment Frame	2	Low-Rise Concrete Moment Frame	Unknown	Moderate -Code	Sd	in
NSF_DS_ C2_1	HAZUS	Concrete Frame w/ Shear Walls	2	Low-Rise Concrete Frame w/ Shear Walls	Unknown	Pre-Code	Sd	in
NSF_DS_ C2_2	HAZUS	Concrete Frame w/ Shear Walls	5	Mid-Rise Concrete Frame w/ Shear Walls	Unknown	Pre-Code	Sd	in



<b>Fragility ID Code</b>	<b>Author</b>	<b>Structure Type</b>	<b>Stories</b>	<b>Description</b>	<b>Ground Motions</b>	<b>Code</b>	<b>Demand Type</b>	<b>Demand Units</b>
NSF_DS_C2_3	HAZUS	Concrete Frame w/ Shear Walls	12	High-Rise Concrete Frame w/ Shear Walls	Unknown	Pre-Code	Sd	in
NSF_DS_C2_4	HAZUS	Concrete Frame w/ Shear Walls	2	Low-Rise Concrete Frame w/ Shear Walls	Unknown	Low-Code	Sd	in
NSF_DS_C2_5	HAZUS	Concrete Frame w/ Shear Walls	5	Mid-Rise Concrete Frame w/ Shear Walls	Unknown	Low-Code	Sd	in
NSF_DS_C2_6	HAZUS	Concrete Frame w/ Shear Walls	12	High-Rise Concrete Frame w/ Shear Walls	Unknown	Low-Code	Sd	in
NSF_DS_PC1_1	HAZUS	Concrete Tilt-Up	1	Concrete Tilt-Up	Unknown	Pre-Code	Sd	in
NSF_DS_PC1_2	HAZUS	Concrete Tilt-Up	1	Concrete Tilt-Up	Unknown	Low-Code	Sd	in
NSF_DS_PC2_1	HAZUS	Precast Concrete Frame	2	Low-Rise Precast Concrete Frame	Unknown	Pre-Code	Sd	in
NSF_DS_PC2_2	HAZUS	Precast Concrete Frame	5	Mid-Rise Precast Concrete Frame	Unknown	Pre-Code	Sd	in
NSF_DS_PC2_3	HAZUS	Precast Concrete Frame	12	High-Rise Precast Concrete Frame	Unknown	Pre-Code	Sd	in
NSF_DS_PC2_4	HAZUS	Precast Concrete Frame	2	Low-Rise Precast Concrete Frame	Unknown	Low-Code	Sd	in
NSF_DS_PC2_5	HAZUS	Precast Concrete Frame	5	Mid-Rise Precast Concrete Frame	Unknown	Low-Code	Sd	in
NSF_DS_PC2_6	HAZUS	Precast Concrete Frame	12	High-Rise Precast Concrete Frame	Unknown	Low-Code	Sd	in
NSF_DS_RM_1	HAZUS	Reinforced Masonry	2	Low-Rise Reinforced Masonry Bearing Walls with Wood or Metal Deck Diaphragms	Unknown	Pre-Code	Sd	in
NSF_DS_RM_2	HAZUS	Reinforced Masonry	5	Mid-Rise Reinforced Masonry Bearing Walls with Wood or Metal Deck Diaphragms	Unknown	Pre-Code	Sd	in



<b>Fragility ID Code</b>	<b>Author</b>	<b>Structure Type</b>	<b>Stories</b>	<b>Description</b>	<b>Ground Motions</b>	<b>Code</b>	<b>Demand Type</b>	<b>Demand Units</b>
NSF_DS_RM_3	HAZUS	Reinforced Masonry	2	Low-Rise Reinforced Masonry Bearing Walls with Precast Concrete Diaphragms	Unknown	Pre-Code	Sd	in
NSF_DS_RM_4	HAZUS	Reinforced Masonry	5	Mid-Rise Reinforced Masonry Bearing Walls with Precast Concrete Diaphragms	Unknown	Pre-Code	Sd	in
NSF_DS_RM_5	HAZUS	Reinforced Masonry	12	High-Rise Reinforced Masonry Bearing Walls with Precast Concrete Diaphragms	Unknown	Pre-Code	Sd	in
NSF_DS_RM_6	HAZUS	Reinforced Masonry	2	Low-Rise Reinforced Masonry Bearing Walls with Wood or Metal Deck Diaphragms	Unknown	Low-Code	Sd	in
NSF_DS_RM_7	HAZUS	Reinforced Masonry	5	Mid-Rise Reinforced Masonry Bearing Walls with Wood or Metal Deck Diaphragms	Unknown	Low-Code	Sd	in
NSF_DS_RM_8	HAZUS	Reinforced Masonry	2	Low-Rise Reinforced Masonry Bearing Walls with Precast Concrete Diaphragms	Unknown	Low-Code	Sd	in
NSF_DS_RM_9	HAZUS	Reinforced Masonry	5	Mid-Rise Reinforced Masonry Bearing Walls with Precast Concrete Diaphragms	Unknown	Low-Code	Sd	in
NSF_DS_RM_10	HAZUS	Reinforced Masonry	12	High-Rise Reinforced Masonry Bearing Walls with Precast Concrete Diaphragms	Unknown	Low-Code	Sd	in
NSF_DS_URM_1	HAZUS	Unreinforced Masonry	2	Low-Rise Unreinforced Masonry Bearing Walls	Unknown	Pre-Code	Sd	in
NSF_DS_URM_2	HAZUS	Unreinforced Masonry	5	Mid-Rise Unreinforced Masonry Bearing Walls	Unknown	Pre-Code	Sd	in
NSF_DS_URM_3	HAZUS	Unreinforced Masonry	2	Low-Rise Unreinforced Masonry Bearing Walls	Unknown	Low-Code	Sd	in
NSF_DS_URM_4	HAZUS	Unreinforced Masonry	5	Mid-Rise Unreinforced Masonry Bearing Walls	Unknown	Low-Code	Sd	in
NSF_DS_S1_1	HAZUS	Steel Moment Resisting Frame	2	Low-Rise Steel Moment Frame	Unknown	Pre-Code	Sd	in
NSF_DS_S1_4	HAZUS	Steel Moment Resisting Frame	2	Low-Rise Steel Moment Frame	Unknown	Low-Code	Sd	in



<b>Fragility ID Code</b>	<b>Author</b>	<b>Structure Type</b>	<b>Stories</b>	<b>Description</b>	<b>Ground Motions</b>	<b>Code</b>	<b>Demand Type</b>	<b>Demand Units</b>
NSF_DS_S2_2	HAZUS	Steel Braced Frame	5	Mid-Rise Steel Braced Frame	Unknown	Pre-Code	Sd	in
NSF_DS_S2_3	HAZUS	Steel Braced Frame	13	High-Rise Steel Braced Frame	Unknown	Pre-Code	Sd	in
NSF_DS_S2_5	HAZUS	Steel Braced Frame	5	Mid-Rise Steel Braced Frame	Unknown	Low-Code	Sd	in
NSF_DS_S2_6	HAZUS	Steel Braced Frame	13	High-Rise Steel Braced Frame	Unknown	Low-Code	Sd	in
NSF_DS_S3_1	HAZUS	Light Metal Frame	1	Steel Light Frame	Unknown	Pre-Code	Sd	in
NSF_DS_S3_2	HAZUS	Light Metal Frame	1	Steel Light Frame	Unknown	Low-Code	Sd	in
NSF_DS_W1_1	HAZUS	Wood Frame	1	Light Wood Frame	Unknown	Pre-Code	Sd	in
NSF_DS_W1_2	HAZUS	Wood Frame	1	Light Wood Frame	Unknown	Low-Code	Sd	in
NSF_DS_W2_1	HAZUS	Wood Frame	2	Commercial and Industrial Wood Frame	Unknown	Pre-Code	Sd	in
NSF_DS_W2_2	HAZUS	Wood Frame	2	Commercial and Industrial Wood Frame	Unknown	Low-Code	Sd	in
NSF_AS_C1_1	HAZUS	Concrete Moment Frame	2	Low-Rise Concrete Moment Frame	Unknown	Pre-Code	Sa	g
NSF_AS_C1_2	HAZUS	Concrete Moment Frame	5	Mid-Rise Concrete Moment Frame	Unknown	Pre-Code	Sa	g
NSF_AS_C1_3	HAZUS	Concrete Moment Frame	12	High-Rise Concrete Moment Frame	Unknown	Pre-Code	Sa	g
NSF_AS_C1_4	HAZUS	Concrete Moment Frame	2	Low-Rise Concrete Moment Frame	Unknown	Low-Code	Sa	g



<b>Fragility ID Code</b>	<b>Author</b>	<b>Structure Type</b>	<b>Stories</b>	<b>Description</b>	<b>Ground Motions</b>	<b>Code</b>	<b>Demand Type</b>	<b>Demand Units</b>
NSF_AS_C1_5	HAZUS	Concrete Moment Frame	5	Mid-Rise Concrete Moment Frame	Unknown	Low-Code	Sa	g
NSF_AS_C1_6	HAZUS	Concrete Moment Frame	12	High-Rise Concrete Moment Frame	Unknown	Low-Code	Sa	g
NSF_AS_C1_7	HAZUS	Concrete Moment Frame	2	Low-Rise Concrete Moment Frame	Unknown	Moderate-Code	Sa	g
NSF_AS_C2_1	HAZUS	Concrete Frame w/ Shear Walls	2	Low-Rise Concrete Frame w/ Shear Walls	Unknown	Pre-Code	Sa	g
NSF_AS_C2_2	HAZUS	Concrete Frame w/ Shear Walls	5	Mid-Rise Concrete Frame w/ Shear Walls	Unknown	Pre-Code	Sa	g
NSF_AS_C2_3	HAZUS	Concrete Frame w/ Shear Walls	12	High-Rise Concrete Frame w/ Shear Walls	Unknown	Pre-Code	Sa	g
NSF_AS_C2_4	HAZUS	Concrete Frame w/ Shear Walls	2	Low-Rise Concrete Frame w/ Shear Walls	Unknown	Low-Code	Sa	g
NSF_AS_C2_5	HAZUS	Concrete Frame w/ Shear Walls	5	Mid-Rise Concrete Frame w/ Shear Walls	Unknown	Low-Code	Sa	g
NSF_AS_C2_6	HAZUS	Concrete Frame w/ Shear Walls	12	High-Rise Concrete Frame w/ Shear Walls	Unknown	Low-Code	Sa	g
NSF_AS_PC1_1	HAZUS	Concrete Tilt-Up	1	Concrete Tilt-Up	Unknown	Pre-Code	Sa	g
NSF_AS_PC1_2	HAZUS	Concrete Tilt-Up	1	Concrete Tilt-Up	Unknown	Low-Code	Sa	g
NSF_AS_PC2_1	HAZUS	Precast Concrete Frame	2	Low-Rise Precast Concrete Frame	Unknown	Pre-Code	Sa	g
NSF_AS_PC2_2	HAZUS	Precast Concrete Frame	5	Mid-Rise Precast Concrete Frame	Unknown	Pre-Code	Sa	g
NSF_AS_PC2_3	HAZUS	Precast Concrete Frame	12	High-Rise Precast Concrete Frame	Unknown	Pre-Code	Sa	g



<b>Fragility ID Code</b>	<b>Author</b>	<b>Structure Type</b>	<b>Stories</b>	<b>Description</b>	<b>Ground Motions</b>	<b>Code</b>	<b>Demand Type</b>	<b>Demand Units</b>
NSF_AS_PC2_4	HAZUS	Precast Concrete Frame	2	Low-Rise Precast Concrete Frame	Unknown	Low-Code	Sa	g
NSF_AS_PC2_5	HAZUS	Precast Concrete Frame	5	Mid-Rise Precast Concrete Frame	Unknown	Low-Code	Sa	g
NSF_AS_PC2_6	HAZUS	Precast Concrete Frame	12	High-Rise Precast Concrete Frame	Unknown	Low-Code	Sa	g
NSF_AS_RM_1	HAZUS	Reinforced Masonry	2	Low-Rise Reinforced Masonry Bearing Walls with Wood or Metal Deck Diaphragms	Unknown	Pre-Code	Sa	g
NSF_AS_RM_2	HAZUS	Reinforced Masonry	5	Mid-Rise Reinforced Masonry Bearing Walls with Wood or Metal Deck Diaphragms	Unknown	Pre-Code	Sa	g
NSF_AS_RM_3	HAZUS	Reinforced Masonry	2	Low-Rise Reinforced Masonry Bearing Walls with Precast Concrete Diaphragms	Unknown	Pre-Code	Sa	g
NSF_AS_RM_4	HAZUS	Reinforced Masonry	5	Mid-Rise Reinforced Masonry Bearing Walls with Precast Concrete Diaphragms	Unknown	Pre-Code	Sa	g
NSF_AS_RM_5	HAZUS	Reinforced Masonry	12	High-Rise Reinforced Masonry Bearing Walls with Precast Concrete Diaphragms	Unknown	Pre-Code	Sa	g
NSF_AS_RM_6	HAZUS	Reinforced Masonry	2	Low-Rise Reinforced Masonry Bearing Walls with Wood or Metal Deck Diaphragms	Unknown	Low-Code	Sa	g
NSF_AS_RM_7	HAZUS	Reinforced Masonry	5	Mid-Rise Reinforced Masonry Bearing Walls with Wood or Metal Deck Diaphragms	Unknown	Low-Code	Sa	g
NSF_AS_RM_8	HAZUS	Reinforced Masonry	2	Low-Rise Reinforced Masonry Bearing Walls with Precast Concrete Diaphragms	Unknown	Low-Code	Sa	g
NSF_AS_RM_9	HAZUS	Reinforced Masonry	5	Mid-Rise Reinforced Masonry Bearing Walls with Precast Concrete Diaphragms	Unknown	Low-Code	Sa	g
NSF_AS_RM_10	HAZUS	Reinforced Masonry	12	High-Rise Reinforced Masonry Bearing Walls with Precast Concrete Diaphragms	Unknown	Low-Code	Sa	g
NSF_AS_URM_1	HAZUS	Unreinforced Masonry	2	Low-Rise Unreinforced Masonry Bearing Walls	Unknown	Pre-Code	Sa	g



<b>Fragility ID Code</b>	<b>Author</b>	<b>Structure Type</b>	<b>Stories</b>	<b>Description</b>	<b>Ground Motions</b>	<b>Code</b>	<b>Demand Type</b>	<b>Demand Units</b>
NSF_AS_URM_2	HAZUS	Unreinforced Masonry	5	Mid-Rise Unreinforced Masonry Bearing Walls	Unknown	Pre-Code	Sa	g
NSF_AS_URM_3	HAZUS	Unreinforced Masonry	2	Low-Rise Unreinforced Masonry Bearing Walls	Unknown	Low-Code	Sa	g
NSF_AS_URM_4	HAZUS	Unreinforced Masonry	5	Mid-Rise Unreinforced Masonry Bearing Walls	Unknown	Low-Code	Sa	g
NSF_AS_S1_1	HAZUS	Steel Moment Resisting Frame	2	Low-Rise Steel Moment Frame	Unknown	Pre-Code	Sa	g
NSF_AS_S1_4	HAZUS	Steel Moment Resisting Frame	2	Low-Rise Steel Moment Frame	Unknown	Low-Code	Sa	g
NSF_AS_S2_2	HAZUS	Steel Braced Frame	5	Mid-Rise Steel Braced Frame	Unknown	Pre-Code	Sa	g
NSF_AS_S2_3	HAZUS	Steel Braced Frame	13	High-Rise Steel Braced Frame	Unknown	Pre-Code	Sa	g
NSF_AS_S2_5	HAZUS	Steel Braced Frame	5	Mid-Rise Steel Braced Frame	Unknown	Low-Code	Sa	g
NSF_AS_S2_6	HAZUS	Steel Braced Frame	13	High-Rise Steel Braced Frame	Unknown	Low-Code	Sa	g
NSF_AS_S3_1	HAZUS	Light Metal Frame	1	Steel Light Frame	Unknown	Pre-Code	Sa	g
NSF_AS_S3_2	HAZUS	Light Metal Frame	1	Steel Light Frame	Unknown	Low-Code	Sa	g
NSF_AS_W1_1	HAZUS	Wood Frame	1	Light Wood Frame	Unknown	Pre-Code	Sa	g
NSF_AS_W1_2	HAZUS	Wood Frame	1	Light Wood Frame	Unknown	Low-Code	Sa	g
NSF_AS_W2_1	HAZUS	Wood Frame	2	Commercial and Industrial Wood Frame	Unknown	Pre-Code	Sa	g



<b>Fragility ID Code</b>	<b>Author</b>	<b>Structure Type</b>	<b>Stories</b>	<b>Description</b>	<b>Ground Motions</b>	<b>Code</b>	<b>Demand Type</b>	<b>Demand Units</b>
NSF_AS_ W2_2	HAZUS	Wood Frame	2	Commercial and Industrial Wood Frame	Unknown	Low- Code	Sa	g



## **Fragility Database Documentation**

The fragility database contains the following fields:

### **ID –**

Numeric identifier.

### **Fragility ID Code –**

Unique ID code for each fragility. Each ID code corresponds to data for a set of three fragility curves. The general form for structural fragility curves is SF\_AA\_BB, where AA corresponds to the structure type (e.g., AA = C1 for concrete moment frame, C2 for concrete frame with shear walls), and BB is a numeric counter to uniquely identify each fragility set. The general form for nonstructural fragility curves is NSF\_CC\_AA\_BB, where AA and BB are the same as for structural fragilities, and CC is either “DS” for drift-sensitive or “AS” for acceleration-sensitive.

### **Author –**

Identifies the person(s) or entity(ies) who provided each fragility set.

### **Structure Type –**

Describes the structure type of the fragility set. The structure type is always one of the following:

- Concrete Moment Frame
- Concrete Frame w/ Shear Walls
- Concrete Frame w/ Unreinforced Masonry Infill Walls
- Concrete Tilt-Up
- Precast Concrete Frame
- Reinforced Masonry
- Unreinforced Masonry
- Steel Moment Resisting Frame
- Steel Braced Frame
- Light Metal Frame



- Steel Frame w/ CIP Concrete Shear Walls
- Steel Frame w/ Unreinforced Masonry Infill Walls
- Wood Frame
- Other

**Stories –**

Identifies the number of stories used for the model building when constructing fragilities. A value of “0” indicates multiple story levels were considered (for fragility surfaces).

**Description –**

A textual description of the model building used when constructing fragilities.

**Ground Motions –**

Ground motion records used for time-history analyses when constructing fragilities.

**Code –**

The level of seismic demand required by the building code when a model building is designed.

**Damage Type –**

Either Structural or Nonstructural.

**Demand Type –**

The type of seismic demand associated with a particular fragility set. Demand is typically spectral acceleration ( $S_a$ ) computed at the model building’s natural period or PGA for fragilities provided by the MAE Center. When fragilities are adapted from HAZUS, the hazard parameter is spectral displacement ( $S_d$ ), where spectral displacement and spectral acceleration can be approximately related by

$$S_d = S_a (9.78 \cdot T^2)$$



Where  $S_d$  is in units of inches,  $S_a$  is in units of g, and the natural period,  $T$ , is in units of seconds. Parametric fragilities are calibrated to use PGA, 0.2 second  $S_a$ , or 1.0 second  $S_a$ , regardless of the natural period of the model building, as indicated.

### **Demand Unit –**

The units associated with each demand type. Units are g's for all fragility sets except those adapted directly from HAZUS, which use inches.

### **Limit States –**

The limit states which define the transitions between damage states for each fragility set.

#### *Period Calculations*

T Eqn Type, T Eqn Param0, T Eqn Param1, and T Eqn Param2 provide data required to estimate the natural period of a building to which a fragility set has been assigned.

#### When T Eqn Type = 1

$$T_1 = a$$

Where

$$a = \text{T Eqn Param0}$$

#### when T Eqn Type = 2

$$T_1 = a * \text{NO\_STORIES}$$

Where

$$a = \text{T Eqn Param0}$$

#### when T Eqn Type = 3



$$T_1 = b * (a * NO\_STORIES)^c$$

Where

$$a = \text{T Eqn Param0}$$

$$b = \text{T Eqn Param1}$$

$$c = \text{T Eqn Param2}$$

### **Frag Eqn Type–**

Fragility equation type. The fragility equation type is either 1 or 2, where 1 corresponds to

$$P(LS / Y) = \Phi \left( \frac{\ln(Y) - \lambda}{\beta} \right)$$

In which Y is a hazard parameter (PGA, Sa, or Sd), and  $\Phi$  indicates the cumulative normal distribution function. Fragility equation type 2 corresponds to

$$P(LS / S_a) = \Phi \left( \frac{\ln(S_a) - (\alpha_{11} + \alpha_{12}T)}{(\alpha_{13} + \alpha_{14}T)} \right)$$

when  $0.87 \leq T(\text{sec})$

and

$$P(LS / S_a) = \Phi \left( \frac{\ln(S_a) - (\alpha_{11} + \alpha_{12}0.87)}{(\alpha_{13} + \alpha_{14}0.87)} + (0.87 - T) \frac{\ln(S_a) - \alpha_{21}}{\alpha_{22}} \right)$$

when  $0 < T < 0.87(\text{sec})$

in which Sa is spectral acceleration at the natural period of a given structure, and  $\Phi$  indicates the cumulative normal distribution function as it did for equation type 1.

### **Parameters –**

The number of parameters needed to define the given fragility set. The number is typically 6, which is 3 pairs of  $\lambda$ ,  $\beta$  parameters. In the case of fragility surfaces (fragility equation type 2, above), the number is 18, which is 3 sets of 6  $\alpha$  terms.

### **Median and Beta Parameters**



For fragility equation type 1, there are three pairs of parameters which are used to define the three transitions between damage states. The median parameters are substituted for  $\lambda$  in the equation for fragility equation type 1, and the beta parameters are likewise substituted for  $\beta$ . The number following each parameter description indicates which transition the parameter describes, where “0” is a transition between Insignificant and Moderate damage, “1” is a transition between Moderate and Heavy, and “2” is a transition between Heavy and Complete damage.

*FS Param (Fragility Surface Parameters)*

The fragility surface parameters function similarly to median and beta parameters, except that there are 6 parameters per fragility curve rather than 2. Considering PL1, PL2, and PL3 to be the transition limits between Insignificant and Moderate, Moderate and Heavy, and Heavy and Complete damage, the parameters should be substituted into the equations given above for fragility equation type 2 as follows:

**Table C4.2.1-3 Correlations of database entries,  $\alpha$  terms, and limit states for fragility surfaces**

	PL1	PL2	PL3
$\alpha_{11}$	FS Param0	FS Param6	FS Param12
$\alpha_{12}$	FS Param1	FS Param7	FS Param13
$\alpha_{13}$	FS Param2	FS Param8	FS Param14
$\alpha_{14}$	FS Param3	FS Param9	FS Param15
$\alpha_{21}$	FS Param4	FS Param10	FS Param16
$\alpha_{22}$	FS Param5	FS Param11	FS Param17



**APPENDIX D – DIRECT ECONOMIC LOSS EXAMPLE FOR BUILDINGS**

**SYSTEMATIC TREATMENT OF UNCERTAINTY IN  
CONSEQUENCE-BASED RISK MANAGEMENT OF  
SEISMIC REGIONAL LOSSES**

Liang Chang, Junho Song, Joshua Steelman and Jerome F. Hajjar

*Mid-America Earthquake Center  
1241 Newmark Civil Engineering Laboratory  
205 North Mathews Avenue  
University of Illinois at Urbana-Champaign  
Urbana, Illinois 61801*



The Mid-America Earthquake (MAE) center aims to treat various uncertainties inherent in its Consequence-based Risk Management (CRM) in a systematic manner. In order to achieve this goal, a Task Group on Interdisciplinary Coordination (TGIC) of the MAE center develops a probabilistic framework to estimate the uncertainty in social and economic losses in a region caused by seismic hazard. This document presents the probabilistic framework under development with a numerical example. The total direct loss of an inventory of three buildings is estimated with its uncertainty quantified. We incorporate the uncertainties in the intensity of a scenario earthquake, inventory identification, performance of structural/non-structural components, content loss, liquefaction hazard, and damage states. Examples on the use of a probabilistic hazard map in regional loss estimation and on the direct loss of a bridge inventory are currently under development.

## I. Inventory data and scenario seismic hazard

For simplicity, this example considers the total loss of three building inventory items in the Memphis test bed region. Table 1 lists the structural and occupancy types of the inventory items, the fundamental periods ( $T$ ) of the structures, the mean ( $\lambda_{S_a}$ ) and standard deviation ( $\beta_{S_a}$ ) of the natural logarithm of the spectral acceleration ( $S_a$ ) at each inventory location, and their assessed structural values ( $M$ ). URM denotes unreinforced masonry building.

Table 1. Example data and scenario hazard

No.	Structural type	Occupancy type	$T$ (sec)	$\ln S_a$		$M$ (US \$)
				$\lambda_{S_a}$	$\beta_{S_a}$	
1	Concrete	Industrial	0.95	-1.710	0.887	136,400
2	URM	Commercial	0.60	-1.463	0.827	415,393
3	URM	Industrial	0.60	-1.514	0.840	811,346

## II. Structural damage

### II-1. Structural damage fragility and limit-state exceedance probability

The fragility  $P(LS_i | S_a)$  is defined as the conditional probability that a certain type of structure will exceed the prescribed limit state  $LS_i$  for a given spectral acceleration  $S_a$ . The fragilities developed by the MAE center can be described as

$$P(LS_i | S_a) = \Phi\left(\frac{\ln S_a - \lambda_i}{\beta_i}\right) \quad (1)$$



where  $\Phi(\cdot)$  is the cumulative density function (CDF) of the standard normal distribution, and  $\lambda_i$  and  $\beta_i$  are the fragility parameters for the  $i$ -th limit state of a given structural type. This form of fragility is being internally referred as “Type I.”

There also exist MAE center fragilities described in terms of drift (Wen et al. 2004).

$$P(LS_i | S_a) = \Phi \left( - \frac{\lambda_C^i - \lambda_{D|S_a}}{\sqrt{\beta_C^2 + \beta_{D|S_a}^2 + \beta_M^2}} \right) \quad (2)$$

where  $\lambda_C^i$  denotes the natural logarithm of the median drift capacity for the  $i$ -th limit state,  $\lambda_{D|S_a}$  is the natural logarithm of the median drift demand determined from a fitted power law equation (Cornell et al. 2002) for a given spectral acceleration, and  $\beta_C$ ,  $\beta_{D|S_a}$  and  $\beta_M$  are the standard deviation of the natural logarithm of the capacity, demand and model error, respectively. When the power law is defined as  $D = a_1(S_a)^{a_2}$ , the parameters of the Type I fragilities are

$$\lambda_i = \frac{(\lambda_C^i - \ln a_1)}{a_2} \quad (3a)$$

$$\beta_i = \frac{\sqrt{\beta_C^2 + \beta_{D|S_a}^2 + \beta_M^2}}{a_2} \quad (3b)$$

The exceedance probability for an unknown spectral acceleration is derived as

$$P(LS_i) = \Phi \left( \frac{\lambda_{S_a} - \lambda_i}{\sqrt{\beta_i^2 + \beta_{S_a}^2}} \right) \quad (4a)$$

$$P(LS_i) = \Phi \left( - \frac{\lambda_C^i - \lambda_{D|S_a = m_{S_a}}}{\sqrt{\beta_C^2 + \beta_{D|S_a}^2 + a_2^2 \beta_{S_a}^2 + \beta_M^2}} \right) \quad (4b)$$

where  $m_{S_a} = e^{\lambda_{S_a}}$  is the median of the spectral acceleration.

MAE Center building damage estimation is based on the use of four damage states, with three thresholds, or behavioral limit states, to define the boundaries of the individual damage states. The three limit states may generally be referred to as PL1, PL2, and PL3, where the higher numbers indicate limit states at the boundaries of more severe damage states. Table 2 lists the fragility parameters for the three limit states considered; Immediate Occupancy (IO) for PL1, Life Safety (LS) for PL2, and Collapse Prevention (CP) for PL3. The exceedance probabilities  $P(LS_i)$  computed by Eq. (4a) are also listed. Other behavioral limit states may be used for various levels of PL, such as First Yield, or Plastic Mechanism Initiation, instead of IO, LS, or CP, when some other behavior more closely represents a threshold of expected damage level.



Table 2. Fragility parameters and limit state exceedance probabilities (structural damage)

Inventory items		Limit states, $LS_i$		
		PL1(IO)	PL2(LS)	PL3(CP)
1	$\lambda_i$	-1.991	-1.523	-1.175
Concrete	$\beta_i$	0.509	0.392	0.425
Bracci (3-story)	$P(LS_i)$	0.608	0.423	0.293
2	$\lambda_i$	-1.890	-1.200	-0.693
URM	$\beta_i$	0.300	0.300	0.330
Wen (2-story)	$P(LS_i)$	0.686	0.383	0.194
3	$\lambda_i$	-1.890	-1.200	-0.693
URM	$\beta_i$	0.300	0.300	0.330
Wen (2-story)	$P(LS_i)$	0.663	0.362	0.182

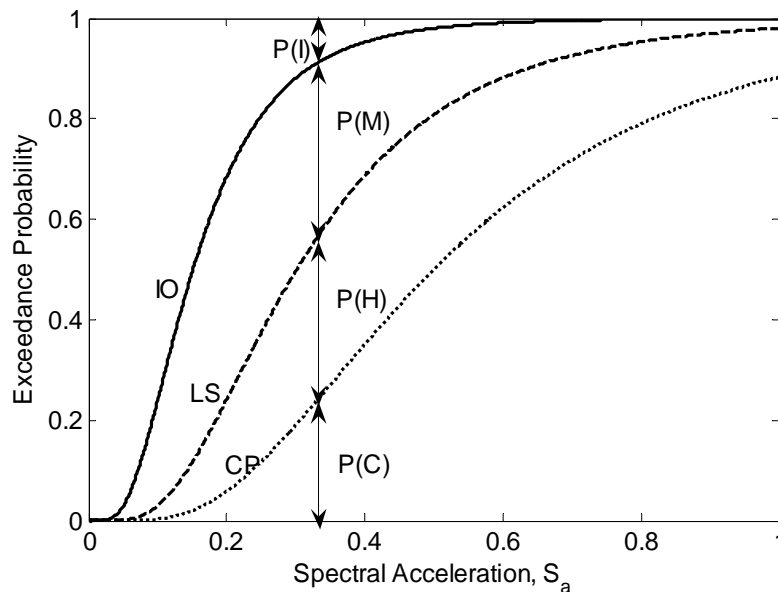


Figure 1. Computing probabilities of damage states

## II-2. Probability of structural damage states by ground shaking

Bai et al. (2006) proposed four distinct states for structural damages by ground shaking: Insignificant (I), Moderate (M), Heavy (H), and Complete (C). As illustrated in Figure 1, we can compute the probabilities of the four damage states from the limit-state exceedance probabilities as follows.



$$P(I) = 1 - P(PL1) \quad (5a)$$

$$P(M) = P(PL1) - P(PL2) \quad (5b)$$

$$P(H) = P(PL2) - P(PL3) \quad (5c)$$

$$P(C) = P(PL3) \quad (5d)$$

We compute the damage state probabilities from the limit-state exceedance probabilities reported in Table 2 by using Eq. (5) and report in Table 3.

Table 3. Probabilities of structural damage states

Inventory items	Probability of damage states			
	I	M	H	C
1 (Concrete)	0.392	0.185	0.130	0.293
2 (URM1)	0.314	0.304	0.189	0.194
3 (URM2)	0.337	0.301	0.181	0.182

### II-3. Consideration of structural damages caused by ground failure

A structure can be damaged not only by ground shaking, but also by ground failure such as soil liquefaction. If we use four states (I, M, H and C) for the damages by ground failure as well, and assume structural damage by ground shaking and that by ground failures are statistically independent of each other, the probability that a structure will exceed a certain damage state either by ground shaking or ground failure is obtained as

$$P_{COMB}[DS \geq I] = 1 \quad (6a)$$

$$P_{COMB}[DS \geq M] = P_{GS}[PL1] + P_{GF}[PL1] - P_{GS}[PL1] \cdot P_{GF}[PL1] \quad (6b)$$

$$P_{COMB}[DS \geq H] = P_{GS}[PL2] + P_{GF}[PL2] - P_{GS}[PL2] \cdot P_{GF}[PL2] \quad (6c)$$

$$P_{COMB}[DS \geq C] = P_{GS}[PL3] + P_{GF}[PL3] - P_{GS}[PL3] \cdot P_{GF}[PL3] \quad (6d)$$

where  $P_{COMB}[DS \geq X]$  denotes the probability that a structure will exceed a damage state  $X$  either by ground failure or ground shaking, and  $P_{GS}$  and  $P_{GF}$  denote the probabilities of exceedance by ground shaking and ground failure, respectively. Then, the combined probabilities of damage states are computed as

$$P_{COMB}[DS = I] = 1 - P_{COMB}[DS \geq M] \quad (7a)$$

$$P_{COMB}[DS = M] = P_{COMB}[DS \geq M] - P_{COMB}[DS \geq H] \quad (7b)$$

$$P_{COMB}[DS = H] = P_{COMB}[DS \geq H] - P_{COMB}[DS \geq C] \quad (7c)$$

$$P_{COMB}[DS = C] = P_{COMB}[DS \geq C] \quad (7d)$$



In this example, the probability of “Complete” ground failure,  $P_{GF}[DS \geq C] = P_{GF}[DS = C]$  is defined as the probability that the liquefaction potential index (LPI) is greater than 15. An algorithm has been developed and documented within the MAE Center to evaluate this probability,  $P(LPI > 15)$ . The proposed algorithm evaluates the complete ground failure probabilities of the three buildings in the example as 1.51% (Concrete), 1.96% (URM1) and 1.93% (URM2), respectively. In this example, we also assume that a ground failure either causes Complete (C) or Insignificant (I) damages only. Therefore,  $P_{GF}[DS \geq M]$  and  $P_{GF}[DS \geq H]$  are also the same as  $P(LPI > 15)$ . Combining these ground failure probabilities with the probabilities of structural damages caused by ground shaking (Table 3) by Eqs. (6) and (7), the combined probabilities of structural damages are obtained and reported in Table 4.

Table 4. Probabilities of structural damage after liquefaction hazard is considered

Inventory items	Combined probability of damage states			
	I	M	H	C
1 (Concrete)	0.386	0.182	0.128	0.304
2 (URM1)	0.308	0.298	0.185	0.209
3 (URM2)	0.330	0.295	0.177	0.197

#### II-4. Mean and standard deviation of damage ratio

The damage ratios of inventory items are critical inputs to social and economic loss models. Bai et al. (2006) proposed a probabilistic model for the structural damage ratios to account for the uncertainty in structural damages. They assume that a structure is subjected to one of the four damage states (I, M, H and C) with the probabilities computed by Eq. (7). For a given damage state, the damage ratio follows the beta distribution with a prescribed range. The mean of the Beta distribution is assumed to be at the midpoint of the range while the standard deviation is given as one-third of the length of the range. Table 5 shows the proposed range, mean and standard deviation of Beta distribution for each damage state.

Table 5. Probabilistic model for structural damage ratio (Bai et al. 2006)

Damage states, $DS_i$	Range of Beta distribution (%)	Mean of damage ratio, $\mu_{D/DS_i}$ (%)	Standard deviation of damage ratio, $\sigma_{D/DS_i}$ (%)
1: Insignificant	[0, 1]	0.5	0.333
2: Moderate	[1, 30]	15.5	9.67
3: Heavy	[30, 80]	55	16.7
4: Complete	[80, 100]	90	6.67



The mean and variance of the damage ratio ( $D$ ) of an inventory item are computed by

$$\mu_D = \sum_{i=1}^4 [P(DS_i) \cdot \mu_{D|DS_i}] \quad (8a)$$

$$\begin{aligned} \sigma_D^2 &= E[D^2] - \mu_D^2 \\ &= \sum_{i=1}^4 \{P(DS_i) \cdot E[D^2 | DS_i]\} - \mu_D^2 \\ &= \sum_{i=1}^4 [P(DS_i) \cdot (\sigma_{D|DS_i}^2 + \mu_{D|DS_i}^2)] - \mu_D^2 \end{aligned} \quad (8b)$$

where  $P(DS_i)$ ,  $i = 1, \dots, 4$  denotes the combined probabilities of the  $i$ -th damage state such as those shown in Table 4, and  $\mu_{D|DS_i}$  and  $\sigma_{D|DS_i}$  are the conditional mean and standard deviation of Beta distribution given  $DS_i$  damage state, shown in Table 5. The means and variances of the damage ratios of the three inventory items in this example are computed by Eq. (8) and listed in Table 6.

Table 6. Mean and variance of structural damage ratios

Inventory	Mean, $\mu_D$	Variance, $\sigma_D^2$
1: Concrete	0.374	0.156
2: URM1	0.338	0.127
3: URM2	0.323	0.125

### III. Non-structural damage

#### III-1. Probabilistic models for non-structural damage states

In order to estimate the probabilities of non-structural damage states, we adopt the HAZUS non-structural fragility curves developed for four limit-states: Slight, Moderate, Extensive and Complete. As illustrated in Figure 2, five damage states, None (N), Slight (S), Moderate (M), Extensive (E) and Complete (C) are derived from the four limit-states. To be consistent with the probabilistic model on the structural damage, we combine the damage states N and S and name it Insignificant (I). The other HAZUS damage states M, E and C are renamed to Moderate (M), Heavy (H) and Complete (C), respectively.

For each damage state, HAZUS assigns a deterministic damage ratio. Consider the damage ratios given in Figure 3a. If a non-structural component is in Moderate state, for example, the damage ratio is assumed to be ‘b’ exactly. To be consistent with the beta-



distribution-based probabilistic model proposed for structural damage, we introduce four ranges of non-structural damage states whose boundaries are midpoints between the HAZUS damage ratio values (See Figure 3b). Then, we assume that the mean of the damage ratio in each interval is at its midpoint and the standard deviation is one third of the interval length. There exist two types of non-structural damages: acceleration-sensitive and drift-sensitive. Tables 7 and 8 show the probabilistic models obtained by the aforementioned procedure.

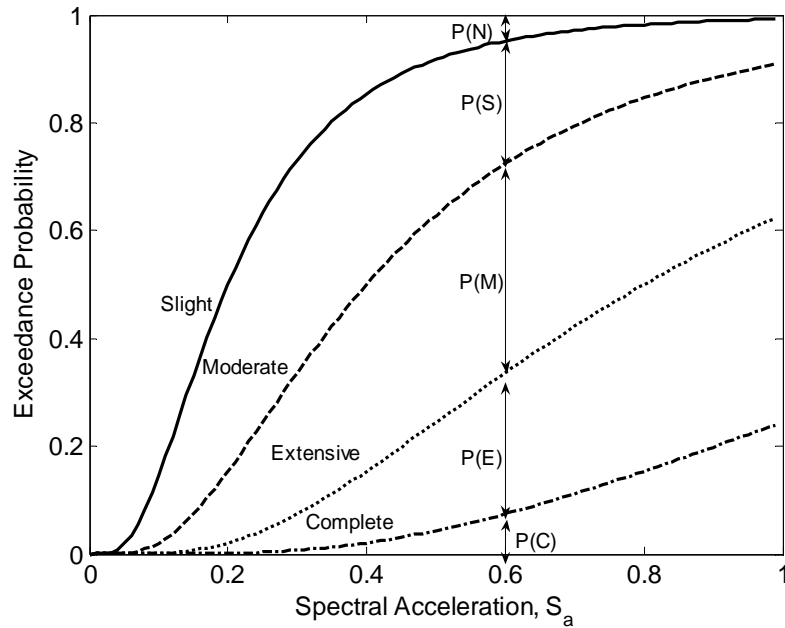


Figure 2. Acceleration-sensitive non-structural fragility curves (HAZUS)

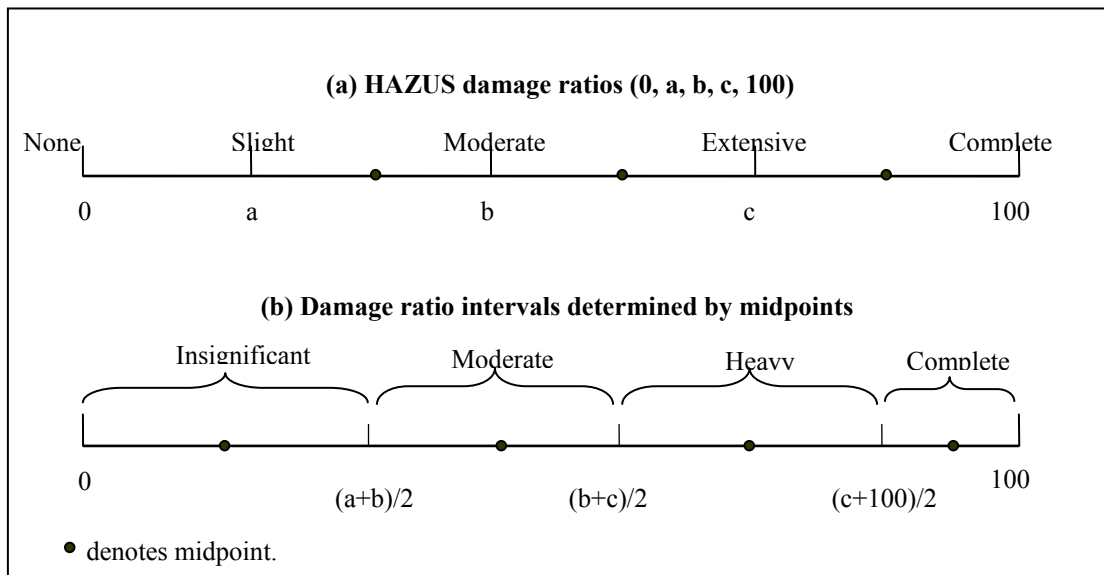


Figure 3. Probabilistic model for non-structural damage ratios

Table 7. Probabilistic model for acceleration-sensitive non-structural damage ratio

Damage states, $DS_i$	Range of Beta distribution (%)	Mean of damage ratio, $\mu_{D DS_i}$ (%)	Standard deviation of damage ratio, $\sigma_{D DS_i}$ (%)
1: Insignificant	[0, 6]	3.0	2.0
2: Moderate	[6, 20]	13.0	4.67
3: Heavy	[20, 65]	42.5	15.0
4: Complete	[65, 100]	82.5	11.7

Table 8. Probabilistic model for drift-sensitive non-structural damage ratio

Damage states, $DS_i$	Range of Beta distribution (%)	Mean of damage ratio, $\mu_{D DS_i}$ (%)	Standard deviation of damage ratio, $\sigma_{D DS_i}$ (%)
1: Insignificant	[0, 6]	3.0	2.0
2: Moderate	[6, 30]	18.0	8.0
3: Heavy	[30, 75]	52.5	15.0
4: Complete	[75, 100]	87.5	8.3

### III-2. Acceleration-sensitive non-structural damage

HAZUS acceleration-sensitive non-structural fragilities are given in terms of spectral accelerations. By combining the uncertainties of spectral acceleration by Eq. (4a), we can compute the exceedance probabilities  $P(LS_i)$  for acceleration-sensitive non-structural damage. Table 9 shows the HAZUS fragility parameters and the computed exceedance probabilities.

Table 9. Fragility parameters and limit state exceedance probabilities (acceleration-sensitive non-structural damage)

Inventory items		Limit states, $LS_i$		
		Moderate (M)	Extensive (E)	Complete (C)
1 Concrete	$\lambda_i$	-0.9162	-0.2231	0.47
	$\beta_i$	0.68	0.68	0.68
	$P(LS_i)$	0.239	0.0917	0.0256
2 URM	$\lambda_i$	-0.9162	-0.2231	0.47
	$\beta_i$	0.65	0.65	0.65
	$P(LS_i)$	0.302	0.119	0.033
3 URM	$\lambda_i$	-0.9162	-0.2231	0.47
	$\beta_i$	0.65	0.65	0.65
	$P(LS_i)$	0.287	0.112	0.0309



The probabilities of the four damage states are then computed by

$$P(I) = 1 - P(\text{Moderate}) \quad (9a)$$

$$P(M) = P(\text{Moderate}) - P(\text{Extensive}) \quad (9b)$$

$$P(H) = P(\text{Extensive}) - P(\text{Complete}) \quad (9c)$$

$$P(C) = P(\text{Complete}) \quad (9d)$$

Table 10 shows the computed probabilities of the damage states.

Table 10. Probabilities of acceleration-sensitive non-structural damage states

Inventory items	Probability of damage states			
	I	M	H	C
1 (Concrete)	0.761	0.147	0.066	0.026
2 (URM1)	0.698	0.182	0.086	0.033
3 (URM2)	0.713	0.175	0.081	0.031

Non-structural damages caused by ground failure are taken into account by the procedure in Eqs. (6) and (7). Table 11 shows the probabilities after liquefaction hazard is considered.

Table 11. Probabilities of acceleration-sensitive non-structural damage after combining liquefaction hazard

Inventory items	Combined probability of damage states			
	I	M	H	C
1 (Concrete)	0.750	0.145	0.065	0.040
2 (URM1)	0.685	0.179	0.085	0.052
3 (URM2)	0.700	0.171	0.080	0.050

The means and variances of the damage ratios are computed by Eq. (8) and listed in Table 12.



Table 12. Mean and variance of acceleration-sensitive non-structural damage ratios

Inventory	Mean, $\mu_D$	Variance, $\sigma_D^2$
1: Concrete	0.102	0.035
2: URM1	0.123	0.043
3: URM2	0.118	0.041

### III-3. Drift-sensitive non-structural damage

The HAZUS fragility curves for drift-sensitive non-structural damage are given in terms of spectral displacement instead of spectral acceleration. As shown in Table 1, the uncertainties in the seismic intensity are quantified in terms of spectral acceleration. Hence, we derive the mean and variance of the logarithm of the spectral displacement from those of spectral acceleration. When the units of spectral acceleration and displacement are the gravity acceleration (g) and inches, respectively, the spectral displacement ( $S_d$ ) is described in terms of the spectral acceleration by

$$S_d = 9.8 S_a T_e^2 \quad (10)$$

where  $T_e$  is the fundamental period of the structure shown in Table 1. Then, the mean and variance of the natural logarithms of the spectral displacement are computed as

$$\lambda_{S_d} = \lambda_{S_a} + \ln(9.8 T_e^2) \quad (11a)$$

$$\beta_{S_d}^2 = \beta_{S_a}^2 \quad (11b)$$

Table 13 shows the results of the conversion.

Table 13. Conversion from spectral acceleration to spectral displacement

Inventory items	$\lambda_{S_a}$	$\lambda_{S_d} = \lambda_{S_a} + \ln(9.8 T_e^2)$	$\beta_{S_d}^2 = \beta_{S_a}^2$
1: Concrete	-1.710	0.470	0.887
2: URM1	-1.463	-0.202	0.827
3: URM2	-1.514	-0.253	0.840

This conversion allows us to follow all the procedures developed for the acceleration-sensitive non-structural damages. Tables 14-17 show the results of the computations.



Table 14. Fragility parameters and limit state exceedance probabilities (drift-sensitive non-structural damage)

Inventory items		Limit states, $LS_i$		
		Moderate (M)	Extensive (E)	Complete (C)
1 Concrete	$\lambda_i$	0.3646	1.5041	2.1972
	$\beta_i$	0.98	0.93	1.03
	$P(LS_i)$	0.532	0.211	0.102
2 URM	$\lambda_i$	0.0770	1.2179	1.9095
	$\beta_i$	1.23	1.23	1.03
	$P(LS_i)$	0.425	0.169	0.055
3 URM	$\lambda_i$	0.0770	1.2179	1.9095
	$\beta_i$	1.23	1.23	1.03
	$P(LS_i)$	0.412	0.162	0.052

Table 15. Probabilities of drift-sensitive non-structural damage states

Inventory items	Probability of damage states			
	I	M	H	C
1 (Concrete)	0.468	0.321	0.109	0.102
2 (URM1)	0.575	0.256	0.114	0.055
3 (URM2)	0.588	0.251	0.110	0.052

Table 16. Probabilities of drift-sensitive non-structural damage considering liquefaction

Inventory items	Combined probability of damage states			
	I	M	H	C
1 (Concrete)	0.461	0.316	0.107	0.116
2 (URM1)	0.564	0.251	0.112	0.074
3 (URM2)	0.576	0.246	0.108	0.070

Table 17. Mean and variance of drift-sensitive non-structural damage ratios

Inventory	Mean, $\mu_D$	Variance, $\sigma_D^2$
1: Concrete	0.228	0.082
2: URM1	0.185	0.066
3: URM2	0.180	0.065



#### IV. Contents Loss

HAZUS uses the acceleration-sensitive non-structural fragilities to determine the states of contents loss. For each content loss state, a deterministic loss ratio is assigned. Table 18 shows a probabilistic model proposed for the content loss ratios to be consistent with the models for structural/non-structural damage ratios. Table 19 shows the means and variances of the content loss ratios of the buildings in this example.

Table 18. Probabilistic model for content loss ratio

Damage states, $DS_i$	Range of Beta distribution (%)	Mean of damage ratio, $\mu_{D DS_i}$ (%)	Standard deviation of damage ratio, $\sigma_{D DS_i}$ (%)
1: Insignificant	[0, 3]	1.5	1.0
2: Moderate	[3, 15]	9.0	4.0
3: Heavy	[15, 37.5]	26.25	7.5
4: Complete	[37.5, 50]	43.75	4.17

Table 19. Mean and variance of the contents loss ratios

Inventory	Mean, $\mu_D$	Variance, $\sigma_D^2$
1: Concrete	0.059	0.011
2: URM	0.071	0.013
3: URM	0.069	0.013

#### V. Consideration of inventory uncertainty

There exist uncertain errors in identifying the structural types of inventory items by remote sensing. For example, a concrete building could be mistakenly classified into the URM building category. We may assume a probability of accurate identification, denoted by  $p_{id}$ , to account for this uncertainty. This means there is  $(1 - p_{id})$  probability that the structure belongs to any of the *other* structural types in the inventory. Then, the mean of the damage ratio is adjusted as

$$\mu_{\bar{D}} = p_{id}\mu_D + (1 - p_{id})\mu_{D_r} \quad (12)$$

where  $\mu_{\bar{D}}$  is the mean damage ratio with the inventory uncertainty considered,  $\mu_D$  is the mean damage ratio based on the identified structure type such as those reported in Tables 6, 12, 17 and 19, and  $\mu_{D_r}$  is the mean damage ratio for unknown structural type. The latter, denoted as “representative” mean damage ratio, is estimated as the weighted average of the mean damage ratios based on the other identified structural types except for the originally predicted structure type, that is,



$$\mu_{D_r} = \frac{1}{N} \sum_{j=1}^{N_{id}} n_j \cdot \mu_D^j \quad (13)$$

where  $N_{id}$  is the number of representative structure types identified, i.e., the total number of structure types minus 1;  $n_j$  is the number of the inventory items identified as the  $j$ -th representative structural type,  $j=1, \dots, N_{id}$ ;  $N = \sum_{j=1}^{N_{id}} n_j$  is the total number of representative inventory items (excluding the originally predicted structures); and  $\mu_D^j$  is the mean damage ratio estimated based on the  $j$ -th representative structural type at the given site. Note that for this example, the hazard will be assumed constant with respect to structure type. In fact, each structure type can have its own period, and a calculation should be performed for each period to estimate an appropriate spectral acceleration. When the hazard is *transformed* from spectral acceleration to spectral displacement for drift-sensitive damage estimation, the period *is* used.

In this example, the representative damage ratio is computed as

$$\mu_{D_r} = \mu_D^{URM} \quad (14a)$$

for inventory item I1, and

$$\mu_{D_r} = \mu_D^{con} \quad (14b)$$

for inventory item I2 and I3.

where  $\mu_D^{con}$  and  $\mu_D^{URM}$  respectively denote the mean damage ratio estimated based on the identifications as concrete and URM buildings. Assuming  $p_{id} = 0.85$ , the mean damage ratio is updated as

$$\mu_{\tilde{D}} = 0.85\mu_D + 0.15\mu_{D_r} \quad (15)$$

For the first inventory item identified as a concrete building, the adjusted mean damage ratio is

$$\mu_{\tilde{D}} = 0.85\mu_D^{con} + 0.15\mu_D^{URM} \quad (16)$$

The adjusted variance of the damage ratio is

$$\begin{aligned} \sigma_{\tilde{D}}^2 &= E[\tilde{D}^2] - \mu_{\tilde{D}}^2 \\ &= 0.85[(\mu_D^{con})^2 + (\sigma_D^{con})^2] + 0.15[(\mu_D^{URM})^2 + (\sigma_D^{URM})^2] - \mu_{\tilde{D}}^2 \end{aligned} \quad (17)$$

For the second and third inventory items identified as URM buildings, the adjusted means and variances of the damage ratios are

$$\mu_{\tilde{D}} = 0.15\mu_D^{con} + 0.85\mu_D^{URM} \quad (18a)$$

$$\begin{aligned} \sigma_{\tilde{D}}^2 &= E[\tilde{D}^2] - \mu_{\tilde{D}}^2 \\ &= 0.15[(\mu_D^{con})^2 + (\sigma_D^{con})^2] + 0.85[(\mu_D^{URM})^2 + (\sigma_D^{URM})^2] - \mu_{\tilde{D}}^2 \end{aligned} \quad (18b)$$



Table 20 shows the structural/non-structural damage ratios and the content loss ratios adjusted by Eqs. (16)–(18).

Table 20. Means and variances of damage ratios and content loss ratios adjusted by inventory uncertainty

Inventory buildings		$\mu_{\tilde{D}}$	$\sigma_{\tilde{D}}^2$
1: Concrete	SD	0.359	0.151
	NA	0.102	0.035
	ND	0.218	0.079
	CL	0.059	0.011
2: URM	SD	0.356	0.134
	NA	0.123	0.042
	ND	0.198	0.071
	CL	0.071	0.013
3: URM 2	SD	0.340	0.132
	NA	0.118	0.041
	ND	0.191	0.069
	CL	0.069	0.013

Notation: SD: structural damage, NA: acceleration-sensitive non-structural damage, ND: drift-sensitive non-structural damage, CL: content loss

## VI. Loss estimation

As a simple example of social and economic losses caused by seismic hazard, we consider the loss of an inventory item defined by

$$Loss_i = M_i (\alpha_i^{SD} \tilde{D}_i^{SD} + \alpha_i^{NA} \tilde{D}_i^{NA} + \alpha_i^{ND} \tilde{D}_i^{ND} + \alpha_i^{CL} \tilde{D}_i^{CL}) \quad (19)$$

where  $M_i$  is the total assessed value of the  $i$ -th inventory item;  $\alpha_i^{SD}$ ,  $\alpha_i^{NA}$  and  $\alpha_i^{ND}$  are the fractions of the values of structural and non-structural (acceleration- and drift-sensitive) components;  $\alpha_i^{CL}$  is the ratio of the contents value to the structural assessed value;  $\tilde{D}_i^{SD}$ ,  $\tilde{D}_i^{NA}$  and  $\tilde{D}_i^{ND}$  are the damage ratios of the  $i$ -th inventory item adjusted by the inventory uncertainty; and  $\tilde{D}_i^{CL}$  is the adjusted content loss ratio. Table 21 shows the fractions of structural and non-structural values of commercial and industrial occupancies defined by HAZUS. In this example, we assume  $\alpha^{CL}$  to be 150, 100 and 150% for the inventory items 1, 2 and 3, following the assumption by HAZUS that  $\alpha^{CL}$  can be 50, 100 or 150% only.



Table 21. Fraction (%) of structural and non-structural values

Occupancy type	$\alpha^{SD}$	$\alpha^{NA}$	$\alpha^{ND}$
Commercial	29.4	43.1	27.5
Industrial	15.7	72.5	11.8

The total loss of the inventory is obtained by aggregating the losses of the inventory items, that is,

$$Loss = \sum_{i=1}^N Loss_i \quad (20)$$

Then mean of the total loss is estimated as

$$\mu_{Loss} = \sum_{i=1}^N M_i (\alpha_i^{SD} \mu_{\bar{D}_i^{SD}} + \alpha_i^{NA} \mu_{\bar{D}_i^{NA}} + \alpha_i^{ND} \mu_{\bar{D}_i^{ND}} + \alpha_i^{CL} \mu_{\bar{D}_i^{CL}}) \quad (21)$$

Assuming the damage ratios of different inventory items are conditionally independent given a seismic intensity, the variance of the total loss is computed as

$$\sigma_{Loss}^2 = \sum_{i=1}^N M_i^2 \left[ (\alpha_i^{SD})^2 \sigma_{\bar{D}_i^{SD}}^2 + (\alpha_i^{NA})^2 \sigma_{\bar{D}_i^{NA}}^2 + (\alpha_i^{ND})^2 \sigma_{\bar{D}_i^{ND}}^2 + (\alpha_i^{CL})^2 \sigma_{\bar{D}_i^{CL}}^2 \right] \quad (22)$$

The coefficient of variation (c.o.v.) of the total loss is

$$\delta_{Loss} = \frac{\sigma_{Loss}}{\mu_{Loss}} \quad (23)$$

The mean, standard deviation and c.o.v. of the total loss of the example inventory are estimated as 0.365 (million US\$), 0.208(million US\$) and 56.84 %, respectively.

Consider Loss Ratio ( $L_r$ ), which is the total loss normalized by the sum of structural, non-structural and content values in a region, that is,

$$L_r = \frac{Loss}{\sum_{i=1}^N M_i (\alpha_i^{SD} + \alpha_i^{NA} + \alpha_i^{ND} + \alpha_i^{CL})} = \frac{Loss}{\sum_{i=1}^N M_i (1 + \alpha_i^{CL})} = \frac{Loss}{M_{total}} \quad (24)$$

Then, mean and standard deviation of the loss ratio are  $\mu_{Loss} / M_{total}$  and  $\sigma_{Loss} / M_{total}$ , respectively. The c.o.v. of the loss ratio is the same as that of the total loss. For the example inventory, the mean and standard deviation of the loss ratio are estimated as 11.42% and 6.48 %, respectively.

Given the estimated mean and standard deviation, and an assumed distribution type, we can find the probability distribution of the loss ratio. We hereby assume the loss ratio follows the lognormal distribution. The lognormal distribution requires two parameters  $\lambda$  and  $\beta$ , which are the mean and standard deviation of the natural logarithm of the quantity.



These parameters are obtained from the estimated mean and standard deviation of the loss ratio as follows.

$$\beta = \sqrt{\ln[1 + (\sigma / \mu)^2]} \quad (25a)$$

$$\lambda = \ln \mu - 0.5\beta^2 \quad (25b)$$

The lognormal parameters of the loss ratio in the example are  $\lambda = -2.31$  and  $\beta = 0.529$ . The probability density function (PDF) of the loss ratio is defined as

$$f_{L_r}(l_r) = \frac{1}{\sqrt{2\pi}\beta l_r} \exp\left[-\frac{1}{2}\left(\frac{\ln l_r - \lambda}{\beta}\right)^2\right] \quad (26)$$

Figure 4 plots the PDF of the loss ratio of the example inventory.

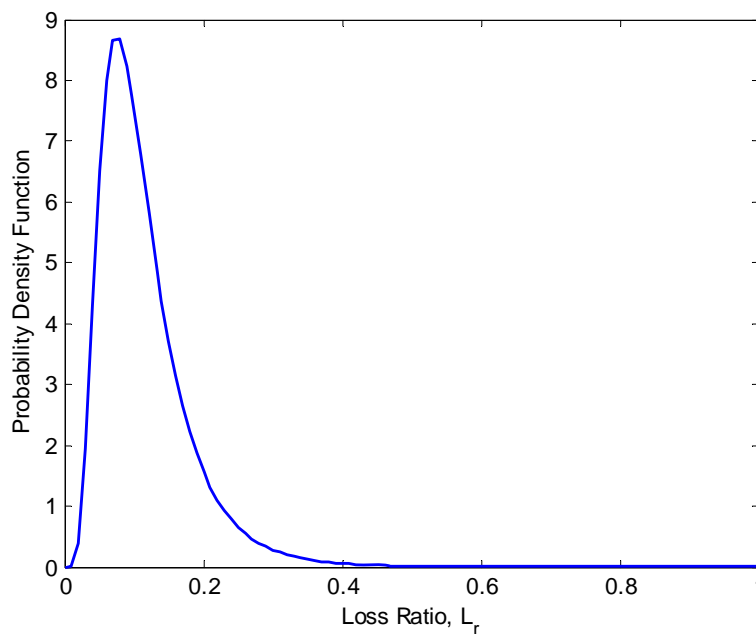


Figure 4. Probability density function of loss ratio



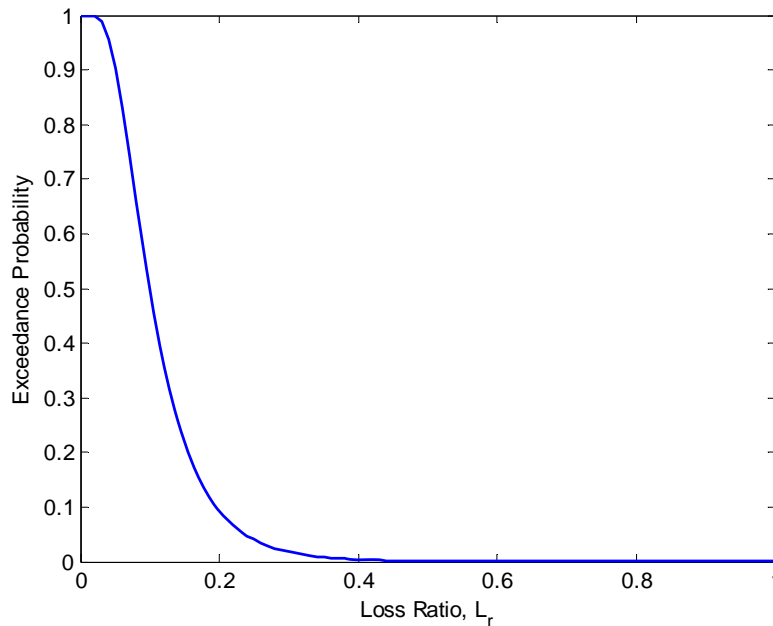


Figure 5. Exceedance probability of loss ratio

We can also estimate the probability that the loss ratio will exceed a certain threshold. This is often referred as complementary cumulative distribution function (CCDF). The CCDF of the lognormal distribution is

$$C_{L_r}(l_r) = 1 - \Phi \left[ \frac{\ln(l_r) - \lambda}{\beta} \right] \quad (27)$$

The exceedance probability of the loss ratio is plotted in Figure 5. Table 22 lists the exceedance probabilities at selected thresholds of loss ratio.

Table 22. Probability of exceedance

Loss ratio (%)	Probability of exceedance, % (lognormal distribution)
0	100.00
1	100.00
5	90.24
10	49.43
20	9.27
30	1.83
40	0.42
50	0.11



Based on the estimated uncertainty in the loss ratio, we can predict the loss ratio by an interval with a certain level of confidence. An interval that encloses the true loss ratio with probability  $1 - \alpha$  (or an interval with ‘confidence level’  $1 - \alpha$ ) is

$$[\exp(\lambda - k_{\alpha/2}\beta), \exp(\lambda + k_{\alpha/2}\beta)] \quad (28)$$

where  $k_{\alpha/2} = \Phi^{-1}(1 - \alpha/2)$ . Table 23 shows the coefficient values for selected confidence levels and the corresponding confidence intervals.

Table 23. Confidence intervals on loss ratio

Confidence level, $1 - \alpha$ (%)	$k_{\alpha/2}$	Confidence interval (%)
60	0.8416	[6.36, 15.49]
70	1.0364	[5.73, 17.17]
80	1.2816	[5.04, 19.55]
90	1.6449	[4.16, 23.70]
95	1.9600	[3.52, 28.00]
99	2.5758	[2.54, 38.78]



## **APPENDIX: Data flow chart**

Figure 6 illustrates the data flow of the proposed procedure with equation numbers shown.



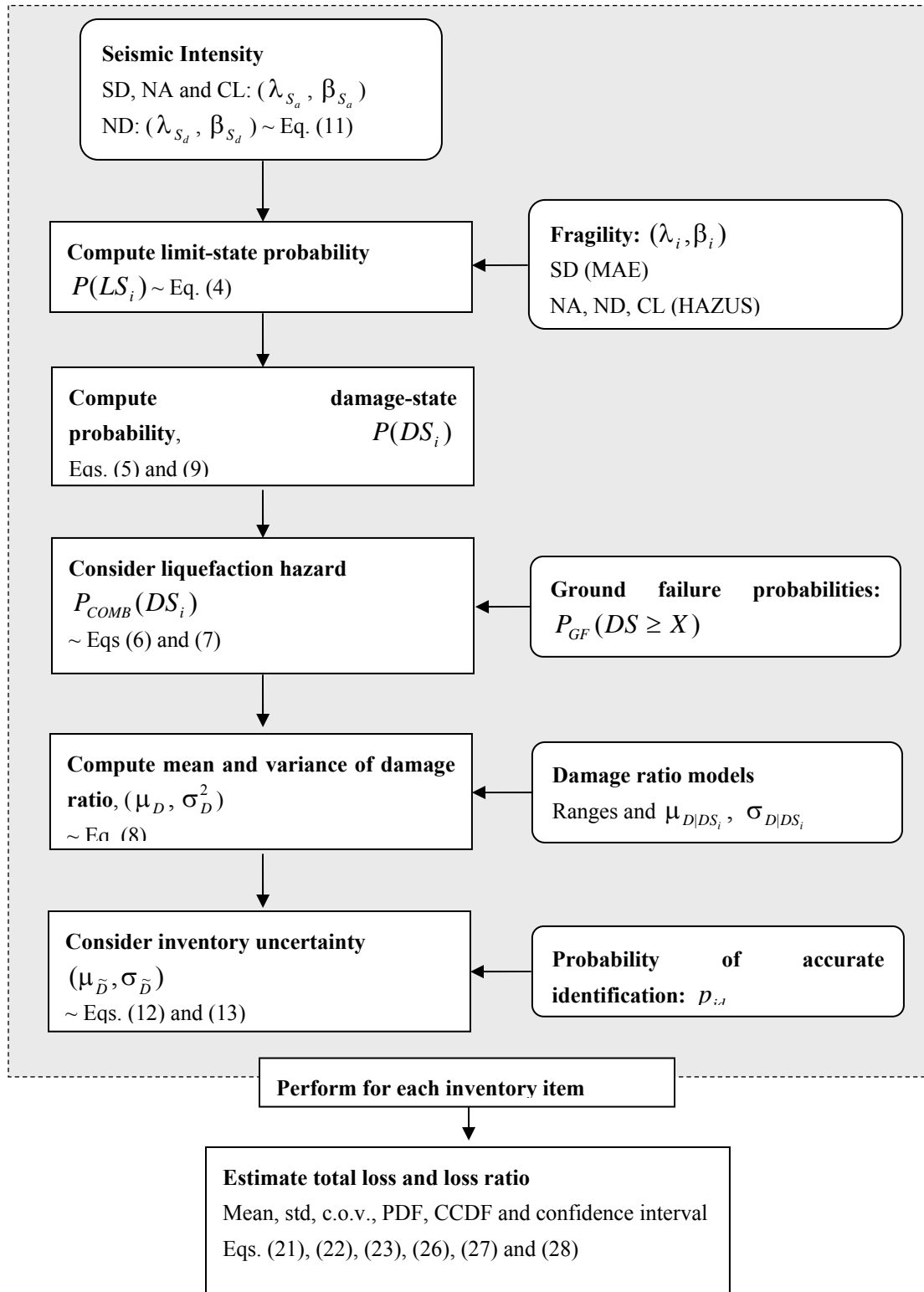


Figure 6. Data flow chart of probabilistic estimation of seismic regional loss

